Technische Universität München
TUM School of Engineering and Design

Influence of Fluid Properties on Lubricant Return for Low-GWP Refrigerants

Bernd Heithorst

Vollständiger Abdruck der von der TUM School of Engineering and Design der Technischen Universität München zur Erlangung eines

DOKTORS DER INGENIEURWISSENSCHAFTEN (DR.-ING.)

genehmigten Dissertation.

Vorsitz:
Prof. Dr. Oliver Lieleg
Prüfer*innen der Dissertation:
1. Prof. Dr.-Ing. Thomas Sattelmayer
2. Prof. Dr.-Ing. Arne Speerforck
3. Hon.-Prof. Dr.-Ing. Alexander Kolb

Die Dissertation wurde am 16.01.2023 bei der Technischen Universität München eingereicht und durch die TUM School of Engineering and Design am 18.07.2023 angenommen.

To my family

Acknowledgements

This thesis evolved during my time as research and teaching associate at the Institute of Thermodynamics, Technical University of Munich. The work published in this thesis was inspired by and carried out after the Project PVCool funded by the Qatari National Research Fund (project grant NPRP8-1908-2-760). The financial support during the project is gratefully acknowledged.

First, I want to thank Prof. Dr.-Ing. Thomas Sattelmayer for the opportunity to work as a research and teaching associate at the institute, for his great scientific knowledge, and for his strategic advice. I would like to thank Prof. Dr.-Ing. Arne Speerforck and Prof. Dr.-Ing. Alexander Kolb for reviewing the thesis and for the examination. I would also like to thank Prof. Dr.-Ing Oliver Lieleg for chairing the examination.

I am deeply grateful to Dr.-Ing. Markus Spinnler for the opportunity to conduct the PVCool project, for his trust and support during the project and the work on the thesis, for his optimism, and above all for his friendship, which will remain despite his much too early decease. This thesis would not have been possible without him.

I am sincerely grateful to Dr.-Ing. Florian Kiefer for his support, the countless discussions through all the years, the proofreading, and his friendship. Furthermore, I want to express my gratitude towards my colleagues Dr.-Ing. Alexander Kroiss, Dr.-Ing. Mayameen Reda, Dr.-Ing. Andreas Kastl, and Dr.-Ing. Alexander Präbst for their scientific support, friendship and the cheerful moments at the institute. A big thank you to all my students supporting me during the PVCool project.

Many thanks to Dr.-Ing. Christoph Hirsch for the numerous discussions, especially during the critical phase of the dissertation. A big thank you to the workshop and administrative staff of the institute, especially Gerhard Giel, Jens Hümmer, Thomas Schleussner, Helmut Koller and Helga Bassett.

It is impossible to find suited words to express my gratitude to my family. With their encouragement and selfless financial support, my parents made my studies possible. Without the backing, endless patience, and the unconditional love of my wife Melanie, it would have been impossible to complete the work summarized in this thesis. Last but not least, a heartfelt thank you to my children Gregor and Marianna, who continuously remind me of what is really important in life.

Oberhaching, 2024 Bernd Heithorst

Abstract

In refrigeration cycles, stable lubricant return to the compressor is required to prevent compressor failure. If the load of variable speed compressors is reduced, the lubricant return at some point fails in vertical parts of the suction line. This limits the operation range of variable speed compressors.

Currently, the refrigeration industry faces a transition to refrigerants with low global warming potential. However, an operation limit to guarantee stable lubricant return is not available for these refrigerants. The present work aims to determine this operation limit for refrigerants with low global warming potential and polyol ester lubricants.

The stability of the liquid wall film in the two-phase annular flow in vertical parts of the suction line depends on the fluid properties of both vapor and liquid phase. The liquid phase consists of the lubricant with dissolved refrigerant. Therefore, it is challenging to determine its fluid properties. A tool chain consisting of three elements was developed to predict the fluid properties. First, a composition of polyol esters is determined that matches target properties for density and viscosity. Secondly, the solubility of the refrigerant in the mixture of polyol esters and the density of the liquid phase are determined with the *Perturbated-Chain Statistical Associating Fluid Theory*. Thirdly, the mixture viscosity of the liquid phase is calculated. Based on the predicted fluid properties, the limit for part-load operation is determined by means of a two-phase flow model. The results serve as design guideline for the diameter of the suction line to ensure lubricant return in the operation range of variable speed compressors.

Kurzfassung

Ein stabiler Schmiermittelrücklauf zum Verdichter ist erforderlich, um Schaden am Verdichter von Kompressionskälteanlagen zu vermeiden. Wird die Leistung von drehzahlgeregelten Verdichtern reduziert, bricht der Schmiermittelrücklauf in vertikalen Teilen der Saugleitung ab einem bestimmten Punkt zusammen. Dadurch wird der Betriebsbereich von Verdichtern mit variabler Drehzahl eingeschränkt.

In der Kältetechnik findet derzeit ein Übergang zu Kältemitteln mit geringem Treibhauspotenzial statt. Allerdings ist für diese Kältemittel kein Auslegungskriterium für den Teillastbetrieb definiert, das den Schmiermittelrücklauf sicherstellt. In der vorliegenden Arbeit soll diese Betriebsgrenze für Kältemittel mit niedrigem Treibhauspotenzial und Polyolester-Ölen ermittelt werden.

Die Stabilität des Flüssigkeitsfilms in der zweiphasigen Ringströmung in vertikalen Bereichen der Saugleitung hängt von den thermophysikalischen Eigenschaften der Dampf- und Flüssigphase ab. Die Herausforderung besteht darin, die Eigenschaften der flüssigen Phase zu bestimmen, da diese aus Schmieröl und darin gelöstem Kältemittel besteht. Zur Vorhersage der thermophysikalischen Eigenschaften wurden verschiedene aufeinander aufbauende Elemente entwickelt. Zuerst wird eine Zusammensetzung von Polyolestern bestimmt, die bestimmten Zieleigenschaften für Dichte und Viskosität entspricht. Anschließend werden die Löslichkeit des Kältemittels im Polyolesteröl und die Dichte der Mischung mit der *Perturbated-Chain Statistical Associating Fluid Theory* bestimmt. Schließlich wird die Mischungsviskosität der flüssigen Phase berechnet. Basierend auf den berechneten thermophysikalischen Eigenschaften wird die Grenze für den Teillastbetrieb mit Hilfe eines Modells der Zwei-Phasen-Strömung in der Saugleitung bestimmt. Das Ergebnis kann zur Auslegung des Durchmessers der Saugleitung genutzt werden, um die Schmiermittelrückführung im Betriebsbereich von drehzahlgeregelten Verdichtern zu gewährleisten.

Contents

List of Figures

List of Tables

Nomenclature

Abbreviations

AB	Alkylbenzene lubricant
AC	Air conditioning
CFC	Chlorofluorocarbon
DiPE	Di-pentaerythritol hexaalkyl ester
EoS	Thermal equation of state
FP	Freezing point
GWP	Global warming potential
HC	Hydrocarbon
HCFC	Hydrochlorofluorocarbon
HFC	Hydrofluorocarbon
HFO	Hydrofluoroolefin
MO	Mineral lubrication oil
MP	Melting point
NMR	Nuclear magnetic resonance spectroscopy
PAG	Polyalkylene glycol lubricant
PAO	Polyalphaolefin lubricant
PC SAFT	Perturbated-Chain Statistical Associating Fluid Theory
PCP SAFT	Perturbated-Chain Polar Statistical Associating Fluid Theory
PE	Pentaerythritol tetraalkyl ester
POE	Polyolester lubricant
PP	Pour point
PR	Peng-Robinson

PV	Photovoltaic(s)
SRK	Soave-Redlich-Kwong
VG	Viscosity grade
VI	Viscosity index

Constants

h	$\mathrm{J\,s}$	Plank constant
k_B	$\mathrm{J\,K^{-1}}$	Boltzmann constant
N_A	$\mathrm{mol^{-1}}$	Avogadro constant
R	$\mathrm{J\,mol^{-1}\,K^{-1}}$	Universal gas constant

Latin Letters

A	$\mathrm{m^2}$	Area
a_i		Empirical coefficients in various equations
AAD	%	Absolute average deviation
B	−	Parameter in the free volume model
Bias	%	Average deviation
D	m	Inner pipe diameter
E	J	Energy
EER	−	Energy efficiency ratio
F	J	Helmholtz free energy
f	−	Friction factor
Fr	−	Froude number
Fr^*	−	Modified Froude number
G_m	$\mathrm{J\,mol^{-1}}$	Molar Gibb's free enthalpy
$G_\mathrm{m}^{\neq}$	$\mathrm{J\,mol^{-1}}$	Molar free energy of activation for viscous flow
g	$\mathrm{m\,s^{-2}}$	Gravitational acceleration constant
H	J	Enthalpy
h	$\mathrm{J\,kg^{-1}}$	Mass specific enthalpy
J	$\mathrm{kg\,m^{-2}\,s^{-1}}$	Mass flux
k_{ij}	−	Binary interaction coefficient of i and j
L	m	Length

l	Å	Parameter in the Free Volume Model
LR	–	Liquid ratio in two-phase flow
M	$\mathrm{kg\,mol^{-1}}$	Molecular weight
m	–	PC SAFT parameter: number of segments
$\mathfrak{m}$	kg	Mass
$\dot{\mathfrak{m}}$	$\mathrm{kg\,s^{-1}}$	Mass flow rate
MD	%	Maximum deviation
n	–	Number of data points or components in a mixture
OCR	–	Oil circulation ratio
p	Pa	Pressure
P	W	Power
$\dot{Q}$	W	Heat flow
R	m	Inner pipe radius
r	m	Coordinate in radial direction
Re	–	Reynolds number
Res	–	Residual
T	°C or K	Temperature
ΔT_{SH}	K	Superheat
u	J	Square well potential in PC SAFT
V_{m}	$\mathrm{m^3\,mol^{-1}}$	Molar volume
$\Delta\overline{V}_{\mathrm{m}}$	$\mathrm{m^3\,mol^{-1}}$	Molar volume change of mixing
v	$\mathrm{m\,s^{-1}}$	Velocity
w_i	–	Mass fraction of component i in a mixture
x_i	–	Mole fraction of component i in a mixture
Z	–	Compressibility factor
z	m	Coordinate in flow direction

Greek Letters

α	$\mathrm{m^2\,s^{-2}\,mol^{-1}}$	Free volume coefficient
γ	–	Activity coefficient
δ	m	Film thickness
δ_{v}^{+}	–	Dimensionless film thickness
ϵ	–	Normalized deviation

ε	J	PC SAFT parameter: potential depth
η	$\mathrm{J\,mol^{-1}}$	Chemical potential
ι	D	Dipole moment
κ_i	$\mathrm{Pa^{1-i}\,s}$	Friction parameters in f-theory
$\tilde{\kappa}_i$	–	Reduced friction parameters in f-theory
λ	–	Width of square well potential in PC SAFT
μ	Pa s	Dynamic viscosity
ν	$\mathrm{m^2\,s^{-1}}$	Kinematic viscosity
ϖ_j	–	Mass weighed fraction of potential depth ε_j of component j
ρ	$\mathrm{kg\,m^{-3}}$	Density
σ	Å	PC SAFT parameter: segment diameter
ς	$\mathrm{N\,m^{-1}}$	Surface tension
τ	$\mathrm{N\,m^{-2}}$	Shear stress
φ	–	Fugacity coefficient
ψ	Pa	Fugacity
ω	–	Effective mass fraction in mixture viscosity model of Yokozeki

Subscripts

0	Pure component parameter
a	Attractive
act	Activation
atm	Atmospheric
c	Property at the critical point
calc	Calculated
Comp	Compressor
cond	Condensation
crit	Critical point for lubricant return
d	Dense liquid
dp	Dipole contribution
dil	Diluted gas
disp	Dispersive contribution

el	Electric
Evap	Evaporator
evap	Evaporation
exp	Experimental data
FP	Freezing point
fr	Flow reversal
g	Gas
hc	Hard chain contribution
hor	Horizontal
I	Interface
in	Inlet
l	Liquid
Lub	Lubricant
m	Molar quantity
max	Maximum
min	Minimum
Mix	Mixture of pentaerythritol tetraalkyl esters
mod	Modeled data
MP	Melting point
out	Outlet
PP	Pour point
r	Repulsive
Ref	Refrigerant
s	Smooth pipe
sat	Saturation
TS	Test section
v	Vapour
vert	Vertical
w	Wall

Superscripts

$\overline{\boxtimes}$	Mixture property
E	Excess property
id	Ideal mixture property
res	Residual property

1 Introduction

1.1 Background and Motivation

Solar heating and cooling gained increased attention in the past decades to reduce the carbon dioxide footprint in the thermal conditioning of buildings. Regarding solar cooling, the coupling of photovoltaic (PV) panels with mechanical vapor compression chillers shows a higher efficiency compared to sorption chillers driven with solar thermal collectors. Additionally, they also became the economically favorable option in this comparison due to the decrease of PV module prices [1].

With respect to solar heating with a combination of heat pump and PV, a part of the required electricity of the heat pump can be covered by the PV system. Variable speed compressors can be used to adapt the compressor power to the available PV power to increase the economically favorable self-supply [2].

The technical constraints that limit the part-load operation of the compressor are not considered in most publications that examine variable speed compressors to efficiently exploit the solar resources or to reduce electricity cost with variable electricity prices (e.g. [3–6]). A reason for this is the scarce experimental data on operation constraints in literature.

Besides the technically limiting components in the compressor drive, also the return of the lubricant oil from the refrigeration cycle to the compressor can be an important constraint for part-load operation of variable speed compressors [7].

1.2 Lubricants in the Refrigeration Cycle

The lubricant oil is needed in refrigeration cycles only in the compressor to reduce friction and minimize wear of the sliding parts [8]. During the compression and at the compressor outlet valves very fine droplets of lubrication oil are entrained in the refrigerant vapor flow [9–11]. Oil separation devices can be applied in the compressor or in the discharge line, but increase the pressure loss. Additionally, they do not fully separate the oil [12]. In small scale systems, oil separation is usually limited to simple devices inside the compressor crankcase.

Once the lubricant entered the discharge line, it circulates together with the refrigerant in the refrigeration cycle depicted in Figure 1.1. If not explicitly mentioned, the following explanations refer to the subcritical refrigeration cycle depicted in Figure 1.1a.

The mass flow rate of the lubricant $\dot{m}_{\mathrm{Lub}}$ is usually related to the total mass flow rate in the oil circulation ratio OCR according to Equation (1.1).

$$\mathrm{OCR} = \frac{\dot{m}_{\mathrm{Lub}}}{\dot{m}_{\mathrm{Lub}} + \dot{m}_{\mathrm{Ref}}} \tag{1.1}$$

$\dot{m}_{\mathrm{Ref}}$ is the mass flow rate of the refrigerant. The OCR depends on the rotational speed of the compressor and on oil separation inside the compressor or in the discharge line. TOYAMA ET AL. [9] found that an oil separation plate reduces the amount of emitted oil by a factor of three. For a scroll compressor with oil separation plate, they found OCR = 1% for a rotational speed of 60 Hz and OCR = 3% for a rotational speed of 90 Hz.

XU AND HRNJAK [13] compared the oil discharge of a scroll compressor with a cooling capacity of 10 kW and an automotive swash-plate compressor with a displacement volume of 155 cm^3. They measured a range of 1.2% < OCR < 1.8% for the scroll compressor and of 0.4% < OCR < 3% for the swash-plate compressor. The OCR increases continuously with rising compressor speed for both compressor types. The stronger influence of the compressor speed on the OCR for the swash-plate compressor compared to the scroll compressor is explained with the absence of any oil separation devices in this case.

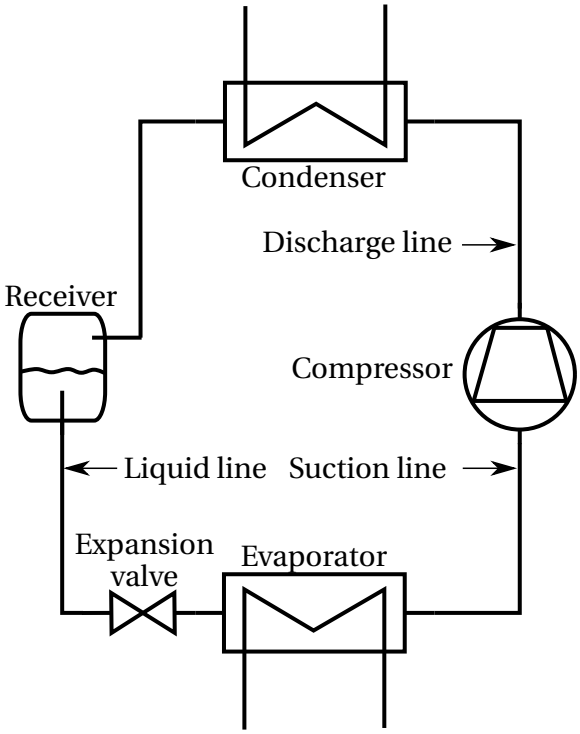

(a) Subcritical refrigeration cycle.

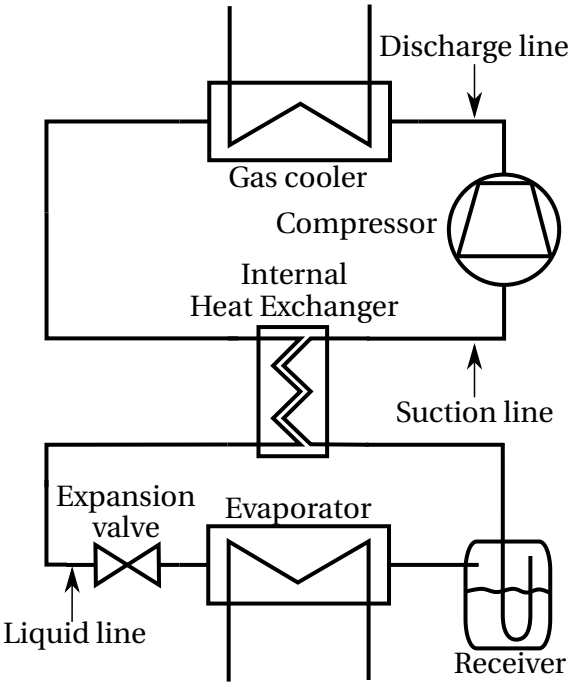

(b) Refrigeration cycle with supercritical heat extraction for refrigerant R744 (CO_2).

Figure 1.1: Refrigeration cycle setup.

HWANG ET AL. [14] measured an OCR of 1.1% in steady-state compressor operation and up to 10% during the compressor start-up for an automotive CO_2 air conditioning system.

The comparison of the literature on oil discharge shows that the amount of lubricant is small compared to the refrigerant. Nevertheless, it has a negative influence on the performance of the other refrigeration cycle components:

- In the condenser, the lubricant dissolves in the liquefied refrigerant. The reduced condensation temperature of a refrigerant-lubricant mixture compared to pure refrigerant is beneficial whereas the increased viscosity of the liquid is detrimental to the heat transfer. All in all, the influence of lubricant on the heat transfer is low [15].

- In the evaporator, the liquid phase at the inlet is refrigerant rich. The lubricant remains in the liquid phase due to its very low vapor pressure [16]. The oil concentration in the liquid rises continuously towards the evaporator outlet. At the evaporator outlet, the refrigerant vapor is superheated[1]. On the one hand, the presence of oil in the evaporator leads to an improved surface wetting [18, 19]. On the other hand, it leads to a certain amount of refrigerant dissolved in the lubricant that does not evaporate and thus to a smaller heat flow than for a pure refrigerant flow [20]. The higher viscosity of refrigerant-lubricant mixtures leads to a negative effect on the refrigerant distribution in microchannel evaporators [21]. LOTTIN ET AL. [22] found that a very small amount (OCR = 0.1%) is beneficial for heat transfer, but higher OCRs have a negative effect.
- The vapor pressure is lower for a mixture of refrigerant and lubricant compared to the pure refrigerant [20]. This leads to a slightly higher pressure ratio between high and low pressure side of the compressor.
- Pressure losses in the pipes and heat exchangers increase with rising OCR [23, 24].

It is essential that the lubricant returns to the compressor to prevent a decrease of the lubricant level in the oil sump below the critical level for proper lubrication [23]. CREMASCHI ET AL. [7] experimentally investigated the oil retention in the different components of the refrigeration cycle in steady-state operation. In their test setup, the largest amount of lubricant was retained in the condenser and the suction line. The mass of retained oil was proportional to the OCR in steady state operation. The suction line was identified as the most critical component for oil retention.

For nominal operation conditions, the liquid forms an annular film at the wall of the suction line. The shear stress between the liquid film and the refrigerant vapor core flow leads to a movement of the liquid film in flow direction of

[1] In air conditioning or domestic heat pump systems with R744 (CO_2), the system setup is different compared to the system setup of other common refrigerants (see Figure 1.1b in comparison to Figure 1.1a). The reason is that R744 is in a supercritical state for common operation temperatures of the heat sink. The receiver is located after the evaporator due to the high pressures on the discharge side of the compressor. In this case, the refrigerant vapor is saturated at the evaporator outlet. Nevertheless, the refrigerant is superheated directly after the receiver in the internal heat exchanger [17].

the refrigerant and thus back to the compressor. The lubricant transport in the suction line is a bottleneck, because the liquid film in the suction line shows the highest viscosity values in the refrigeration cycle due to the low temperature and relatively low amount of dissolved refrigerant. Additionally, the shear force that drives the lubricant transport is low in the suction line. [7]

Beside the oil retention in steady-state operation, different oil traps can lead to a failure of lubricant return. For example, a large amount of oil can be trapped in the receiver due to phase separation of the liquid phase into a refrigerant rich and a lubricant rich phase [25, 26]. Furthermore, oil traps in the pipe work have to be avoided especially in pipe junctions by an appropriate design. For details see OWEN [26, p.1.17ff].

Even if the oil return works well for nominal operation conditions, potentially critical situations for oil return may occur varying the load of a variable speed compressor. Reducing the compressor speed leads to a decrease of the refrigerant vapor mass flux in the suction line. For decreasing mass flux, there is a point when the shear force at the liquid-vapor interface is not sufficient to transport the lubricant upwards in vertical parts of the suction line, so called suction risers [27, 28]. In this case, the oil accumulates at the deepest location in the pipe. The locally increased oil concentration leads to a transition in the flow regime. The lubricant is then transported in a surge upwards the pipe. This can lead to a liquid slug if the surge enters the compression volume, as the lubricant is incompressible. Liquid slugs can lead to severe damages in the compressor.

The critical mass flux J_{crit} for lubricant return is defined as the lowest mass flux that leads to a stable lubricant return in vertical suction lines [27, 28]. Reducing the suction line diameter decreases the critical mass flux J_{crit} and also the oil retention in steady-state operation. Albeit, a lower diameter leads to higher pressure losses in the suction line at full-load operation of the variable speed compressor [23, 26]. A trade-off must be found between the reduction of pressure losses at full load and the operation limit at part-load.

Beside the suction line diameter, the critical mass flux J_{crit} depends on the density and viscosity of the vapor and liquid phase [28].

1.3 Low Global Warming Potential Refrigerants

The refrigeration industry is facing a transformation due to the stricter legislation on green house gas emissions for refrigerants. In Europe, the fluorinated greenhouse gases regulation [29] decreases the amount of refrigerants with high global warming potential (GWP) on the market gradually down to 20% of the amount of 2014 until 2030. Therefore, alternatives to the common hydrofluorocarbon (HFC) refrigerants are economically favored. In automotive air conditioning, HFC refrigerants were banned completely.

Alternatives to HFC refrigerants are natural refrigerants as R744 (CO_2), hydrocarbon (HC) refrigerants R290 (propane), R600a (isobutane), and R1270 (propene) or hydrofluoroolefin (HFO) refrigerants, as R1234yf (2,3,3,3-Tetrafluoropropene) or its structural isomer R1234ze (1,3,3,3-Tetrafluoropropene). All alternative refrigerants have a GWP < 5. This is much lower compared to e.g. the frequently applied HFC refrigerant R134a with GWP = 1300 [30]. The common disadvantage of these alternatives to HFC refrigerants is their flammability. While HC refrigerants are grouped in safety class A3 (low toxicity, high flammability), HFO refrigerants R1234yf and R1234ze belong to safety class A2L (low toxicity, mild flammability) [31]. Charge minimization and additional safety measures can be necessary to fulfill safety requirements [32]. The natural refrigerants R717 (ammonia) and R718 (water) are not considered in this thesis. R717 (ammonia) is toxic and is therefore not applied in residential or automotive air conditioning (AC) systems. R718 (water) requires a very different system setup using centrifugal compressors [33].

Natural refrigerants are nothing new in refrigeration. Rather, they have been the first substances applied as refrigerants in history [34]. Nevertheless, fluid properties of mixtures of natural refrigerants or HFOs with lubricants are widely not available. As a consequence, also values for the critical mass flux for lubricant return in vertical suction lines are not available for low GWP refrigerants in literature.

The identification of the critical mass flux for low GWP refrigerants was therefore defined as the main objective of the study at hand.

1.4 Refrigeration Lubricants

1.4.1 Tasks and Requirements

Lubricants fulfill different tasks in refrigeration compressors [8, 35]:

- Reduction of friction between the sliding parts of the compressor and minimization of wear.
- Sealing of the compression volume.
- Cooling of the mechanical components.
- Reduction of noise generated by the moving parts.

To fulfill the mentioned tasks, the lubricant must show the following characteristics [8, 35, 36]:

- Sufficiently high viscosity at compressor operation conditions to lubricate sliding parts. Viscosity reductions due to elevated temperatures and dissolved refrigerant have to be considered.
- Low viscosity at low temperatures to reduce oil retention in the suction line.
- High chemical and thermal stability as the lubricant cannot be changed during the lifetime of the refrigeration plant.
- Compatibility with other components, such as refrigerant, metals, and sealing material.
- Miscibility with the refrigerant.
- No wax formation over the entire temperature operation range of the evaporator, as waxes would clog the evaporator.
- A high dielectric strength for applications in hermetic compressors[2].

[2] In hermetic compressors, the motor and compressor are placed in one sealed casing. Thus, the electric motor coil is in contact with the lubricant oil. To prevent a current between stator and rotor or casing of the electric motor, the lubricant needs a sufficient dielectric strength. [8] In open compressors, the compressor is working with an external drive. A dynamic sealing is required for the driving shaft. The dielectric strength of the lubricant is irrelevant in this case.

A conclusion drawn from this list is that trade-offs between the different requirements on refrigeration lubricants are necessary. A higher viscosity in the compressor improves the protection against wear, but increases the energy demand and pressure losses in the pipes and heat exchangers. A good miscibility with the refrigerant is required for a proper lubricant return, but a high solubility of the refrigerant in the lubricant reduces the viscosity of the lubricating film in the compressor. [8]

In other words, the lowest viscosity sufficient to lubricate the compressor at the highest operation temperature should be selected to guarantee proper lubrication and the best possible efficiency of the refrigeration cycle [36].

1.4.2 Types of Refrigeration Lubricants

In the following, the most relevant types of refrigeration lubricants are presented and compared with each other regarding their compatibility with low-GWP refrigerants.

- **Mineral oil (MO):** As the name suggests, MOs are derived from fossil resources. Therefore, the lubricants consist of a wide range of classes of components: paraffins, naphthenes, aromatics, and non-hydrocarbons. The low cost is an advantage of MOs. Mineral oil lubricants were widely applied with Chlorofluorocarbon (CFC) and Hydrochlorofluorocarbon (HCFC) refrigerants [8]. They are not miscible with HFC refrigerants in a wide range due to the high dipole moment of these refrigerants [36]. In contrast, HC refrigerants show a very high solubility with MO lubricants. This requires a high viscosity with HC refrigerant applications. An oil sump heating is beneficial to reduce the amount of dissolved refrigerant at cold start conditions [35].

- **Polyalkylene glycol (PAG)** is derived from the controlled polymerization of propene oxide and ethylene oxide. The properties of PAGs can be adjusted very versatilely with modifications of the average molecular weight and the ratio of propene oxide to ethylene oxide [8]. They show a low dielectric strength and are therefore not applied in hermetic compressors. PAGs are widely miscible with HFC refrigerants. This made them the preferred lubricant in automotive air conditioning of combustion engine vehicles, as open compressors are used in this case[2] [8, 36]. PAGs show a pronounced miscibility gap with HC refrigerants. This limits their applicability with HC refrigerants [35].

- **Polyalphaolefins (PAO)** are synthesized through a controlled oligomerization of linear α-olefins. The viscosity is adjusted by the degree of polymerization of the olefin and the branching of the α-olefins. Chemically, PAOs are similar to MOs and do not show a polarity. The viscosity-temperature relation and the low temperature behaviour are better compared to MO lubricants. They are miscible with (H)CFC refrigerants, but immiscible with R134a [8, 35].

- **Polyol Esters (POE)** are synthesized combining carboxylic acids and an alcohol from the group of neopentyl polyols. Due to the vast possibilities of combining differently structured alcohols and carboxylic acids, a wide viscosity range is covered by POEs. The properties of the lubricant can be optimized to specific applications or refrigerants [8]. POEs are compatible with a wide range of refrigerants, i.a. HFC refrigerants [8, 35]. Additionally, their high dielectric strength makes them an attractive solution for widely used hermetic compressors in small scale applications. Therefore, POEs gained a high market share. The liquid lubrication film sustains higher loads compared to MO lubricants because of the polarity of the carboxylic-groups [35]. They have an excellent thermal and chemical stability provided that the system is free of moisture [36].

The compatibility of the different lubricants and refrigerants according to OWEN [8] and BOCK AND PUHL [35] is summarized in Table 1.1.

Table 1.1: Compatibility of refrigerants and lubricants.

Refrigerant		Owen [8]				Bock and Puhl [35]		
		MO	PAG	PAO	POE	MO	PAO	POE
HFC	R134a		x		x			x
	R410A		x		x			x
HC	R290	x			x	x	x	x
	R600a	x	x	x	x	x	x	x
	R1270	n.a.	n.a.	n.a.	n.a.	x	x	x
CO_2	R744		x		x			x

n.a.: not available.

Both, Owen [8] and Bock and Puhl [35] do not indicate the lubricant compatibility with HFO refrigerants. Karnaz [37] found immiscible mixtures for temperatures below 20°C for alkylbenzene (AB), MO and PAO lubricants with R1234ze. In contrast, miscibility was observed with POE lubricants down to $T = -60$°C. In a review article on recent developments in HFO research, Nair [38] concluded that R1234yf is better compatible with POEs then with PAGs.

The comparison shows that POE lubricants are compatible with all low GWP-refrigerants in contrast to all other lubricant types. POEs are applicable also in hermetic compressors due to their high dielectric strength. The dominance of PAGs in the automotive industry is expected to decrease with the rising market share of electric vehicles that do not have belt driven air conditioning compressors anymore.

Therefore, it was decided to focus on POE lubricants in the study at hand.

The solubility in POE lubricants varies for the different refrigerants. Therefore, the viscosity of the lubricant should be adapted to the refrigerant it is applied with.

The viscosity of lubricants is characterized with two different numbers:

- **Viscosity grade (VG):**
  Essentially, the VG describes the kinematic viscosity at a temperature of 40°C in mm^2s^{-1} in a range of ±10%. The viscosity grade is defined in DIN3448.

- **Viscosity Index (VI):**
  The temperature influence on the viscosity of the pure lubricant is characterized in the VI. It relates the viscosity at 40°C and 100°C[3] and is calculated according to ISO 2909. The VI is higher for lubricants that have a low temperature influence on the viscosity. A high VI is desirable for lubricants to obtain a high viscosity in the hot compressor and a low viscosity in the refrigeration cycle to reduce pressure losses and oil retention [36].

To ensure proper lubrication, BOCK AND PUHL [35] recommend different viscosity grades for different refrigerants. For HFC refrigerants the viscosity grade should be in a range of 32 < VG < 55 while for hydrocarbons a higher VG in a range of 68 < VG < 100 is required. For supercritical refrigeration cycles with R744 (CO_2), a viscosity grade in the range of 80 < VG < 120 is recommended. This shows that a wide range of lubricant viscosity grades have to be covered to determine the critical mass flux for different refrigerants in combination with practically relevant lubricants.

Different additives are added to the lubricant to improve certain properties. For example, anti-wear additives improve the tribologic properties of the lubricant. They are used especially in lubricants for the refrigerant R744 (CO_2) because of the high pressures and temperatures [35]. They contain surface active elements as phosphorus or sulfur to protect the metal surface and are important in case of mixed film or boundary lubrication [36]. Rust inhibitors prevent oxidation of steel components. Antifoam agents or profoaments are used to adjust the foaming properties. Foam reduces compressor noise but excessive foaming may lead to failure of lubrication [8]. Especially for hermetic refrigeration applications, it is important that additives are as stable as the lubricant. Additionally, they have to be compatible to all system components and soluble in the refrigerant to avoid deposits e.g. in the expansion valve. [8] The additives used in commercial lubricants and their concentration are proprietary knowledge of the manufacturers.

[3] In previous versions of ISO 2909, the VI was calculated with the viscosity at 37.8°C (≙100°F) and 98.9°C (≙210°F) [39]. These temperatures are often found in literature.

1.5 Thermophysical Properties of Liquid Refrigerant-Lubricant Mixtures

To determine the critical mass flux for lubricant return J_{crit}, density and viscosity of liquid and vapor phase are required.

Density and viscosity of the vapor phase are easy to obtain, as the vapor phase consists of pure refrigerant.[4] The density and viscosity of the liquid phase lead to difficulties, because the liquid phase is a mixture of lubricant and dissolved refrigerant. Especially the liquid viscosity of the pure lubricant and pure refrigerant may differ by some orders of magnitude. Thus, the liquid viscosity strongly depends on the concentration of the dissolved refrigerant. In turn, the solubility depends on the applied refrigerant and lubricant as well as on the temperature and pressure in the respective point of operation.

The density and viscosity of refrigerant-lubricant mixtures is often published in form of Daniels plots. A Daniels plot for a mixture of R134a and a POE with a VG of 22 is depicted in Figure 1.2. These graphs consist of two elements. In the viscosity diagram (Figure 1.2a), the kinematic viscosity $\overline{\nu}$[5] is plotted over temperature T for different lubricant mass fractions $w_{\text{l,Ref}}$. In the solubility diagram (Figure 1.2b), the vapor pressure p_{v} of the saturated mixture is plotted over the temperature T for different refrigerant mass fractions $w_{\text{l,Ref}}$.

For a specific temperature and pressure in the respective component of the refrigeration cycle, the mass fraction $w_{\text{l,Ref}}$ of the refrigerant in the liquid can be retrieved from the solubility plot in Figure 1.2b. With the obtained refrigerant mass fraction $w_{\text{l,Ref}}$, the viscosity $\overline{\nu}$ can be read from the viscosity graph in Figure 1.2a.

Often, isobars are depicted in the viscosity diagram of Daniels plots for easier handling. Following an isobar from lower to higher temperatures in Figure 1.2a, a peculiarity in the mixture viscosity can be observed. Against the

[4] The vapor pressure of pure POE lubricants (see Section 2.2.4) is very low in comparison to the vapor pressure of pure refrigerant. Therefore, the vapor phase can be considered as pure refrigerant.

[5] In the present study, properties of mixtures are indicated with a line over the symbol: $\overline{\boxtimes}$. In case of the kinematic viscosity $\overline{\nu}$, the mixture consists of the lubricant with dissolved refrigerant.

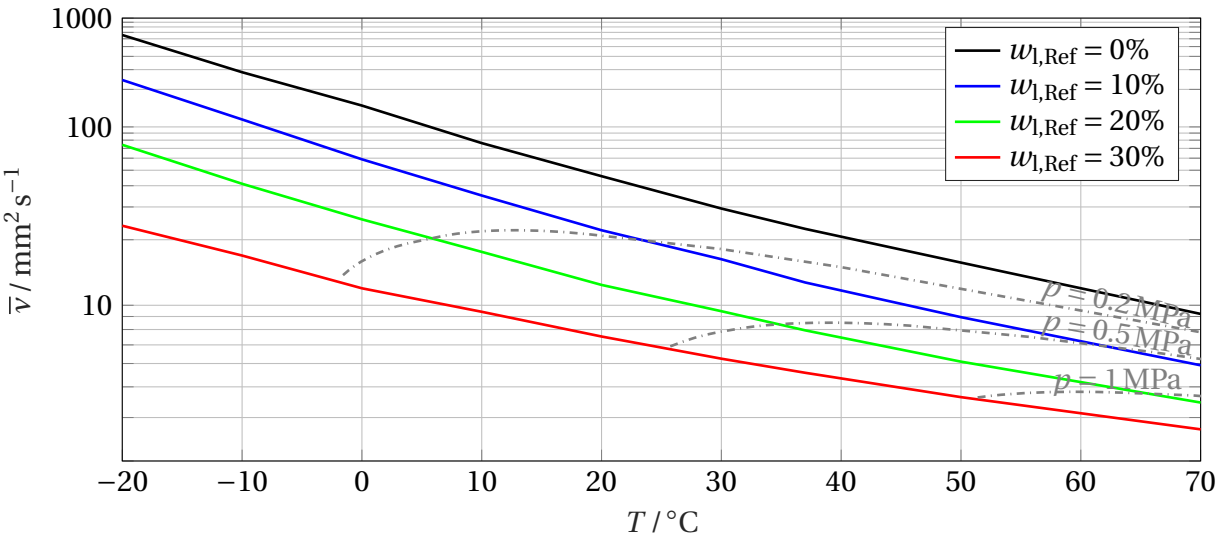

(a) Viscosity diagram.

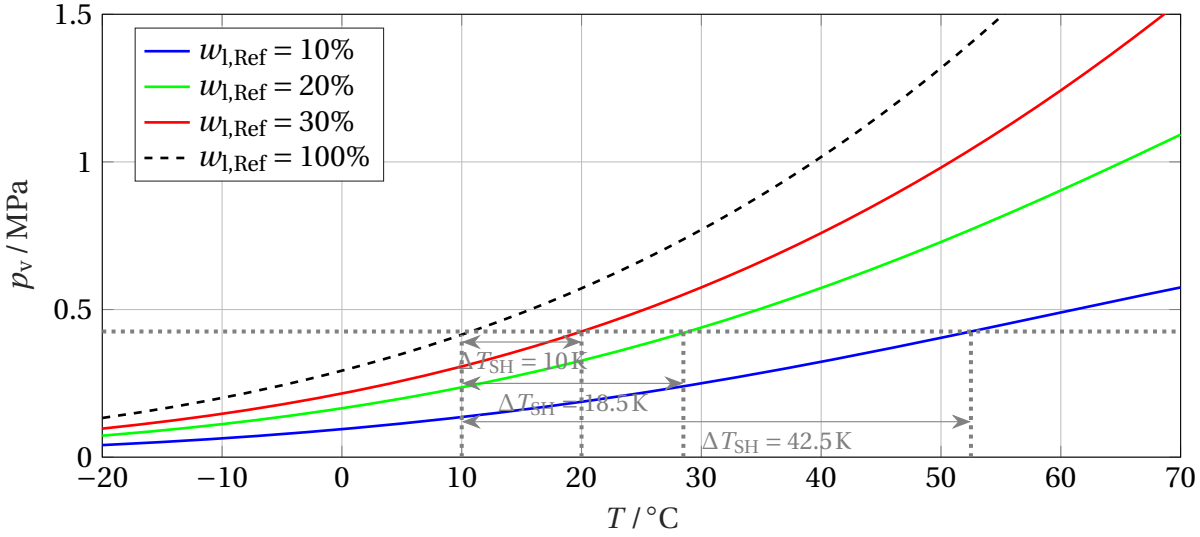

(b) Solubility diagram.

Figure 1.2: Daniels plot for R134a and a POE lubricant with a VG of 22. Data source: [35].

expected behavior, the mixture viscosity $\overline{\nu}$ increases with rising temperature T until it reaches a maximum. Subsequently, it falls continuously, as it would be expected for an increasing temperature. The reason is that the refrigerant concentration decreases with increasing superheat ΔT_{SH} of the refrigerant vapor, as depicted in Figure 1.2b for an evaporation temperature of $T_{evap} = 10°C$. At lower temperatures, the decreasing concentration of refrigerant has a higher

influence on the mixture viscosity compared to the rising temperature. At higher temperatures, the refrigerant concentration is already significantly reduced and the temperature influence on the mixture viscosity becomes dominant leading to a decreasing mixture viscosity at constant pressure.

Regarding POE lubricants, also the composition of the lubricant influences the solubility. BIANCARDI ET AL. [25] found that R407C was completely miscible with one POE with a VG of 32 while it was immiscible with a differently composed POE of the same VG of another manufacturer. CAVESTRI [40] investigated the solubility and viscosity of HFC refrigerants with POE lubricants and found differences in the solubility for POEs with the same VG that were synthesized with branched and mixed carboxylic acids, respectively. This means that Daniels plots cannot be readily transferred from one lubricant to another, even if the lubricants have the same VG.

Especially for HC refrigerants, Daniels plots are scarce in literature. The book of BOCK AND PUHL [35] only contains one diagram for R290 (propane) and a POE with a VG of 68 for temperatures $T > 50°C$, which cannot be applied to conditions in the suction line. Furthermore, one diagram for R1270 (propene) and a POE with a VG of 100 is published. Mixture data of POEs and HFOs are not available in BOCK AND PUHL [35]. In OWEN [8], no data is available at all on HC or HFO refrigerants and POE lubricants. Furthermore, the scientific literature on the mixture properties of HC and HFO refrigerants with POE lubricants is scarce, as it will be shown in Chapters 4 and 5 dealing with the solubility and viscosity of refrigerant-lubricant mixtures. In contrast, mixture properties of R744 (CO_2) with POE lubricants are well investigated in numerous scientific publications.

Both, the scarcity of mixture properties in the available literature and the difficulties in the transfer of mixture data from one lubricant to another lead to the requirement of a predictive approach to calculate the liquid mixture viscosity and density in order to determine the critical mass flux for lubricant return in upward vertical flow.

1.6 Scope and Structure of the Thesis

Scope and structure of the thesis orient on the main objective to calculate the critical mass flux for lubricant return for low-GWP refrigerants.

The critical mass flux depends on the inner diameter of the suction line and the fluid properties of the liquid and vapor phase of the two-phase flow. A significant part of the thesis covers the development of a tool chain to predict the density and viscosity of the liquid phase. These properties depend on the applied fluids, refrigerant and POE lubricant, as well as on the process parameters pressure and temperature.

The POE lubricant is considered as a mixture of different pure polyol esters. The influence of lubricant additives on density and viscosity of the liquid phase is neglected. Also the refrigerant is not necessarily a pure component. The refrigerants labeled with R4xx and R5xx are a mixture of different refrigerants. Subsequently, the liquid film in the two-phase flow is considered as a multi-component mixture of the refrigerant(s) and the pure polyol esters.

Figure 1.3 shows the flow of information in the thesis at hand. The fluid properties of pure refrigerants are well known and available from computer programs as *CoolProp* [41] or *REFPROP* [42], which model the properties with a thermal equation of state based on two known properties.

In contrast, there is no database for the fluid properties of the pure polyol esters similar to refrigerants. Therefore, the literature on the properties of polyol ester lubricants is reviewed in Chapter 2. The influence of the structure of the polyol esters on the fluid properties is described. Different pure polyol ester lubricants that are investigated profoundly are selected to form the basis for the polyol ester mixtures.

In Chapter 3, an algorithm is developed that aims to calculate a mixture composition of polyol esters, which matches target values for the lubricant properties. Target data are either desired properties of the mixture or known properties of existing POE lubricants. The algorithm is based on mixture laws for density, viscosity and molecular weight of the POE lubricant.

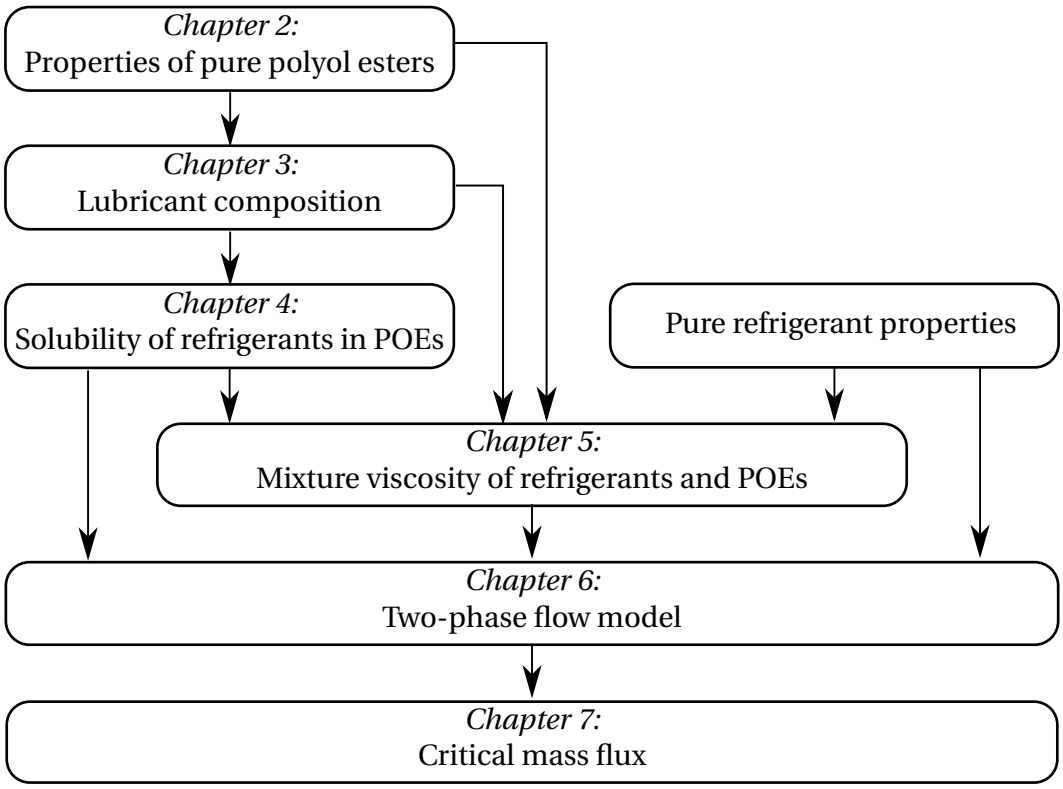

Figure 1.3: Structure of the thesis.

Chapter 4 contains the modeling of the refrigerant solubility in the lubricant based on the *Perturbated-Chain Polar Statistical Associating Fluid Theory* (PCP SAFT) of GROSS AND VRABEC [43]. The required pure component parameters of refrigerants and lubricants are summarized and the interaction of the components in the multi-component mixtures is modeled.

The resulting refrigerant concentration in the mixture and the composition of the lubricant are subsequently used in Chapter 5 to model the liquid mixture viscosity. Different mixture laws and viscosity models previously used in literature for refrigerant-lubricant mixtures are assessed regarding their capability to predict the mixture viscosity for the wide range of viscosity grades and refrigerants required in this study. The model that shows the lowest deviations between experimental results and predictions is selected for the prediction of the mixture viscosity.

In Chapter 6, the model to calculate the critical mass flux of two-phase flow is presented. Correlations required to calculate the shear stress at the interfacial boundary of the two-phase flow are compared with each other regarding their applicability to the two-phase flow of refrigerants and lubricants in the suction line based on available experimental data.

Deviations to the available literature data are calculated in each step of the modeling process.

Finally, the critical mass flux for low GWP lubricants is computed in Chapter 7. The influence of the different parameters on the critical mass flux is discussed for relevant examples. A minimum cooling capacity for lubricant return is derived from the critical mass flux and tabulated analogously to existing data for HFC refrigerants.

The findings obtained in the development of the algorithm to predict the fluid properties of refrigerant-lubricant mixtures and the results of the critical mass flux calculations are summarized in Chapter 8. Potential for improvements in the derivation of the fluid properties is discussed.

2 Polyol Ester Lubricants

Polyol ester lubricants were developed for the aviation industry as lubricant for turbine bearings during and after World-War II [44]. Beginning with the phase out of CFC and HCFC refrigerants due to their ozone depletion potential in the 1990s, the refrigeration industry searched for compatible lubricants for HFC refrigerants. POEs were found to be one of the most suitable options due to their good lubricating properties and good miscibility with HFC refrigerants. Furthermore, they have excellent thermal and chemical stability in the presence of a refrigerant and a good viscosity-temperature behavior. [36] They are compatible with commonly used sealing materials [45]. POEs show a high hygroscopicity. If the POE is contaminated with water, the molecules decompose at high temperatures. Therefore, it is crucial to protect POEs from water and moisture contact [45].

The aim of this chapter is to find different polyol esters that can be applied as components in the POE mixtures used in the subsequent parts of the study. First, the structure and synthesis of polyol esters are introduced in Section 2.1. Then, the influence of the molecular structure on the fluid properties is analyzed in Section 2.2. A literature review on the fluid properties of polyol esters is presented. Based on the results of the literature review and the requirements on lubricants in refrigeration applications, some polyol esters with sufficiently investigated properties are selected to form the basis for the POE mixtures in Section 2.3.

2.1 Composition and Synthesis of Polyol Ester Lubricants

The advantage of POEs is that the required fluid properties can be adjusted with modifications of the structure of both polyol and carboxylic acid. This allows to modify the viscosity grades in a broad range between 5 and 400 [8].

During the synthesis of POEs, a neopentyl polyol and carboxylic acids react to the POE. The advantage of neopentyl polyols in contrast to other alcohols used for ester synthesis is that they do not contain a hydrogen atom attached to the beta carbon atom[1] in the molecule. This eliminates a mechanism for high temperature rearrangement and thus increases thermal stability. [8, 45]

Different neopentyl polyols can be used for POE synthesis. Table 2.1 gives an overview on the frequently used neopentyl polyols.

Table 2.1: Neopentyl polyols for synthesis of POEs. Source: [8].

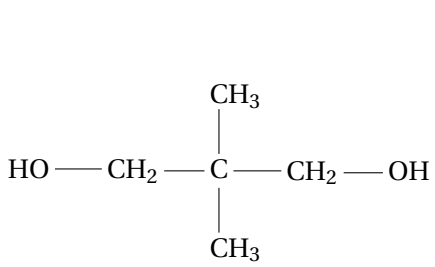

Neopentylglycol

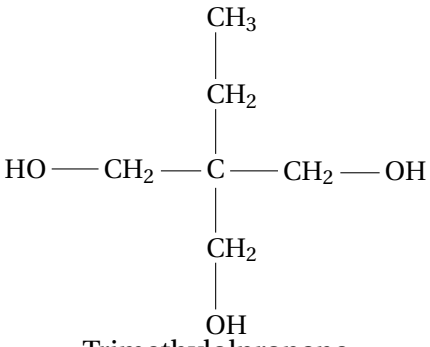

Trimethylolpropane

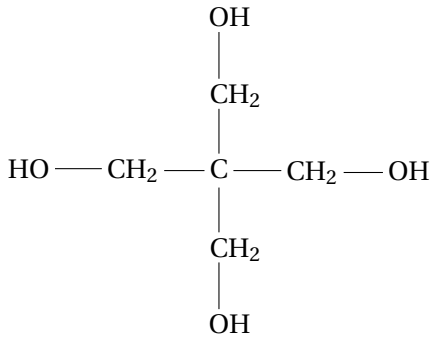

Pentaerythritol

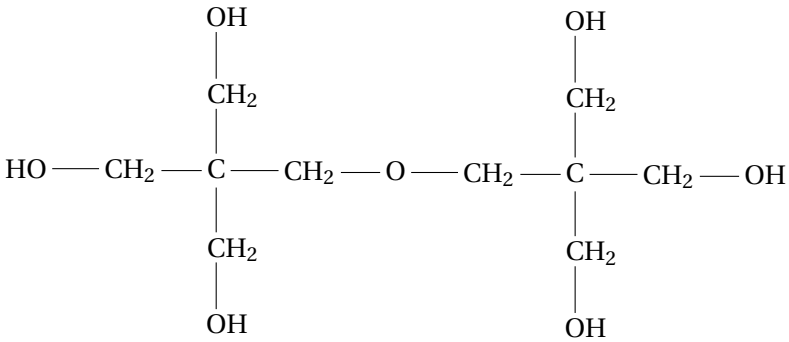

Di-Pentaerythritol

The functionality[2] of the neopentyl polyol strongly influences the fluid properties of the POE. A higher functionality leads to a higher viscosity and a higher density of the POE [46]. For low viscosity lubricants (VG < 10), usually neopentylglycol is used, whereas lubricants with VG > 150 are based on

[1] The beta carbon is the carbon beside the carbon attached with the OH group, i.e. the central carbon for the neopentyl polyols depicted in Table 2.1

[2] The number of OH-groups of the neopentyl polyol

di-pentaerythritol or complex esters. Complex esters are synthesized from polyfunctional acids and polyfunctional alcohols that form oligomeric polyesters [36]. For the intermediate viscosity range, either pure pentaerythritol or a mixture of pentaerythritol with either neopentylglycol or di-pentaerythritol is used [36]. Due to the wide viscosity range required to cover the relevant refrigeration applications, both pentaerythritol and di-pentaerythritol are considered in the following as alcohols for POE synthesis. Complex esters are not considered, because data on the fluid properties is not available.

The monofunctional carboxylic acids used for POE synthesis consist of the carboxylic COO group and a linear or branched alkyl group [36], as depicted in Figure 2.1.

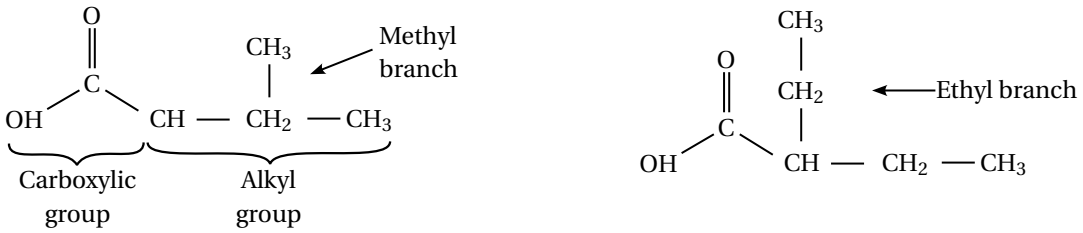

(a) Carboxylic acid with methyl branch at third carbon-atom

(b) Carboxylic acid with ethyl branch at second carbon-atom

Figure 2.1: Exemplary structure of carboxylic acids.

Some carboxylic acids used in POE synthesis are shown in Table 2.2 to illustrate differences in structure and their nomenclature. The structure of all carboxylic acids that appear in this thesis are listed in Appendix A.1. The labels shown in the last column of Table 2.2 are subsequently used for the carboxylic acids. The labeling is based on the following rule:

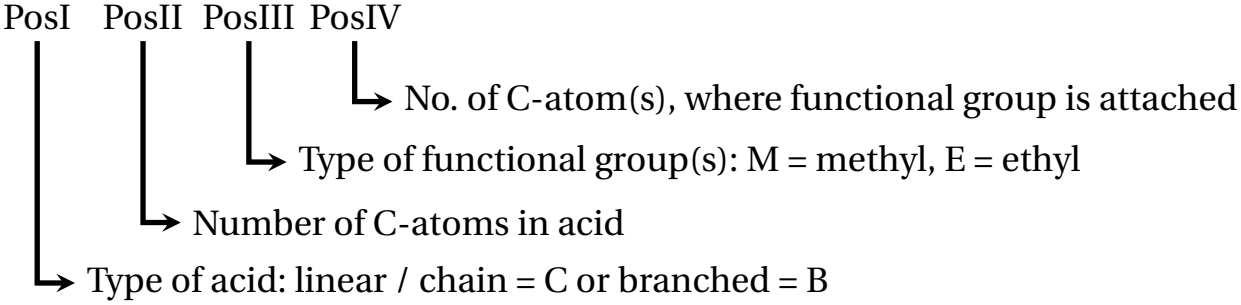

Table 2.2: Carboxylic acids for synthesis of POEs.

	Carbon Number in Acid, Structure	Name	Label
Linear	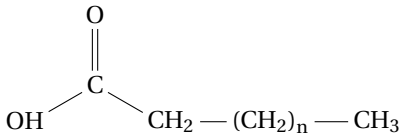	n=0: Propanoic acid n=1: Butyric acid n=2: Valeric / Pentanoic acid n=3: Hexanoic acid n=4: Heptanoic acid n=5: Octanoic acid n=6: Nonanoic acid	C3 C4 C5 C6 C7 C8 C9
Branched	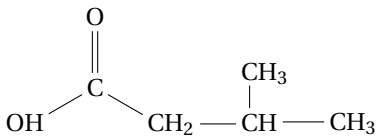	3-Methylbutyric acid	B5M3
	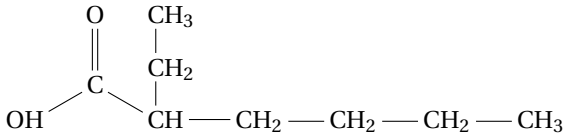	2-Ethylhexanoic acid	B8E2
	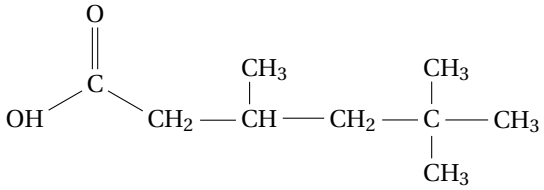	355-Trimethylhexanoic acid	B9M355

For example, B8E2 means a branched carboxylic acid with 8 carbon atoms and an ethyl functional group connected at the second carbon-atom (counting from the carboxylic group). Regarding the synthesized polyol ester, the abbreviation of the alcohol prefixes the label of the carboxylic acid, e.g a pentaerythritol ester of 2-ethylhexanoic acid is labeled as PEB8E2. A dipentaerythritol ester of the same acid is labeled as DiPEB8E2. This system is based on labeling often implemented in scientific publications[3], but additionally distinguishes between all possible isomers. It is believed that spelling out the complex scientific naming of the polyol esters in the text confuses the

[3]E.g. PENSADO ET AL. [47] simply use the label PEB8 for a pentaerythritol ester of 2-ethylhexanoic acid. FEDELE ET AL. [48] use the label PEBM5 for a pentaerythritol ester of 2-methylbutyric acid. In the present thesis, this is PEB5M2.

reader. Therefore, only the labeling introduced here is used in the following. For the scientific names of the respective carboxylic acid, the reader is referred to Table A.1 in the Appendix.

To synthesize POE lubricants, carboxylic acids and an alcohol are mixed with 5% to 10% excess of carboxylic acids compared to stoichiometry in presence of an inert agent (e.g. benzene or toluene). The mixture is heated to temperatures between 408 K and 505 K. The methylol-groups of the alcohol react with the OH-group of the carboxylic acid [49].

Figure 2.2 shows the reaction of pentaerythritol and pentanoic acid (C5). A generalized reaction scheme for the synthesis of linear PEs and DiPEs can be found in Appendix A.2.

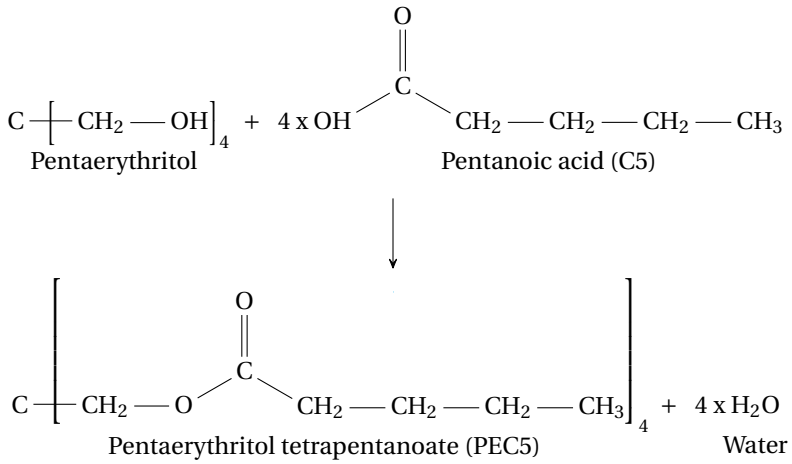

Figure 2.2: Reaction of pentaerythritol and pentanoic acid (C5) to pentaerythritol tetrapentanoate (PEC5).

For each connection between methylol-group and carboxylic acid a water molecule is split off. The water of reaction is removed with help of the inert agent. The reaction is completed, when it is not possible to extract any more water from the mixture. Excess carboxylic acids are removed by distillation [49].

The high thermal stability of POEs in comparison to other lubricants results from the strong dipole moments of the carboxylic group, as the COO group is thermally more stable than a C-C group. The high dipole moment negatively affects the hydrolytic stability, though [45].

If a POE lubricant is contaminated with water, hydrolysis occurs at high temperatures. Hydrolysis can be described by the reversion of the reaction mechanism described in Figure 2.2.

In industrial synthesis, several different carboxylic acids are reacting with one type of alcohol to a base-stock for POE lubricants in a single step. This results in molecules, where different carboxylic acids are connected to one alcohol molecule [50]. Nevertheless, density and viscosity of POEs are mainly determined for POEs of a single type of carboxylic acid in scientific literature. NIEDZIELSKI [50] reports that blending POEs of a single carboxylic acid leads to metastable mixtures that can undergo an equilibration process if they are exposed to high temperatures. The viscosity of the metastable blend of POEs with a single carboxylic acid is similar to a POE synthesized in a single step with an equal composition of carboxylic acids, though.

2.2 Influence of Molecule Structure on Fluid Properties

The bottleneck to describe the influence of the molecular structure on different fluid properties is the limited availability of scientific literature. There is a significant need for research to properly characterize the influence of the molecule structure on the fluid properties. An overview of the available literature is given in Table B.1 in the Appendix.

The influence of the molecule structure on the fluid properties is analyzed by comparing literature data on polyol esters that are synthesized with a single type of carboxylic acid, i.e. pentaerythritol tetraalkyl esters (PE) and dipentaerythritol hexaalkyl esters (DiPE). The data for pure PEs or DiPEs differs significantly in different publications. Nevertheless, the influence of the structure on the fluid properties can be described qualitatively.

The aim of this section is to establish a scientifically founded database for the properties of different PEs and DiPEs, which is subsequently used in the determination of the lubricant composition as well as in the calculation of the density and viscosity of POE lubricants or refrigerant-lubricant mixtures.

2.2.1 Density

Density data of PEs and DiPEs is scarce in scientific literature compared to viscosity data. Especially for branched PEs, the database is limited. It contains only density data of PEs with a functional group attached to the second carbon atom in the carboxylic acid. Regarding the density of di-pentaerythritol esters, publications are available only for two linear and one branched DiPE. The available data is evaluated and depicted in Figure 2.3.

For the values depicted in Figure 2.3a[4], the literature data is interpolated at a temperature of 40°C and atmospheric pressure. The data of PEs can be found for lower molecular weights $M < 760\,\mathrm{g\,mol^{-1}}$ and the data of DiPEs at higher molecular weights $M > 750\,\mathrm{g\,mol^{-1}}$. The density of both, PEs and DiPEs, decreases with rising molecular weight. The density of branched PEs is slightly lower compared to their respective linear isomers.

Comparing DiPEs and PEs with the same carboxylic acid (e.g. PEC5 and DiPEC5), the density of DiPEs is slightly higher compared to the respective PEs. This is in agreement with KISHORE AND SHOBHA [46]. They found increasing density for rising functionality of the polyol comparing trimethylolpropane and pentaerythritol esters.

The temperature influence on the density is depicted in Figure 2.3b. The density ρ of polyol esters depends linearly on temperature. The gradient of the density with respect to temperature $\partial\rho/\partial T$ is calculated regressing the density data to a polynomial of first order in a temperature range of $5°\mathrm{C} < T < 90°\mathrm{C}$. Figure 2.3b shows the gradient of the density $\partial\rho/\partial T$ over the molecular weight M for the different polyol esters. Additionally, Figure C.1 in the Appendix shows the development of the measured density over temperature at atmospheric pressure. The temperature influence on the density is important for the determination of the POE mixture composition in Chapter 3, because

[4] The marker form in the figure represents the structure of the carboxylic acid of the polyol ester. To distinguish PEs and DiPEs of the same carboxylic acid, the depicted structure of the carboxylic acid is marked with a '6' for DiPEs, as di-pentaerythritol has a functionality of six in contrast to pentaerythritol, which has a functionality of four (see Section 2.1).
The vertical dotted lines correlate the number of carbon-atoms in the carboxylic acid to the molecular weight for PEs. This should help the reader to distinguish the markers for similar length of the alkyl group.
The exact location of the data-point is marked with the black dot (or other markers in case of the pour point).

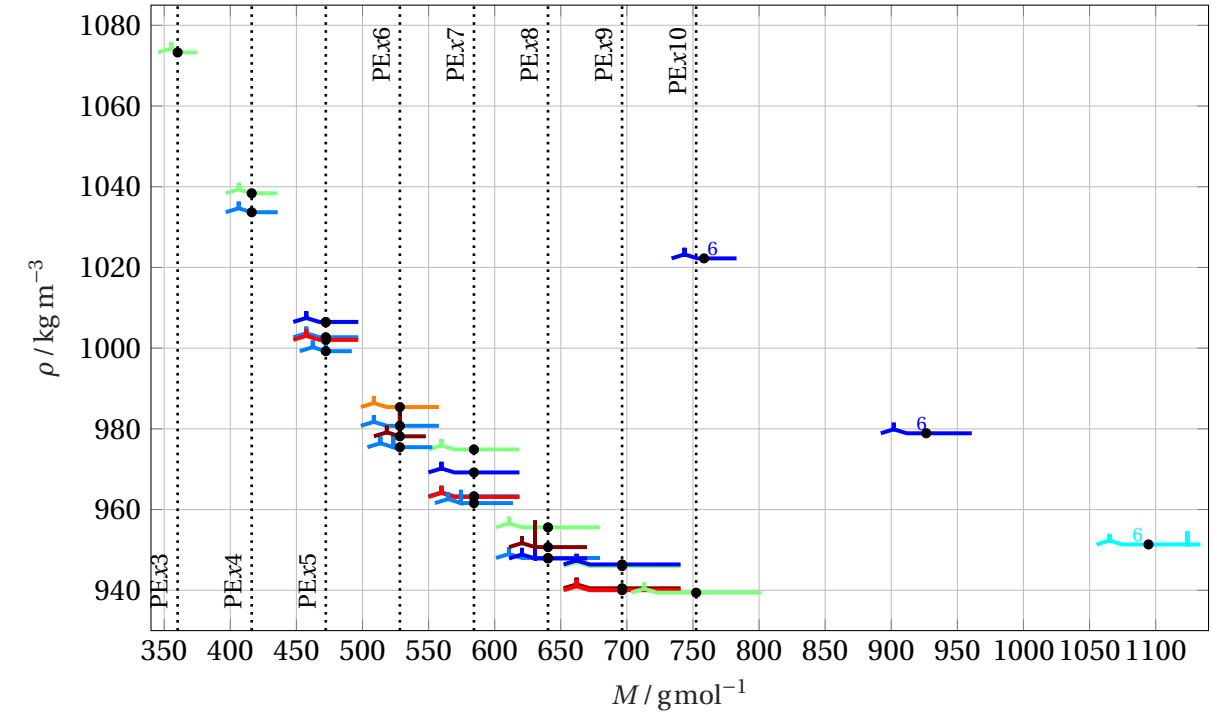

(a) Density ρ over molecular weight M at $T = 40°C$.

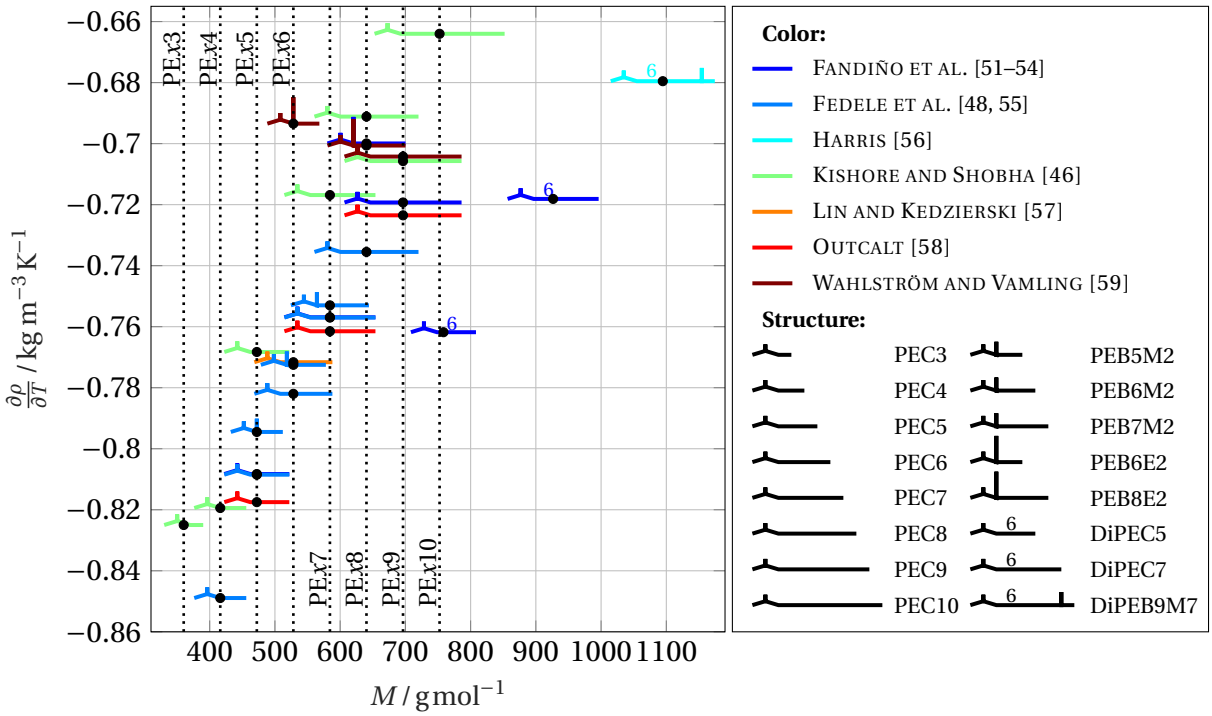

(b) Density gradient $\partial\rho/\partial T$ at atmospheric pressure over molecular weight M.

Figure 2.3: Density of PEs in literature.[4]

density and viscosity values at different temperature levels are used in the calculation. The gradient of the density $\partial\rho/\partial T$ of linear PEs shows an approximately linear trend and is rising with the molecular weight of the PEs. The gradient of the density differs significantly for different publications investigating the same PE.

Regarding the branched PEs, the density gradient of the PEs with a methyl active group is only slightly higher, while the values for PEs with an ethyl active group differ significantly from their linear isomers.

The density gradient of DiPEs is significantly higher compared to PEs of the same carboxylic acid.

For both density and gradient of the density, the data of the different publications show the same trend but differ significantly. The highest deviation in the density data is visible in Figure 2.3a for PEC7. The difference between the data of FEDELE ET AL. [55] and KISHORE AND SHOBHA [46] is $\Delta\rho = 11.6\,\mathrm{kg\,m^{-3}}$ or 1.2%. The difference between FEDELE ET AL. [55] and FANDIÑO ET AL. [52] is $\Delta\rho = 5.9\,\mathrm{kg\,m^{-3}}$. This greatly exceeds the estimated measurement uncertainties stated in the respective publications. It is likely that the deviations in the density data of the same polyol ester between different publications are the result of different impurities in the samples. Different sources for contamination are possible:

- Incompletely reacted molecules,
- reactants of the synthesis, or
- contamination in the reactants:
  - Pentaerythritol is usually contaminated with a small amount of di-pentaerythritol. This leads to di-pentaerythritol esters in the synthesis.[5]
  - The ester acid can be contaminated with other ester acids.[6]

[5] The pentaerythritol purity is indicated e.g. with 98% in the publication of WAHLSTRÖM AND VAMLING [59] and FANDIÑO ET AL. [52].

[6] The purity of the ester acids indicated by the manufacturer was 97% for ester acid C9 in FANDIÑO ET AL. [52] and 96% in WAHLSTRÖM AND VAMLING [59]. Other ester acid purities are 99% in both publications. In other publications, the ester acid purity is not indicated.

- Contamination with water from the reaction or air moisture is also possible.

These contamination of the sample alter the measured density and thus influence the comparability with other publications.

The data of the pure PEs and DiPEs summarized in the present section is subsequently used in the modeling process for the calculation of the lubricant composition (Chapter 3) and for the validation of the PC SAFT EoS (Section 4.4).

2.2.2 Viscosity

The viscosity of pentaerythritol tetraalkyl esters is reported in numerous scientific publications. Linear PEs are investigated more profoundly compared to branched PEs and DiPEs.

Figure 2.4 compares the kinematic viscosity of different PEs at 40°C and 100°C. Regarding the kinematic viscosity at 40°C depicted in Figure 2.4a, the viscosity of linear PEs with more than 3 carbon atoms in the acid rises continuously with molecular weight. KISHORE AND SHOBHA [46] explain the peculiarity of the higher viscosity of PEC3 compared to PEC4 at 40°C with an insufficient increase in the free volume for free rotation of the molecules at temperatures near the melting point. Considering linear PEs, the measurement range is largest for PEC5. The values differ by ±8% from the mean value. This is much more than the estimated measurement uncertainties summarized in Table B.3. The reasons for the deviations are presumably differences in the measurement systems and impurities of PEs and DiPEs as described in Section 2.2.1. Details on the viscosity measurement are often not given in older publications.

For linear DiPEs, the viscosity of DiPEC4 and DIPEC5 is higher than of DiPEC6 for both 40°C and 100°C. Therefore, it seems that the explanation of the vicinity to the melting point for the higher viscosity of PEC3 in comparison to PEC4 [46] does not apply for linear DiPEs.

The viscosity of branched PEs is higher compared to their linear isomers. This is related to the reduced flexibility of the molecule [36]. An exception is PEB4M2 at 40°C. BOHNER ET AL. [60] state that PEB4M2 was supercooled at 40°C. A behavior similar to PEC3 would be expected, which is not the case.

Regarding the branching of the carboxylic acid, the following conclusions can be drawn qualitatively:

- Ethyl functional groups lead to a higher increase in viscosity than methyl functional groups (see PEB5M2 vs. PEB6E2, PEB7M2 vs. PEB8E2).
- Di-methyl functional groups show the highest viscosity in the dataset (PEB7M22, PEB8M22, PEB8M44, PEB8M55).
- Symmetry in branching leads to a higher viscosity in comparison to functional groups that are attached at the beginning or end of the carboxylic chain (compare PEB8M22, PEB8M44, PEB8M55).

Beside these general conclusions, some peculiarities exist: The viscosity of PEB5M2 is higher compared to PEB6M2 and PEB7M2 [61]. The lowest temperature in the measurement of PEB5M2 was $T = 0.5$°C [61]. Thus, it is not likely that there is a vicinity to the melting point at $T = -40$°C reported by CHAO ET AL. [62] and a subsequent influence on the viscosity as for PEC3 in the data of KISHORE AND SHOBHA [46]. Also PEB6E2 and PEB8E2 exhibit a similar viscosity although PEB8E2 has a longer alkyl chain. An hypothesis to explain this phenomenon is that the influence of symmetry of the carboxylic acid dominates the influence of the alkyl chain length.

Regarding the temperature influence on viscosity, the kinematic viscosity at 100°C is depicted in Figure 2.4b. The differences in the viscosity of branched and linear PEs are much smaller at high temperatures. The branched PEs have a larger viscosity decrease for rising temperatures compared to linear PEs. Generally, the temperature influence on the viscosity increases, if the distance between the carboxylic COO group and the branch of the carboxylic acid increases. BOYDE [36] relates this to the flexibility of the molecule. A long, linear alkyl group in the carboxylic acid leads to the highest flexibility. Branching reduces the flexibility.

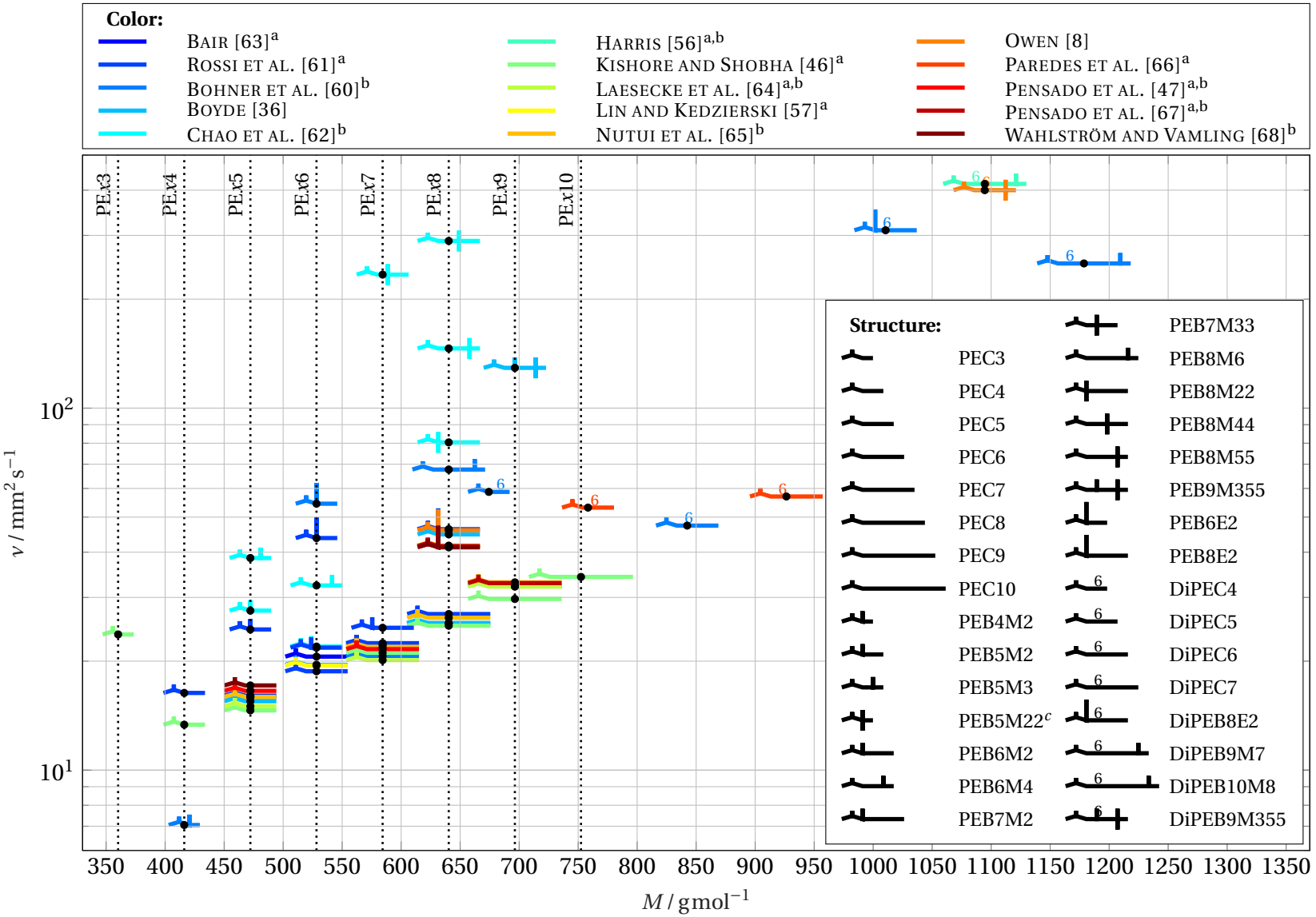

Figure 2.4: (a) Kinematic viscosity of PEs for $T = 40°C$.[4]

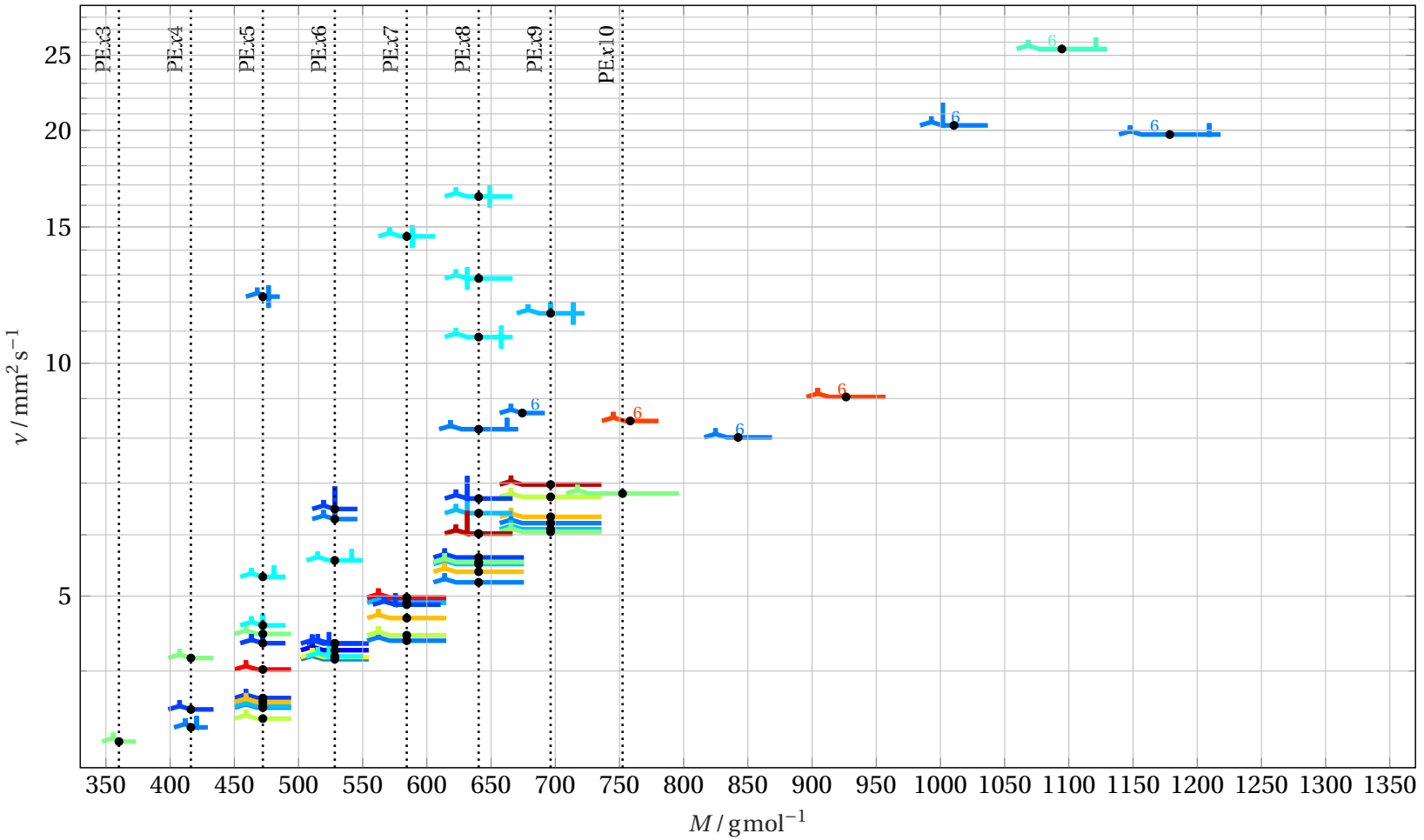

a: In these publications, the dynamic viscosity μ is given. The density data of the following publications is used to calculate the kinematic viscosity ν: PEC4, PEC6, PEC8: [55]; PEC5: [53]; PEC7, PEC9: [52]; PEC10: [46]; PEB5M2, PEB6M2, PEB7M2: [48], DiPEC5, DiPEC7: [54], DiPEB9M7: [56].
b: In these publications, the viscosity is not given for 40°C and 100°C. The values were inter- or extrapolated using the *Ubbelohde-Walther* Equation (3.23).
c: PEB5M22 is solid at 100°F(≙37.8°C) [60]. The only known value for the viscosity is at 210°F (≙98.9°C). As it is not possible to fit the Ubbelohde-Walther equation (c.f. footnote b) with a single value, the viscosity at 210°F (≙98.9°C) is depicted.

Figure 2.4: (b) Kinematic viscosity of PEs for $T = 100°C$.[4]

The shown PEs and DiPEs cover a very wide range of viscosity grades $7 < VG < 420$. However, branched PEs and DiPEs that have a high VG also show a stronger decrease in viscosity for rising temperatures (i.e. a lower viscosity index) compared to linear PEs.

Models that relate the kinematic viscosity to molecular weight for linear PEs were developed by NIEDZIELSKI [50] and EYCHENNE AND MOULOUNGUI [69]. These PEs show a clear trend for all publications found in literature, allthough the deviations between the different publications are high, as depicted in Figure 2.4. Regarding branched PEs, it seems very difficult to model the influence of the molecular structure on the viscosity e.g. by group contribution methods with an acceptable accuracy. One reason is the scarce data on branched PEs, where the branch is connected to the alkyl group at other than the second carbon atom in the carboxylic acid (e.g. PEB6M3, PEB6M4). Such data would be required to investigate the influence of symmetry in branching on the viscosity. Another reason is the strong difference in viscosity between the different types of branches. While methyl-groups only slightly influence the viscosity, di-methyl groups show a huge influence on the viscosity. Further research is required to extend the database of branched PEs, especially regarding the position of the branches in the carboxylic acid.

The viscosity data of the single PEs and DiPEs is used in the modeling process for the calculation of the lubricant composition in Chapter 3 and for the calculation of the mixture viscosity of refrigerants and lubricants in Chapter 5.

2.2.3 Low Temperature Behavior

At low temperatures, PEs crystallize and form wax-like structures [36]. This has to be avoided in refrigeration cycles as the evaporator can be clogged leading to a low pressure failure. For the characterization of the low temperature behavior, the pour point (PP) is defined in the norm ISO 3016, as the lowest temperature at which a sample of the lubricant pours or flows when it is cooled with a standardized procedure [8, 70]. The reason for the loss in fluidity is either the steady increase in viscosity for a decreasing temperature or crystallization [8]. Unfortunately, not all publications that describe the low temperature beha-

vior of PEs and DiPEs use the same standardized procedure. Some authors indicate the freezing point (FP) or melting point (MP) instead.

Figure 2.6 depicts the data for PP, MP or FP in the different publications. The different quantities (PP, FP, MP) make it difficult to compare the results. Especially, for PEB6E2 the difference between the MP of WAHLSTRÖM AND VAMLING [59] ($T_{MP} = 37°C$) and PP of BOHNER ET AL. [60] ($T_{PP} = -34.4°C$) is striking. WAHLSTRÖM AND VAMLING [59] report crystallization at room temperature for PEB6E2. BOYDE [36] states that esters tend to supercooling[7]. So, possibly BOHNER ET AL. [60] measured the PP with a severely supercooled PEB6E2 sample.[8]

Nevertheless, some general aspects can be concluded:

- PP values of linear PEs show a minimum for PEC5.[9] The rising PP for PEs with larger alkyl groups is due to their tendency to form wax-like structures as they pack efficiently [36].
- BOYDE [36] states that branching prevents solidification for long alkyl groups. This is not confirmed by the available data of PEs. Only PEB5M2, PEB8M44, PEB8M55 show a lower PP compared to their linear isomers.
- Branching with a methyl functional group appears to have a small influence on the PP (PEB5M2, PEB5M3, PEB6M2).
- A high degree of symmetry in branching with di-methyl and di-ethyl functional groups appears to reduce the PP significantly as it is visible for PEB8M55. If the branching is unsymmetrical, it appears to increase the melting point (PEB6M22, PEB7M22, PEB7M33, PEB8M22).

[7] A matter may remain in a metastable liquid state even below the transition temperature from liquid to solid state. The fluid is called supercooled liquid in this case. [71]

[8] Severe supercooling was also observed by CHAO ET AL. [62] for PEB7M33. They report that PEB7M33 remained liquid for more than two years in supercooled state until it was seeded with small amounts of PEB7M22 and solidified within some hours in a refrigerator. CHAO ET AL. [62] suggest to use additives to inhibit crystallization. However, pour point depressing additives are not compatible with HFC or HFO refrigerants [8].

[9] Although no quantitative data for PEC3 and PEC4 is available, KISHORE AND SHOBHA [46] related the abnormally high measured viscosity for PEC2 and PEC3 at low temperatures to the vicinity to the melting point. The lowest temperatures in the viscosity dataset are for 90°C for PEC2 and 40°C for PEC3. A lower PP for PEC4 compared to PEC5 cannot be ruled out, but appears unlikely.

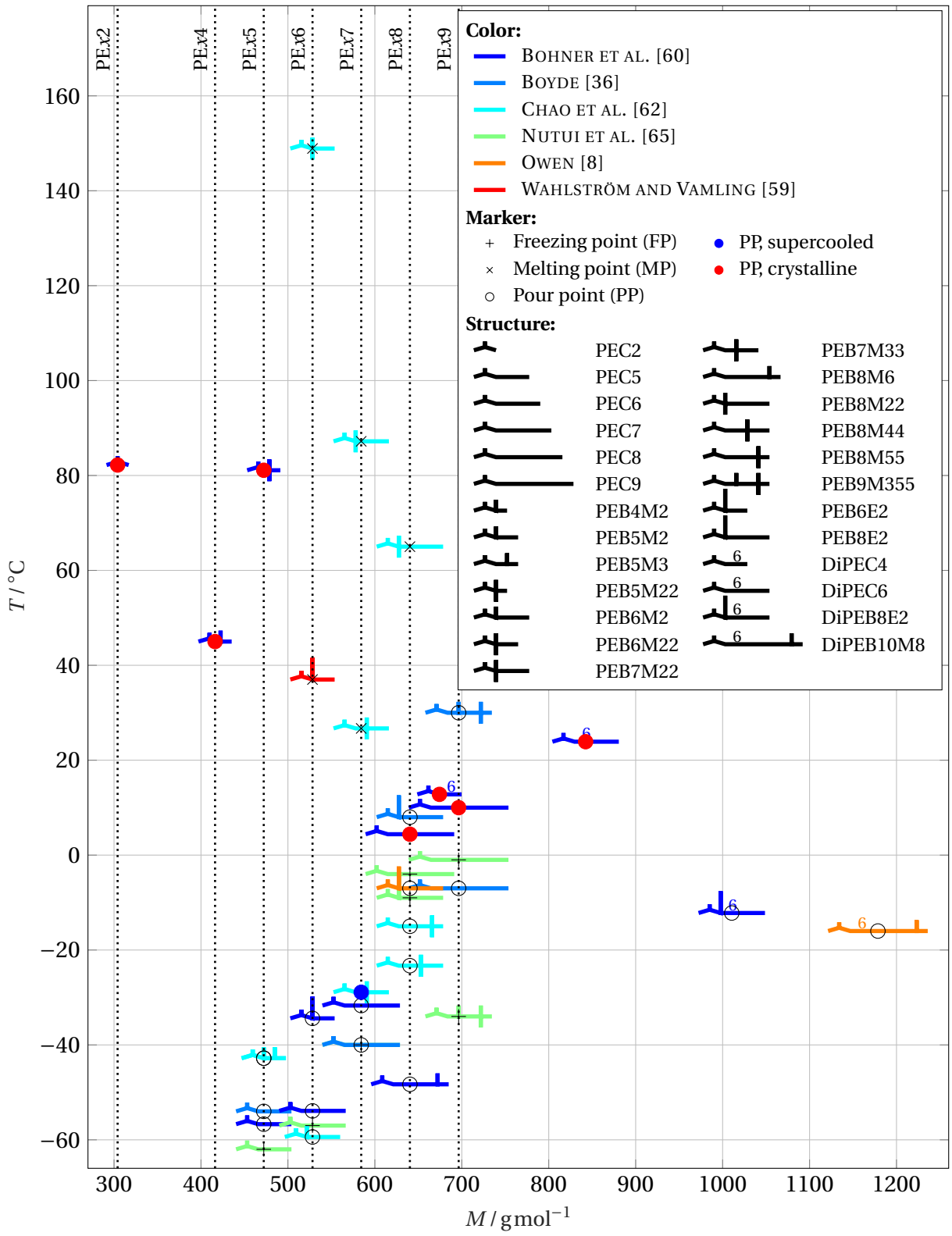

Figure 2.6: Pour point, melting point or freezing point temperature of PEs and DiPEs.[4]

Structural diversity in a mixture of different PEs improves the low temperature properties [50, 62], but only resolves the issue to some extent [36]. To verify the low temperature properties of a lubricant mixture in combination with a certain refrigerant, floc tests are required as the refrigerant can also act as precipitant to compounds of the lubricant [35].

The data presented in this section is subsequently used in the selection of suitable PEs and DiPEs for refrigeration applications.

2.2.4 Volatility

The volatility of POEs generally decreases with increasing molecular weight and increases by reducing the flexibility of the molecules with branched carboxylic acids [36]. This is confirmed by vapor pressure measurements of PEC5, PEC7, PEC9 and PEB8E2 conducted by RAZZOUK ET AL. [16]. Additionally, GARCÍA ET AL. [72] measured the vapor pressure of DiPEC5, DiPEC7 and DiPEB9M7.

The measured vapor pressure of both publications is depicted in Figure 2.7. The vapor pressure of DiPEs is lower compared to the PEs with the same carboxylic acid. While the vapor pressure of the linear PEs decreases with rising molecular weight, the vapor pressure of PEB8E2 is higher than of PEC7 despite the higher molecular weight. The same effect is visible comparing DiPEB9M7 and DiPEC7. BOYDE [36] relates this to the reduced flexibility in branched PE and DiPE molecules that prevents a close packing and therefore reduces attractive intermolecular forces.

In older publications, the volatility of the polyol esters was characterized measuring the flash point of the lubricant. CHAO ET AL. [62] found that the flash point of esters increases as the position of branching moves away from the carboxylic group.

RAZZOUK ET AL. [16] and GARCÍA ET AL. [72] used their measured vapor pressure data to correlate the pure component parameters for the PC SAFT EoS of the respective PEs and DiPEs. The values of the PC SAFT parameters found in both publications are used in Section 4.4 to model the solubility.

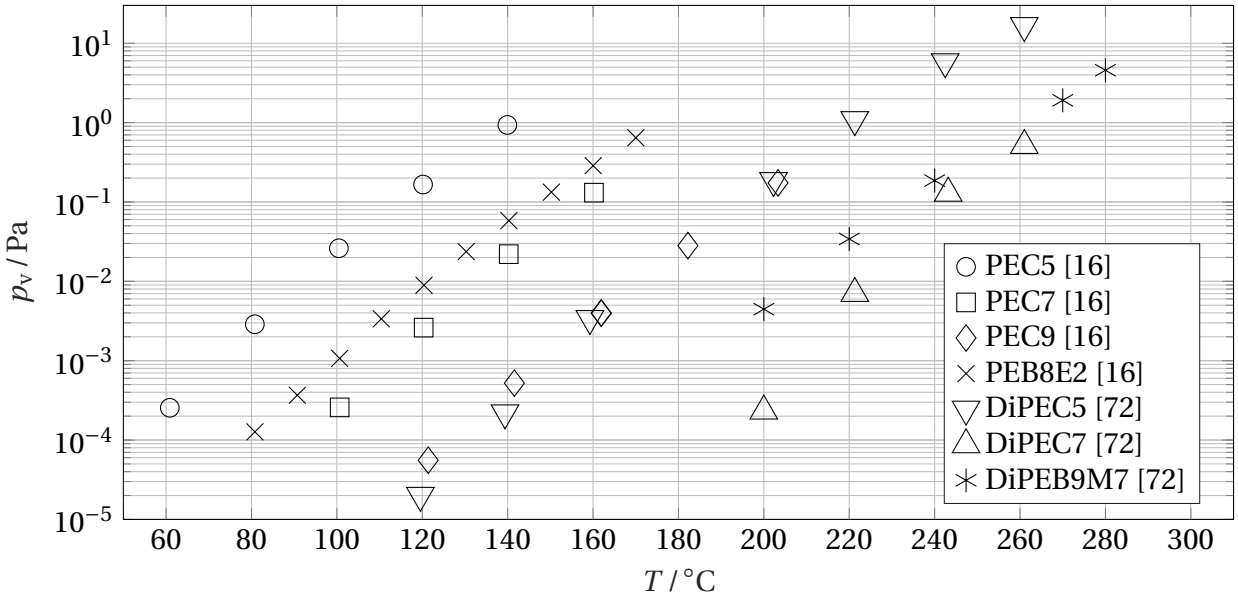

Figure 2.7: Vapor pressure of PEs and DiPEs.

2.2.5 Conclusions from the Analysis of Fluid Properties of PEs and DiPEs

For the same polyol ester, the fluid properties determined in different publications showed large deviations. Literature data especially for branched pentaerythritol esters and di-pentaerythritol esters is scarce. Both issues make it difficult to design a model that predicts the fluid properties based on the structure of the polyol ester. Additionally, the viscosity and the low temperature behavior of branched PEs vary strongly for small differences in the structure of the carboxylic acids. These variations do not always show a clear trend and are sometimes contradicting. Further research on the fluid properties of branched PEs is required to reliably predict the influence of branching on the fluid properties.

Based on these findings, it was decided to consider the POE lubricant as a multi-component mixture of different polyol esters. A mixture of different pentaerythritol tetraalkyl esters and di-pentaerythritol hexaalkyl esters is different to a real lubricant. In the synthesis of (commercial) POEs, different polyols react with different carboxylic acids in a single reactor. This leads to molecules with different carboxylic acids. Nevertheless, the findings of NIEDZIEL-

SKI [50] suggest that the properties of a mixture of different pentaerythritol tetraalkyl esters and di-pentaerythritol hexaalkyl esters are similar to polyol esters reacted in a single step with a similar composition of carboxylic acids. Thus, it is expected that the approach of considering a POE lubricant as a multi-component mixture of different PEs and DiPEs leads to similar results compared to POEs with molecules of different carboxylic acids.

2.3 Selection of PEs and DiPEs for Lubricant Mixtures

POE lubricants must meet the requirements for refrigeration applications introduced in Section 1.4.1. A low pour point is desirable for refrigeration lubricants. Additionally, the viscosity index should be high so that lubricants have a good fluidity at low temperatures and a sufficient lubricity at high temperatures in the compressor [8]. A trade-off has to be made between both requirements. Linear PEs with lower molecular weight (e.g. PEC5) have a low pour point but also a low viscosity index. In contrast, linear PEs with high molecular weight (e.g. PEC9) have a high viscosity index but also elevated pour points (c.f. Sections 2.2.2 and 2.2.3). Structural diversity in the PE mixture improves the pour point to some extent [36]. Branched PEs exhibit a higher viscosity compared to linear PEs but a low viscosity index. These are the reasons, why POE lubricants generally do not consist of a single component.

Beside the requirements mentioned above, a broad viscosity range is required as lubricants with various viscosity grades are recommended for the considered refrigerants (see Section 1.4.2). Therefore, various PEs and DiPEs are required as base lubricants for POE mixtures. The following criteria for the selection of PEs and DiPEs are applied:

- Density and viscosity data of the PE or DiPE are available for the temperature operation range of the suction line (i.e. low temperatures) and optimally also for elevated pressures in the operation range of refrigeration cycles ($1\,\text{bar} < p < 100\,\text{bar}$).

- Data of density and viscosity should have their origin in the same research group to make sure that data were generated with identical samples.
- PEs and DiPEs should cover a broad viscosity range to allow mixtures to have a wide range of viscosity grades. This means that results are applicable to different refrigerants.

Applying the criteria mentioned above, the polyol esters summarized in Table 2.3 are selected to form a pool of base lubricants for POE mixtures.

Table 2.3: PEs and DiPEs used as basis for POE mixtures.

PE / DiPE	M $\frac{g}{mol}$	Source of ν	$\nu\|_{40°C}$ $\frac{mm^2}{s}$	$\nu\|_{100°C}$ $\frac{mm^2}{s}$	VI -	Source of ρ	$\rho\|_{15°C}$ $\frac{kg}{m^3}$
PEC5	472	[64]	15.0	3.5	112	[58]	1023
PEC7	584	[64]	19.6	4.4	139	[58]	982
PEC9	696	[64]	29.9	6.6	186	[58]	958
PEB5M2	472	[61]	24.6	4.5	90	[48]	1019
PEB8E2	640	[67]	42.4	6.0	79	[51]	965
PEB9M355	696	[36]	129.2	11.6	70	calc.[a]	959
DiPEC5	759	[66]	52.9	8.4	133	[54]	1041
DiPEC7	927	[66]	56.2	9.0	139	[54]	997
DiPEB9M7	1096	[56]	414.1	26.1	84	[56]	968

a: Calculated with PC SAFT EoS (see Section 4.4).

Most viscosity data does not cover the temperature operation range of the suction line. This is problematic because of the high influence of the temperature on the viscosity. The lowest temperatures of the conducted experiments were found in the publication of LIN AND KEDZIERSKI [57]. LAESECKE ET AL. [64] and [61] conducted measurements near $T = 0°C$. All other authors conducted measurements at significantly higher temperatures. The data of LAESECKE ET AL. [64] is preferred over the data of LIN AND KEDZIERSKI [57], because it covers all relevant linear PEs. For PEB8E2, DiPEC5 and DiPEC7 only data at a temperature of $T \geq 30°C$ are available in PENSADO ET AL. [67] and PAREDES ET AL. [66], respectively. For PEB5M2 and DiPEB9M7 viscosity data are only available at atmospheric pressure in ROSSI ET AL. [61] and HARRIS [56], re-

spectively. Unfortunately, for PEB9M355 only viscosity data at 40°C and 100°C is available in BOYDE [36]. There is no density data on PEB9M355 in literature known to the author. PEB9M355 is required because of its exceptionally high viscosity grade. Furthermore, it is a component in commercial lubricants, as it was identified in nuclear magnetic resonance spectroscopy (NMR) measurements of a commercial lubricant by MORAIS ET AL. [73]. To overcome the lack of data, the density of PEB9M355 was calculated with the PC SAFT EoS (see Section 4.4). The quality of the data of the lubricants PEB6M2, PEB7M2, and PEB6E2 is comparable to PEB5M2 or DiPEB9M7. Nevertheless, these polyol esters are not considered as suitable lubricants for POE mixtures. This is due to the following reasons: The PP of PEB6E2 is very high (see Figure 2.6). Therefore, the application in refrigeration seems to be disadvantageous. The viscosity of PEB6M2 and PEB7M2 is only slightly higher compared to their respective linear isomers (see Figure 2.4). Considering these lubricants would not increase the capability of the database.

The density and viscosity of the different selected pure PEs and DiPEs described in Section 2.2 are subsequently used in the modeling process of the mixture properties.

3 Composition of POE Lubricants

In this chapter, an algorithm is developed that determines the composition of a POE mixture in a way that the fluid properties of the mixture match given target data. The mixture consists of the different PEs and DiPEs selected in Section 2.3.

This algorithm can be applied for different purposes:

- Engineering: In the design process of the lubricant, a composition is determined that shows desired properties.
- Reverse engineering: A composition of PEs and DiPEs is determined that matches the fluid properties of a lubricant of unknown composition.

In the subsequent parts of the thesis, the algorithm is applied for reverse engineering. Especially for the mixture viscosity of refrigerants and lubricants, the amount of available data on binary mixtures of refrigerants with a PE or DiPE are not sufficient to parametrize and validate the mixture models. Therefore, mixture data of refrigerants and commercial POE lubricants have to be considered.

The composition of POE lubricants is usually proprietary knowledge of the manufacturer. Nevertheless, it is important to have a detailed knowledge about the lubricant composition to predict the fluid properties of refrigerant-lubricant mixtures. Mixture properties as e.g. the molecular weight can be calculated only with a known composition and are required in many fluid property models. There are correlations that estimate the molecular weight of a lubricant, e.g. RAZZOUK ET AL. [16] estimated the molecular weight based on its viscosity at 40°C. They use the correlation of EYCHENNE AND MOULOUNGUI [69] that relates the viscosity of linear PEs at 40°C to the molecular weight. However, if the lubricant contains branched PEs with a much higher viscosity

compared to linear PEs (see Figure 2.4), the molecular weight is significantly overestimated with this approach. This limits the applicability of this lumped parameter approach to lubricants with low viscosity grades VG < 32, because these lubricants may consist of linear PEs only. As lubricants with much higher viscosity grades of 55 ≤ VG ≤ 100 are required for applications with natural refrigerants (see Section 1.4.2), the reverse engineering approach is promising to overcome this limitation. Additionally, it offers the possibility to study the influence of the lubricant composition on the mixture properties. The knowledge of the lubricant composition builds the basis for the multi-component approach chosen in the present thesis to model solubility and viscosity of refrigerant-lubricant mixtures.

In Section 3.1 viscosity models used in literature for polyol esters are discussed. The modeling of density and viscosity of polyol esters is presented in Section 3.2. Furthermore, suitable mixture laws for mixtures of polyol esters are selected. These mixture laws are implemented in an algorithm that calculates the mixture composition based on target properties of the lubricant mixture. The development of the algorithm is described in Section 3.3. Subsequently, the algorithm is assessed in Section 3.4 based on POE mixtures of known composition from literature. In Section 3.5, the composition of lubricant mixtures with different viscosity grades is calculated that show similar fluid properties as reference POE lubricants. These lubricant mixtures are used in the subsequent chapters in the solubility (Chapter 4) and viscosity (Chapter 5) modeling of the liquid refrigerant-lubricant mixtures.

3.1 Literature Review on Viscosity Models for Polyol Esters

In the following, different approaches to model the viscosity of pure and mixed polyol esters are presented. They are subsequently used to model the mixture viscosity of polyol esters or multi-component refrigerant-lubricant mixtures. The applicability and accuracy of the different models is assessed in the subsequent chapters.

It was observed that the dynamic viscosity μ of liquids below the normal boiling point can be expressed with an exponential approach according to Equation (3.1) [74, p.119].

$$\mu = a_1 \exp\left(\frac{a_2}{T}\right) \tag{3.1}$$

This type of equation is often named *Arrhenius*-type [75]. This empiric correlation is the basis for many other viscosity models.

3.1.1 Eyring Theory of Viscous Flow

EYRING ET AL. [76, 77] considered the viscous flow of liquids as similar to a chemical reaction. A molecule is moved from one equilibrium position to another across a potential barrier in a lattice of neighboring molecules. Based on the *absolute rate theory*, Equation (3.2) was derived [77, p.484].

$$\mu = \frac{N_\mathrm{A} h}{V_\mathrm{m}} \exp \frac{G_\mathrm{m}^{\neq}}{RT} \tag{3.2}$$

In this equation N_A is the Avogadro constant, V_m is the molar Volume, h is the Plank constant, $G_\mathrm{m}^{\neq}$ is the molar free energy of activation of viscous flow, R is the gas constant and T is the temperature [77]. There are different approaches to model the free energy of activation of viscous flow $G_\mathrm{m}^{\neq}$. For example, EWELL AND EYRING [76] state that molecules need a hole in the fluid where they can flow into. Therefore, they used the energy of evaporation $\Delta E_\mathrm{m,evap}$ required to form a hole inside the liquid to model $G_\mathrm{m}^{\neq}$.

Mixture Law Based on Eyring Equation

An equation for the mixture viscosity of different fluids can be derived based on the *Eyring equation* (3.2) and considering viscous flow as an isothermal process without changes in the composition. Equation (3.3) describes the resulting equation for mixtures of different components [77–79].

$$\ln(\overline{\mu}\overline{V}_\mathrm{m}) = \sum_i x_i \ln(\mu_{0,i} V_{\mathrm{m},0,i}) + \frac{\overline{G}_\mathrm{m}^{\neq,\mathrm{E}}}{RT} \tag{3.3}$$

In this equation, x_i is the mole fraction, $\mu_{0,i}$ the viscosity, and $V_{\mathrm{m},0,i}$ the molar volume of pure component i. $\overline{G}_\mathrm{m}^{\neq,E}$ is the excess free energy of activation of

viscous flow, according to Equation (3.4).

$$\overline{G}_{\mathrm{m}}^{\neq} = \sum_i G_{0,i}^{\neq} + \overline{G}_{\mathrm{m}}^{\neq,\mathrm{E}} \tag{3.4}$$

For ideal mixtures $\overline{G}_{\mathrm{m}}^{\neq,E}$ vanishes leading to Equation (3.5).

$$\ln(\overline{\mu}^{\mathrm{id}}\overline{V}_{\mathrm{m}}) = \sum_i x_i \ln(\mu_{0,i} V_{\mathrm{m},0,i}) \tag{3.5}$$

There are different approaches to model the excess free energy of activation of viscous flow $\overline{G}_{\mathrm{m}}^{\neq,E}$. Some approaches based on the *Eyring equation* are assessed for mixture viscosity of polyol esters in Section 3.2.4 and refrigerant-lubricant mixtures in Chapter 5.

If the molar volume $V_{\mathrm{m},0,i}$ of the different components i in an ideal mixture is similar, Equation (3.5) can be reduced to the earlier published *Arrhenius equation*. According to GRUNBERG AND NISSAN [80], ARRHENIUS[1] proposed Equation (3.6) for the viscosity of mixtures.

$$\log(\overline{\mu}^{\mathrm{id}}) = \sum_i x_i \log(\mu_{0,i}) \tag{3.6}$$

GRUNBERG AND NISSAN [80] found that this equation is suited to describe the mixture viscosity of ideal mixtures.

3.1.2 Free Volume Theory

COHEN AND TURNBULL [82] developed the idea that statistical distribution of molecules occasionally opens voids between the molecules that allow diffusive displacements of molecules. They assume that the fluid consists of hard spheres. The average free volume can be calculated as the difference between the volume of the cage of surrounding molecules and the volume of the sphere

[1] GRUNBERG AND NISSAN [80] cite the publication of ARRHENIUS [81] "On the internal friction of dilute aqueous solutions". However, Equation (3.6) or a similar equation cannot be found in the publication of ARRHENIUS.

itself. They used the *Stokes-Einstein* relation to derive an equation for the viscosity based on their theoretical equation for the diffusion constant. They observed that the results for a constant temperature agree well with the empirical relationship for viscosity and free volume expressed by DOOLITTLE [83] in Equation (3.7).

$$\mu = a_1 \exp\left(\frac{a_2}{V_{\mathrm{m,free}}}\right) \tag{3.7}$$

Here, $V_{\mathrm{m,free}}$ is the average molecular free volume.

ALLAL ET AL. [75] derived a model based on the free volume concept. Their model contains a term for the dilute gas viscosity μ_{dil} and a term that characterizes the viscosity contribution in a dense state μ_{d} according to Equation (3.8).

$$\mu = \mu_{\mathrm{dil}} + \mu_{\mathrm{d}} \tag{3.8}$$

ALLAL ET AL. [75] use the dilute-gas viscosity μ_{dil} model of CHUNG ET AL. [84] based on the *Chapman-Enskog* theory. The dense fluid contribution term μ_{d} is based on a mechanistic dumbbell model in which molecules are described by spheres that are interconnected with springs. The relaxation function for the ratio of shear stress and shear rate leads to an expression for the viscosity contribution for a dense fluid μ_{d} as described in Equation (3.9).

$$\mu_{\mathrm{d}} = \frac{\rho l \left(\alpha\rho + pM/\rho\right)}{\sqrt{3RTM}} \exp\left[B\left(\frac{\alpha\rho + pM/\rho}{RT}\right)^{3/2}\right] \tag{3.9}$$

The model has three adjustable parameters: l, α, and B.

For fluids of high density, as those considered in the present thesis, the dilute-gas viscosity is several orders of magnitudes smaller than the dense fluid viscosity $\mu_{\mathrm{dil}} \ll \mu_{\mathrm{d}}$. Thus the dilute gas viscosity μ_{dil} is often neglected, e.g. in PENSADO ET AL. [47].

Mixture Laws for the Free Volume Theory

With suitable mixture laws for the model parameters, it is also possible to use the free volume theory to calculate the mixture viscosity based on the pure fluid parameters.

For the free volume theory of ALLAL ET AL. [75], the mixture laws according to Equations (3.10-3.12) [85] are implemented for mixtures of polyol esters[2].

$$\bar{l} = \sum_i x_i \log(l_i) \tag{3.10}$$

$$\overline{\alpha} = \sum_i \sum_j x_i x_j \sqrt{\alpha_i \alpha_j} \tag{3.11}$$

$$\frac{1}{\overline{B}} = \sum_i \frac{x_i}{B_i} \tag{3.12}$$

3.1.3 Friction-Theory

The idea of the *friction theory* (f-theory) for viscosity modeling is to model the viscosity based on attractive and repulsive contributions similar to thermal equations of state (see Chapter 4.2.2). QUIÑONES-CISNEROS ET AL. [87] derive the theoretical background of the f-theory with Newtons law of viscosity and a discretization perpendicular to the surface of the fluid film. Nevertheless, the setup of the equations appears rather empiric.

Similar to the free volume theory of ALLAL ET AL. [75], QUIÑONES-CISNEROS ET AL. [87] use the dilute-gas viscosity μ_{dil} by CHUNG ET AL. [84]. The dense liquid viscosity μ_{d} is split into one term for repulsive contributions and another term for attractive contributions to the shear stress. Both terms are modeled with a series of polynomials as described in Equation (3.13).

$$\mu = \mu_{\mathrm{dil}} + \mu_{\mathrm{d}} = \mu_{\mathrm{dil}} + \sum_{i=1}^{n} \kappa_{\mathrm{a},i}\, p_{\mathrm{a}}^{i} + \sum_{i=1}^{n} \kappa_{\mathrm{r},i}\, p_{\mathrm{r}}^{i} \tag{3.13}$$

The friction parameters $\kappa_{\mathrm{a},i}$ and $\kappa_{\mathrm{r},i}$ are temperature dependent. Repulsive pressure contributions p_{r} and attractive pressure contributions p_{a} are calculated with an EoS. The authors employ the theory for several different EoS, such as *Soave-Redlich-Kwong, Peng-Robinson* [87] or the *Perturbated-Chain Statistical Associating Fluid Theory* (PC SAFT) [88]. As the PC SAFT EoS is used for the solubility modeling in the present thesis (see Chapter 4), this approach

[2] For mixtures of refrigerants and lubricants, the mixture laws of ZÉBERG-MIKKELSEN ET AL. [86] are used as described in Section 5.2.

is also applied here. In the PC SAFT version of the f-theory [88], a cubic approach ($n = 2$) is used for both attractive and repulsive pressure contribution. Moreover, two adjustable scaling parameters μ_a and μ_r are introduced in the friction parameters $\kappa_{\mathrm{a},i}$ and $\kappa_{\mathrm{r},i}$, to improve the model accuracy according to Equations (3.14) and (3.15).

$$\kappa_{\mathrm{a},i} = \mu_\mathrm{a} \frac{\tilde{\kappa}_{\mathrm{a},i}}{p_\mathrm{c}^i} \tag{3.14}$$

$$\kappa_{\mathrm{r},i} = \mu_\mathrm{r} \frac{\tilde{\kappa}_{\mathrm{r},i}}{p_\mathrm{c}^i} \tag{3.15}$$

In these Equations, $\tilde{\kappa}_{\mathrm{a},i}$ and $\tilde{\kappa}_{\mathrm{r},i}$ are the reduced friction parameters. p_c is the pressure at the critical point. The reduced friction parameters $\tilde{\kappa}_{\mathrm{a},i}$ and $\tilde{\kappa}_{\mathrm{r},i}$ are modeled according to Equations (3.16) and (3.17).

$$\tilde{\kappa}_{\mathrm{a},i} = \sum_{j=0}^{2} \left(a_{\mathrm{a},i,j,0} + \sum_{k=1}^{3} \frac{a_{\mathrm{a},i,j,k}}{m^j} \left[\exp\left(k \frac{T_\mathrm{c}}{T} - k \right) - 1 \right] \right) \tag{3.16}$$

$$\tilde{\kappa}_{\mathrm{r},i} = \sum_{j=0}^{2} \left(a_{\mathrm{r},i,j,0} + \sum_{k=1}^{3} \frac{a_{\mathrm{r},i,j,k}}{m^j} \left[\exp\left(k \frac{T_\mathrm{c}}{T} - k \right) - 1 \right] \right) \tag{3.17}$$

T_c is the temperature at the critical point and m is the number of segments of the respective fluid in the PC SAFT model (see Section 4.2.2). QUIÑONES-CISNEROS ET AL. [88] stress that the properties at the critical point p_c and T_c must be calculated with the PC SAFT EoS. Tabulated literature data should not be used. The reason for this is the known deviation near the critical point of the PC SAFT EoS for many substances. All in all, this leads to 48 parameters $a_{\mathrm{a},j,k}$ and $a_{\mathrm{r},j,k}$. The parameters for $a_{i=2,j,k=1}$ and $a_{i=2,j=0,k}$ are set to zero [88]. The remaining 38 parameters are regressed to a database of smoothed experimental viscosities of n-alkanes from methane to n-octadecane and are considered as universal [88]. Consequently, only the two scaling parameters μ_a and μ_r have to be computed for every fluid [88].

Mixture Laws for the F-Theory

Regarding the f-theory of QUIÑONES-CISNEROS ET AL. [88], mixture laws are applied to the friction parameters $\kappa_{\mathrm{a},i}$ and $\kappa_{\mathrm{r},i}$ (see Equations (3.14, 3.15)). The

mixture laws are described in Equations (3.18) and (3.19)) [88].

$$\overline{\kappa}_{\mathrm{a},i} = \sum_j \varpi_j \kappa_{\mathrm{a},i,j} = \sum_j \varpi_j \mu_{\mathrm{a},j} \frac{\tilde{\kappa}_{\mathrm{a},i,j}}{p^i_{\mathrm{c},j}} \tag{3.18}$$

$$\overline{\kappa}_{\mathrm{r},i} = \sum_j \varpi_j \kappa_{\mathrm{r},i,j} = \sum_j \varpi_j \mu_{\mathrm{r},j} \frac{\tilde{\kappa}_{\mathrm{r},i,j}}{p^i_{\mathrm{c},j}} \tag{3.19}$$

ϖ_j describes a mass weighed fraction of the potential depth ε_j of the PC SAFT EoS (see Section 4.2.2) for the mixture component j.[3] ϖ_j is calculated according to Equation (3.20) [88].

$$\varpi_j = \frac{x_j m_j \varepsilon_j M_j^{-1}}{\sum_k x_k m_k \varepsilon_k M_k^{-1}} \tag{3.20}$$

The calculated friction parameters of the mixture $\overline{\kappa}_{\mathrm{a},i}$ and $\overline{\kappa}_{\mathrm{r},i}$ are subsequently used with Equation (3.13) to calculate the mixture viscosity $\overline{\mu}$.

3.1.4 Empirical Correlations

COMUÑAS ET AL. [89] extended the exponential viscosity model of Equation (3.1) to cover the pressure influence on the dynamic viscosity, as described in Equation (3.21).

$$\mu(p,T) = a_1 \exp\left(\frac{a_2}{T - a_3}\right) \exp\left[a_4 \ln\left(\frac{p + a_5(T)}{p_{\mathrm{Ref}} + a_5(T)}\right)\right], \tag{3.21}$$

$a_{1\ldots4}$ are temperature-independent parameters and a_5 is a polynomial of second order regarding temperature according to Equation (3.22).

$$a_5(T) = a_{5,0} + a_{5,1} T + a_{5,2} T^2. \tag{3.22}$$

The equation was also used by PENSADO ET AL. [67] for PEC9 and PEB8E2.

Another equation that is frequently used to model the kinematic viscosity of polyol ester lubricants is the two-parameter *Ubbelohde-Walther* equation[4]

[3] Please note that i is used in Equations (3.18,3.19) for the order of the contribution term (linear: $i = 1$, or quadratic: $i = 2$) according to Equation (3.13) and not for a component.

[4] The value of 0.8 in this equation is found in the German norm DIN51563 [90]. In Anglo-American publications a value of 0.7 is frequently used. The difference is negligible for the kinematic viscosity of pure lubricants considered in the present thesis in the temperature operation range of the suction line.

described in Equation (3.23) [90].

$$\log_{10}\left[\log_{10}(\nu+0.8)\right] = a_1 + a_2\ \log_{10}(T) \tag{3.23}$$

In the following Section 3.2, Equations (3.21) and (3.23) are used to model the viscosity of the pure polyol esters.

3.2 Modeling of Density and Viscosity of Polyol Esters

The fluid properties of PEs and DiPEs were discussed on the basis of the available data in literature in the previous Chapter 2. In the following, the density and viscosity of the different pure PEs and DiPEs are modeled. Additionally, it is evaluated whether mixtures of different polyol esters can be considered as ideal mixtures. Assuming an ideal mixture would simplify the determination of the lubricant composition, which is the aim of the present chapter.

In the following, the deviations between modeled and experimental data will be discussed with the absolute average deviation AAD, the maximum deviation MD, and the mean deviation Bias according to Equations (3.24-3.26).

$$\text{AAD} = \frac{\sum_{j=1}^{n} |\epsilon(p_j, T_j)|}{n} \tag{3.24}$$

$$\text{MD} = \max\left(|\epsilon(p_j, T_j)|\right)\Big|_{j=1\ldots n} \tag{3.25}$$

$$\text{Bias} = \frac{\sum_{j=1}^{n} \epsilon(p_j, T_j)}{n} \tag{3.26}$$

In these equations, $\epsilon(p_j, T_j)$ is the normalized deviation of data point j represented by the pressure p_j and the temperature T_j. n is the number of data points. The normalized deviation is calculated according to:

$$\epsilon(T_j, p_j) = \frac{\zeta_{\text{mod}}(T_j, p_j) - \zeta_{\text{exp}}(T_j, p_j)}{\zeta_{\text{exp}}(T_j, p_j)}. \tag{3.27}$$

ζ stands for the respective property of the mixture. The indices 'mod' and 'exp' indicate the modeled and experimental data, respectively.

3.2.1 Density of Pure PEs and DiPEs

The density of the polyol esters is modeled with a polynomial of second order in temperature and pressure, as shown in Equation (3.28).

$$\rho = a_{00} + a_{10}T + a_{01}p + a_{20}T^2 + a_{11}Tp + a_{02}p^2 \tag{3.28}$$

The coefficients are determined with the Matlab® *fit* library. The calculated coefficients, the AAD, and the MD of the model can be found in Table 3.1. The values of MD are lower than the measurement accuracies in the respective publications as summarized in Table 2.2.1.

Table 3.1: Deviation of the density between polynomial fit and measurements for pure PEs and DiPEs.

PE / DiPE	Data Source	$10^{-3}\,a_{00}$ $\frac{\mathrm{kg}}{\mathrm{m^3}}$	a_{10} $\frac{\mathrm{kg}}{\mathrm{K\,m^3}}$	$10^{9}\,a_{01}$ $\frac{\mathrm{kg}}{\mathrm{Pa\,m^3}}$	$10^{6}\,a_{20}$ $\frac{\mathrm{kg}}{\mathrm{K^2\,m^3}}$	$10^{9}\,a_{02}$ $\frac{\mathrm{kg}}{\mathrm{Pa^2\,m^3}}$	$10^{15}\,a_{11}$ $\frac{\mathrm{kg}}{\mathrm{Pa\,K\,m^3}}$	AAD %	MD %
PEC5	[58]	1.26	-0.856	-658	62.7	4.43	-5.19	0.014	0.046
PEC7	[58]	1.21	-0.811	-573	78.8	4.09	-7.02	0.013	0.049
PEC9	[58]	1.18	-0.778	-556	82.1	3.93	-7.84	0.009	0.027
PEB5M2	[48]	1.28	-0.973	-172	285.2	2.91	-2.83	0.007	0.019
PEB8E2	[51]	1.15	-0.588	-297	-177.3	3.08	-1.52	0.006	0.022
PEB9M355	calc.[a]	1.35	-1.874	898	1766	1.70	-5.45	0.035	0.107
DiPEC5	[54]	1.25	-0.695	-328	-104.5	3.31	-5.56	0.010	0.055
DiPEC7	[54]	1.20	-0.688	-230	-50.3	2.97	-5.24	0.012	0.053
DiPEB9M7	[56]	1.18	-0.788	0	172.0	0	0	0.002	0.005

a: Calculated with PC SAFT EoS (see Section 4.4).

3.2.2 Density of Mixtures of Polyol Esters

The molar volume of a mixture $\overline{V}_\mathrm{m}$ is composed according to Equation (3.29) [91, p.159].

$$\overline{V}_\mathrm{m} = \sum_i x_i V_{\mathrm{m},0,i} + \Delta\overline{V}_\mathrm{m} \tag{3.29}$$

$V_{\mathrm{m},0,i}$ is the molar volume of the pure component i and $\Delta\overline{V}_\mathrm{m}$ the molar volume change of mixing. For an ideal mixture, $\Delta\overline{V}_\mathrm{m}$ vanishes [91, p.175], leading to

Equation (3.30).

$$\overline{V}_{\mathrm{m}}^{\mathrm{id}} = \sum_i x_i V_{\mathrm{m},0,i} \tag{3.30}$$

The molar volume V_{m} is related to the density ρ through the molecular weight M in Equation (3.31).

$$V_{\mathrm{m}} = \frac{M}{\rho} \tag{3.31}$$

Combining Equations (3.30) and (3.31) leads to Equation (3.32).

$$\frac{\overline{M}}{\overline{\rho}^{\mathrm{id}}} = \sum_i x_i \frac{M_i}{\rho_{0,i}} \tag{3.32}$$

The molecular weight of the mixture $\overline{M}$ is calculated according to Equation (3.33).

$$\overline{M} = \sum_i x_i M_i \tag{3.33}$$

In order to obtain a mixture law for the density of ideal mixtures, Equation (3.32) is divided by the molecular weight of the mixture $\overline{M}$. This leads to Equation (3.34).

$$\frac{1}{\overline{\rho}^{\mathrm{id}}} = \sum_i \frac{x_i M_i}{\overline{M}\rho_{0,i}} = \sum_i \frac{w_i}{\rho_{0,i}} \tag{3.34}$$

Here, w is the mass fraction of the components i, which is defined according to Equation (3.35).

$$w_i = x_i \frac{M_i}{\overline{M}} \tag{3.35}$$

In the following, it is examined, whether mixtures of polyol esters can be considered as ideal mixtures as assumed in Equation (3.30).

FANDIÑO ET AL. [92] measured the compressed liquid density of different PE mixtures with a VG of 32: a binary mixture of PEB8E2 and PEC5 and a binary mixture of PEB8E2 and PEC7. The compressed liquid density of the pure polyol esters PEC5, PEC7, and PEB8E2 was investigated by the same authors in FANDIÑO ET AL. [52, 53]. Thus, it is assumed that differences in the measurement setup and impurities of the lubricant samples do not play a role.

To test, whether the mixture of different polyol esters can be considered as an ideal mixture, the mixture data investigated by FANDIÑO ET AL. [92] is compared to data calculated with an ideal mixture law applied to the data of the components of the binary mixtures.

According to Equation (3.29) and (3.30), the difference between the molar volume $\overline{V}_\mathrm{m}$ and the molar volume of the ideal mixture $\overline{V}_\mathrm{m}^\mathrm{id}$ is the molar volume change of mixing $\Delta\overline{V}_\mathrm{m}$ described in Equation (3.36).

$$\Delta\overline{V}_\mathrm{m} = \overline{V}_\mathrm{m} - \overline{V}_\mathrm{m}^\mathrm{id} \tag{3.36}$$

Consequently, the ratio of molar volume change of mixing $\Delta\overline{V}_\mathrm{m}$ to molar volume $\overline{V}_\mathrm{m}$ describes the deviation of the ideal mixture from the real mixture according to Equation (3.37).

$$\frac{\overline{V}_\mathrm{m}^\mathrm{id} - \overline{V}_\mathrm{m}}{\overline{V}_\mathrm{m}} = \frac{-\Delta\overline{V}_\mathrm{m}}{\overline{V}_\mathrm{m}} \tag{3.37}$$

The ratio of $\Delta\overline{V}_\mathrm{m}$ to $\overline{V}_\mathrm{m}$ is depicted in Figure 3.1.

Figure 3.1 shows that the ratio of molar volume change of mixing to the molar volume is $\Delta\overline{V}_\mathrm{m}/\overline{V}_\mathrm{m} < 0.22\%$ for both mixtures. This is more than the uncertainty resulting from the density measurements of approximately 0.014% and the uncertainty of the weight of <0.01%, as stated in the publication of FANDIÑO ET AL. [92]. Nevertheless, the molar volume change of mixing $\Delta\overline{V}_\mathrm{m}$ is negligible compared to the molar volume of the mixture $\overline{V}_\mathrm{m}$ and it appears reasonable to assume an ideal behavior of the PE mixture.

3.2.3 Viscosity of Pure PEs and DiPEs

In the following, the parameters of the respective viscosity models are regressed to the experimental viscosity data of each PE or DiPE (c.f. Table 2.3). To improve the accuracy in the pressure regime relevant for the suction line, only data with a pressure $p < 10\,\mathrm{MPa}$ was considered in the parameter regression. The nonlinear least-squares solver *lsqnonlin* in Matlab® is used to determine the model parameters.

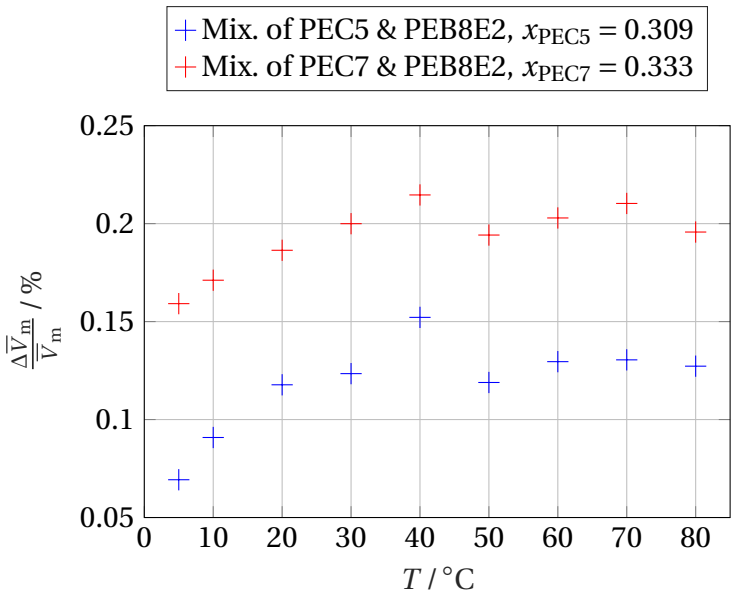

Figure 3.1: Ratio of molar volume change of mixing $\Delta\overline{V}_m$ to molar volume $\overline{V}_m$ for binary PE mixtures. Data source of compressed liquid density: Mixture [92], PEC5 [53], PEC7 [53], PEB8E2 [52].

Free Volume Theory

The free volume parameters contains three adjustable parameters: l, α, and B (see Equation (3.9)). Table 3.2 shows the computed values and the deviations between the modeled viscosity and the measurements for the used PEs and DiPEs (see Table 2.3)[5]. The maximum deviations of most PEs and DiPEs are in an acceptable range with MD < 6%. Nevertheless, higher MD occur for PEB5M2, PEB9M355, and DiPEB9M7. In these cases, the problem is that the solver cannot find a combination of the free volume parameters that matches the strong temperature influence on viscosity. This has to be kept in mind, for the application of the free volume model for mixtures of refrigerants and lubricants in Chapter 5, if the lubricant contains any of the named branched PEs. Additionally to mixtures of refrigerants and lubricants, the free volume model is applied to mixtures of polyol esters in the following Section 3.2.4.

[5]The calculated free volume theory parameters of the refrigerant can be found in Table D.1 in the Appendix.

Table 3.2: Free volume model parameters and deviations to viscosity measurements for implemented PEs and DiPEs.

Component	Data Source	Free Volume Parameters			Deviation		
		α	l	B	AAD	MD	Bias
		$\frac{\mathrm{Jm^3}}{\mathrm{molkg}}$	Å	10^{-3}	%	%	%
PEC5	[64]	395	0.2015	2.567	1.76	2.85	-0.04
PEC7	[64]	563	0.1828	1.646	0.93	2.03	-0.01
PEC9	[64]	792	0.1413	1.115	3.09	5.84	-0.13
PEB5M2	[61]	176	0.1490	11.62	8.35	18.69	-0.94
PEB8E2	[67]	687	0.04101	1.778	2.86	5.01	-0.10
PEB9M355	[36]	460	0.01391	4.565	8.70	18.49	-1.05
DiPEC5	[66]	952	0.08252	0.8633	3.04	4.49	-0.11
DiPEC7	[66]	1244	0.07946	0.6141	2.78	4.53	-0.10
DiPEB9M7	[56]	792	0.01683	2.103	6.91	20.52	-0.72

F-Theory

In the f-theory for the PC SAFT EoS, the two scaling parameters μ_a and μ_r (see Equation (3.20)) have to be adjusted for every fluid. The parameters and the deviations to the measurements for the considered PEs and DiPEs are summarized in Table 3.3[6]. The parameter regression leads to low AAD for the lin-

Table 3.3: F-theory model parameters and deviations to viscosity measurements for implemented PEs and DiPEs.

Component	Data Source	f-theory Parameters		Deviation		
		μ_a	μ_r	AAD	MD	Bias
		10^{-7}Pas	10^{-7}Pas	%	%	%
PEC5	[64]	−129.3	174	10.04	31.14	−1.59
PEC7	[64]	8.288	104.5	5.66	24.04	−0.59
PEC9	[64]	21.43	69.38	7.44	15.83	−0.74
PEB5M2	[61]	−1490	78.44	22.86	50.45	−7.05
PEB8E2	[67]	−373.1	80.40	12.55	32.79	−2.41
PEB9M355	[36]	7877	2742	41.58	76.32	−22.34
DiPEC5	[66]	−75.19	171.1	7.64	12.88	−0.71
DiPEC7	[66]	−17.65	51.59	6.87	11.14	−0.55
DiPEB9M7	[56]	−1099	505.8	16.76	66.88	−5.67

[6]The f-theory parameters for the refrigerants can be found in Table D.2 in the Appendix.

ear PEs PEC7 and PEC9 as well as for the linear DiPEs DiPEC5 and DiPEC7. For PEC5 as well as for branched PEs and DiPEs, the deviations are very high. Additionally, the values of the scaling parameters differ significantly for different PEs and DiPEs. The solver cannot find a homogeneous set of parameters for the considered polyol esters. This is related to the model architecture. The universal parameters $a_{\mathrm{a},i,j,k}$ and $a_{\mathrm{r},i,j,k}$ of Equations (3.16) and (3.17) were fitted to the viscosity of n-alkanes with a much lower molecular weight than PEs or DiPEs. Therefore, high deviations are expected for the application of the f-theory to mixtures of refrigerant-lubricant mixtures in Chapter 5.

Empiric Correlations

The empiric equation of *Comuñas* (Equation (3.21)) is used to model the viscosity of all selected PEs and DiPEs (see Table 2.3), except for PEB9M355. The viscosity of PEB9M355 cannot be modeled with Equation (3.21) as the model has seven adjustable parameters, but only two viscosity values are reported in BOYDE [36]. Here, the two-parameter *Ubbelohde-Walther* Equation (3.23) is used. As the *Ubbelohde-Walther* equation gives the kinematic viscosity ν, the dynamic viscosity μ is calculated with the kinematic viscosity ν and the density ρ estimated with the PC SAFT EoS.

AAD, MD, and Bias of the pure PE and DiPE modeled with Equations (3.21) and (3.23) can be found in Table 3.4. The calculated parameters of the polyol esters can be found in Table D.3 in the Appendix.

Table 3.4: Deviation of the viscosity between empiric equation of *Comuñas* (Equation (3.21)) and measurement data for pure PEs and DiPEs.

PE / DiPE	Data Source	AAD %	MD %	Bias %
PEC5	[64]	1.63	4.59	−0.367
PEC7	[64]	2.43	5.91	−0.081
PEC9	[64]	1.53	4.4	−0.04
PEB5M2	[61]	2.56	5.43	−0.101
PEB8E2	[67]	0.83	1.99	−0.01
DiPEC5	[66]	0.31	0.85	−0.002
DiPEC7	[66]	0.63	1.48	−0.006
DiPEB9M7	[56]	0.95	2.23	−0.013

The maximum deviations of the linear PEs as well as of PEB5M2 and DiPEB9M7 are slightly higher than the estimated measurement uncertainty. For the other PEs and DiPEs, the maximum deviations are within the estimated measurement uncertainty. The AAD of PEB9M355 modeled with the *Ubbelohde-Walther* Equation (3.23) is zero as the two-parameter equation is fitted with two viscosity values.

Comparing the deviations of the different viscosity models, only the empiric Equation (3.21) of COMUÑAS ET AL. [89] leads to a MD in the range of the measurement uncertainty for polyol ester lubricants. Therefore, this equation is used in the following to model the dynamic viscosity μ of the pure PEs and DiPEs except for PEB9M355, which is modeled with the *Ubbelohde-Walther* Equation (3.23).

3.2.4 Viscosity of Mixtures of Polyol Esters

In the following, the different models for the mixture viscosity $\overline{\mu}$ presented in Section 3.1 are compared to experimental results for a binary mixture of polyol esters.

LUGO ET AL. [85] measured the dynamic viscosity of the same mixture samples that were used by FANDIÑO ET AL. [92] for the measurements of the compressed liquid density of the mixture. Their focus was on identifying the viscosity-pressure coefficient of the mixture for high pressures $p < 60\,\mathrm{MPa}$.

In the following, only the experimental results at a pressure of 0.1 MPa are compared, because low pressures are more characteristic for the suction line. The mixture viscosity $\overline{\mu}$ of the experiments and the different models are compared in Figure 3.2. Beside the mixture viscosity, the viscosity of the pure components is depicted, as these build the margin for the mixture viscosity.

For both cases, the mixtures PEC5-PEB8E2 (Figure 3.2a) and PEC7-PEB8E2 (Figure 3.2b), the comparison of calculated mixture viscosity and the experimental viscosity data lead to similar results. For low temperatures $T \leq 40°\mathrm{C}$, the experimental mixture viscosity is slightly underestimated by the different viscosity models. For the intermediate temperature range $40°\mathrm{C} \leq T \leq 60°\mathrm{C}$,

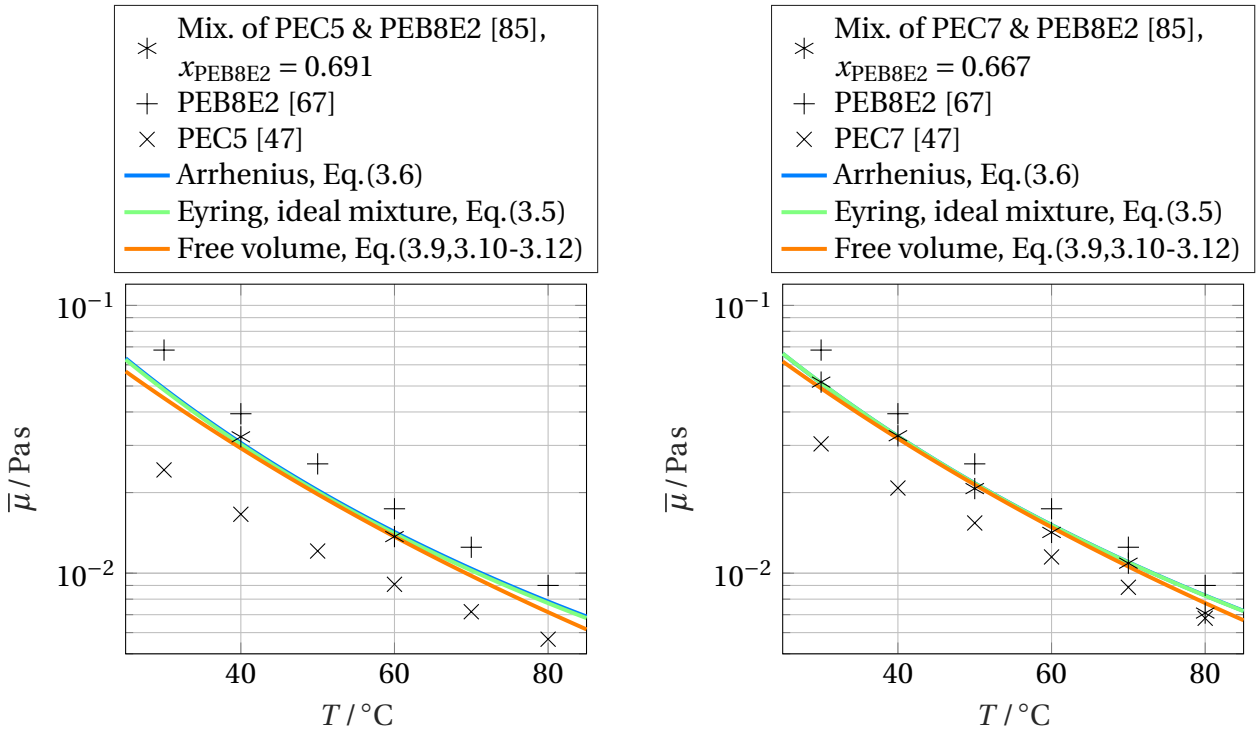

(a) Mixture of PEC5 and PEB8E2.

(b) Mixture of PEC7 and PEB8E2.

Figure 3.2: Dynamic viscosity of PE-mixture at atmospheric pressure.

the mixture viscosity models agree well with the experimental data. For high temperatures $T > 60°C$, only data for the mixture of PEC7 and PEB8E2 is available (Figure 3.2b). For $T = 70°C$, the models agree well with the experiments, wheras there is a strong overprediction for $T = 80°C$. Comparing the different viscosity models, it can be seen that the free volume model predicts slightly lower viscosity values compared to the models of *Arrhenius* and *Eyring*.

Regarding the aim of the present chapter to determine the composition of the lubricant mixture with target values for the properties, it is crucial that the mixture model accurately predicts the mixture viscosity. To demonstrate this, Figure 3.3 compares the composition of the binary mixture given by LUGO ET AL. [85] to the composition that is determined with the experimental mixture viscosity and the inversed mixture models. Figure 3.3b shows that the calculated composition differs significantly from the experimental composition at temperatures $T > 40\,°C$ with an exception for $T = 70\,°C$.

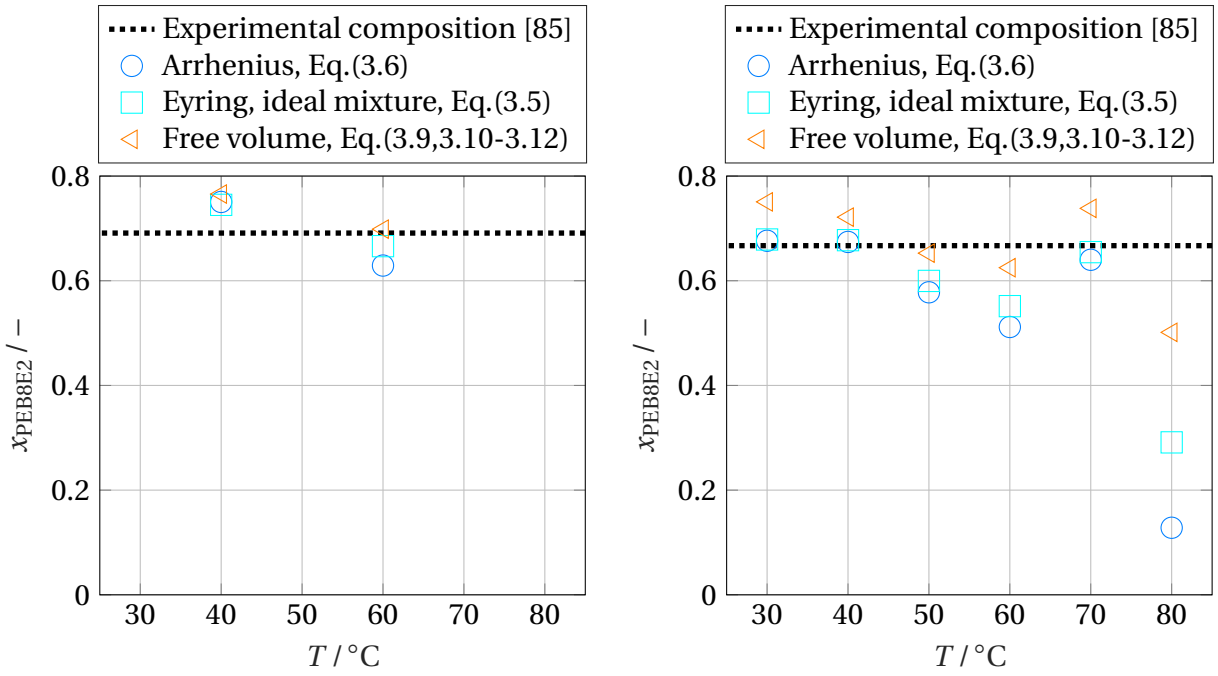

(a) Mixture of PEC5 and PEB8E2.

(b) Mixture of PEC7 and PEB8E2.

Figure 3.3: Comparison of mole fraction of PEB8E2 x_{PEB8E2} between experiments and calculation with inversed mixture viscosity models.

To the knowledge of the author, the publication of LUGO ET AL. [85] is the only one that investigates the mixture viscosity of PEs. Therefore, it is not possible to clarify the origin of the deviations between real and ideal mixtures at elevated temperatures further. It remains unclear if the effect results from a physically relevant influence or from artifacts in the measurements. As a consequence for the determination of the lubricant composition, only target values of the mixture viscosity at temperatures below $T = 50\,°\mathrm{C}$ are considered as a compromise between the accuracy and the amount of available data

In order to select a viscosity mixture law for the determination of the lubricant composition, the AAD of the different viscosity models to the experimental composition is calculated considering only values with a temperature $T < 50°\mathrm{C}$. The values of the AAD can be found in Table 3.5.

Table 3.5: Absolute average deviation AAD for temperatures $T < 50°C$ of the different inverted viscosity models in the calculation of the lubricant composition.

Viscosity Model	AAD / %	
	PEC5 - PEB8E2	PEC7 - PEB8E2
Arrhenius, Eq. (3.6)	6.74	5.13
Eyring, ideal mixture, Eq. (3.5)	6.48	4.38
Free volume [75], Eq. (3.9-3.12)	10.09	7.98

The AAD of the ideal mixture *Eyring* equation is slightly better compared to the *Arrhenius* equation that does not consider the molar volume of the components. Therefore, the *Eyring* equation for ideal mixtures was selected for the calculation of the lubricant composition.

3.3 Algorithm to Determine the Lubricant Composition

The non-linear least squares Matlab® solver *lsqnonlin* is used to determine the composition of the mixture with a minimum deviation between the fluid properties of a mixture of PEs and DiPEs on the one hand and the target data on the other hand. Analogously to the deviation between experimental and modeled data in Equation (3.27), a vector of the normalized deviation ϵ_ζ is set up for the deviation between the properties of the lubricant mixture and the target data, as described in Equation (3.38).

$$\epsilon_\zeta(T) = \frac{\zeta_{\text{Mix}}(T, p_{\text{atm}}) - \zeta_{\text{Target}}(T, p_{\text{atm}})}{\zeta_{\text{Target}}(T, p_{\text{atm}})} \tag{3.38}$$

ζ stands for the respective properties of the mixture: either molecular weight $\overline{M}$ (Equation (3.33)), density $\overline{\rho}$ (Equation (3.34)), or dynamic viscosity $\overline{\mu}$ (Equation (3.5)). In case only kinematic viscosity data is available, the mixture kinematic viscosity $\overline{\nu}$ is calculated with the mixture density $\overline{\rho}$ and the dynamic viscosity $\overline{\mu}$.

The following restrictions are made to select data points for the calculation of the lubricant composition.

- The upper temperature limit is set to $T = 50°C$ (see Section 3.2.4).
- The lower temperature limit is set to $T = 0°C$ to avoid excessive extrapolation of the pure lubricant viscosity (see Table B.3 in the Appendix for the temperature range of the experimental data).
- Only data points at atmospheric pressure or alternatively at the lowest available pressure are considered, because viscosity data of PEB5M2 and PEB9M355 is only available at atmospheric pressure.

The restriction on the pressure of the data points is not an issue as most of the commercial viscosity data is only available at atmospheric pressure. The non-linear least squares solver aims to find a minimum for the residual Res described in Equation (3.39).

$$\text{Res} = \sum_{i}^{n_\mu} (\epsilon_\mu(T_i))^2 + \sum_{i}^{n_\rho} (\epsilon_\rho(T_i))^2 + \sum_{i}^{n_M} (\epsilon_M)^2 \tag{3.39}$$

The number of data points n_ζ for the different fluid properties is usually not equal. There is only one data point for the molecular weight ($n_M = 1$), while usually several values for the viscosity ($n_\mu > 1$) at different temperatures are available. To avoid that the algorithm optimizes primarily one fluid property, the number of data points is equalized to the number of the viscosity data points n_μ. If several density data points are available, a linear fit of the density data is evaluated at the temperature levels of the viscosity data. If only a single data point of the density data is available, the mean density gradient of all PEs $\partial\rho/\partial T = -0.75\,\mathrm{kg\,m^{-3}\,K^{-1}}$ (c.f. Figure 2.3b) is used to estimate the density of the commercial lubricant at different temperature levels. Thus, Equation (3.39) is modified to Equation (3.40).

$$\text{Res} = \sum_{i}^{n_\mu} (\epsilon_\mu(T_i))^2 + \sum_{i}^{n_\mu} (\epsilon_\rho(T_i))^2 + \sum_{i}^{n_\mu} (\epsilon_M)^2 \tag{3.40}$$

If data on molecular weight or density are not available for a commercial lubricant, the respective term is omitted in Equation (3.40).

3.4 Assessment of the Algorithm

The algorithm is assessed with data of a commercial lubricant. A series of publications by MORAIS ET AL. [73, 93, 94] builds a valuable validation case for the prediction of density and viscosity of the pure lubricant as well as for refrigerant-lubricant mixtures in this thesis. In MORAIS ET AL. [73], the composition of carboxylic acids used in the synthesis of the commercial lubricant Emkarate® RL 32-3MAF with a VG of 32 was determined using nuclear magnetic resonance spectroscopy (NMR) [73]. They identified the carboxylic acids C5, C7, B5M, and B9M355 in the mixture. The molecular structure of the carboxylic acids can be found in Table A.1 in the Appendix. Based on the relative integrals of the ^{13}C NMR spectrum of the carbon atoms in the carboxylic acid, they determined the composition of carboxylic acids in the lubricant. Assuming that the mixture consists only of pentaerythritol esters, they calculated the lubricant composition as shown in Table 3.6.

Table 3.6: Composition of Emkarate® RL 32-3MAF determined by MORAIS ET AL. [93].

PE	Composition x_i / %
PEC5	32.7 ± 4.3
PEC7	45.5 ± 2.9
PEB5M3	5.5 ± 2.8
PEB9M355	16.3 ± 1.0

The composition calculated with the algorithm described in Section 3.3 is compared to the reported composition by MORAIS ET AL. [73] in three steps applying different assumptions:

Step 1: The mixture viscosity and density of the lubricant are calculated with the composition determined by MORAIS ET AL. [73].

Step 2: The mixture composition is calculated with the algorithm described in the previous Section 3.3 restricting the PEs in the composition to the ones identified by MORAIS ET AL. [73].

Step 3: The mixture composition is calculated using the algorithm derived in the previous Section 3.3 considering all PEs used for determination of the lubricant composition (see Table 2.3).

In *Step 2* and *Step 3*, the density $\overline{\rho}$ and viscosity $\overline{\mu}$ of the lubricant reported in MORAIS ET AL. [94] are used as target data for the algorithm.

The comparison between the calculated lubricant properties in *Step 1* and the properties measured by MORAIS ET AL. [73, 94] is depicted in Figure 3.4. The

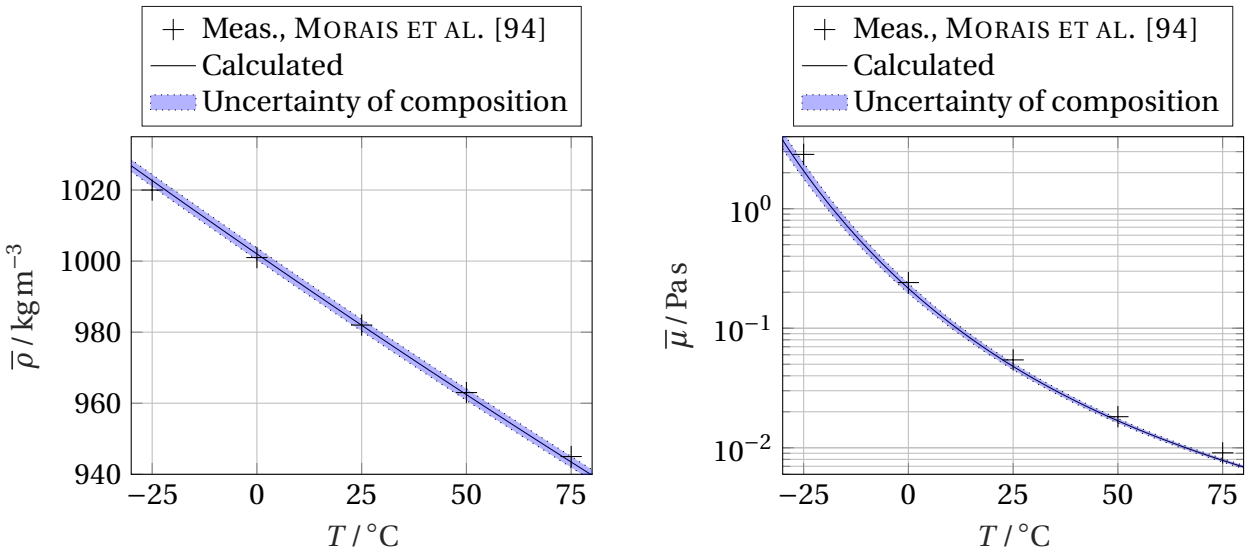

(a) Density $\overline{\rho}$ over temperature T.

(b) Dyn. viscosity $\overline{\mu}$ over temperature T.

Figure 3.4: Comparison of the measured and calculated lubricant properties.

blue area around the curve of the calculated properties shows the influence of the indicated standard deviation of the measured lubricant composition. Regarding the density curve in Figure 3.4a, the deviation between the measurements of MORAIS ET AL. [94] and the calculated density is low. The AAD is 0.12% and the MD is 0.26%. The density slope $\frac{\partial \overline{\rho}}{\partial T}$ of the calculated results is slightly steeper compared to the measured density values.

The calculated viscosity of the mixture is lower than the measured mixture viscosity in the complete temperature interval. The average deviation is -14.1% and the MD 27.1%. The measured mixture viscosity is also outside the area of the influence of the composition measurement uncertainty. Both, the differ-

ence in the density gradient and the lower viscosity of the calculated results emphasize that DiPEs are present in the lubricant mixture.

In *Step 2*, the composition of the lubricant is calculated with the algorithm described in the previous section. As a consequence of the conclusion in *Step 1* that DiPEs are suspected to be part of the mixture, *Step 2* is split into two substeps:

In *Step 2a,* DiPEs are not considered in the mixture. The PEs in the composition are restricted to PEC5, PEC7, PEB5M2 (instead of PEB5M3), and PEB9M355.

In *Step 2b,* DiPEC5 and DiPEC7 are considered as possible mixture components additionally to PEC5, PEC7, PEB5M2, and PEB9M355.

As described above, the composition of carboxylic acids in the POE is determined rather than the mole fraction of PEs in the measurement approach of MORAIS ET AL. [73]. To compare the measurement data with the results of *Steps 2a* and *2b* properly, Figure 3.5 shows the mole fraction of carboxylic acids instead of the mole fraction of the different PEs and DiPEs[7]. Additionally, it is indicated, which amount of the carboxylic acid belongs to the respective PE and DiPE for a better understanding of the difference between *Steps 2a* and *2b*.

In both *Steps 2a* and *2b*, the calculated composition does not contain PEB5M2. In *Step 2a* the computed amount of C5 is significantly lower and the amount of C7 significantly higher compared to the composition measured by MORAIS ET AL. [73] to achieve a higher viscosity.

In *Step 2b*, a mole fraction of $x_{\mathrm{DiPEC5}} = 0\%$ and $x_{\mathrm{DiPEC7}} = 10.1\%$ is calculated. Here, the mole fraction of the linear carboxylic acid C7 is nearly equal to the mole fraction determined by MORAIS ET AL. [73]. The mole fraction of the linear carboxylic acid C5 is within the standard uncertainty of MORAIS ET AL. [73]. The mole fraction of B9M355 is slightly higher compared to the measure-

[7] PEs consist of 4 carboxylic acids while DiPEs consist of 6 carboxylic acids (see Section 2.1). Therefore, there is a difference between the mole fraction of the carboxylic acid and the sum of the mole fraction of a PE and a DiPE of the same carboxylic acid, e.g. $x_{\mathrm{C7}} \neq x_{\mathrm{PEC7}} + x_{\mathrm{DiPEC7}}$.

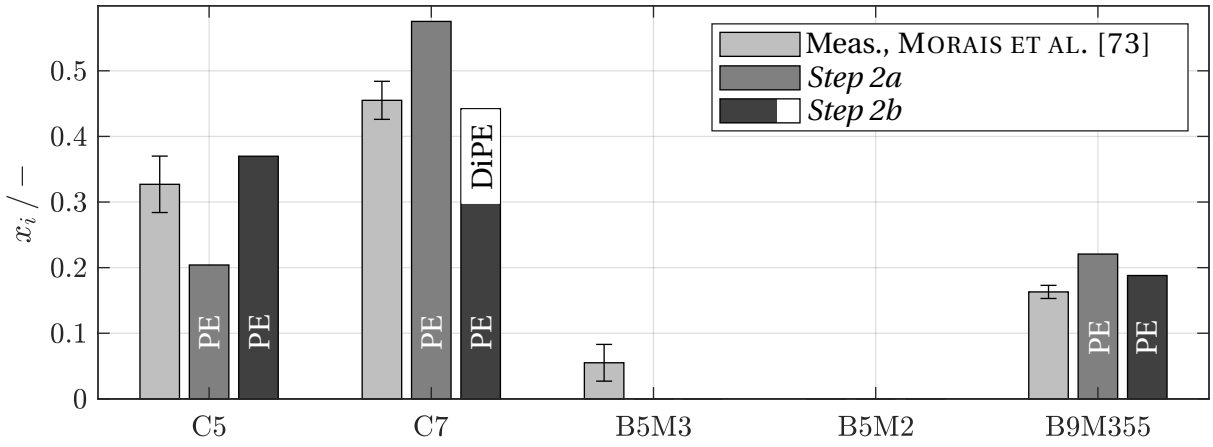

Figure 3.5: Composition of carboxylic acids determined by MORAIS ET AL. [73] and in *Steps 2a* and *2b*.

ment results to compensate the influence of the missing B5M3 on the viscosity. All in all, the algorithm predicts the composition of the different carboxylic acids with a good accuracy. The results of *Step 2b* further substantiate the suspicion that DiPEs are present in the commercial POE investigated by MORAIS ET AL. [73].

In *Step 3*, all PEs and DiPEs introduced in Section 2.3 are now considered for the determination of the lubricant composition. To make this possible, it is necessary to increase the amount of input data, as the Matlab® non-linear least-squares solver requires at least as many equations as unknown variables. Therefore, the *Ubbelohde-Walther* Equation (3.23) is fitted to the viscosity data between 0°C and 50°C and evaluated between the existing measurement values at $T = 12.5$°C and $T = 37.5$°C. Analogously, a polynomial of first order was fitted to the measured density values and evaluated at the same temperatures as the viscosity fit. This way, there are 10 equations for 9 unknown variables.

Figure 3.6 compares the composition of the carboxylic acids in the lubricant experimentally determined by MORAIS ET AL. [73] with the composition determined in *Step 3*. The solver finds a lower residual using the branched lubricant PEB8E2 instead of PEB9M355 and PEB5M2. This is possibly due to the estimated density data of PEB9M355 that is expected to differ from experimental data. Although the deviations are not expected to be large, the influ-

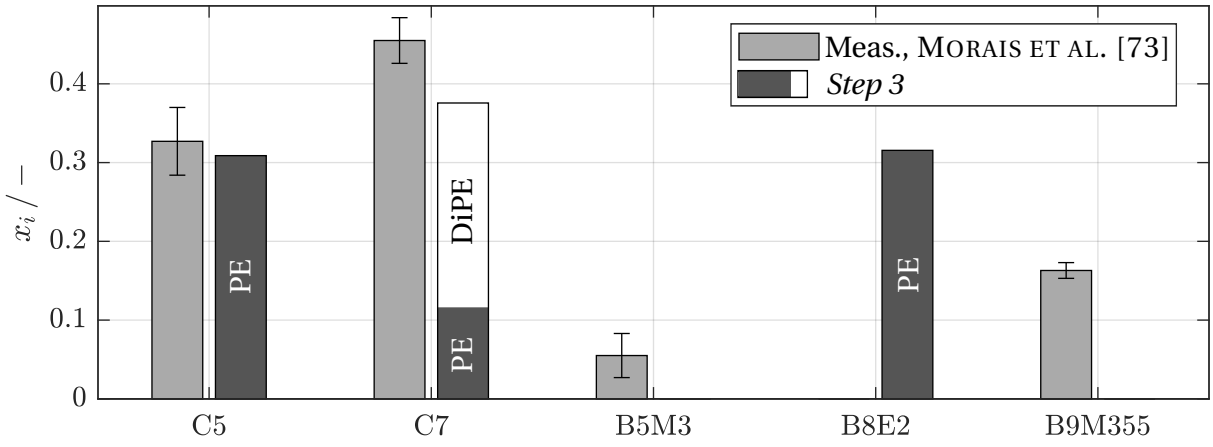

Figure 3.6: Composition of carboxylic acids determined by MORAIS ET AL. [73] and in *Step 3*.

ence on the density calculation can be significant as the density of different PEs is in a narrow range (see Figure 2.3a). This also affects the mole fraction of PEC7, which is significantly lower and DiPEC7, which is significantly higher compared to *Step 2b*. The carboxylic acids C9 and B9M7 do not appear in the mixture. This agrees with the findings of MORAIS ET AL. [73].

Table 3.7: Composition and deviation calculated in the steps of the assessment.

Case	Mole fraction x_i / %						Deviation / %			
	PEC5	PEC7	PEB5M3	PEB8E2	PEB9M355	DiPEC7	AAD$\vert_{\overline{\mu}}$	MD$\vert_{\overline{\mu}}$	AAD$\vert_{\overline{\rho}}$	MD$\vert_{\overline{\rho}}$
Step 1	32.7[a]	45.5[a]	5.5[a]	–	16.3[a]	–	14.1	27.1	0.12	0.26
Step 2a	20.4	57.5	–	–	22.1	–	1.4	2.3	0.75	0.82
Step 2b	38.9	31.2	–	–	19.8	10.1	1.3	1.9	0.13	0.20
Step 3	33.8	12.7	–	34.5	–	18.9	1.0	2.5	0.05	0.11

a: Composition determined by MORAIS ET AL. [73].

A comparison of the lubricant composition of *Steps 2b* and *3* summarized in Table 3.7 shows that it is possible to achieve similar results for mixture viscosity and density with different compositions of PEs. As a consequence, it can

be concluded that the algorithm is not capable to determine the composition of a commercial lubricant mixture out of the wide range of possible PEs and DiPEs, because especially the density values of the different PEs and DiPEs are in a narrow range. Albeit, this was not the objective in the development of the algorithm. The algorithm fulfills the requirement of finding a composition that shows a similar density and viscosity compared to the target data. This is proven by the deviations between the measured properties and the properties of the calculated lubricant composition, as summarized in Table 3.7.

3.5 Commercial Lubricant Mixtures

For the modeling of solubility and viscosity of refrigerant-lubricant mixtures, data on the composition of the lubricant is required. In this section, a composition of different PEs and DiPEs that matches target data of different commercial lubricants is determined using the algorithm developed in Section 3.3.

In the following, different scientific publications are introduced that contain on the one hand information on the POE lubricant allowing to determine a mixture of polyol esters and on the other hand data on solubility and/or mixture viscosity of these lubricants with refrigerants. The publication of CZUBINSKI ET AL. [95] is a valuable case to validate the solubility and viscosity of a polyol ester with R290 (propane). They used a POE of VG = 22. The manufacturer or brand name of the commercial lubricant was not indicated. In BOCK [96] and MARTZ AND JACOBI [97] the commercial lubricant Emkarate® RL68H with VG 68 was used to investigate the solubility of HFO and HFC refrigerants. The publications of MORAIS ET AL. [73, 93, 94] were already introduced in the previous Section 3.4. The lubricant Emkarate® RL32-3MAF used in these publications is considered in the subsequent modeling process as well. Table 3.8 summarizes the properties and meta data of the lubricants used in the mentioned publications.

The molecular weight of RL68H is higher than the molecular weight of the largest PE molecule PEC9 ($M_{\mathrm{PEC9}} = 696\,\mathrm{g\,mol^{-1}}$). This shows that the lubricant consists of a significant amount of DiPEs.

Table 3.8: Properties and meta data of commercial lubricants in literature.

Name	VG	M	$\overline{\rho}$			$\overline{\mu}$		
	$mm^2 s^{-1}$	$g mol^{-1}$	NP	T_{min}	T_{max}	NP	T_{min}	T_{max}
Czu22	22	541 [95]	-	-	-	5 [95]	284 K	354 K
RL32-3	32	560 [73]	5 [94]	248 K	348 K	5 [94]	248 K	348 K
RL68H	68	765 [96]	19[97]	233 K	338 K	5 [98]	296 K	338 K

Regarding the lubricant RL32-3, it was concluded in the previous section that it likely contains DiPEC7 to achieve the viscosity with the composition of carboxylic acids determined in MORAIS ET AL. [73]. Thus, a composition including DiPEC7 with a similar distribution of carboxylic acids as shown in Table 3.6 is determined. Here, PEB5M3 was replaced by its better investigated isomer PEB5M2.

To extend the database of polyol ester mixtures and to incorporate lubricant mixtures with a viscosity grade VG > 68, also lubricant data available in BOCK AND PUHL [35] are used as target data for the algorithm to determine the composition of polyol ester mixtures. The data of the manufacturer *Fuchs* comprise the viscosity-temperature curve ($\overline{\nu}$-T curve) of the pure lubricant in Daniels plots of different refrigerant-lubricant mixtures and the density of the POE at a temperature of $T = 15°C$. Data on the molecular weight M is not available. The $\overline{\nu}$-T data is extracted with help of a Matlab® script. The procedure is described in Appendix E. The $\overline{\nu}$-T curve of the respective lubricant is evaluated in steps of 5 K in a range of $0°C < T < 50°C$ resulting in a vector of 11 viscosity-temperature value pairs.

Table 3.9 summarizes the available information in BOCK AND PUHL [35] of the polyol ester lubricants in a range of $20 < VG < 100$.

The lubricants C55E and C85E are especially designed for the refrigerant R744 (CO_2). They contain additional anti-wear additives [35]. The properties of lubricant C55E are similar to SE55. Nevertheless, the $\overline{\nu}$-T-curve of both lubricants differs significantly in the low temperature regime[8]. Therefore, the composi-

[8]The difference in the viscosity at low temperatures of both lubricants can be observed in Figure 3.7, which compares the viscosity of the considered commercial POEs with the mixture viscosity of the determined polyol ester mixtures

Table 3.9: Properties of commercial POE lubricants in BOCK AND PUHL [35].

Name	VG	VI	PP	Temperature range of $\overline{\nu}$-T curve	Density $\overline{\rho}\vert_{T=15°C}$
	$mm^2 s^{-1}$	-	°C		$kg m^{-3}$
SEZ22	20	134	-57	$-20°C < T < 80°C$	1001
SEZ32	32	140	-57	$-25°C < T < 100°C$	1004
SE55	55	137	-48	$-10°C < T < 80°C$	1009
C55E	55	137	-48	$-40°C < T < 100°C$	1009
SEZ68	68	125	-39	$-25°C < T < 100°C$	970
C85E	80	118	-42	$-20°C < T < 80°C$	993
SEZ80	82	115	-39	$-25°C < T < 100°C$	992
SEZ100	100	100	-30	$-25°C < T < 100°C$	970

tion of both lubricants is calculated separately.

The algorithm described in Section 3.3 is used to calculate a mixture of PEs and DiPEs with similar properties compared to the commercial lubricants summarized in Tables 3.8 and 3.9. The determined compositions and the deviation in the fluid properties between the literature data and the polyol ester mixtures can be found in Table 3.10. The lubricant ID will be used in the subsequent parts of the thesis to refer to the lubricant composition calculated in this section.

Regarding the composition of the polyol ester mixtures, it can be observed that the mole fraction of short linear PEs decreases, while the mole fraction of linear DiPEs increases for a rising VG. Comparing the polyol ester mixtures of the same viscosity grades 22-1 and 22-2 as well as 32-1 and 32-2 with each other, it can be observed that the same VG can be obtained with a combination of linear PEs and either branched PEs (22-1, 32-1) or linear DiPEs (22-2, 32-2). Lubricants of higher viscosity grades VG > 32 always contain either branched PEs or the branched DiPEB9M7. Branched PEs are mainly applied with lubricants of VG ≤ 68, except for lubricant 80-2. For VG > 68 the branched DiPEB9M7 replaces the branched PEs.

For all polyol ester mixtures, the maximum deviation between the determined mixture and the commercial POEs are below 8% regarding viscosity and below 2.4 % regarding density. The highest maximum deviations in viscosity

Table 3.10: Composition of PE mixtures, AAD and MD between commercial lubricant and PE mixture.

ID	Target data source[a]	VG	Mole fraction x_i / %									Deviation / %				
		$\frac{mm^2}{s}$	PEC5	PEC7	PEC9	PEB5M2	PEB8E2	PEB9M355	DiPEC5	DiPEC7	DiPEB9M7	$\overline{AAD\|_{\tilde{\mu}}}$	$\overline{AAD\|_{\tilde{\rho}}}$	$\overline{AAD\|_{\tilde{M}}}$	$\overline{MD\|_{\tilde{\mu}}}$	$\overline{MD\|_{\tilde{\rho}}}$
22-1	Czu22	22	67.6	-	-	-	30.8	-	-	1.6	-	5.1	-	1.7	7.3	-
22-2	SEZ22	20	41.2	33.3	15.4	-	-	-	10.1	-	-	2.3	0.3	-	5.6	0.3
32-1	RL32-3	32	34.4	32.3	-	5.8	-	17.1	-	10.3	-	-	-	-	-	-
32-2	SEZ32	32	16.2	20.0	-	-	-	-	-	63.8	-	1.5	0.7	-	2.6	0.7
55-1	C55E	55	4.4	-	-	-	-	4.1	32.6	58.9	-	2.0	0.0	-	4.9	0.1
55-2	SE55	55	-	5.2	16.4	-	-	17.7	58.3	2.5	-	0.6	0.0	-	1.1	0.0
68-1	RL68H	68	-	-	13.9	-	-	19.7	47.7	18.8	-	4.6	2.3	0.6	5.6	2.3
68-2	SEZ68	68	-	-	18.9	-	-	-	-	65.8	15.4	1.0	1.7	-	1.6	1.8
80-1	C85E	80	-	-	-	-	-	-	-	80.7	19.3	2.4	0.2	-	6.0	0.3
80-2	SEZ80	82	-	-	10.1	17.3	-	18.7	30.5	-	23.5	0.8	0.0	-	1.6	0.0
100-1	SEZ100	100	-	-	-	-	-	-	-	71.7	28.3	3.4	1.9	-	7.3	2.0

a: c.f. Tables 3.8 & 3.9 for details on the commercial lubricants.

are observed for the polyol ester mixtures 22-1 (Czu22) and 100-1 (SEZ100). This emphasizes that the POEs contain polyol esters that are not among the considered PEs and DiPEs. For the POE Czu22, these are likely Trimethylolpropane esters that have a lower viscosity compared to PEs. For SEZ100, this is likely DiPEC9 instead of DiPEC7. This is also emphasized by the high maximum deviation in the density for lubricant 100-1. It is also possible that SEZ100 contains complex esters or viscosity index improving additives.

A high maximum deviation of the density can be observed also for lubricants 68-1 and 68-2. For lubricant 68-1, this can be related to the conflict of either optimizing the molecular weight or the density of the lubricant. Density and molecular weight of the commercial POE RL68H are obtained from different sources (see Table 3.8), what could be a reason for this conflict of optimization. Regarding lubricant 68-2 (SEZ68), it seems likely that it contains some DiPEC9 instead of DiPEC7 similar to SEZ100, because of the high deviation in density.

Figure 3.7 shows a comparison of the commercial POE viscosity and the mix-

ture viscosity of the determined polyol ester mixtures for varying temperature. The viscosity of commercial POE lubricants obtained from scientific literature (c.f. Table 3.8) is available at certain temperature levels and depicted with markers. In contrast, the viscosity data obtained from BOCK AND PUHL [35] is available in form of a continuous $\overline{\nu}$-T-curve and depicted with the dashed lines. The mixture viscosity of the determined polyol ester mixtures is depicted with the solid lines.

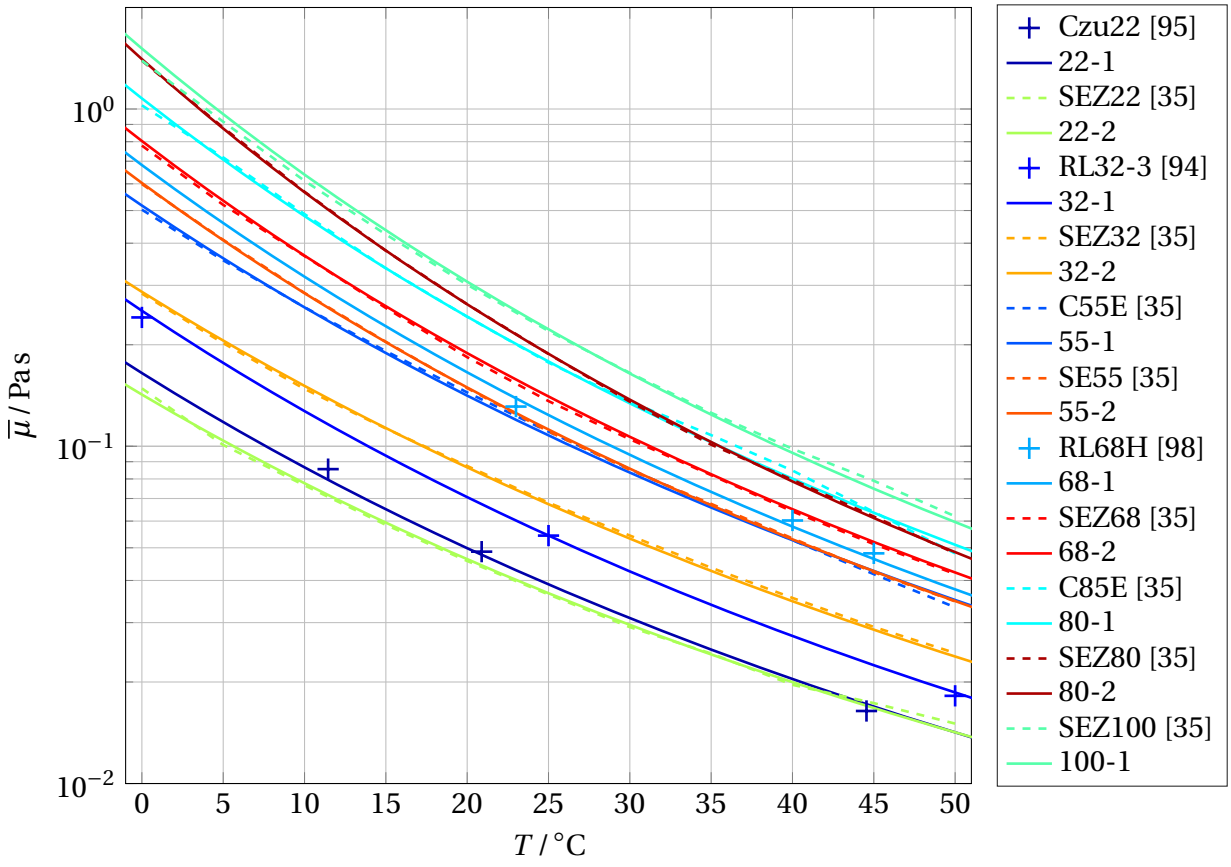

Figure 3.7: Comparison of dynamic viscosity $\overline{\mu}$ over temperature T of commercial lubricants and calculated polyol ester mixtures.

The viscosity of all polyol ester mixtures agrees well with the respective viscosity data of the commercial POEs. Only for lubricant 100-1 it can be observed that it shows a higher viscosity at low temperatures and a lower viscosity at high temperatures compared to the commercial POE SEZ100. This means that the polyol ester mixture 100-1 has a lower viscosity index compared to the

commercial POE SEZ100. This strengthens the hypotheses that a linear DiPE with a longer chain compared to DiPEC7 is present in the commercial POE SEZ100, as the VI increases with the chain length (see Section 2.2.2).

It can be concluded that density and viscosity of the calculated polyol ester mixtures agree well with the commercial lubricants. Improvements could be achieved especially for lubricants with a viscosity grade VG > 68, if DiPEC9 could be considered as a possible component. Unfortunately, no data on density or viscosity is available in literature for DiPEC9.

The compositions of PEs and DiPEs determined in this section are subsequently used in the modeling process of solubility and viscosity of refrigerant-lubricant mixtures.

4 Solubility of Refrigerant-Lubricant Mixtures

The amount of dissolved refrigerant has a strong influence on the density and viscosity of the liquid phase of the two-phase flow. This chapter aims to develop a predictive approach to model the mutual solubility of refrigerants and lubricants.

First of all, experimental results are presented in Section 4.1 to characterize the solubility of different combinations of refrigerants and lubricants and to present the influence of the process parameters on the solubility. Secondly, the state of the art in solubility modeling of refrigerant-lubricant mixtures is described in Section 4.2. Additionally, The PCP SAFT EoS is introduced, which is used to model the solubility in the present study. Missing elements to derive a predictive solubility model are deduced from the state of the art.

Subsequently, a predictive model for the solubility of refrigerant-lubricant mixtures is developed in Sections 4.3-4.5 based on the experimental solubility data. The model architecture is described in Section 4.3. The pure component parameters of PCP SAFT for refrigerants and lubricants are summarized in Section 4.4. To improve the accuracy in the prediction of the solubility, PCP SAFT contains a binary interaction parameter. In Section 4.5, correlations for this parameter are developed for the considered refrigerants and polyol esters to allow predictions of the solubility.

Finally, some example results for the solubility of refrigerants and polyol ester lubricants and for the density of the liquid phase are presented in Section 4.6.

4.1 Literature Data on Solubility of Binary Mixtures of Refrigerants and Pure Polyol Esters

The measurement data on the binary mutual solubility of refrigerants and pure PEs or DiPEs presented in this section form the basis for the modeling of the interaction of refrigerants and polyol esters. An overview on the publications investigating the solubility of refrigerants and pure polyol esters that are relevant for the present thesis can be found in Table 4.1.

Table 4.1: Overview of literature on binary solubility measurement.

		Refrigerant								
Polyolester		R32	R125	R134a	R1234yf	R1234ze	R290	R600a	R1270	R744
PEs	PEC4				[99]	[99]		[100]		[101]
	PEC5				[99]	[102]		[103]		[104]
	PEC6				[105]			[100]		[106]
	PEC7				[105]	[107]		[103]		[108]
	PEC8				[105]			[100]		[109]
	PEC9	[59]	[59]	[59]	[110]	[102]		[110]		[108]
	PEB5M2									[111]
	PEB6M2									[112]
	PEB7M2									[113]
	PEB6E2	[59]	[59]	[59]						[114]
	PEB8E2	[59]	[59]	[59]						[104]
	PEB9M355									
DiPEs	DiPEC5									
	DiPEC7									[115]
	DiPEB9M7									

The solubility of R744 (CO_2) is investigated for most of the polyol esters that are considered as components of the lubricant mixtures (see Table 2.3). Solubility data are only missing for PEB9M355, DiPEC5 and DiPEB9M7. For the HFOs R1234yf and R1234ze as well as for R600a (isobutane), solubility data are available for linear PEs. Literature data on the solubility of branched polyol esters with these lubricants were not found. For the HFCs R32, R125, and R134a, at least the solubility with one linear PE and two branched PEs was invest-

igated by WAHLSTRÖM AND VAMLING [59]. Significant gaps exist in data on the refrigerants R290 (propane) and R1270 (propene). Solubility data of these refrigerants could not be found for any of the considered PEs and DiPEs. Furthermore, the solubility of refrigerants in DiPEs requires further research.

To characterize the solubility of refrigerants and lubricants, some results of the experiments are depicted in Figure 4.1. Due to the very low vapor pressure of PEs and DiPEs (see Figure 2.7), the vapor phase consists nearly of pure refrigerant, whereas the liquid phase is a mixture of lubricant and refrigerant. Each sub-figure shows the vapor pressure p_v on the ordinate and the mole fraction of solved refrigerant in the liquid phase $x_{l,Ref}$ on the abscissa. The dashed lines depict Raoult's law.

The solubility measurements of R134a (Figure 4.1a) are limited to mole fractions of $x_{l,Ref} < 0.6$. For $T = 90°C$, the deviations to Raoult's law are negative for all data points. For $T = 50°C$, the deviations from Raoult's law are negative for low mole fractions, whereas there are some data points with positive deviations for higher mole fractions. Comparing the different polyol esters, it can be seen that the molecular structure of the lubricant does not exhibit a strong influence on the solubility. Nevertheless, the solubility is slightly higher for the branched PEs, which is indicated by a higher mole fraction of solved refrigerant $x_{l,Ref}$ for experiments at a similar pressure level p_v.

R1234yf shows positive deviations from Raoult's law for both depicted temperature levels and the complete range of compositions. FOUAD AND VEGA [116] relate this to the strong repulsive interactions as all fluorine atoms are placed on one side of the double bonded carbon atoms in the R1234yf molecule in contrast to its isomer R1234ze. For the lowest temperature in the dataset $T = 20°C$, the pressure approaches $x_{l,Ref} = 1$ nearly horizontally. This probably results in a global maximum in the vapor pressure for lower temperatures at $x_{l,Ref} < 1$, which implies a miscibility gap in the low temperature regime. The solubility is nearly independent of the PE chain length.

For $T = 10°C$, R744 (CO_2) shows large negative deviations from Raoult's law for refrigerant mole fraction $x_{l,Ref} < 0.8$. Close to the pure refrigerant $x_{l,Ref} = 1$, the deviation is positive. This emphasizes a maximum in the pressure curve in

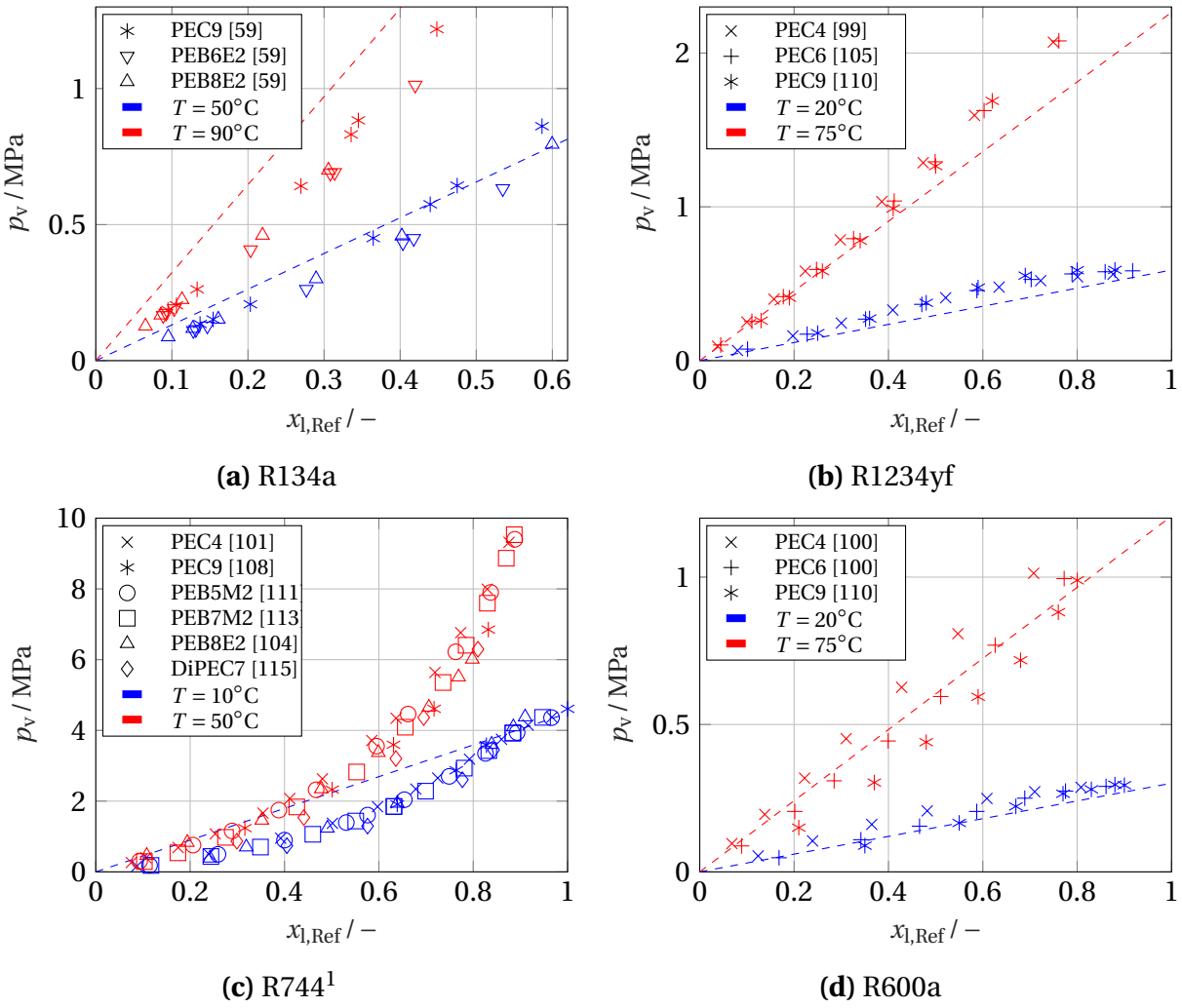

(a) R134a

(b) R1234yf

(c) R744[1]

(d) R600a

Figure 4.1: Solubility measurements of different refrigerants.

the region $0.9 < x_{\mathrm{l,Ref}} < 1$ and thus a miscibility gap. In fact, phase separation of R744 and PEC8 was observed in experiments of FEDELE ET AL. [109]. It was also predicted with the PC SAFT EoS for PEC8 by GARCÍA ET AL. [117] and for PEC7 and PEC9 by FANDIÑO ET AL. [108]. The influence of the molecular structure on the solubility is low.

For $T = 50°\mathrm{C}$, the solubility is slightly higher for molecules with longer chains. The solubility of the branched PEs is within the range of the linear PEs, so

[1] $T = 50°C$ is above the critical temperature of R744 (CO_2) of $T_{\mathrm{crit,R744}} = 304.13°C$ (Source: CoolProp [41]). Therefore, there is no defined vapor pressure of pure R744, which is required for Raoult's law. As a consequence, the line for Raoult's law in Figure 4.1c is missing for $T = 50°C$.

the number of molecules in the carboxylic acid seems to have a higher influence than the branching. The solubility of DiPEC7 is higher compared to the PEs. SUGII ET AL. [118] performed molecular dynamics simulations on the solubility of R744 and PEC6. They identified that the CO_2 molecules mainly interact with the double bonded oxygen atom of the carboxylic group. Additionally, there is unspecific sorption in the alkane tail region. In contrast to that, the distance distribution function of the core carbon atom of the PE molecule and CO_2 molecules is very low in the core region of the PE molecule (i.e. within the carboxylic groups). These findings explain the higher solubility in DiPEC7 compared to PEs and the higher solubility of longer chain PEs.

In contrast to the other refrigerants, the measurements for R600a (isubutane) show a strong influence of the chain length of the alkyl group in the PE molecule on the solubility. The solubility rises with increasing chain length. This shows that there is a stronger interaction of the unpolar isobutane molecules with the alkyl group of the carboxylic acid compared to the polar COO group of the PE molecule.

The comparison of the different phase diagraphs in Figure 4.1 shows that a powerful model is required to capture the different phenomenology of the solubility for various refrigerants.

4.2 State of the Art in Modeling the Mutual Solubility of Refrigerants and Lubricants

This section analyzes the solubility modeling of refrigerant-lubricant mixtures in literature. The fundamentals on solubility modeling are introduced in Section 4.2.1. Different modeling approaches are presented. The model used in the present study is based on the *Perturbated Chain Associating Fluid Theory* of GROSS AND SADOWSKI [119]. The PC SAFT is introduced in Section 4.2.2. The literature on solubility modeling of refrigerant-lubricant mixtures with PC SAFT is presented in Section 4.2.3. Based on the literature review, the need for enhancements on the state-of-the-art in modeling to create a predictive model is described.

4.2.1 Principles of Solubility Modeling

This section introduces the basic concepts of solubility modeling. Possible approaches are briefly summarized. In physical models, the basis of mutual solubility modeling is the equality of the chemical potential of two phases in equilibrium. For a liquid and a vapor phase in equilibrium, this means that the fugacity ψ of a component i in both phases is equal [91, p.204], as described in Equation (4.1).

$$\psi_{\mathrm{v},i} = \psi_{\mathrm{l},i} \tag{4.1}$$

With the definition of the fugacity coefficient $\varphi_i = \psi_i / p_i = \psi_i / (x_i p)$ and the partial pressure p_i of component i, Equation (4.2) for the isofugacity of component i in the phases is derived [120, p.11].

$$x_{\mathrm{v},i}\, p \varphi_{\mathrm{v},i} = x_{\mathrm{l},i}\, p \varphi_{\mathrm{l},i} \tag{4.2}$$

In addition to the isofugacity equations (4.2) for each component, the system of equations of the solubility model contains the summation of the mole fractions of the vapor and liquid phase, respectively. If each phase consists of n components, the summation can be written according to Equation (4.3).

$$\sum_{i=1}^{n} x_{\mathrm{v|l},i} = 1 \tag{4.3}$$

The fugacity of vapor and liquid phase can be calculated in two different ways [97, 121]:

- In the $\varphi - \varphi$ approach, the fugacity coefficient is calculated with a thermal equation of state (EoS). An EoS represents the relationship between temperature, pressure and volume of a mixture for a certain composition [91]. Often applied EoS for the solubility of refrigerant-lubricant mixtures are the *Peng-Robinson* (PR) EoS [122] and the *Soave-Redlich-Kwong* (SRK) EoS [123]. Both, the PR and SRK EoS are based on the *Van der Waals* EoS [122, 123].

  Especially in the more recent literature, the PC SAFT EoS is applied for refrigerant-lubricant mixtures. The PC SAFT model incorporates three

model parameters for each component. The PC SAFT EoS is based on statistical mechanics [120]. It is explained in more detail in Section 4.2.2.

Mixture laws are required for all mentioned EoS to determine the respective model parameters for mixtures.

With the established relationship between volume, pressure and temperature of the mixture in the EoS, the fugacity coefficient of component i is calculated for both liquid and vapor phase according to Equation (4.4) [91, p.142].

$$\ln \varphi_i = \int_0^p \frac{V_{\mathrm{m},i}}{RT} - \frac{1}{p} \mathrm{d}p \tag{4.4}$$

- In the $\gamma - \varphi$ approach, the fugacity coefficient of the vapor phase is calculated with an EoS. The fugacity coefficient of the liquid phase is determined with an activity coefficient model. The activity coefficient γ_i is defined as the ratio of the fugacity coefficient φ_i of component i in a mixture and the fugacity coefficent of the pure substance $\varphi_{0,i}$. Equation (4.2) is then modified to Equation (4.5) [91, p.205].

$$x_{\mathrm{v},i}\, p \varphi_{\mathrm{v},i} = \gamma_i x_{\mathrm{l},i}\, p \varphi_{\mathrm{l},0,i} \tag{4.5}$$

The advantage of this equation is that the fugacity coefficient of the pure component $\varphi_{\mathrm{l},0,i}$ can be obtained, e.g. using an EoS or tabulated data. The activity coefficient can be calculated with a partial derivative of the excess Gibb's free enthalpy $\overline{G}_{\mathrm{m}}^{\mathrm{E}}$ with respect to the mole fractions x_i according to Equation (4.6) [91, p.176f].

$$RT \ln \gamma_i = \overline{G}_{\mathrm{m}}^{\mathrm{E}} - \sum_{k \neq i} x_k \left. \frac{\partial \overline{G}_{\mathrm{m}}^{\mathrm{E}}}{\partial x_k} \right|_{T,p,x_{j \neq k}} \tag{4.6}$$

The Gibb's free enthalpy $\overline{G}_{\mathrm{m}}$ of a mixture can be calculated according to Equation (4.7) [91, p.173].

$$\overline{G}_{\mathrm{m}} = \underbrace{\sum_i \eta_{0,i} x_i + RT \sum_i x_i \ln x_i}_{\overline{G}_{\mathrm{m}}^{\mathrm{id}}} + \underbrace{RT \sum_i x_i \ln \gamma_i}_{\overline{G}_{\mathrm{m}}^{\mathrm{E}}} \tag{4.7}$$

In this equation, $\eta_{0,i}$ represents the chemical potential of the pure component i and γ_i the activity coefficient of the component i. The excess

Gibb's free enthalpy $\overline{G}_{\mathrm{m}}^{\mathrm{E}}$ denotes the deviation from an ideal solution. It can be calculated with different empirical approaches, e.g. of *Flory-Huggins* [124] or *Wilson* [125]. A comprehensive overview on approaches to calculate the excess Gibb's free enthalpy $\overline{G}_{\mathrm{m}}^{\mathrm{E}}$ can be found in STEPHAN AND MAYINGER [91](p.179ff).

In the following, the mutual solubility of refrigerant-lubricant mixtures is modeled with the $\varphi - \varphi$ approach. The PC SAFT EoS is used to determine the fugacity coefficient φ. The reasons to follow this approach are summarized in the following.

Different criteria are considered in the selection of the modeling approach. To fulfill the aims of this study, it is necessary that the model allows predictions of the solubility of refrigerant-lubricant mixtures on the basis of the available solubility measurements in literature. Furthermore, the model should have a high accuracy and a low complexity.

In the following, it is assessed whether the PC SAFT model fulfills the criteria mentioned above.

- **Development of a predictive model:**
  For the PC SAFT EoS, correlations were developed for the model parameters of branched and linear polyol esters by RAZZOUK ET AL. [16]. This allows to estimate the model parameters of a polyol ester, if they are not available in literature. Similar correlations for the model parameters of the PR or SRK EoS were not found in literature.

  Additionally, GARCÍA ET AL. [117] and FOUAD AND VEGA [116] developed correlations for the interaction parameter of refrigerants and lubricants. Even though these correlations do not cover the complete range of polyol esters used in the present thesis, the publications show that the development of correlations for the binary interaction parameter of the PC SAFT EoS is possible. This improves the accuracy of the predictive model.

  The advantage of the PC SAFT EoS in comparison to SRK or P-R is that the pure component parameters do not depend on the critical properties which are not reported for polyol esters.

- **Accuracy:**
  MONSALVO [126] and CZUBINSKI ET AL. [95] compared experimental solubility data to results of the PC SAFT and the PR EoS, respectively. The PC SAFT EoS showed a slightly better AAD to the experimental data compared to the PR EoS in both publications.
- **Complexity:**
  Van der Waals type EoS as the PR or SRK EoS are much less complex than the PC SAFT EoS.

In a nutshell, the PC SAFT EoS fulfills the requirements for a predictive solubility model, whereas this is unclear for other EoS as PR or SRK. The higher complexity compared to a *Van der Waals* type EoS is accepted.

4.2.2 Perturbated Chain Statistical Associating Fluid Theory

The development of the PC SAFT EoS aimed to improve the description of macro-molecular substances with high molecular weights, e.g. polymers [120]. Furthermore, it can be applied also to other substances, as e.g. gases with a small, spherical molecular shape, or solvents. It facilitates a high accuracy in the prediction of thermodynamic state variables and phase equilibria of single substances and mixtures [119].

In the following, the basic concept of the PC SAFT EoS is introduced. For details, it is referred to GROSS [120] and GROSS AND SADOWSKI [119]. The basis of the PC SAFT EoS is an expression for the Helmholtz free energy F according to Equation (4.8).

$$F(T, V_\mathrm{m}, x_{1\ldots n}) = F^\mathrm{id}(T, V_\mathrm{m}, x_{1\ldots n}) + F^\mathrm{res}(T, V_\mathrm{m}, x_{1\ldots n}) \tag{4.8}$$

The Helmholtz free energy F is a thermodynamic potential. Describing the thermodynamic potential in form of a fundamental relation[2] $F = f(T, V, x_{1\ldots n})$ enables the user to calculate all other thermodynamic state variables with partial derivations [91, p. 26]. For details, refer to GROSS [120, p. 7ff]. The ideal

[2] In this context, the term "Equation of state" for PC SAFT appears to be imprecise. However, it is the term exclusively used in literature. Therefore, it is adopted in the following in connection with PC SAFT.

gas contribution of the Helmholtz potential $F^{\mathrm{id}}(T, V_{\mathrm{m}}, x_{1\ldots n})$ is described with the thermal and caloric equation of state of the ideal gas. In the context of PC SAFT, the residual Helmholtz free energy $F^{\mathrm{res}}(T, V_{\mathrm{m}}, x_{1\ldots n})$ is modeled based on statistical mechanics with different contribution terms according to Equation (4.9) [43, 120].

$$F^{\mathrm{res}} = F^{\mathrm{res}}_{\mathrm{hc}} + F^{\mathrm{res}}_{\mathrm{disp}} + F^{\mathrm{res}}_{\mathrm{dp}} \tag{4.9}$$

The original version of the PC SAFT EoS by GROSS AND SADOWSKI [119] comprised only the repulsive and attractive contribution terms $F^{\mathrm{res}}_{\mathrm{hc}}$ and $F^{\mathrm{res}}_{\mathrm{disp}}$, respectively. Later, different approaches (e.g. GROSS AND VRABEC [43] or DOMINIK ET AL. [127]) aimed to extend the model to polar substances with an additional dipole contribution term to the residual Helmholtz energy $F^{\mathrm{res}}_{\mathrm{dp}}$.

The modeling of the contribution terms of Equation (4.9) is described in the following in more detail.

Hard Chain Contribution Term

The repulsive contribution to the residual Helmholtz potential $F^{\mathrm{res}}_{\mathrm{hc}}$ in Equation 4.9 is modeled as a hard chain according to the SAFT concept of CHAPMAN ET AL. [128]. The hard chain is defined as a system of associating spheres with a number of m segments as depicted in Figure 4.2a.

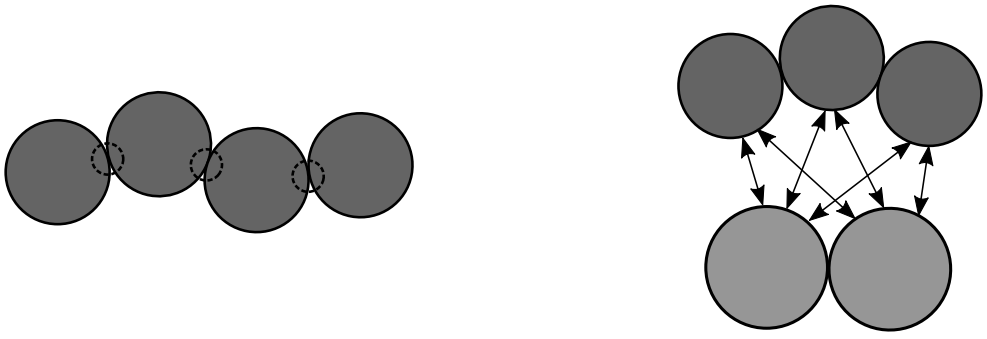

(a) Hard chain in the SAFT concept. Adapted from [120].

(b) Attraction between different chains as summation of all segment to segment interactions. Adapted from [120].

Figure 4.2: Concept of modeling in PC SAFT equation of state.

The spheres are connected irreversibly at two defined bonding spots at each segment. A square well potential function modified with soft repulsion is used to calculate the temperature dependent effective collision diameter [120]. In Figure 4.3, the potential u is depicted as a function of the radial distance r between two uniform segments.

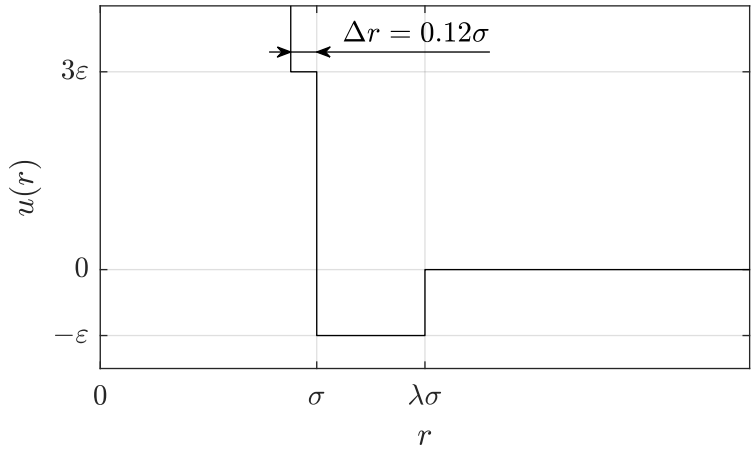

Figure 4.3: Square well potential with soft repulsion of the PC SAFT EoS.

The segment diameter σ and the depth of the potential well ε are introduced as model constants. The soft repulsion of molecules is represented as a step in the potential function with a width of $\Delta r = 0.12\,\sigma$. The width of the potential well is set to $\lambda = 1.4$. [119]

Dispersive Contribution Term

The attractive contributions to the residual Helmholtz potential in Equation (4.9) are collected in a dispersive term $F^{\text{res}}_{\text{disp}}$ [119]. They are modeled as perturbations to the hard chain reference system with the perturbation theory of BARKER AND HENDERSON [129, 130]. GROSS AND SADOWSKI [119] extended the theory from spherical molecules to chain molecules. Consequently, molecules are modeled as chains of spherical segments that show attractive interactions with other chains. The interaction is calculated with a summation of all segment-segment interactions, as depicted in Figure 4.2b. Resulting integrals in the attractive contribution are substituted by power laws to reduce the model complexity. The introduced model constants are fitted to vapor pressure data of n-alkanes. The segment number m of methane was

set to $m = 1$. The resulting model constants are considered universal. Thus, only three model parameters remain: the segment number m, the segment diameter σ and the depth of the square well potential ε.[119]

Dipole Contribution Term

Some refrigerants show a high dipole moment. To consider dipole moments in the solubility modeling, an extension to the PC SAFT EoS of GROSS AND SADOWSKI [119] is required. GROSS AND VRABEC [43] developed a dipole contribution term to the residual Helmholtz potential $F_{\mathrm{dp}}^{\mathrm{res}}$ in Equation (4.9) based on a third-order perturbation theory. Model constants are adjusted to vapor-liquid equilibrium data of molecular simulations. The approach enables the user to apply literature data of dipole moments instead of introducing a new model parameter. The resulting EoS was called PC Polar SAFT or PCP SAFT. If a component without dipole moment ($\iota = 0\,\mathrm{D}$) is used, the dipole contribution vanishes and the PCP SAFT EoS is identical to the PC SAFT EoS.

DOMINIK ET AL. [127] compared two different dipole contribution terms for the PC SAFT EoS. They selected the contribution term of JOG AND CHAPMAN [131], as it leads to physically meaningful polar parameters. This approach was used by FOUAD AND VEGA [116] to model the solubility of low GWP refrigerants in different PEs.

In the present thesis, the PC polar SAFT approach of GROSS AND VRABEC [43] is implemented, as the publication on the Polar PC SAFT EoS of DOMINIK ET AL. [127] lacks some details on how the pure fluid integrals are calculated.

Mixture Laws for Model Parameters

A mixture of different components means that chains of different length, segment size and potential interact. Mixture rules have to be used for the model constants σ and ε to describe the potential well (see Figure 4.3) for the segment-segment interaction of a component i with a component j. GROSS [120] implemented the *Berthelot-Lorentz* combination rules (Equations (4.10) and (4.11)) for the PC SAFT EoS.

$$\sigma_{ij} = \frac{1}{2}(\sigma_i + \sigma_j) \tag{4.10}$$

$$\varepsilon_{ij} = \sqrt{\varepsilon_i \varepsilon_j}(1 - k_{ij}) \tag{4.11}$$

Equation (4.11) contains the binary interaction parameter k_{ij}. It can be adjusted with experimental vapor pressure data of the binary mixture to reduce the deviation between experimental and calculated results. [120]

4.2.3 Modeling of Refrigerant-Lubricant Mixtures with the PCP SAFT EoS

In this section, the required steps to develop a predictive model for the solubility of refrigerants and lubricants based on the PCP SAFT EoS are deduced from the relevant literature in the field. The section is divided in four parts. First, the pure component parameters of the PCP SAFT EoS of refrigerants determined in literature are discussed. Secondly, the determination of the pure component parameters of polyol esters in literature is presented. Thirdly, existing correlations for the binary interaction coefficient k_{ij} are presented. Finally, the architecture of solubility models based on the PC SAFT or PCP SAFT EoS is analyzed.

Model Parameters of Refrigerants

Refrigerants are modeled in different publications with approaches based on PC SAFT. Parameters of many refrigerants, especially natural refrigerants, have already been determined in different publications. GROSS AND SADOWSKI [119] determined the parameters of R744 (CO_2) and the HC refrigerants R290, R600a, and R1270. VINŠ AND HRUBÝ [132] determined the model parameters for HFCs R32 and R125 for the PCP SAFT EoS that is also used in the present study. FOUAD AND VEGA [116] determined the model parameters of HFOs R1234yf and R1234ze for the slightly different Polar PC SAFT EoS of DOMINIK ET AL. [127] (see Section 4.2.2). MONSALVO [126] determined the model parameters of R134a for the original PC SAFT EoS of GROSS AND SADOWSKI [119] without modeling the influence of the dipole moment in a special contribution term to the residual Helmholtz energy (see Equation (4.9)).

Model parameters of the PCP SAFT EoS of GROSS AND VRABEC [43] applied in the present study were not found in literature for R134a, R1234yf, and R1234ze. Consequently, the model parameters of these refrigerants must be calculated in the present thesis. The calculation and the obtained results are described in Section 4.4. For a better overview of the model parameters of all used substances, the parameters taken from literature are also listed in Table 4.3 of Section 4.4.

Model Parameters of Polyol Esters

In the literature on PC SAFT modeling of PEs [16, 72, 115–117, 133] dipole or quadrupole moments of PEs are not considered, although the HOO-groups connecting the alcohol and the ester acid for themselves exhibit a strong dipole moment. Therefore, the PC SAFT parameters calculated in literature can also be used in the PCP SAFT EoS with a dipole moment of $\iota = 0\,\mathrm{D}$. Regarding PEs, RAZZOUK ET AL. [16] calculated the PC SAFT Parameters of PEC5, PEC7, PEC9 and PEB8E2 based on measured vapor pressures (see Section 2.2.4). Analogously, GARCÍA ET AL. [72] determined the PC SAFT parameters of DiPEC5, DiPEC7 and DiPEB9M7.

RAZZOUK ET AL. [16] developed correlations for the segment number m, segment diameter σ and square well potential depth ε for PEs. These correlations make it possible to estimate the model parameters for PEs, even if vapor pressure data of the PEs are not available in literature. Thus, these correlation are crucial to develop a predictive model for the mutual solubility of refrigerants and lubricants. The correlations for the respective model parameters are depicted in Figure 4.4. The figure shows the linear correlations of the respective model parameters over the molecular weight of the PEs. The model parameters determined by RAZZOUK ET AL. [16] with vapor pressure data are depicted with markers. For the correlations of the linear PEs, the model parameters were regressed to a linear polynomial. These correlations are depicted with the solid lines. The only branched PE evaluated by RAZZOUK ET AL. [16] is PEB8E2. For the correlations of branched PEs depicted with the dashed lines, RAZZOUK ET AL. [16] used the slope of the linear PEs and the calculated value of PEB8E2. This is a rough assumption. Additionally, it does not allow to distinguish between different structural isomers (e.g. PEB5M2 and PEB5M3). The

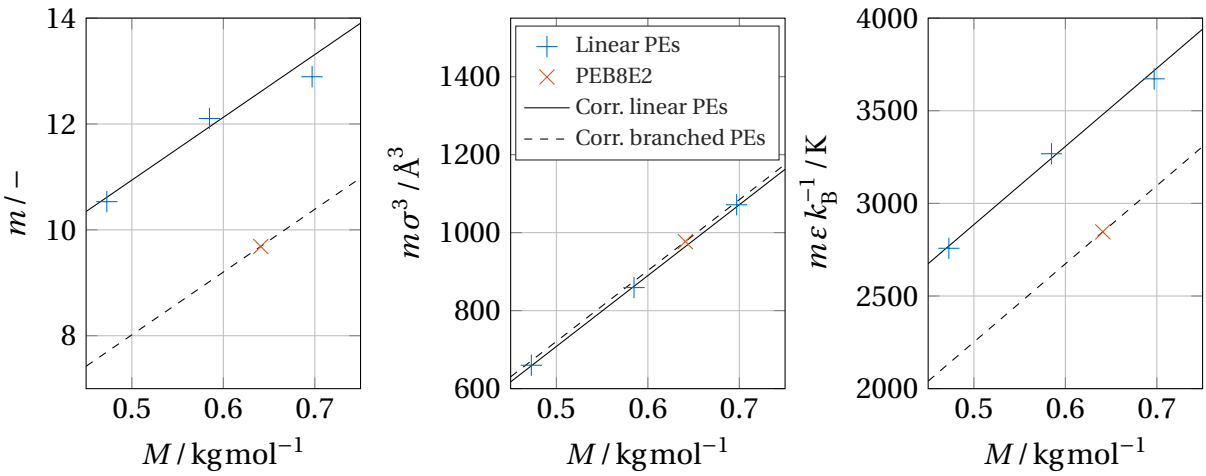

(a) Segment number m. **(b)** Segment diameter σ. **(c)** Potential depth ε.

Figure 4.4: Correlation of pure component PC SAFT parameters according to RAZZOUK ET AL. [16].

validity of this assumption is examined in the present study with a comparison of the experimental liquid density to the predicted values with the PC SAFT EoS in Section 4.4. For a better overview of the model parameters of all used substances, the values of the model parameters are listed in Section 4.4.

Binary Interaction Parameter k_{ij}

The binary interaction parameter k_{ij} is calculated with the experimental vapor pressure data of a binary mixture. Regarding mixtures of refrigerants and pure PEs or DiPEs, different publications developed correlations for the binary interaction parameter k_{ij}. GARCÍA ET AL. [117] developed correlations for R744 (CO_2) and linear as well as branched PEs. They considered k_{ij} as depending only on the molecular weight and not on temperature, according to Equation (4.12).

$$k_{ij} = a_1 + a_2 M \tag{4.12}$$

Later, FOUAD AND VEGA [116] continued this work for different low-GWP refrigerants and linear PEs. They concluded that the accuracy of the model is increased significantly for the HFOs R1234yf and R1234ze using an temperature dependent value of k_{ij}, according to Equation (4.13).

$$k_{ij} = a_1 + a_2 M + a_3 T \tag{4.13}$$

The open points to derive correlations for the binary interaction parameter k_{ij} are summarized in the following:

- FOUAD AND VEGA [116] used the Polar PC SAFT EoS of DOMINIK ET AL. [127]. Thus, the correlations have to be adjusted to the PCP SAFT EoS of GROSS AND VRABEC [43] used in the present study.
- Correlations for branched PEs and DiPEs have to be developed, as well, because these polyol esters are considered in the present thesis.
- Correlations for HC refrigerants R290 (propane) and R1270 (propene) were not found in literature and need to be developed.
- The recalculation of the correlations offers the possibility to consider more recent solubility measurements of refrigerants and PEs than the respective publications of GARCÍA ET AL. [117] and FOUAD AND VEGA [116].

Correlations for the binary interaction parameter are developed in Section 4.5.

Model Architecture

In literature, lumped parameter models have been used so far for solubility modeling of refrigerant and commercial polyol ester lubricants with equations of state based on the PC SAFT EoS. In these lumped parameter approaches, the lubricant is considered as a single component. The PC SAFT parameters of the lubricant are determined with an estimated molecular weight of the commercial lubricant.

RAZZOUK ET AL. [16] estimated the molecular weight of 15 commercial polyol esters based on their viscosity at 40°C and the correlation of EYCHENNE AND MOULOUNGUI [69]. Subsequently, they determine the PC SAFT parameters with the correlations depicted in Figure 4.4 and compared the calculated density of the polyol esters to data from experiments or manufacturers. They conclude that the correlation for branched PEs leads to better results. Nevertheless, deviations are high compared to the difference in density of the linear PEs (see Section 2.2.1). Additionally, this approach is only an option for low

viscosity grades VG < 32 that contain a high degree of linear PEs. A high degree of branched PEs or DiPEs would lead to an overprediction of the PC SAFT parameters. To overcome this issue, a correlation for the viscosity of branched PEs would be required. Based on currently available data, developing such correlations would be very difficult as shown in Section 2.2.2.

GARCÍA ET AL. [117] and FOUAD AND VEGA [116] compared the PC SAFT predictions on the solubility of R744 (CO_2) in commercial polyol esters with experiments from BOBBO ET AL. [134]. Both implemented a similar approach: They used the molecular weight of the polyol esters estimated by BOBBO ET AL. [134] to determine the PC SAFT parameters with the correlations of RAZZOUK ET AL. [16]. The binary interaction parameter with R744 (CO_2) was determined with the correlations of the respective authors (see Figure 4.5a). In both publications it was found that the lumped parameter model leads to accurate results in the prediction of the solubility. This is not astonishing as the influence of the lubricant structure on the solubility is low for R744 (CO_2) (see Figure 4.1c). Problems are expected when the composition of the lubricant plays a more important role for the solubility. This is the case for the hydrocarbon R600a (isobutane) (see Figure 4.1d).

Additionally, it must be highlighted that GARCÍA ET AL. [117] considered lubricants with a VG of 32. FOUAD AND VEGA [116] considered lubricants with VG 32, 46, and 68. The molecular weight of these lubricants was estimated by BOBBO ET AL. [134]. The estimated molecular weights are in a range of $554\,\mathrm{g\,mol^{-1}} \leq M \leq 634\,\mathrm{g\,mol^{-1}}$ and, thus, in the range of pentaerythritol esters. If lubricants of higher viscosity grades are considered, which contain a significant amount of DiPEs, the correlations cannot lead to accurate results as they are made for linear and branched PEs. For example, the lubricant RL68H has a molecular weight of $M = 765\,\mathrm{g\,mol^{-1}}$ (see Table 3.8). The molecular weight of this lubricant is higher compared to the the molecular weight of PEC9 ($M_{\mathrm{PEC9}} = 696.4\,\mathrm{g\,mol^{-1}}$). This means that the lubricant contains a significant amount of DiPE. The PC SAFT parameters would be over predicted using the correlation of RAZZOUK ET AL. [16].

Consequently, a different approach is required in the study at hand. This approach is described in Section 4.3.

4.3 Model Architecture

This section and the following Sections 4.4 and 4.5 describe the development of the predictive solubility model. In this section, the model architecture used in the present study is briefly described. In the following sections, the model parameters of the pure components (Section 4.4) and correlations for the interaction of refrigerants and lubricants (Section 4.5) are introduced.

In the thesis at hand, an approach is pursued that exploits the potential of the PC SAFT EoS. The PC SAFT EoS is made for multi-component mixtures from its origins [119]. This is not only beneficial for mixtures of polyol esters, but also for refrigerant mixtures as R410A, which is a nearly azeotropic blend of refrigerants R125 and R32, each with a mass fraction of $w_{\mathrm{Ref}} = 0.5$ [26].

The PC SAFT parameters and the binary interaction parameters are stored in matrices with dimensions of n x n, with n being the number of components of the mixture: $n = n_{\mathrm{Ref}} + n_{\mathrm{Lub}}$. The binary interaction parameters of similar components (i.e. between different PEs or DiPEs on the one hand and between different refrigerants on the other hand) are set to $k_{ij} = 0$.

The equations of PC SAFT as detailed in GROSS AND SADOWSKI [119, 135] were implemented in Matlab® by the author. The equation system consisting of the isofugacity of each component (Equation (4.2)) of the different phases and the summation of the mole fractions in the different phases (Equation (4.3)) is solved with the Matlab® non-linear least squares solver *lsqnonlin*. It is assumed that the composition of the lubricant in the liquid phase remains equal. This assumption is reasonable as non of the polyol ester components is enriched in the vapor phase, which consists nearly of pure refrigerant.

4.4 PCP SAFT Model Parameters of Pure Components

In the following, the model parameters of the pure components are introduced.

Refrigerants

The calculation of the PCP SAFT parameters of the polar refrigerants R134a, R1234yf, and R1234ze is described in this section. The PC SAFT parameters of the natural refrigerants R290, R600a, R744, and R1270 are adopted from GROSS AND SADOWSKI [119] and the PCP SAFT parameters for R32 and R125 from VINŠ AND HRUBÝ [132]. Vapor pressure and the density of liquid and vapor phase are obtained from *REFPROP* [42] in a range of $240\,\mathrm{K} \leq T \leq 350\,\mathrm{K}$. The values of the PCP SAFT parameters are determined with the *lsqnonlin* algorithm of Matlab®.

Polyol Esters

The PC SAFT parameters of PEC5, PEC7, PEC9, and PEB8E2 were calculated by RAZZOUK ET AL. [16] with vapor pressure data of the PEs. Analogously, GARCÍA ET AL. [72] determined the parameters of DiPEC5, DiPEC7, and DiPEB9M7. The parameters of these polyol esters are adopted in the present thesis. The parameters of the remaining PEs, PEB5M2 and PEB9M355, are calculated with the correlation of RAZZOUK ET AL. [16] depcited in Figure 4.4.

To check, if the assumption on branched PEs in RAZZOUK ET AL. [16] is valid, the experimental density data of PEs (see Table B.2) are compared to the calculated density with the PC SAFT EoS. For PEC5, PEC7, PEC9, PEB8E2, and the DiPEs, the model parameters calculated with vapor pressure data of the PEs were adopted. For all other PEs, the model parameters were calculated with the correlation of RAZZOUK ET AL. [16]. The results are collected in Table 4.2. The rows of the PEs and DiPEs that are modeled with parameters resulting from vapor pressure data are highlighted in gray.

The table shows that the maximum deviations MD are not higher if the model parameters are derived from the correlation of RAZZOUK ET AL. [16] (white rows) compared to the model parameters calculated with vapor pressure data

Table 4.2: Deviation of compressed liquid density between values predicted with the PC SAFT EoS and experimentally determined values.

Lubricant	Authors	n[a] -	AAD %	Bias %	MD %
PEC3	KISHORE AND SHOBHA [46]	11	1.23	1.23	1.79
PEC4	FEDELE ET AL. [55]	40	0.51	-0.07	1.35
	KISHORE AND SHOBHA [46]	12	0.18	0.05	0.4
PEC5	FANDIÑO ET AL. [52]	99	0.92	0.91	2.11
	FEDELE ET AL. [55]	40	0.61	-0.45	1.74
	KISHORE AND SHOBHA [46]	12	0.33	-0.30	0.70
PEC6	FEDELE ET AL. [55]	40	0.60	-0.43	1.67
	LIN AND KEDZIERSKI [57]	24	0.23	-0.03	0.60
PEC7	FANDIÑO ET AL. [53]	99	0.99	0.97	2.30
	FEDELE ET AL. [55]	40	0.55	-0.24	1.53
	KISHORE AND SHOBHA [46]	12	0.49	-0.24	0.88
PEC8	FEDELE ET AL. [55]	40	0.55	-0.27	1.48
	KISHORE AND SHOBHA [46]	12	0.45	-0.45	0.66
PEC9	FANDIÑO ET AL. [53]	88	0.76	0.52	1.99
	KISHORE AND SHOBHA [46]	12	0.49	-0.49	0.66
	WAHLSTRÖM AND VAMLING [59]	10	0.07	-0.01	0.15
PEC10	KISHORE AND SHOBHA [46]	10	0.60	-0.60	0.83
PEB5M2	FEDELE ET AL. [48]	48	0.32	-0.06	0.89
PEB6M2	FEDELE ET AL. [48]	48	0.55	0.53	1.23
PEB7M2	FEDELE ET AL. [48]	48	0.51	0.48	1.21
PEB6E2	WAHLSTRÖM AND VAMLING [59]	10	0.67	-0.67	0.92
PEB8E2	FANDIÑO ET AL. [51]	99	1.47	1.45	3.43
	WAHLSTRÖM AND VAMLING [59]	10	0.41	-0.41	0.57
DiPEC5	FANDIÑO ET AL. [54]	70	2.47	2.47	4.55
DiPEC7	FANDIÑO ET AL. [54]	70	1.68	1.68	3.59
DiPEB9M7	HARRIS [56]	11	1.26	1.26	1.95

a: n is the number of experimental data points.

(gray rows). Additionally, the maximum deviations of branched PEs are not higher compared to linear PEs. Thus, the assumptions made for the slope of the model parameters of branched PEs in the correlation of RAZZOUK ET AL. [16] can be considered as valid to describe branched PEs. Astonishingly, PEB8E2 shows the highest maximum deviation among all PEs, although it is the only branched PE with PC SAFT parameters calculated from vapor pres-

sure data. The reason is that the deviations increase with rising pressure comparing the calculated density values of the PC SAFT EoS with the experimental data of FANDIÑO ET AL. [51]. For atmospheric pressure, the density is predicted accurately with MD = 0.44%. Furthermore, elevated deviations can be observed for the DiPEs. The deviations of the DiPEs calculated in the present study agree with the deviations calculated by GARCÍA ET AL. [72].

The PC SAFT parameters of the fluids used in this thesis are collected in Table 4.3.

Table 4.3: Pure component PC SAFT parameters.

Fluid		M	m	σ	$\varepsilon\, k_B^{-1}$	Source	ι	Source
		$g\,mol^{-1}$	-	Å	K		D	
HFCs	R32	52	2.472	2.797	161.7	[132]	1.978	[136]
	R125	120	3.147	3.120	153.7	[132]	1.563	[136]
	R134a	102	3.262	3.002	162.1	-	2.058	[137]
HFOs	R1234yf	114	2.834	3.364	168.2	-	2.24	[138]
	R1234ze	114	3.294	3.165	171.2	-	1.13	[138]
HCs	R290	44	2.002	3.618	208.1	[119]	0	
	R600a	58	2.262	3.757	216.5	[119]	0	
	R1270	42	1.96	3.536	207.2	[119]	0	
CO_2	R744	44	2.073	2.785	169.2	[119]	0	
PEs	PEC5	472	10.53	3.972	261.8	[16]	0	
	PEC7	584	12.10	4.141	270.0	[16]	0	
	PEC9	696	12.89	4.364	284.8	[16]	0	
	PEB5M2	472	7.699	4.435	277.7	Corr.	0	
	PEB6M2	528	8.352	4.522	283.9	Corr.	0	
	PEB7M2	584	9.016	4.594	289.2	Corr.	0	
	PEB6E2	528	8.352	4.522	283.9	Corr.	0	
	PEB8E2	640	9.686	4.655	293.9	[16]	0	
	PEB9M355	696	10.35	4.705	297.7	Corr.	0	
DiPEs	DiPEC5	759	20.28	3.682	230.8	[72]	0	
	DiPEC7	927	24.64	3.770	240.4	[72]	0	
	DiPEB9M7	1096	19.51	4.353	250.5	[72]	0	

Corr.: Calculated with correlation of RAZZOUK ET AL. [16] for branched PEs.

4.5 Correlation for the Binary Interaction Parameter k_{ij}

In this section, correlations for the binary interaction parameter k_{ij} of Equation (4.11) are derived. In Section 4.5.1, the values for the binary interaction parameter k_{ij} are calculated based on the measurement data of refrigerants and polyol esters introduced in Section 4.1. The linear approach in temperature and molecular weight of Equation (4.13) is used to model the obtained vales of k_{ij}. The binary mixture data are not available for all required combinations of refrigerants and lubricants. Therefore, the parameters of Equation (4.13) are regressed to solubility data of refrigerants with commercial lubricants for the missing combinations of refrigerants and lubricants in Section 4.5.2. Here, the mixture of refrigerant and commercial POE is considered as a multi-component mixture of the refrigerant(s) and different PEs and DiPEs.

4.5.1 Binary Mixtures of Refrigerants and Pure Polyol Esters

In the following, correlations for the binary interaction parameter k_{ij} in Equation (4.11) are developed based on the available solubility measurements between refrigerants and linear and branched PEs, respectively (c.f. Table 4.1).

Correlations for the binary interaction parameter k_{ij} are determined in the following in three steps:

1. The binary interaction parameter k_{ij} is regressed against the values of every isotherm of the solubility measurements for each combination of polyol ester and refrigerant. The objective function of the optimization is the AAD of calculated and measured vapor pressure p_{v} at different mole fractions of the refrigerant x_{Ref}. The optimization is performed with the Matlab® solver *fmincon*.
2. The parameters a_1, a_2, and a_3 of Equation (4.13) are fitted to the values of k_{ij} for all isotherms and all branched and linear PEs, respectively.

3. The vapor pressure p_v in phase equilibrium is computed with the modeling approach described in Section 4.3 considering the correlation for the binary interaction parameter k_{ij} in Equation (4.13). The deviation to the experimental vapor pressure data is calculated.

The calculated parameters a_1, a_2, and a_3 for the k_{ij} correlation in Equation (4.13) and the deviations of the vapor pressure data are summarized in Table 4.4.

Table 4.4: Calculated parameters for k_{ij} correlation.

(a) Parameters for linear PEs.

	Parameters			AAD					
	a_1	a_2	$10^4\ a_3$	PEC4	PEC5	PEC6	PEC7	PEC8	PEC9
Refrigerant	-	$\mathrm{mol\,kg^{-1}}$	$\mathrm{K^{-1}}$	%	%	%	%	%	%
R1234yf	−0.0754	0.1373	0.9649	2.00	1.73	2.46	2.81	4.72	1.90
R1234ze	−0.09864	0.1818	1.404	1.61	2.15		2.67		3.31
R600a	0.03589	−0.02419	0	1.34	2.52	3.62	1.85	3.97	4.76
R744	−0.0812	0.2126	2.111	6.31	4.76	7.06	11.09	10.47	6.77

(b) Parameters for branched PEs.

	Parameters			AAD				
	a_1	a_2	$10^4\ a_3$	PEB5M2	PEB6M2	PEB7M2	PEB6E2	PEB8E2
Refrigerant	-	$\mathrm{mol\,kg^{-1}}$	$\mathrm{K^{-1}}$	%	%	%	%	%
R32	−0.146	0.1977	3.347				3.78	6.36
R125	−0.1064	0.1516	2.985				1.29	3.05
R134a	−0.09333	0.1866	2.096				2.98	3.32
R744	−0.04136	0.1583	2.907	5.53	7.98	11.24	6.12	7.89

Figure 4.5 shows the binary interaction parameter k_{ij} over the molecular weight M of the polyol ester for the refrigerants R744 (CO_2), R134a, and R600a (isobutane) at different temperature levels.

The influence of the temperature on k_{ij} is shown in the color of the markers and lines in the diagram. The markers represent the calculated values of the binary interaction parameter k_{ij} of each isotherm, calculated in the first step. The dotted and the dashed-dotted lines show the k_{ij} correlations for linear and branched PEs, respectively. To compare the resulting correlations of the present study with literature, the correlations of FOUAD AND VEGA [116] and

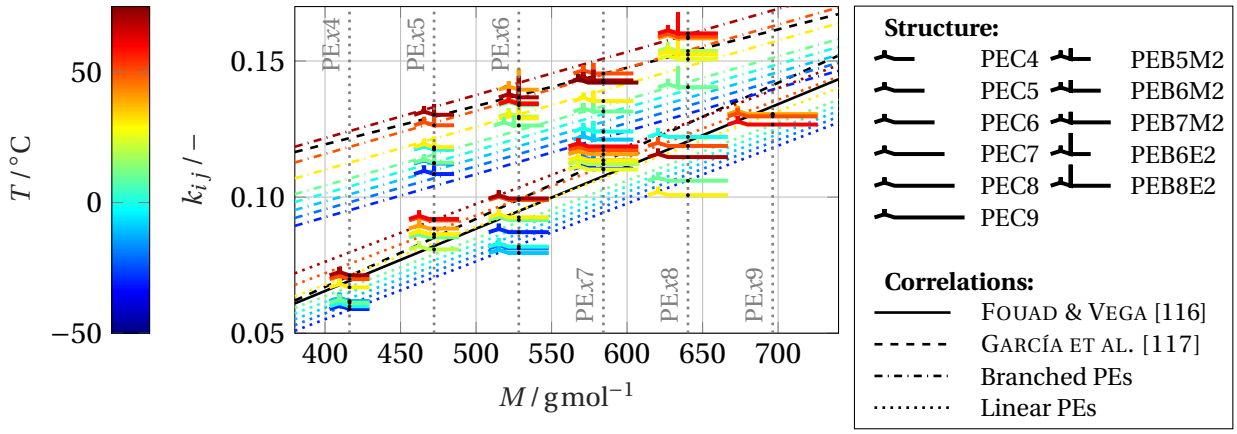

(a) R744

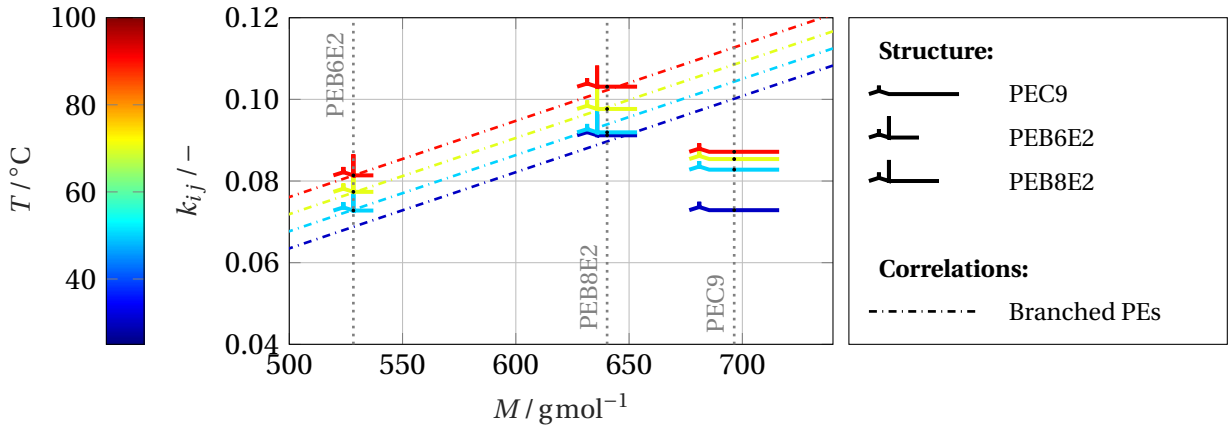

(b) R134a

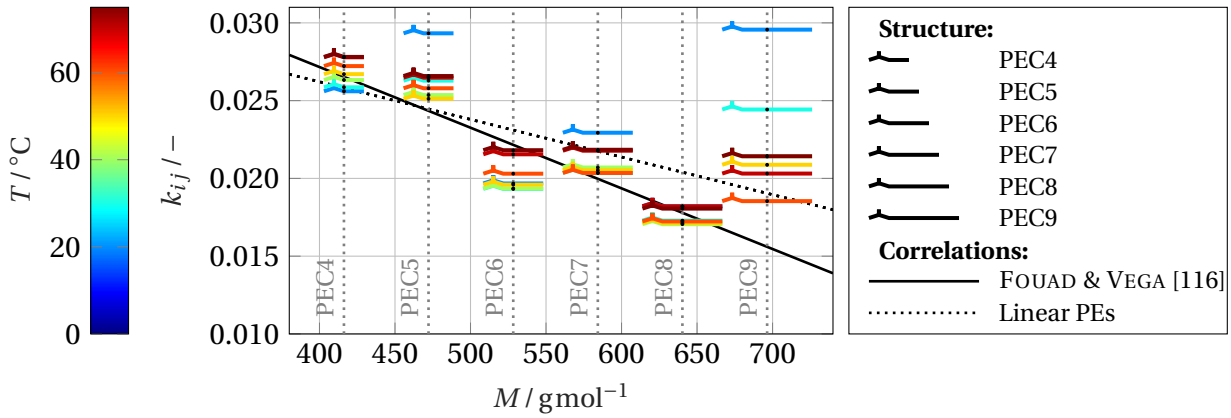

(c) R600a

Figure 4.5: Binary interaction parameter k_{ij} of different refrigerants and PEs. Lines depict correlations for k_{ij}.

GARCÍA ET AL. [117] are depicted as well. Diagrams on the other refrigerants can be found in Figures F.1 and F.2 in the Appendix.

The values of k_{ij} are positive for all PEs. This means that the interaction between a segment of refrigerant and lubricant is stronger than predicted with the interaction of segments of the same components (see Equation (4.11)). Furthermore, the values of k_{ij} are higher for the polar HFC and HFO refrigerants compared to the non-polar hydrocarbon refrigerants. Also for R744 (CO_2) that has a quadrupole moment, high values of k_{ij} are found. A potential reason is that the polarity of the COO groups of the PEs and the quadrupole moment of R744 (CO_2) are not considered in the modeling. The problem is that the polarity of PEs is not described in literature to the knowledge of the author. Considering the quadrupole moment of R744 would require an additional quadrupole contribution term to the Helmholtz free energy in Equation (4.9), as developed e.g. by GROSS [139]. Regarding the aim of the present study to develop an approach to predict the solubility of refrigerant-lubricant mixtures, the high values of k_{ij} underline the necessity to develop correlations for k_{ij} for mixtures of refrigerants and polyol esters used in this study.

Regarding the calculated values of k_{ij} of R744 and the linear PEs in Figure 4.5a, it is striking that the trend of the k_{ij} values of PEC5, PEC7 and PEC9 is slightly higher compared to the trend of the k_{ij} values of PEC4, PEC6 and PEC8. The mixture solubility data of R744 with PEC5, PEC7, and PEC9 that is used to calculate the values of k_{ij} were published by FANDIÑO ET AL. [104, 108]. In contrast, the mixture solubility data of R744 with PEC4, PEC6, and PEC8 were published by the group of FEDELE, BOBBO AND PERNECHELE [101, 106, 109]. PERNECHELE ET AL. [101] and BOBBO ET AL. [106] considered a temperature range of $-30°C < T < 70°C$ while FANDIÑO ET AL. [104, 108] published results in the range of $10°C < T < 60°C$. Considering the entire temperature range, it seems reasonable to consider the temperature influence on the binary interaction parameter k_{ij} for PEs and the refrigerant R744. The gradient $\partial k_{ij}/\partial M$ for linear PEs is similar to the correlation of FOUAD AND VEGA [116] and slightly lower compared to GARCÍA ET AL. [117], who used a different dataset as some of the measurement results had not been published at that time. Regarding the branched PEs, the temperature influence is stronger compared

to the linear PEs. The gradient $\partial k_{ij}/\partial M$ of the correlation for branched PEs is slightly higher compared to the correlation of GARCÍA ET AL. [117] most likely because the low temperature data of PEB5M2 and PEB7M2 were not available at the time of the publication of GARCÍA ET AL. [117].

Regarding R134a in Figure 4.5b, the database is much smaller compared to R744. As the solubility data on PEC9 is the only available data for linear PEs, it is not possible to calculate a value for parameter a_2 that describes the influence of the molecular weight on k_{ij}.

Regarding R600a in Figure 4.5c, only data of linear PEs are available. The values of k_{ij} are significantly lower compared to the other refrigerants. Another pecularity of R600a is the negative trend of k_{ij} with rising molecular weight M of the polyol ester. The calculated values for k_{ij} do not show a clear trend regarding the influence of the temperature. Therefore, it was decided to set the temperature paramter $a_3 = 0$ in Equation (4.13) for R600a. The correlation determined in the study at hand differs slightly from the correlation of FOUAD AND VEGA [116], because recently published solubility data of R600a with PEC9 of SUN ET AL. [110] was considered in the present study.

4.5.2 Multi-Component Mixtures of Refrigerants and Commercial POEs

It was shown in Section 4.1 that significant gaps exist for solubility measurements of

- DiPEs with all refrigerants,
- the hydrocarbon refrigerants R290 and R1270 with all polyol esters,
- the hydrocarbon R600a (isobutane) with branched PEs,
- the HFOs R1234yf and R1234ze with branched PEs, and
- the HFCs R32, R125, and R134a with linear PEs.

For these refrigerant-lubricant combinations, correlations for the binary interaction parameter k_{ij} could not be determined in the previous Section 4.5.

In the present section, correlations for k_{ij} are developed for these combinations of refrigerant and lubricant based on some assumptions and solubility data of refrigerants and commercial lubricants.

Literature Database

In the following, the solubility database that is used in the development of correlations for the binary interaction parameter k_{ij} is presented. The studies introduced in this section do not represent the complete research in the field. Rather, they represent special details that are relevant to reach the aims of the study. Especially in older studies, data on the lubricant (viscosity, density, molecular weight) is scarce. Nevertheless, this data is required to determine a composition of polyol esters with similar properties (cf. Section 3.3). Additionally, data about the mixture viscosity is valuable to parametrize the mixture viscosity models with consistent data on solubility and viscosity. Therefore, the database introduced here is used in Chapter 5 in the parametrization of the viscosity models as well. Table 4.5 gives an overview of the studies used in this section.

Parameter Regression

In the following, the gaps in the k_{ij}-correlations developed in Section 4.5.1 are filled. The parameters of Equation (4.13) are regressed to the experimental data of the cases summarized in Table 4.5. Table 4.6 describes which parameters are regressed ('r'), calculated with binary mixture data ('C'), or determined by assumptions ('A') for the respective case. The checkmarks indicate that the respective parameter is allready known either from the calculations of the binary mixture data in Section 4.5.1 or from a previously calculated case.

The regression is performed with the Matlab® solver for constrained multivariable problems *fmincon*, because this solver lead to results that were independent of the starting conditions in contrast to the non-linear least-squares solver *lsqnonlin*. The objective function of the parameter regression is the AAD (Equation (3.24)) of the vapor pressure p_v between the PCP SAFT EoS and the respective experimental data.

Table 4.5: Literature on solubility of refrigerants in polyol ester lubricants.

ID	Source	Ref.	Lubricant		Solubility			Viscosity		
			VG $\frac{mm^2}{s}$	Comm. Lub. Name[a]	NP	T_{min} K	T_{max} K	NP	T_{min} K	T_{max} K
L1	MORAIS ET AL. [73]	R32	32	RL32-3	28[b,c]	248	348			
L2	CAVESTRI [40]	R32	32	RL32S	47	248	398	47	248	398
L3	MORAIS ET AL. [73]	R125	32	RL32-3	32[b]	248	348			
L4	CAVESTRI [40]	R125	32	RL32S	48	248	398	48	248	398
L5	MARTZ AND JACOBI [97]	R125	68	RL68H	64	232	338			
L6	MORAIS ET AL. [73]	R134a	32	RL32-3	37[b,c]	248	348			
L7	CAVESTRI [40]	R134a	32	RL32S	45	243	398	45	243	398
L8	MARTZ AND JACOBI [97]	R134a	68	RL68H	49	227	357			
L9	MORAIS ET AL. [93]	R1234yf	32	RL32-3	32[b]	248	348	33	248	348
L10	MORAIS ET AL. [93]	R1234ze	32	RL32-3	24[b]	248	348	21	248	348
L11	BOCK [96]	R1234ze	68	RL68H	53[d]	267	334			
L12	CZUBINSKI ET AL. [95]	R290	22	Czu22	22	283	353	20	283	353
L13	FERNANDO ET AL. [140]	R290	32	RL32CF	132	253	313			
L14	GINIES ET AL. [141]	R1270	68	-	36	253	334	38	255	334
L15	MARCELINO NETO AND BARBOSA [79, 142]	R744	68	-	43	285	348	10[e]	309	350

a: Table 3.8 contains information on all lubricants except for RL32CF and RL32S.

b: Solubility data of $x_{Ref} < 0.01$ are omitted as the ratio of uncertainty to measured value is very high.

c: The data in tables S5 and S7 in the supplementary data of MORAIS ET AL. [73] contain some typos.

d: The concentration in Table A.3 of BOCK [96] is misnamed as mole fraction. It is obviously mass fraction.

e: Mole fractions for T=55.5°C and T=76.5°C are mixed up in Table 1 of MARCELINO NETO AND BARBOSA [79]. In the respective figures, they are reproduced correctly.

Table 4.6: Case setup to regress k_{ij}-correlations.

			Linear PEs			Branched PEs			DiPEs		
Ref.	Case ID	Lub. ID	a_1	a_2	a_3	a_1	a_2	a_3	a_1	a_2	a_3
R32	L1	32-1	C1	r	C1	✓	✓	✓	r[a]		A1
R125	L3	32-1	C1	r	C1	✓	✓	✓	r[a]		A1
	L5	68-1	✓[b]	✓[b]	✓[b]	✓	✓	✓	r	r	A1
R134a	L6	32-1	C1	r	C1	✓	✓	✓	r[a]		A1
	L8	68-1	✓[b]	✓[b]	✓[b]	✓	✓	✓	r	r	A1
R1234yf	L9	32-1	✓	✓	✓	r	r	A1	r[a]		A1
R1234ze	L10	32-1	✓	✓	✓	r	r	A1	r[a]		A1
	L11	68-1	✓	✓	✓	✓[c]	✓[c]	✓[c]	r	r	A1
R290	L12	22-1	A2	A2	A2	r[d]		A1	-[e]	-[e]	-[e]
	L13	32-2	A2	A2	A2	-	-	-	r[a]		A1
	L13	32-1	A2	A2	A2	r	r	A1	✓[f]		A1
R1270	L14	68-1	A2	A2	A2	r[g]		A1	r	r	A1
R744	L15	68-1	✓	✓	✓	✓	✓	✓	C2	r	C2

Legend:

✓: Parameter is available because it was determined with binary solubility data of Refrigerant and PEs (see Section 4.5.1) or in a previously conducted regression (in this case see the respective remark).

- : The lubricant mixture does not contain the respective group of polyol esters (see Table 3.10).

r : Parameter is regressed in this case.

Assumptions:

A1: The temperature parameter a_3 is adopted from the respective linear PE.

A2: The respective parameter is adopted from R600a (see Table 4.4a).

Calculations:

C1: The parameters are calculated with the available binary mixture data of PEC9 and the respective refrigerant of WAHLSTRÖM AND VAMLING [59].

C2: The parameters are calculated with the available binary mixture data of R744 and DiPEC7 of FANDIÑO ET AL. [115].

Remarks:

a: DiPEC7 is the only DiPE in the lubricant 32-1 (see Table 3.10). Thus, the following parameter was regressed: $a_{12} = a_1 + a_2 M_{\mathrm{DiPEC7}}$.

b: The parameter is adopted from Case L3 for R125 and from Case L6 for R134a.

c: The parameter is adopted from Case L10.

d: PEB8E2 is the only branched PE in the mixture (see Table 3.10). Thus, the following parameter was regressed: $a_{12} = a_1 + a_2 M_{\mathrm{PEB8E2}}$.

e: Lubricant 22-1 contains $x_{\mathrm{DiPEC7}} = 1.6\%$ (see Table 3.10). This was considered negligible.

f: DiPEC7 is the only DiPE in the mixture. The parameter a_{12} is adopted from Case L13 with lubricant 32-2 (see line above).

g: PEB9M355 is the only branched PE in the mixture (see Table 3.10). Thus, the following parameter was regressed: $a_{12} = a_1 + a_2 M_{\mathrm{PEB9M355}}$.

The regression of the parameters requires much computation time, as the PCP SAFT EoS is solved at every data point of the experiment in every iteration. In order to reduce the numerical effort, assumptions are made to decrease the number of parameters that are regressed. The temperature parameter a_3 of branched PEs and DiPEs is assumed to be equal to the temperature parameter of the linear PEs, if binary solubility data of branched PEs and DiPEs with the respective refrigerant are not available. HC refrigerants show the poorest database for k_{ij} (see Table 4.1). For the HCs R290 and R1270, it is assumed that the parameters for R600a and linear PEs, determined in section 4.5 also apply to the other hydrocarbon refrigerants R290 and R1270.

Regarding refrigerants R125, R134a, and R1234ze, Table 4.1 shows that the parameters of Equation (4.13) for DiPEs are calculated in different cases with the lubricants 32-1 and 68-1 for the same refrigerant. The DiPE-parameters calculated with lubricant 68-1 are finally considered, because the concentration of DiPEs is significantly higher in this lubricant compared to lubricant 32-1 (see Table 3.10). Nevertheless, it was found that the parameters computed in the regression with cases of both lubricants, 32-1 and 68-1, agree well for the same refrigerant.

Regarding refrigerant R290, the trade name of the lubricant was not indicated in FERNANDO ET AL. [140]. The available information on the pure lubricant of this publication is not sufficient to calculate a composition of polyol esters with similar properties with the algorithm described in Section 3.3. Therefore, the solubility data are used with the two lubricant compositions 32-1 and 32-2 of the same VG as the commercial lubricant used by FERNANDO ET AL. [140]. For refrigerant R290 and branched PEs, the parameter a_1 differs significantly for cases L12 and L13. For case L12, the $a_1 = 0.0337\,\mathrm{mol\,kg^{-1}}$ is calculated.[3] For case L13, the following parameters are calculated in the parameter regression: $a_2 = -0.024\,\mathrm{mol\,kg^{-1}}$ $a_1 = 0.076$. Subsequently, the average value of cases L12 and L13 is used: $a_1 = 0.5\,(0.076 + 0.0337)\,\mathrm{mol\,kg^{-1}} = 0.0548\,\mathrm{mol\,kg^{-1}}$.

For some refrigerants further assumptions are required for the molecular

[3] As PEB8E2 is the only branched PE in lubricant 22-1 used in case L12, it is not possible to determine the parameter a_2 of Equation (4.13). Instead, parameter $a_{12,L12}$ is used in the parameter regression. $a_{12,L12}$ is calculated according to $a_{12,L12} = a_1 + M_{\mathrm{PEB8E2}}\,a_2$. With the parameter $a_2 = -0.024\,\mathrm{mol\,kg^{-1}}$ of case L13, this leads to $a_1 = 0.0337\,\mathrm{mol\,kg^{-1}}$.

weight parameter a_2, if only cases are available, where the combined parameter a_{12} is calculated. These are listed below.

- **R32 - DiPEs:** Parameter a_2 is assumed equal to R125.
- **R1234yf - DiPEs:** Parameter a_2 is assumed equal to R1234ze.
- **R290 - DiPEs:** Parameter a_2 is assumed equal to R1270.
- **R1270 - Branched PEs:** Parameter a_2 is assumed equal to R290.

The derived parameters a_1, a_2, and a_3, of Equation (4.13) are summarized in Table 4.7.

Table 4.7: Parameters of correlations for binary interaction parameter k_{ij}.

	Linear PEs			Branched PEs			DiPEs		
	$10\ a_1$	$10\ a_2$	$10^4\ a_3$	$10\ a_1$	$10\ a_2$	$10^4\ a_3$	$10\ a_1$	$10\ a_2$	$10^4\ a_3$
Ref.	-	$\mathrm{mol\,kg^{-1}}$	$\mathrm{K^{-1}}$	-	$\mathrm{mol\,kg^{-1}}$	$\mathrm{K^{-1}}$	-	$\mathrm{mol\,kg^{-1}}$	$\mathrm{K^{-1}}$
R32	−1.61	2.37	2.16	−1.46	1.98	3.35	−1.06	0.599	2.16
R125	−1.57	2.28	2.25	−1.06	1.52	2.99	−1.12	0.599	2.25
R134a	−1.50	2.24	2.28	−0.933	1.87	2.1	−1.28	0.466	2.28
R1234yf	−0.754	1.37	0.965	−0.835	1.56	0.965	−0.706	0.673	0.965
R1234ze	−0.986	1.82	1.40	−1.11	1.82	1.40	−0.839	0.673	1.40
R290	0.359	−0.242	0	0.548	−0.24	0	0.0883	0.00265	0
R1270	0.359	−0.242	0	0.653	−0.24	0	0.0502	0.00265	0
R744	−0.812	2.13	2.11	−0.414	1.58	2.91	−2.06	2.10	3.01

A graphical representation of the correlations can be found in Figure F.3 in the Appendix.

Deviation to Experimental Data

Subsequently, the correlation for the binary interaction parameter k_{ij} are used to determine the deviation between values from experiments and the PCP SAFT EoS. The deviations of the vapor pressure p_v and the density of the liquid phase ρ_l are summarized in Table 4.8.

The cases L1, L3, L6, L9, and L10 are based on the measurements of MORAIS ET AL. [73, 93, 94]. The deviation in the vapor pressure p_v is moderate in these

Table 4.8: Deviation of vapor pressure p_v and liquid density ρ_l between calculation with PCP SAFT EoS and experiments.

			Vapor Pressure p_v			Liquid Density ρ_l		
			AAD	Bias	MD	AAD	Bias	MD
Ref.	Case ID	Lub. ID	%	%	%	%	%	%
R32	L1	32-1	8.99	2.31	30.75	–	–	–
	L2	32-1	28.01	−23.66	99.67	4.31	4.29	28.26
R125	L3	32-1	6.24	3.37	64.87	–	–	–
	L4	32-1	13.69	−7.67	99.67	4.03	4.00	13.11
	L5	68-1	9.79	−0.82	105.03	2.16	2.05	5.62
R134a	L6	32-1	6.22	−1.70	27.07	–	–	–
	L7	32-1	15.31	−5.84	62.42	9.18	8.47	22.87
	L8	68-1	14.68	−13.85	44.21	2.03	2.03	4.47
R1234yf	L9	32-1	4.55	3.53	25.07	0.88	0.88	2.15
R1234ze	L10	32-1	7.05	2.65	20.29	1.04	1.04	2.86
	L11	68-1	2.10	−0.55	10.36	–	–	–
R290	L12	22-1	10.89	8.52	25.80	–	–	–
	L13	32-1	4.24	−3.46	11.42	–	–	–
R1270	L14	68-1	7.64	5.86	20.37	–	–	–
R744	L15	68-1	7.12	0.38	53.21	1.29	1.26	3.79

cases. The deviation in the liquid density ρ_l is low for cases L9 and L10, as well. The liquid density is not reported for cases L1, L3, and L6.

The measurement data of CAVESTRI [40] used for cases L2, L4, and L7 show a high scattering in the data for both vapor pressure and liquid density. The high values of AAD and MD of the pressure data are related to this issue. Nevertheless, the high values for the Bias of the density shows that the density is over-predicted in these cases with the PCP SAFT EoS. This emphasizes a different composition with a higher amount of PEs with a longer alkyl group compared to the assumed composition in lubricant 32-1, because the density decreases with the length alkyl group (see Figure 2.3a).

The reason for the high maximum deviation of case L5 is that phase separation is predicted by the PCP SAFT model for $T > 60°C$. This leads to a strong increase in the calculated pressure. In the experiments, no phase separation is observed. If the respective data point is omitted, the calculated deviation is reduced to AAD = 8.3% and MD = 26.7%.

Regarding case L12 using the data of CZUBINSKI ET AL. [95], the AAD is above 10%. The reason is that the parameter a_1 for branched PEs was determined as the average of cases L12 and L13. This affects the deviation of case L12 stronger than the deviation in case L13. Nevertheless, it can be stated that the AAD of the vapor pressure p_v is below 8% for the low GWP refrigerants R1234yf, R1234ze, R290, R1270, and R744, except for case L12.

All in all, the calculated solubility and the density of the liquid phase are found to be in good agreement with the experimental data, especially for low GWP refrigerants.

The designed predictive model is used in Chapters 6 and 7 to determine the amount of dissolved refrigerant and the liquid density of the liquid phase in the two-phase flow in the suction line.

4.6 Example Phase and Density Diagrams

In the following, some example results for composition and liquid density of refrigerant-lubricant mixtures modeled with the PCP SAFT EoS are presented. Mixtures of R290 with lubricants 80-2 and R1234yf with lubricant 32-1 are considered.

The composition of the refrigerant-lubricant mixtures is described in phase diagrams (Figures 4.6a and 4.6c). In these diagrams, the pressure of the system p is depicted over the mole fraction of the refrigerant x_{Ref}. Only the boiling point curve is depicted, because the dew point curve cannot be distinguished from the right margin of the figure ($x_{\mathrm{Ref}} = 1$) and the abscissa in the graphical representation due to the low vapor pressure of polyol esters in comparison to refrigerants. Therefore, the abscissa is only labeled with the liquid mole fraction of the refrigerant $x_{\mathrm{l,Ref}}$. Above the boiling point curve, the system consists of a single liquid phase. Below the boiling point curve[4], the system consists of a liquid and a vapor phase. The composition of the liquid phase can be determined from the intersection of a horizontal line at the respective pressure

[4] Generally, between the boiling point curve and the dew point curve.

with the boiling point curve. The vapor phase consists of nearly pure refrigerant $x_{\mathrm{v,Ref}} \approx 1$, as the dew point curve is similar to the right margin of the figure.

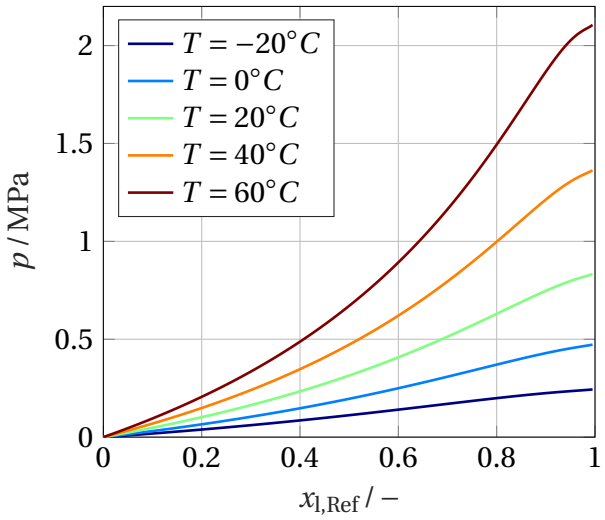

(a) Phase diagram of R290 and lubricant 80-2.

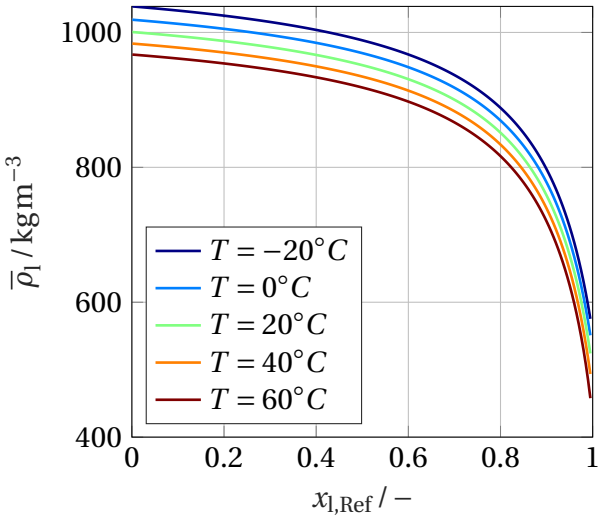

(b) Liquid density of R290 and lubricant 80-2.

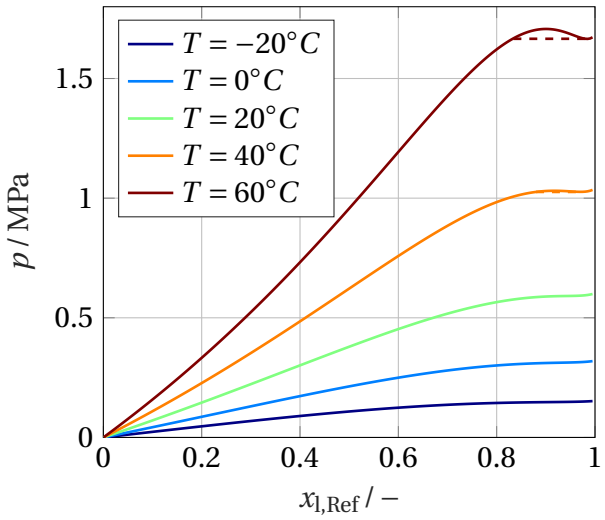

(c) Phase diagram of R1234yf and lubricant 32-1.

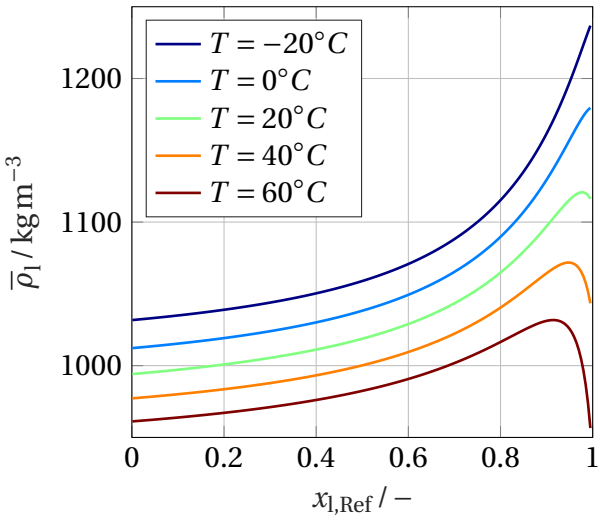

(d) Liquid density of R1234yf and lubricant 32-1.

Figure 4.6: Examples for solubility and density calculations with the PCP SAFT EoS.

The phase diagram of R290 in Figure 4.6a shows continuously rising boiling point curves for all temperatures. In the phase diagram of R1234yf in Figure 4.6c, the boiling point curves increase continuously with rising refrigerant

mole fraction for temperatures $T < 40°C$. The boiling point curves for higher temperatures $T \geq 40°C$ exhibit a maximum. For pressures above the dashed three-phase-line, phase separation occurs in the liquid phase. It is not the aim of this study to discuss phase phenomena in detail. The interested reader is referred to the publication of QUIÑONES-CISNEROS ET AL. [143] that investigates phase phenomena in mixtures of R744 (CO_2) and lubricants. For this study, it is important that phase separation of the liquid phase does not occur for the operation parameters of the suction line, because the two-phase flow model is limited to a single liquid phase.

Regarding the liquid density $\overline{\rho}_\mathrm{l}$ of mixtures of R290 with lubricant 80-2 depicted in Figure 4.6b, a constant decrease can be observed from pure lubricant $x_{\mathrm{l,Ref}} = 0$ to pure refrigerant $x_{\mathrm{l,Ref}} = 1$. The curve is very steep for high refrigerant mole fractions $x_{\mathrm{l,Ref}} > 0.8$.

The liquid density $\overline{\rho}_\mathrm{l}$ of mixtures of R1234yf and lubricant 32-1 is depicted in Figure 4.6d. Here, the variations in the liquid density $\overline{\rho}_\mathrm{l}$ with increasing mole fraction are much lower compared to mixtures of R290 and lubricant 80-2. The reason is that the density of the pure lubricant $\rho|_{x_{\mathrm{l,Ref}}=0}$ is similar to the density of pure refrigerant $\rho|_{x_{\mathrm{l,Ref}}=1}$.

5 Viscosity of Refrigerant-Lubricant Mixtures

This chapter describes the liquid mixture viscosity of refrigerants and lubricants. First of all, the literature on measurements of the liquid mixture viscosity is presented in Section 5.1. Subsequently, viscosity models that were applied in literature for mixtures of refrigerant and lubricants are described in Section 5.2. In Section 5.3, the modeling process to derive a predictive model for the mixture viscosity is described.

5.1 Literature Data on the Viscosity of Mixtures of Refrigerants and Polyol Esters

In this section, a database of mixture viscosity measurement data is developed that subsequently serves in the parametrization of the viscosity models in Section 5.3. Section 5.1.1 contains the literature on binary mixtures of refrigerants and lubricants while Section 5.1.2 comprises the literature on mixtures of refrigerants with commercial lubricants.

5.1.1 Binary Mixtures of Refrigerants and Polyol Esters

To the knowledge of the author, there are only three publications on measurements of the mixture viscosity of pure PEs and refrigerants. PENSADO ET AL. [144, 145] measured the viscosity of R744 and PE mixtures at a low lubricant concentration and for pressures that are significantly higher than saturation to ensure that the mixture is in liquid state. Thus, these experiments are not relevant for the investigated phenomena in the suction line of a refrigeration

cycle. In the suction line, the concentration of the lubricant in the liquid phase is high and the liquid is in saturated state. In the third publication of WAHLSTRÖM AND VAMLING [68], the mixture viscosity of PEC5 and PEB8E2 in the HFC refrigerants R134a and R125 was measured. The measurement uncertainty of the viscosity was estimated to be less than 4%. The measured kinematic mixture viscosity $\overline{\nu}$ of mixtures with the same refrigerant and different PEs is depicted in Figure 5.1 over the mole fraction of the refrigerant. Additionally, the viscosity of an ideal mixture of the respective components calculated with Equations (3.5) and (3.30) is shown.

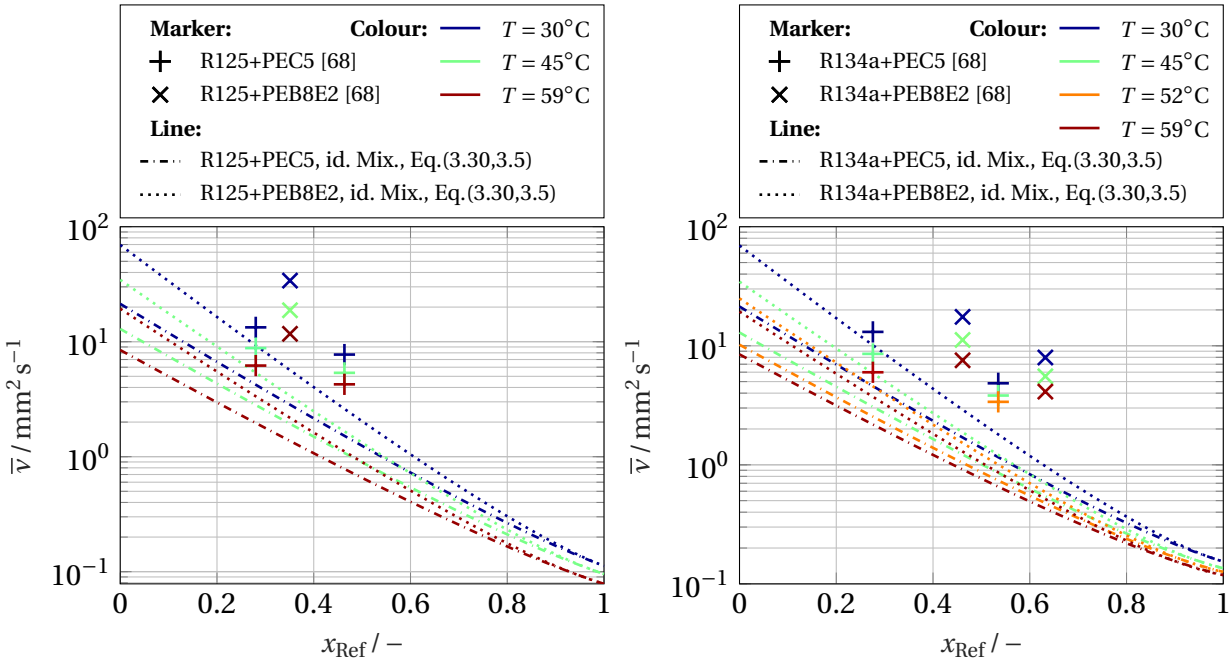

(a) Mixtures of R125 and PEs.

(b) Mixtures of R134a and PEs.

Figure 5.1: Kinematic viscosity of refrigerant and PE mixtures. The measurement results were published by WAHLSTRÖM AND VAMLING [68].

The measured mixture viscosity shows a strong positive deviation from the respective ideal mixture. For mixtures with the branched polyol ester PEB8E2, the deviation is stronger compared to mixtures with the linear polyol ester PEC5. The amount of data is not sufficient to parametrize a viscosity model analogously to the parametrization of the solubility model. Therefore, the

database to parametrize and assess the mixture viscosity models is expanded with data of mixtures of refrigerants and commercial lubricants, as described in the following section.

5.1.2 Multi-Component Mixtures of Refrigerants and Commercial POEs

There are only a few publications available that experimentally determined the viscosity of mixtures of refrigerants with POE lubricants. The meta data of these publications are summarized in Table 5.1.[1] The Case ID was adopted from the literature on solubility (see Table 4.5). Additionally to the literature on refrigerants and commercial lubricants, the experiments of WAHLSTRÖM AND VAMLING [68] on mixtures of refrigerants with PEs, presented in Section 5.1.1, were added (cases L16 - L19). Thus, the table gives a complete overview on the cases subsequently used for the parametrization of the viscosity models.

5.2 Literature Review on Viscosity Modeling of Refrigerant-Lubricant Mixtures

The aim of this section is to identify suitable viscosity models to predict the mixture viscosity of refrigerants and lubricants. Models that use an excessive number of parameters to reduce the deviation to a certain measurement dataset (e.g. the models in [40, 147]) are not considered. First, models that are based on physical relationships are presented in Section 5.2.1. Subsequently, empirical models are summarized in Section 5.2.2

[1] Additionally to the cases mentioned in Table 5.1, THÉBAULT AND VAMLING [146] published the viscosity of HFCs in a polyol ester lubricant of VG 150. This lubricant cannot be represented reliably with the data of the available PEs and DiPEs. Therefore, the measurement data are not considered in the present study.

Table 5.1: Literature on viscosity of refrigerants in polyol ester lubricants.

ID	Source	Ref.	Lubricant		Viscosity				
			VG $\frac{mm^2}{s}$	Lub. Name[a]	NP	T_{min} K	T_{max} K	w_{max} -	Uncert. %
L2	CAVESTRI [40]	R32	32	RL32S	47	248	398	0.30	n/a
L4		R125	32	RL32S	48	248	398	0.70	n/a
L7		R134a	32	RL32S	45	243	398	0.70	n/a
L9	MORAIS ET AL. [94]	R1234yf	32	RL32-3	33	248	348	0.31	±1 %
L10		R1234ze	32	RL32-3	21	248	348	0.25	±1 %
L12	CZUBINSKI ET AL. [95]	R290	22	Czu22	20	283	353	0.25	±2 %
L14	GINIES ET AL. [141]	R1270	68	n.a.	38	255	334	0.30	n/a
L15	MARCELINO NETO AND BARBOSA [79]	R744	68	n.a.	10[b]	309	350	0.22	±1 %
L16	WAHLSTRÖM AND VAMLING [68]	R125	16	PEC5	6	303	332	0.18	±4%
L17		R134a	16	PEC5	6	303	331	0.20	±4%
L18		R125	42	PEB8E2	3	303	333	0.09	±4%
L19		R134a	42	PEB8E2	6	303	332	0.22	±4%

a: Table 3.8 contains information on the named commercial lubricants except for RL32S. Data on PEC5 and PEB8E2 can be found in Table 2.3.

b: Mole fractions for T = 55.5°C and T = 76.5°C are apparently mixed up in Table 1 of MARCELINO NETO AND BARBOSA [79]. In the respective figures of the publication, they are reproduced correctly.

n.a.: not available

5.2.1 Physically Motivated Models

Especially in the past 20 years, the implementation of physically motivated models in the representation of refrigerant-lubricant mixtures gained increased attention.

Models based on Eyring's Theory

There are several models based on Eyring's theory introduced in Section 3.2.3 that were used to model refrigerant-lubricant mixtures. Equation (3.5) represents the mixture viscosity based on the viscosity of the pure components. It is repeated here for a better readability.

$$\ln(\overline{\mu}\overline{V}_\mathrm{m}) = \underbrace{\sum_i x_i \ln(\mu_{0,i} V_{\mathrm{m},0,i})}_{\text{ideal Mixture}} + \frac{\overline{G}_\mathrm{m}^{\neq,\mathrm{E}}}{RT}$$

The difference between the viscosity of the real mixture and of an ideal mixture is expressed in the term $\overline{G}_\mathrm{m}^{\neq,\mathrm{E}}(RT)^{-1}$. In Figure 5.1 it is shown that there is a high positive deviation of the real mixture from the ideal mixture. This emphasizes that the excess activation energy for viscous flow $\overline{G}_\mathrm{m}^{\neq,\mathrm{E}}$ plays a crucial role in the modeling of refrigerant-lubricant mixtures. There are different approaches to find a suitable expression for $\overline{G}_\mathrm{m}^{\neq,\mathrm{E}}$ in literature. WEI AND ROWLEY [78] found that the excess free energy of activation $\overline{G}_\mathrm{m}^{\neq,\mathrm{E}}$ is proportional to the excess Gibb's free enthalpy $\overline{G}_\mathrm{m}^{\mathrm{E}}$ and introduced the proportionality factor a in Equation (5.1).

$$\overline{G}_\mathrm{m}^{\neq,\mathrm{E}} = -aG_\mathrm{m}^{\mathrm{E}} \tag{5.1}$$

They found that $a = 0.25$ leads to accurate results in the prediction of non-aqueous solutions. The excess Gibb's free enthalpy $\overline{G}_\mathrm{m}^{\mathrm{E}}$ is calculated with the fugacity coefficient φ_i of the component i in the mixture and the fugacity coefficient $\varphi_{0,i}$ of the pure component i according to Equation (5.2) [91, p.177].

$$\overline{G}_\mathrm{m}^{\mathrm{E}} = RT \sum_i x_i \ln\left(\frac{\varphi_i}{\varphi_{0,i}}\right) \tag{5.2}$$

MACÍAS-SALINAS ET AL. [148] suggest to simply use Equation (5.3).

$$\overline{G}_\mathrm{m}^{\neq,\mathrm{E}} = \overline{G}_\mathrm{m}^{\mathrm{E}} \tag{5.3}$$

The approach of MACÍAS-SALINAS ET AL. [148] was used in MARCELINO NETO AND BARBOSA [149] to model a mixture of R600a and an alkylbenzene of VG = 6. CZUBINSKI ET AL. [95] tried this approach to model a mixture of R290 and a polyol ester with VG = 22, but achieved a large deviation from the experimental results. A similar approach was also used by SUN ET AL. [150] to model mixtures of R1234yf and R1234ze with a lubricant of VG = 75. They achieved very low deviations (AAD < 4%) between modeled and experimental mixture viscosity.

Another model based on the Eyring's theory is the model of KATTI AND CHAUDHRI [151]. They used the term described in Equation (5.4) to model the excess energy of activation $\overline{G}_{\mathrm{m}}^{\neq,\mathrm{E}}$.

$$\overline{G}_{\mathrm{m}}^{\neq,\mathrm{E}} = a x_1 x_2 \tag{5.4}$$

Here, an empirical coefficient a for the excess activation energy of viscous flow is introduced. This approach was used in MARCELINO NETO AND BARBOSA [121] for mixtures of R600a (isobutane) and a polyol ester lubricant of VG 6. MARCELINO NETO AND BARBOSA [79] extended this equation with an analogous approach to the modeling of the excess Gibb's free enthalpy $\overline{G}_{\mathrm{m}}^{\mathrm{E}}$ of REDLICH AND KISTER [152] for asymmetric mixtures [91, p. 181] according to Equation (5.5).

$$\overline{G}_{\mathrm{m}}^{\neq,\mathrm{E}} = a_0 x_1 x_2 + a_1 (2x_1 - 1)(x_1 - x_1^2) + a_2 (2x_1 - 1)^2 (x_1 - x_1^2) \tag{5.5}$$

They used Equation (5.5) to model a mixture of R744 (CO_2) and a polyol ester of VG 68.

Model of Grunberg and Nissan

Although the earlier equation for binary mixtures of GRUNBERG AND NISSAN [80] described in Equation (5.6) has its origins in the viscosity equation for ideal mixtures of *Arrhenius* (Equation (3.6)), it is equivalent to the approach of KATTI AND CHAUDHRI [151] (Equations (3.5) and (5.4)), if the mixture components have similar molar volumes $V_{\mathrm{m},0}$.

$$\ln(\overline{\mu}) = x_1 \ln(\mu_1) + x_2 \ln(\mu_2) + a x_1 x_2 \tag{5.6}$$

The molar volume of polyol esters is much higher compared to the molar volume of refrigerants. Nevertheless, the influence of the molar volume on the viscosity is minor compared to the influence of the excess activation energy of viscous flow $\overline{G}_{\mathrm{m}}^{\neq,\mathrm{E}}$. Therefore, it is expected that the equations of GRUNBERG AND NISSAN [80] and KATTI AND CHAUDHRI [151] lead to similar results and the equation of GRUNBERG AND NISSAN [80] is not considered in the final evaluation. The equation of GRUNBERG AND NISSAN [80] was used in numerous publications on the mixture viscosity of refrigerant and lubricants (i.a. [94, 121, 144, 153]).

Friction Theory

The f-theory based on the PC SAFT EoS [88] was used to model the mixture viscosity of R290 and a VG 22 polyol ester in CZUBINSKI ET AL. [95], a mixture of R744 (CO_2) and a VG 68 polyol ester in MARCELINO NETO AND BARBOSA [154] and mixtures of R134a and different dimethylethers in MONSALVO [126]. A different version of the f-theory [87] that does not rely on a universal set of parameters was used by QUIÑONES-CISNEROS ET AL. [143] to qualitatively predict the influence of phase separation on the liquid viscosity for mixtures of R744 (CO_2) and polyol esters.

In the study at hand, the PC SAFT version of the f-theory version was introduced for pure PEs and DiPEs in Section 3.2.3. It is subsequently used for the refrigerant-lubricant mixtures, as well. The model does not contain any adjustable parameters for fluid mixtures.

Free Volume Theory

The free volume theory of ALLAL ET AL. [75] was used by MONSALVO ET AL. [155] for mixtures of R134a and dimethylethers and by PENSADO ET AL. [144] for mixtures of R744 (CO_2) and different PEs for low lubricant concentrations.

In the present study, the free volume theory was introduced for pure PEs and DiPEs in Section 3.2.3. Different mixture laws can be applied to the free volume parameters. Preliminary tests for this study revealed that the free volume theory leads to a similar trend compared to the measured mixture viscosity, if the mixture laws of ZÉBERG-MIKKELSEN ET AL. [86] (Equations (5.7-5.9)) are applied.

$$\overline{\alpha} = \sum_i x_i \alpha_i \tag{5.7}$$

$$\overline{l} = \sum_i x_i l_i \tag{5.8}$$

$$\overline{B}^{-1} = \sum_i B_i^{-1} \tag{5.9}$$

Implementing these mixture laws, the model does not contain any adjustable parameters for fluid mixtures.

5.2.2 Empirical Models

Several empiric models were used to describe the viscosity of refrigerant-lubricant mixtures. These are described in the following.

Model of Kendall and Potter

The empiric mixture law of KENDALL AND POTTER [156] in Equation (5.10) was developed for liquids that do not show association or dissociation.

$$\overline{\mu}^a = \sum_i x_i \mu_i^a \tag{5.10}$$

The model contains the adjustable parameter a. KENDALL AND POTTER [156] found that $a = 1/3$ predicts the mixture viscosity of the considered non-aqueous solutions well. The model was used by BAUSTIAN ET AL. [157] for mixtures of the HCFC refrigerant R113 and mineral oil as well as alkylbenzene lubricants.

Model of Jensen and Jackman

The correlation of JENSEN AND JACKMAN [158] was developed for the mixture viscosity of refrigerants and lubricants in pool boiling.

$$\overline{\mu} = \mu_{\text{Ref}} \exp\left[(1 - w_{\text{Ref}})\left(\frac{\mu_{\text{Lub}}}{\mu_{\text{Ref}}}\right)^a\right], \text{ with } a = 0.3 \tag{5.11}$$

The values of the mixture viscosity approach the pure refrigerant viscosity for $w_{\text{Ref}} \rightarrow 1$. This is reasonable because the refrigerant mass fraction is high in pool boiling processes, if the lubricant does not accumulate. In contrast the mixture viscosity does not approach the pure lubricant viscosity for $w_{\text{Lub}} \rightarrow 1$. The model was used by BAUSTIAN ET AL. [157] for mixtures of the HCFC refrigerant R113 and mineral oil as well as alkylbenzene lubricants.

Model of Yokozeki

YOKOZEKI [159] presented a modified version of the ARRHENIUS Equation (3.6), with an "effective mass fraction" ω according to Equation (5.12).

$$\ln \overline{\mu} = \sum_i \omega_i \ln(\mu_i), \text{ with } \omega_i = \frac{M_i^a x_i}{\sum_j M_j^a x_j} \tag{5.12}$$

The exponent a is an adjustable parameter. YOKOZEKI [159] obtained a value of $a = 0.58$ in a parameter regression to experimental data on mixtures of HCFC and HFC refrigerants in different lubricants.

Model of Thebault and Vamling

THÉBAULT AND VAMLING [146] modified the *Ubbelohde-Walther* equation (3.23) for pure lubricants by adding an additional term for the influence of the refrigerant mass fraction on the viscosity, as described in Equation (5.13).

$$\ln\left[\ln\left(\overline{\nu}+0.7\right)\right] = a_1 + a_2 \ln(T) + a_3 w_{\mathrm{Ref}} M_{\mathrm{Ref}}^{a_4} \tag{5.13}$$

In this equation, the kinematic viscosity $\overline{\nu}$ is in $\mathrm{mm^2\,s^{-1}}$, the temperature T is in K, and the molecular weight of the refrigerant M_{Ref} is in $\mathrm{g\,mol^{-1}}$. The model was inspired by the parallel lines of pure lubricants and mixtures with a certain refrigerant mass fraction observed in Daniels plots. The parameters a_1 and a_2 have to be adjusted against the kinematic viscosity of the pure lubricant $\overline{\nu}_{\mathrm{Lub}}$. THÉBAULT AND VAMLING [146] suggested to use $a_3 = -151.2$ and $a_4 = -0.8728$ as universal parameters.

5.3 Development of the Liquid Mixture Viscosity Model

This section describes the modeling process of the liquid mixture viscosity of refrigerants and lubricants. In Section 5.3.1, the adjustable parameters of the different liquid mixture viscosity models are determined. In Section 5.3.2, the different models are compared for example cases. The deviations between calculated values and measurement data for the liquid mixture viscosity are presented. These values serve as a basis for the model selection.

5.3.1 Parametrization of the Viscosity Models

In this section, the adjustable parameters of the different liquid mixture viscosity models described in the previous Section 5.2 are regressed to the meas-

urement data described in Table 5.1[2]. The non-linear unconstrained multivariable solver *fminunc* of Matlab® is used. The target value of the optimization is the AAD (see Equation (3.24)) of modeled and measured data of the liquid mixture viscosity. After regressing the model parameters to the literature data, universal correlations for all considered refrigerant-lubricant mixtures are determined for each model.

In the following, the parametrization is described for the respective viscosity models. The calculated parameters are depicted in Figure 5.2.

Model of Wei and Rowley

The model of WEI AND ROWLEY [78] described in Equation (5.1) contains a proportionality factor a that links the the activation energy for viscous flow $\overline{G}_{\mathrm{m}}^{\neq,\mathrm{E}}$ with the excess Gibb's free enthalpy $\overline{G}_{\mathrm{m}}^{\mathrm{E}}$. The proportionality factor a of Equation (5.1) is considered as temperature dependent and fitted to every isotherm of the mixture viscosity data. The regressed values for a are depicted in Figure 5.2a for all cases and at every temperature level in the range of $-25°\mathrm{C} < T < 60°\mathrm{C}$. The values of the proportionality factor a have a very wide range of $-22 < a < 126$. Due to the extreme values of a for mixtures of HFC refrigerants R125 and R134a with pure PEs (Cases L16-L19), the mean value of a does not represent most of the cases. The median value $a = 7.54$ was chosen instead and is depicted in the dashed line in Figure 5.2a. Nevertheless, large deviations between predicted and measured values of the mixture viscosity are expected for the model of *Wei and Rowley*.

The reason for the large difference in the model parameter a between the different cases are explained in the following. Using the excess Gibb's enthalpy $\overline{G}_{\mathrm{m}}^{\mathrm{E}}$ to model the activation energy for viscous flow $\overline{G}_{\mathrm{m}}^{\neq,\mathrm{E}}$ leads to problems regarding the aim to develop a predictive model for the mixture viscosity. These are illustrated in the Figure 5.3.

Figure 5.3a shows the excess Gibb's free enthalpy $\overline{G}_{\mathrm{m}}^{\mathrm{E}}$ of mixtures of different refrigerants with lubricant 32-1 over the mole fraction of the refrigerant x_{Ref}

[2]The model of *Macías-Salinas et al.*, the free volume theory and the f-theory do not contain adjustable parameters. Therefore, they are not mentioned in this section.

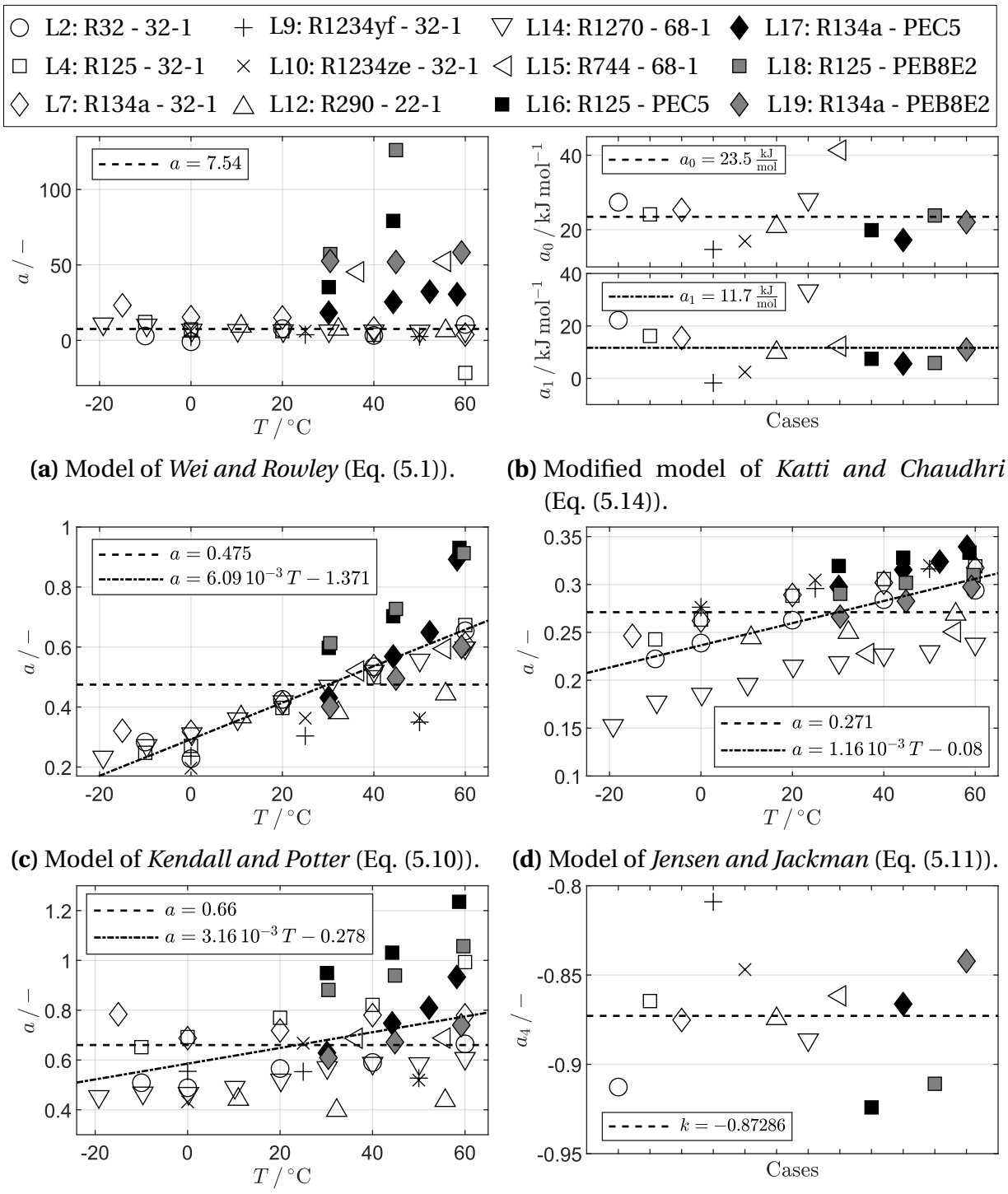

(a) Model of *Wei and Rowley* (Eq. (5.1)).

(b) Modified model of *Katti and Chaudhri* (Eq. (5.14)).

(c) Model of *Kendall and Potter* (Eq. (5.10)).

(d) Model of *Jensen and Jackman* (Eq. (5.11)).

(e) Model of *Yokozeki* (Eq. (5.12)).

(f) Model of *Thébault and Vamling* (Eq. (5.13)).

Figure 5.2: Parametrization of viscosity models.

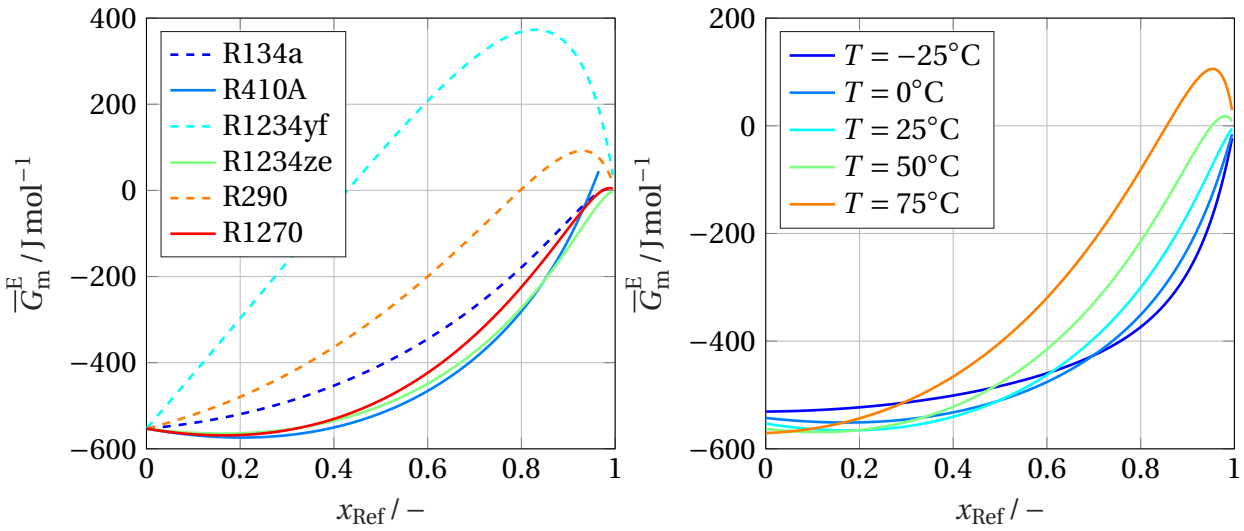

(a) Different refrigerants with lubricant 32-1 at $T = 25$°C.

(b) R134a with lubricant 32-1.

Figure 5.3: Excess Gibb's free enthalpy of refrigerant-lubricant mixtures.

at a constant temperature. In Figure 5.3b, the influence of the temperature on the excess Gibb's free enthalpy $\overline{G}^{\mathrm{E}}_{\mathrm{m}}$ is depicted for refrigerant R134a and lubricant 32-1. This results in the following issues:

- The negative excess Gibb's free enthalpy $\overline{G}^{\mathrm{E}}_{\mathrm{m}}$ for the pure lubricant ($x_{\mathrm{Ref}} = 0$) is the result of considering the lubricant as a mixture of different components. If the lubricant was considered as a single component, the excess Gibb's free enthalpy of the pure lubricant would be $\overline{G}^{\mathrm{E}}_{\mathrm{m}} = 0\,\mathrm{J\,mol^{-1}}$. As a consequence of the negative excess Gibb's free enthalpy $\overline{G}^{\mathrm{E}}_{\mathrm{m}}$ at $x_{\mathrm{Ref}} = 0$, the modeled viscosity of the pure lubricant differs from the ideal mixture in the models of *Wei and Rowley* and *Macías-Salinas et al.*.
- The change in sign of the excess Gibb's free enthalpy $\overline{G}^{\mathrm{E}}_{\mathrm{m}}$, as it can be observed for R410A, R1234yf, and R290 in Figure 5.3a and for $T \geq 50$°C in Figure 5.3b leads to a change of the sign in the deviation of the mixture viscosity between the ideal and the real mixture in the models of *Wei and Rowley* and *Macías-Salinas et al.*. Albeit, the deviation of the mixture viscosity between the real and the ideal mixture are uniformly positive in the available measurement data for all considered cases[3].

[3]This can be observed in Figure 5.1 as well as in Figures 5.4 for some example cases. In Figure 5.4, the ideal

The results presented above show that the model of *Wei and Rowley* requires the excess Gibb's free enthalpy $\overline{G}_{\mathrm{m}}^{\mathrm{E}}$ to be consistently positive or negative for all considered temperature levels and mixtures. This requirement is not fulfilled for all cases considered in this study. The sign of the excess Gibb's free enthalpy $\overline{G}_{\mathrm{m}}^{\mathrm{E}}$ is determined by the deviation of the solubility of the refrigerant-lubricant mixture from *Raoult's* law. If the model was applied to mixtures that show a uniform deviation of the solubility from *Raoult's* law, as e.g. for hydrocarbon refrigerants, the model of *Wei and Rowley* might become an option.

Model of Katti and Chaudhri

In preliminary tests for the present study, it was observed on the one hand that fitting the parameter a of the simple Equation (5.4) of KATTI AND CHAUDHRI [151] to measurement data often leads to higher values for the mixture viscosity of refrigerant and lubricant compared to the viscosity of the pure lubricant. The reason is that the maximum of the energy of activation of viscous flow $\overline{G}_{\mathrm{m}}^{\neq,\mathrm{E}}$ is fixed at $x_{\mathrm{Ref}} = 0.5$. On the other hand, the three-parameter equation (5.5) of MARCELINO NETO AND BARBOSA [79] led to an overfitting for cases L15 - L19 that only contain few measurement points. To overcome both issues, Equation (5.5) was simplified to a two-parameter model as shown in Equation (5.14).

$$\overline{G}_{\mathrm{m}}^{\neq,\mathrm{E}} = a_0 x_1 x_2 + a_1 (2x_1 - 1)(x_1 - x_1^2) \tag{5.14}$$

This led to the best results for the considered cases in the present study. The parameters a_0 and a_1 are considered as temperature independent.

The results of the parameter regression are depicted in Figure 5.2b. Although the single cases can be represented quite accurately with Equation (5.14), the values of the coefficients a_0 and a_1 differ significantly for the different cases. In order to derive global parameters, the mean values of all cases $a_0 = 23.5\,\mathrm{kJ\,mol^{-1}}$ and $a_1 = 11.7\,\mathrm{kJ\,mol^{-1}}$ were chosen and are depicted in Figure 5.2b with the dashed and dashed-dotted line, respectively. Nevertheless, significant deviations are expected applying the global parameters to the single cases.

mixture viscosity is not depicted. Nevertheless, the model of *Macías-Salinas et al.* results in values close to the ideal mixture for both depicted cases.

Model of Kendall and Potter

The model of KENDALL AND POTTER [156] (Equation (5.10)) contains a single adjustable parameter a. The results of the parameter regression are shown in Figure 5.2c. The parameter shows a small variation between the different cases. This is astonishing because of the simplicity of the model equation. The regression reveals a clear temperature dependence of the parameter a. Therefore, the parameter is described with a linear polyonomial according to Equation (5.15) depicted in the dashed-dotted line in Figure 5.2c instead of the mean value of all regressed values depicted with the dashed line.

$$a = 6.09\ 10^{-3}\ T - 1.371, \text{ with } [T] = \text{K}. \tag{5.15}$$

Model of Jensen and Jackman

The model of JENSEN AND JACKMAN [158] (Equation (5.11)) contains a single adjustable parameter a. The results of the regression are depicted in Figure 5.2d. The variations of the parameter a between the different cases are higher compared to the model of *Kendall and Potter* (see Figure 5.2c). Especially for case L14 (R1270 - lubricant 68-1) the value of a differs significantly from the other cases. The parameter a shows a clear temperature dependence. Therefore, the parameter a is described with a linear polynomial according to Equation (5.16).

$$a = 1.16\ 10^{-3}\ T - 0.080, \text{ with } [T] = \text{K}. \tag{5.16}$$

Model of Yokozeki

The model of YOKOZEKI [159] (Equation (5.12)) contains a single adjustable parameter. The results of the regression are depicted in Figure 5.2e. The determined values of parameter a differ significantly for the different cases. Most values are in a range of $0.4 < a < 0.8$. The mixture viscosity of R125 shows higher values in a range of $0.88 < a < 1.25$. The regressed parameters show a dependence on temperature. Allthough the temperature dependence is smaller compared to the models of *Kendall and Potter* (see Figure 5.2c) and *Jensen and Jackman* (see Figure 5.2d), it is considered in the linear polyonomial for

parameter a described in Equation (5.17).

$$a = 3.16\ 10^{-3}\ T - 0.278, \text{ with } [T] = \text{K}. \tag{5.17}$$

Model of Thebault and Vamling

The model of THÉBAULT AND VAMLING [146] (Equation (5.13)) contains 4 adjustable parameters. As the temperature influence on the mixture viscosity is considered in parameter a_2, the parameters a_1, a_3, and a_4 are considered as not temperature dependent. In a first step, the parameters a_1 and a_2 are determined, because these parameters only depend on the kinematic viscosity of the pure lubricant. Subsequently, the values of parameters a_3 and a_4 are determined for the refrigerant-lubricant mixture of all cases. In the regression of parameters a_3 and a_4, the values determined by THÉBAULT AND VAMLING [146] were chosen as starting values. The value of parameter $a_3 = -151.2$ remained nearly unchanged for all cases. The obtained values for a_4 are shown in Figure 5.2f. They are in a rather small range of $-0.92 < a < -0.81$. The mean value of all cases $a_4 = -0.8728$ is depicted in the dashed line and subsequently considered as a global value. It is nearly identical to the value of a_4 determined by THÉBAULT AND VAMLING [146].

5.3.2 Assessment of the Viscosity Models

In the following, the obtained global parameters for the respective models are used to calculate the mixture viscosity. First, different models are compared to measurement data at a constant temperature for two example cases to demonstrate the qualitative behavior of the different mixture viscosity models. Subsequently, the models are compared quantitatively.

Figure 5.4 shows the predicted mixture viscosity $\overline{\mu}$ over the refrigerant mole fraction x_{Ref} in the mixture. The cases L9 (R1234yf and POE 32-1) and L12 (R290 and POE 22-1) were selected as example cases, because these refrigerants are often applied alternatives to HFCs. For both cases, the f-theory of QUIÑONES-CISNEROS ET AL. [88] (Equations (3.13-3.20)) as well as the models of *Wei and Rowley* (Equation (5.1)), and *Macías-Salinas et al.* (Equation (5.3)) show large deviations from the measurement data and do not even

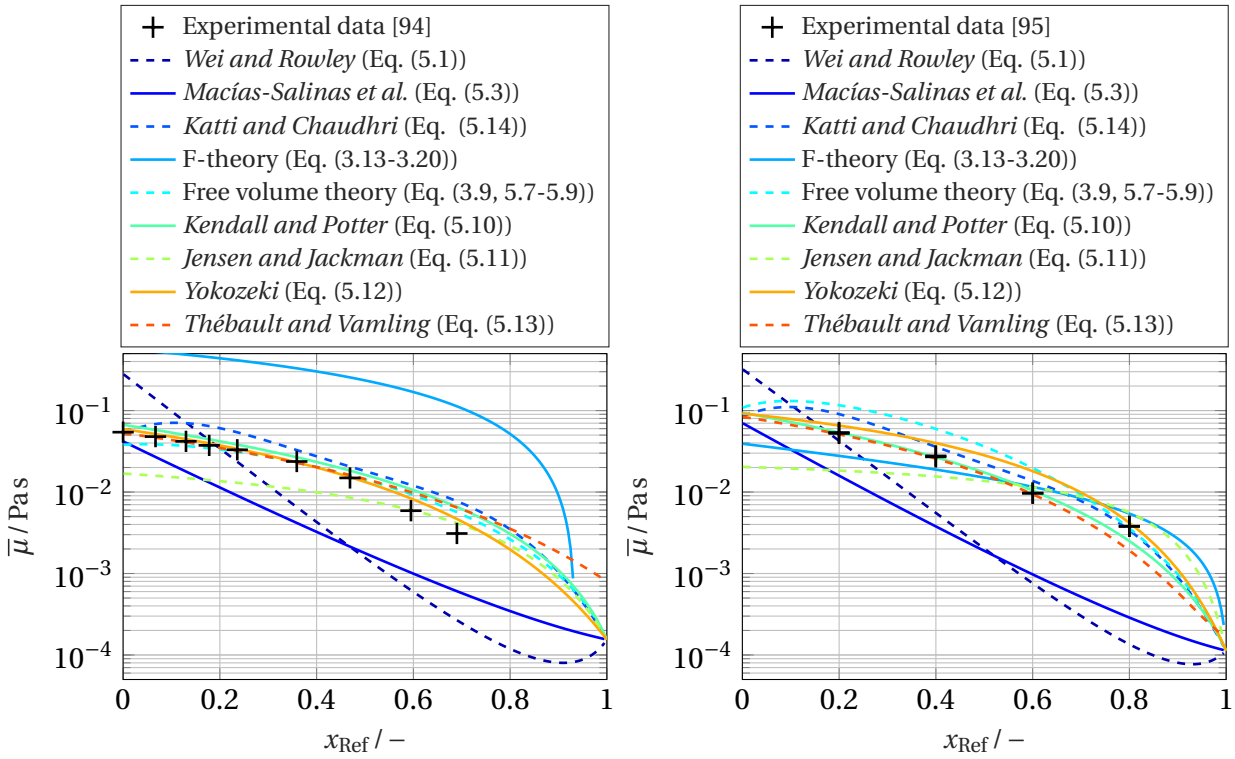

(a) L9: R1234yf - POE 32-1, $T = 25°C$.

(b) L12: R290 - POE 22-1, $T = 11°C$.

Figure 5.4: Comparison of mixture viscosity models.

qualitatively represent the measurement data. The model of *Jensen and Jackman* (Equation (5.11)) under-predicts the measurement data at low refrigerant mole fractions, because this model is designed for conditions close to pure refrigerant. The opposite can be observed for the model of *Thébault and Vamling* (Equation (5.13)) for case L9 in Figure 5.4a. This model is designed to work properly for high lubricant concentrations. The other models predict the mixture viscosity qualitatively correct for both cases. The best representation of the experimental data is the model of *Yokozeki* (Equation (5.12)) for case L9 (Figure 5.4a) and the model of *Kendall and Potter* (Equation (5.10)) for case L12 (Figure 5.4b).

In the following, the models are compared to the measurement data quantitatively. The deviation of the modeled mixture viscosity to the experimental data is summarized in Table 5.2. The overall deviation is calculated as a weighed average with the number of measurement points n indicated in the

table. As expected, the models of *Wei and Rowley* (Equation (5.1)) and *Macías-Salinas et al.* (Equation (5.3)) fail due to the ambiguity of the excess Gibb's enthalpy $\overline{G}_{\mathrm{m}}^{\mathrm{E}}$ for the different cases in combination with a global value of the proportionality factor in Equation (5.1). The two-parameter model based on the model of *Katti and Chaudhri* (Equation (5.14)) leads to the best results of the models based on the Eyring's theory.

The f-theory (Equations (3.13-3.20)) shows acceptable results for case L12 and for the cases with binary mixture (L16 - L19), whereas the deviations are enormous for the other cases. This can be explained with the high deviation between the scaling parameters μ_{a} and μ_{r} of the different PEs and DiPEs (see Table 3.3). The linear PEs, linear DiPEs, and the branched PE PEB8E2 show moderate scaling parameters. In contrast, the values of the scaling parameters of PEB5M2, PEB9M355, and DiPEB9M7 are very high. As an additive mixture law is applied for the attractive and repulsive viscosity contributions (see Equations (3.18, 3.19)), the components with high scaling parameters determine the mixture behavior. This leads to the enormous deviations for this model. This effect occurs only, if the lubricant contains a significant amount of PEB5M2, PEB9M355, or DiPEB9M7. This is not the case for L12 with the low VG lubricant 22-1 or in the cases for the binary mixtures of refrigerants and lubricants (L16-L19).

The free volume model of ALLAL ET AL. [75] (Equations (3.9, 5.7-5.9)) fails for the binary mixture cases of HFCs with PEB8E2 L18 and L19 and for case L12. In case L12, lubricant 22-1 is used that contains 30.8% of PEB8E2 (see Table 3.10). Thus, the issue seems to be related to the free volume parameters of PEB8E2, although the average and maximum deviation between modeled values and measurement data of pure PEB8E2 are low (see Table 3.2). All in all, the free volume theory shows the lowest AAD among the physically motivated models.

Regarding the overall deviation, the rather simple empirical models show a better performance compared to the physically motivated models, except for the model of *Jensen and Jackman*. The higher deviations observed for the latter model were expected, as it was developed for a different application. The other empirical models of *Kendall and Potter*, *Yokozeki*, and *Thébault and Vamling* show an acceptable AAD for predictive viscosity models. As the

Table 5.2: Deviation between experimental data and viscosity models.

(a) Models 1-3.

Case ID	n	*Wei and Rowley* (Eq. (5.1))			*Macías-Salinas et al.* (Eq. (5.3))			*Katti and Chaudhri* (Eq. (5.14))		
		AAD %	Bias %	MD %	AAD %	Bias %	MD %	AAD %	Bias %	MD %
L2	47	98.3	−31.5	671.8	85.9	−85.9	98.4	45.8	−17.1	200.3
L4	48	75.6	−65.6	114.2	84.2	−84.2	97.1	28.4	2.5	72.8
L7	45	78.5	−73.1	103.1	87.8	−87.8	97.8	31.7	1.3	135.5
L9	33	81.6	7.9	230.1	67.7	−67.7	86.9	57.0	54.9	252.3
L10	21	82.2	64.6	230.3	73.2	−73.2	93.4	51.7	48.4	129.5
L12	20	69.5	−67.3	96.4	83.0	−83.0	92.4	42.8	34.3	98.9
L14	34	66.3	−34.6	94.6	96.3	−96.3	98.3	52.3	−52.3	68.5
L15	10	98.2	−98.2	99.8	97.9	−97.9	99.4	84.2	−84.2	92.1
L16	6	72.7	−72.7	82.3	78.3	−78.3	84.3	40.9	40.9	67.5
L17	6	60.2	−60.2	72.9	75.3	−75.3	82.7	84.5	84.5	122.8
L18	3	82.5	−82.5	83.3	85.8	−85.8	86.3	6.2	−6.2	14.7
L19	6	84.5	−84.5	88.3	88.3	−88.3	90.4	15.8	15.8	29.0
All Cases		80.2	−40.7	671.8	84.0	−84.0	99.4	43.9	3.9	252.3

(b) Models 4-6.

Case ID	n	F-Theory (Eq. (3.13-3.20))			Free Volume Theory (Eq. (3.9, 5.7-5.9))			*Kendall and Potter* (Eq. (5.10))		
		AAD %	Bias %	MD %	AAD %	Bias %	MD %	AAD %	Bias %	MD %
L2	47	1429.9	1429.9	4114.1	48.3	−48.2	86.7	27.2	−5.1	166.5
L4	48	1767.0	1767.0	6899.6	26.9	−21.9	72.9	18.1	−5.1	77.7
L7	45	3073.0	3073.0	29631.3	24.1	−19.5	78.7	30.0	−9.2	220.6
L9	33	1332.7	1332.7	3286.7	27.8	−4.2	82.6	24.1	24.1	97.0
L10	21	1283.5	1283.5	2771.2	29.2	−6.6	111.7	20.6	16.5	91.8
L12	20	33.2	−9.0	66.0	128.1	127.6	245.0	19.2	8.4	74.3
L14	34	1188.0	1188.0	3524.2	41.2	40.8	119.7	16.6	−9.1	56.5
L15	10	1259.4	1259.4	2107.6	37.0	−37.0	57.4	13.5	−1.8	29.8
L16	6	29.9	29.9	54.6	2.9	−1.8	9.2	16.7	−16.7	21.4
L17	6	46.7	46.7	103.3	18.6	18.6	31.5	7.7	−4.8	11.1
L18	3	16.0	16.0	24.5	99.9	99.9	104.8	14.6	−14.6	15.5
L19	6	71.6	71.6	113.8	143.9	143.9	174.0	13.7	13.7	26.1
All Cases		1490.4	1487.4	29631.3	42.3	1.3	245.0	21.8	0.0	220.6

Table 5.2: Deviation between experimental data and viscosity models.

(c) Models 7-9.

Case ID	*n*	*Jensen and Jackman* (Eq. (5.11))			*Yokozeki* (Eq. (5.12))			*Thébault and Vamling* (Eq. (5.13))		
		AAD %	Bias %	MD %	AAD %	Bias %	MD %	AAD %	Bias %	MD %
L2	47	150.2	121.5	647.8	27.4	22.4	146.3	25.9	−14.4	104.4
L4	48	105.3	41.5	492.0	24.5	−24.0	64.0	30.4	11.3	276.2
L7	45	81.0	32.0	562.3	30.3	−15.6	169.8	33.9	−5.0	226.0
L9	33	42.7	−41.1	93.7	15.4	14.2	131.9	17.5	12.0	173.6
L10	21	52.8	−50.9	94.2	14.0	8.8	71.7	16.1	4.3	71.9
L12	20	56.5	26.8	140.7	54.2	54.2	172.7	19.4	−1.7	53.2
L14	34	465.0	465.0	1953.1	71.2	71.2	111.1	16.0	−10.4	33.8
L15	10	1471.4	1471.4	2048.1	24.5	22.4	64.3	10.3	0.4	24.2
L16	6	52.6	−52.6	63.9	26.2	−26.2	36.2	11.9	−11.9	15.1
L17	6	41.2	−41.2	60.2	7.2	−4.5	8.6	7.4	−1.5	13.9
L18	3	29.7	−29.7	45.5	20.6	−20.6	21.9	11.1	−11.1	11.6
L19	6	11.8	1.0	16.2	13.4	13.4	21.7	16.8	16.8	27.8
All Cases		181.6	133.1	2048.1	31.3	12.2	172.7	22.9	−1.0	276.2

model of *Kendall and Potter* shows slightly better values for AAD and Bias it was decided to chose this model to predict the liquid mixture viscosity of the two-phase flow in the subsequent parts of the study. The high maximum deviations present in all models remain an unsolved problem.

The predictive model for the liquid mixture viscosity is subsequently used in Chapters 6 and 7 to determine the viscosity of the liquid phase in the two-phase flow in the suction line.

6 Two-Phase Flow in Suction Risers

This chapter deals with the flow phenomena that occur in vertical parts of the suction line with upward refrigerant vapor flow, so called suction risers. First, the different flow regimes relevant in vertical suction lines are introduced in Section 6.1. Based on the transition between the flow regimes, a criterion that describes the operation limit for a safe lubricant return in the suction line is described in Section 6.2. In Section 6.3, different modeling approaches of the two-phase flow published in literature are described. A modeling approach for the present study is selected. In Section 6.4, experiments to determine the operation limit for lubricant return are introduced. Subsequently, the experimental data is used in Section 6.5 to assess different correlations for the interfacial friction factor, which represents the empiric closure of the two-phase flow model. Finally, the experimental data is used to validate the prediction of the operation limit calculated with the two-phase flow model in Section 6.6.

6.1 Flow Phenomena

The flow regime of vertical two-phase flow depends on the volume ratio of the liquid and gaseous phase. For nominal operation conditions of refrigeration cycles, the oil circulation ratio is small (see Section 1.2). Therefore, also the liquid ratio of the two-phase flow in the vertical suction line is small. The low liquid ratio leads to *annular flow*. The liquid forms a continuous film along the channel walls. The gaseous phase builds a continuum in the core of the channel. The gaseous core may contain entrained liquid droplets, especially at high velocities. The liquid wall film can contain entrained gas or vapor bubbles. [160, 161]

SETHI AND HRNJAK [162] observed horizontal, inclined and vertical two phase flow in suction lines for the refrigerants R1234yf and R134a with a POE lubricant of a VG of 32. The total mass flux of refrigerant and lubricant in the test section with an inner diameter of 10.2 mm was varied in a range of $36\,\mathrm{kg\,m^{-2}\,s^{-1}} < J < 170\,\mathrm{kg\,m^{-2}\,s^{-1}}$. Figure 6.1 qualitatively describes the development of the flow regime for decreasing mass flux J in the vertical suction line based on the observations of SETHI AND HRNJAK [162]. In practical applications, a decrease of the mass flux results from a reduced compressor speed of a variable speed compressor. The liquid phase is depicted in gray, the vapor phase in white. The thickness of the liquid film is depicted larger than in reality for a better understanding.

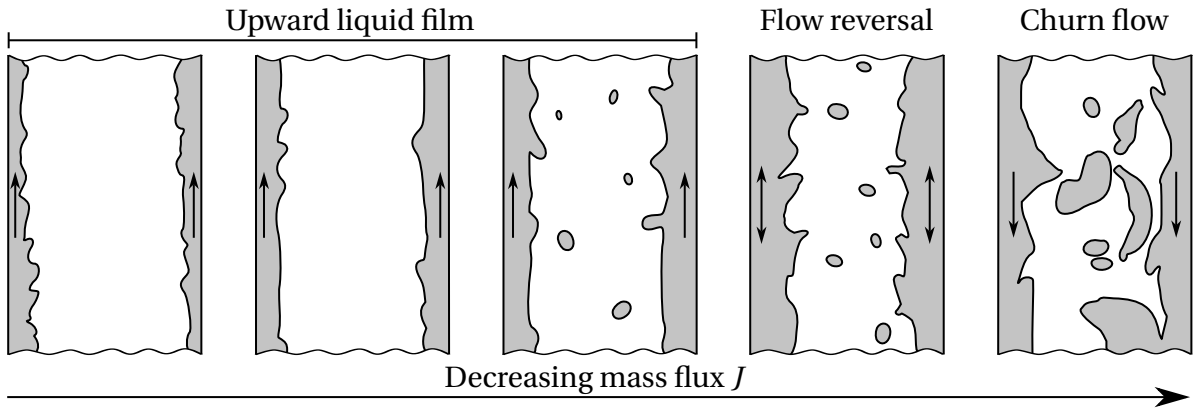

Figure 6.1: Two-phase flow in vertical suction line for different mass fluxes.

At a high mass flux, an annular flow with small ripples is observed. With decreasing mass flux the small ripples partly disappear and the film becomes smoother. With a further decrease, larger waves occur. Entrainment of liquid droplets in the gas core is observed in this regime as droplets are sheared off the large waves. The liquid film thickness increases and the pressure loss in flow direction decreases with decreasing mass flux for an upward liquid film. A further decrease of the mass flux leads to a reversal of the flow direction of the liquid film. [162] This point is called *flow reversal* [161]. The shear forces at the interfacial boundary are no longer sufficient to overcome the gravitational forces of the dense liquid film. In this flow regime, the pressure loss in flow direction increases with decreasing mass flux. If the vapor velocity is

decreased further, the wall film becomes unstable and collapses. This results in an oscillatory upward and downward movement of the liquid phase in the suction line [162] and consequently high local pressure fluctuations [160, 161]. HEWITT AND HALL-TAYLOR [161] designate the term *churn flow* for this flow regime.

6.2 Criterion for Stable Lubricant Return

Based on the fluid phenomena described in the previous Section 6.1, different researchers designed stability criteria in form of a minimum mass flux that leads to a stable lubricant return. This threshold is subsequently called critical mass flux for lubricant return J_{crit}.

Regarding the operation of refrigeration cycles, it is important that the lubricant returns continuously at a low liquid ratio. If churn flow occurs, it is possible that large amounts of incompressible liquid fill the compression volume. In this case very high mechanical stresses act on the boundaries of the compression volume during compression. This phenomenon is called liquid slug [163] and can lead to severe damage of the compressor.

To explain the difference in the criteria that were used to calculate the critical mass flux J_{crit}, the velocity profile $v_{\mathrm{l}}(x)$ of the liquid film is depicted schematically for a decreasing vapor mass flux J_{v} in Figure 6.2. At a high mass flux, the velocity profile shows positive values over the complete liquid film. The velocity gradient at the wall is positive $\frac{\partial v_{\mathrm{l}}}{\partial x}\big|_{x=0} > 0$. If the refrigerant vapor mass flux is reduced, a point is reached where the velocity gradient at the wall becomes $\frac{\partial v_{\mathrm{l}}}{\partial x}\big|_{x=0} = 0$. This means that the shear stress calculated according to Equation (6.1) for Newtonian fluids becomes $\tau_{\mathrm{w}} = \tau|_{x=0} = 0$ at the wall.

$$\tau = \mu \frac{\partial v}{\partial x} \tag{6.1}$$

HEWITT AND HALL-TAYLOR [161, p. 66] showed with an analytic model that the point of zero wall shear stress is not identical, but closely related to the point of the minimum of the pressure loss.

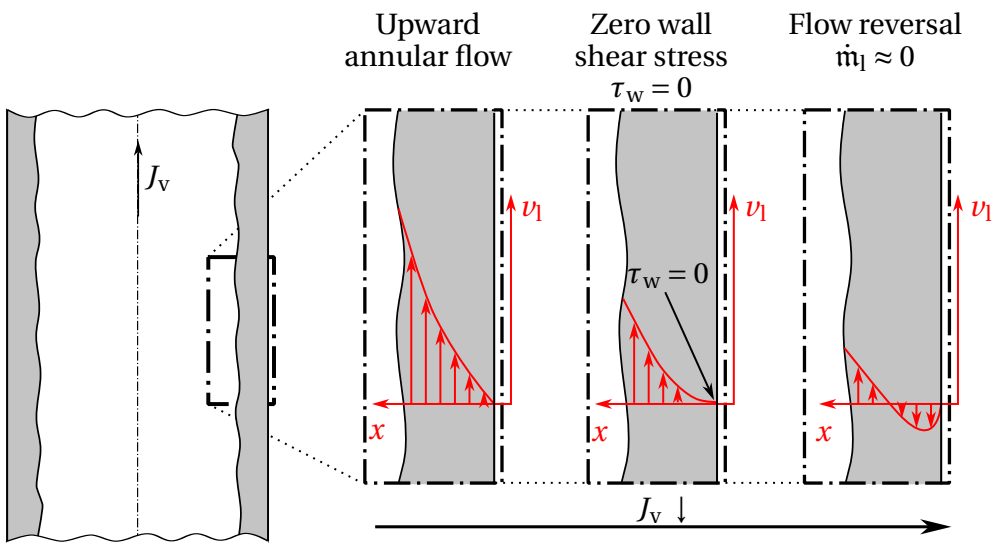

Figure 6.2: Velocity profile in liquid film for decreasing vapor mass flux J_v.

If the vapor mass flux is reduced below the point of zero wall shear stress, a part of the liquid film near the wall moves downward, while near the vapor core, the liquid is still torn upwards by the vapor core. This point is identified in experiments as the point of flow reversal.

JACOBS ET AL. [27] established a criterion for the critical mass flux J_{crit} based on the correlation for flooding[1] and flow reversal of WALLIS [164][2]. WALLIS [164] assumed that in analogy to the single-phase turbulent flow, the average turbulent stresses are related to the average momentum flux of the flow components, $\rho_v v_v (A_v/A)^{-1}$ and $\rho_l v_l (A_l/A)^{-1} = \rho_l v_l (1 - A_v/A)^{-1}$, respectively. A_v/A is the void fraction of the two-phase flow. A is the cross sectional area of the pipe. A_v and A_l are the area of vapor and liquid phase in the cross-section, respectively. WALLIS [164] related the momentum flux of vapor and liquid phase to hydrostatic forces in dimensionless groups according to Equations (6.2) and (6.3).

[1] In *flooding* experiments, a liquid is injected perpendicular to the gas flow in a vertical pipe with upward gaseous flow. For low gas velocities, the liquid flows downwards in the pipe. When the gas flow rate is increased, large waves form on the liquid film that eventually climb upwards in the pipe. This transition is called *flooding*. There is a considerable hysteresis in the mass flux J for flooding and flow reversal in experiments [161, p.14].

[2] This publication was cited in HEWITT AND HALL-TAYLOR [161, p. 17]. The original publication was not found. The derivation of the correlation is also described in detail in WALLIS [165, p. 336 ff].

$$\mathrm{Fr}_\mathrm{v}^* = \frac{v_{\mathrm{v,crit}}\rho_\mathrm{v}}{\sqrt{gD\rho_\mathrm{v}(\rho_\mathrm{l}-\rho_\mathrm{v})}} \tag{6.2}$$

$$\mathrm{Fr}_\mathrm{l}^* = \frac{v_{\mathrm{l,crit}}\rho_\mathrm{l}}{\sqrt{gD\rho_\mathrm{l}(\rho_\mathrm{l}-\rho_\mathrm{v})}} \tag{6.3}$$

These dimensionless groups Fr_v^* and Fr_l^* are modified Froude numbers[3]. WALLIS [165, p. 339] found that the occurrence of flooding can be described by Equation (6.4).

$$\mathrm{Fr}_\mathrm{v}^* + a_1\mathrm{Fr}_\mathrm{l}^* = a_2 \tag{6.4}$$

For a turbulent liquid film, it is $a_1 = 1$. The value of a_2 depends on the inlet geometry and is in the range of $0.725 < a_2 < 1$ for vertical tubes [165, p. 339].

JACOBS ET AL. [27] conducted flooding and flow reversal experiments with refrigerants R12 and R22 in combination with MO lubricants. Correlating the data for flow reversal, they neglected the contribution of the liquid film in Equation (6.4). Thus, only the modified Froude number of the vapor phase Fr_v^* remains on the left side of Equation (6.4). They obtained a value of $\sqrt{\mathrm{Fr}_\mathrm{v}^*} = \sqrt{a_2} = 0.85$ and used this value with Equation (6.2) to calculate the critical mass flux $J_{\mathrm{crit,Jacobs}}$ for lubricant return, as described in Equation (6.5).

$$J_{\mathrm{crit,Jacobs}} = J|_{\dot{m}\approx 0} = v_{\mathrm{v,crit}}\rho_\mathrm{v} = \mathrm{Fr}_\mathrm{v}^*\sqrt{gD\rho_\mathrm{v}\left(\overline{\rho}_\mathrm{l}-\rho_\mathrm{v}\right)} \tag{6.5}$$

This correlation is often found in literature as the *Jacobs*-limit.

MEHENDALE AND RADERMACHER [28] found in experiments on flow reversal of HFC refrigerants and different lubricants that the *Jacobs*-limit under-predicted the mass flux, at which they observed the beginning of flow-reversal for most of their experiments. They relate the difference between experiments and prediction to the neglected influence of liquid ratio and viscosity in the *Jacobs*-limit (Equation (6.5)). Also SETHI AND HRNJAK [162] found that the mass flux of the *Jacobs*-limit under-predicts the point of flow reversal. They found that the predicted mass flux with the *Jacobs*-limit rather corresponds to the flow transition from annular to churn flow for R1234yf and a POE lubricant of VG = 32.

[3] The Froude number relates inertia forces to gravity and is often defined differently depending on the application. The most common definitions are $\mathrm{Fr} = v/\sqrt{gL}$ [166] and $\mathrm{Fr} = v^2/(gL)$ [167]

It is also possible to argue that the point of flow reversal is not suited for a definition of the critical mass flux. At the point of flow reversal, the liquid film mass flow rate in the vertical suction line is $\dot{m}_{l,vert} \approx 0$, as shown in Figure 6.2. This point cannot represent a steady-state operation in the suction line, because the liquid film mass flow rate is $\dot{m}_{l,hor} > 0$ in horizontal or downward parts of the suction line upstream of the vertical section. The oil accumulates at the lowest position, if $\dot{m}_{l,vert} < \dot{m}_{l,hor}$. This leads to an increase of the liquid ratio over time at this location. At some point, the locally increased liquid ratio results in a flow transition to slug- or churn flow with the consequences described above. Thus, a more conservative criterion is required.

In contrast to the point of flow reversal, the mass flow rate of the liquid film is positive at the point of zero wall shear stress. MEHENDALE AND RADERMACHER [28] first used the point of zero wall shear stress of the liquid film as the criterion for a stable lubricant return, according to Equation (6.6).

$$J_{crit} = J|_{\tau_w=0} \tag{6.6}$$

The problem of this criterion is that the point of zero wall shear stress cannot be determined easily in experiments. To overcome this limitation, MEHENDALE AND RADERMACHER [28] developed a model for the two-phase flow in the vertical suction line to calculate the value of the critical mass flux J_{crit}. The boundary conditions of the model guarantee a steady-state operation ($\dot{m}_{l,vert} = \dot{m}_{l,hor}$). The modeling process is explained in the subsequent section.

In the present study, Equation (6.6) is used to define the critical mass flux.

6.3 State of the Art in Modeling of Annular Flow

This section describes the modeling approaches for the two-phase annular flow of refrigerant and lubricant in vertical suction lines found in literature.

Simple, analytic models for two-phase flow gained increased attention in the 1960's to describe boiling in nuclear power plants and to derive safety requirements [160]. Modeling approaches for different flow regimes of two-phase flow are described e.g. in MAYINGER [160]. A comprehensive derivation of a

diabatic model for annular flow can be found in the book of HEWITT AND HALL-TAYLOR [161]. The models described in the following can be considered as adiabatic derivatives of their model.

Models for the two-phase flow in vertical suction lines were published by MEHENDALE [168] and KESIM ET AL. [169]. The modeling approach of MEHENDALE [168] was subsequently used e.g. by LEE [170], CREMASCHI [23], RADERMACHER ET AL. [171], and SETHI AND HRNJAK [172].

For the present study, it was decided to adopt the modeling approach of MEHENDALE [168], because the model of KESIM ET AL. [169] used the point of flow reversal to calculate the critical mass flux. Additionally, the model of MEHENDALE [168] describes the pressure gradient in flow direction more accurately compared to the model of KESIM ET AL. [169].

In the following, the model of MEHENDALE [168] is briefly described. The complete derivation can be found in the original publication or e.g. in SETHI AND HRNJAK [172]. The basis of the two-phase models are the steady-state, incompressible and adiabatic Navier-Stokes equations for momentum and continuity in a two dimensional, cylindrical coordinate system. The following assumptions are made [28, 161, 172]:

- The flow is incompressible, adiabatic, hydrodynamically fully developed and in chemical equilibrium[4].
- The flow is axisymmetric to the pipe center with a uniform film thickness.
- The flow is in annular flow regime.
- Entrainment of liquid droplets in the vapor phase and of vapor bubbles in the liquid film is neglected.
- Density and viscosity are constant in the respective phase.
- The liquid film is a Newtonian fluid.
- The liquid film is laminar.
- The vapor core consists of pure refrigerant.

[4]The suction line is downstream of the evaporator. In the evaporator, the liquid mixture composition changes from a refrigerant rich to a lubricant rich phase (see Section 1.2). Thus, it is reasonable to assume a liquid phase saturated with refrigerant and chemical equilibrium between both phases. Additionally, the pipes of refrigeration cycles are well insulated. Nevertheless, considering the pipes as adiabatic is a simplification of the real process.

Figure 6.3 illustrates the simplified system for the model derivation.

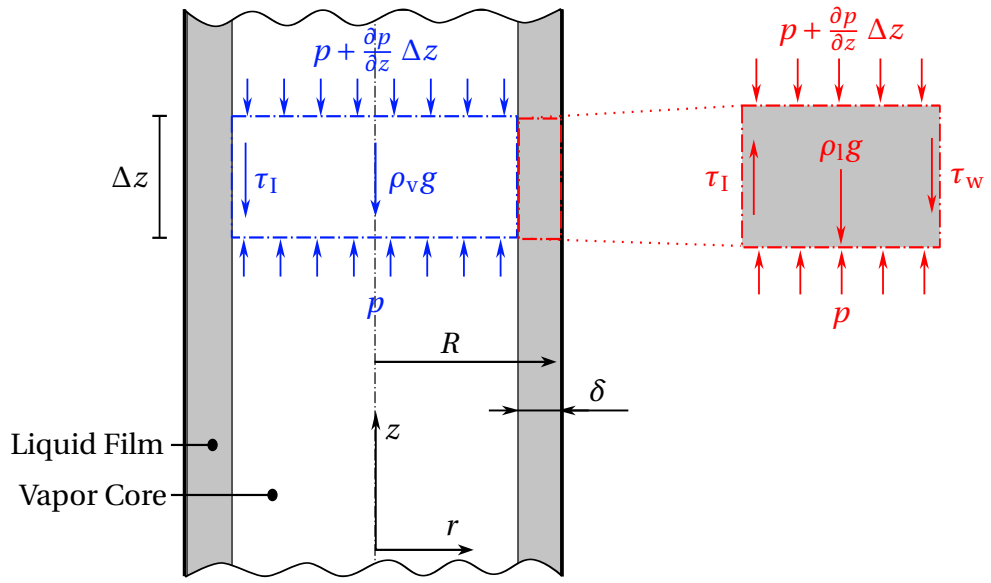

Figure 6.3: Acting forces on liquid and vapor phase of the two-phase flow.

The momentum equation contains the second derivative of the velocity with respect to the radius. Therefore, the momentum equation is integrated twice to obtain the velocity profile over the radius. The interfacial shear stress τ_I according to Equation (6.7) is used as a boundary condition for the momentum equation.

$$\tau_\mathrm{I} = \tau|_{r=R-\delta} = -\mu_\mathrm{l} \frac{\partial u}{\partial r}\bigg|_{r=R-\delta} \tag{6.7}$$

Additionally, the zero-slip boundary condition at the channel center is applied for the vapor core and the no-slip condition at the wall for the liquid film.

Equations (6.8) and (6.9) are derived to calculate the dependent variables film thickness δ and pressure gradient in flow direction $\partial p/\partial z$ from the system variables vapor mass flow rate $\dot{m}_\mathrm{v}$, fluid properties, and pipe geometry [28, 172].

$$\dot{m}_l = \frac{2\pi\overline{\rho}_l}{\overline{\mu}_l}\left\{\left[\tau_I(R-\delta)+\frac{(R-\delta)^2}{2}\left(\frac{\partial p}{\partial z}+\overline{\rho}_l g\right)\right]\left[\frac{R^2-(R-\delta)^2}{2}\ln\left(\frac{R}{R-\delta}\right)\right]\right\} \quad (6.8)$$
$$-\frac{\pi\overline{\rho}_l}{8\overline{\mu}_l}\left(\frac{\partial p}{\partial z}+\overline{\rho}_l g\right)\left[R^2-(R-\delta)^2\right]^2$$

$$\frac{\partial p}{\partial z} = -\rho_v g - \frac{2\tau_I}{R-\delta} \quad (6.9)$$

In these equations, R is the inner radius of the pipe, δ is the film thickness, and g is the gravitational acceleration. Equation (6.8) is derived by an integration of the velocity profile over the liquid film. Equation (6.9) follows from a force balance on the vapor core, as depicted in Figure 6.3. [28, 172]

The liquid mass flow rate $\dot{m}_l$ is calculated in Equation (6.10) with the process parameters oil circulation ratio OCR, refrigerant mass fraction in the liquid w_{Ref} and the mass flow of refrigerant $\dot{m}_{Ref}$ and lubricant $\dot{m}_{Lub}$. The vapor mass flow rate $\dot{m}_v$ is calculated in Equation (6.11) considering the vapor phase as pure refrigerant and subtracting the amount of dissolved refrigerant in the liquid phase $w_{Ref}\dot{m}_l$ from the total refrigerant mass flow rate $\dot{m}_{Ref}$.

$$\dot{m}_l = \frac{\mathrm{OCR}(\dot{m}_{Ref}+\dot{m}_{Lub})}{1-w_{Ref}} \quad (6.10)$$

$$\dot{m}_v = \dot{m}_{Ref} - w_{Ref}\dot{m}_l \quad (6.11)$$

Three unknown variables remain in Equations (6.8) and (6.9): the film thickness δ, the pressure gradient $\partial p/\partial z$, and the interfacial shear stress τ_I. To close the system of equations, a correlation for the interfacial shear stress τ_I is required [28, 172]. The empirical friction factor f_I according to Equation (6.12) was introduced to calculate the interfacial shear stress τ_I with the mean velocity of the vapor v_v and liquid phase v_l and the vapor density ρ_v [172].

$$\tau_I = \frac{1}{2} f_I \rho_v (v_v - v_l)^2 \quad (6.12)$$

Often, the assumption is made that the vapor velocity is much higher than the liquid film velocity: $v_v \gg v_l$ [161, p. 88].

Research on two phase annular flow in the past 60 years lead to countless friction factor correlations. Some of them are described in the following.

Interfacial Friction Factor

WALLIS [165, p.320] compared the influence of the waviness of the liquid film in two phase flow on the one hand and the surface roughness of the inner pipe wall in single phase flow on the other hand on the shear stress. He concluded that the type of shear stress correlation for rough surfaces in single phase flow can be used for two-phase annular flow. This results in the correlation for the interfacial friction factor f_I depending on the dimensionless film thickness δ/D as expressed in Equation (6.13).

$$f_\mathrm{I} = 0.005\left(1 + 300\frac{\delta}{D}\right) \tag{6.13}$$

This correlation was very successful because of its simplicity and effectiveness and was often modified to improve the accuracy. It was also used by MEHENDALE [168] in the context of the two-phase flow in suction lines.

BELT ET AL. [173] found that the *Wallis*-correlation of Equation (6.13) tends to under-predict the interfacial friction factor for a large film thickness $\delta/D > 0.02$ and to over-predict it for small film thickness of $\delta/D < 0.005$. Furthermore, they found that large waves rolling upwards in co-current vertical flow have a much larger influence on the interfacial friction factor compared to small ripple waves. They did not neglect the liquid film velocity in Equation (6.12) and considered it to be equal to the velocity of the large roll waves. This lead to the correlation for the interfacial friction factor described in Equation (6.14).

$$f_\mathrm{I} = 3.413\ 10^{-3}\ + 1.158\frac{\delta}{D} \tag{6.14}$$

Another correlation for the interfacial friction factor used for the two-phase flow of refrigerants and lubricants was developed by SETHI AND HRNJAK [172]. They used the approach of ASALI ET AL. [174] described in Equation (6.15).

$$f_\mathrm{I} = f_\mathrm{s}\left(1 + a_1\,\mathrm{Re}_\mathrm{v}^{a_2}\,\mathrm{Re}_\mathrm{l}^{a_3}\left(\delta_\mathrm{v}^{+}\right)^{a_4}\mathrm{We}^{a_5}\right) \tag{6.15}$$

SETHI AND HRNJAK [172] left out the Weber-number[5] We in their publication, most likely because data on the surface tension ς of POE lubricants is not

[5] The Weber-number relates the drag force to the cohesion force in two-phase flow: $\mathrm{We} = \rho L v^2/\varsigma$ [175] with the surface tension ς.

available. In Equation (6.15), f_s is the friction factor for single phase flow of the vapor in a smooth pipe calculated according to Equation (6.16) [172].

$$f_s = 0.046\,\mathrm{Re}_v^{-0.2} \tag{6.16}$$

The Reynolds-numbers for liquid-phase Re_l and vapor-phase Re_v are calculated according to Equations (6.17) and (6.18), respectively [172].

$$\mathrm{Re}_l = \frac{J_l D}{4\mu_l} \tag{6.17}$$

$$\mathrm{Re}_v = \frac{J_v D}{\mu_v} \tag{6.18}$$

δ_v^+ is a dimensionless number relating the film thickness to the vapor properties and the interfacial shear stress τ_i according to Equation (6.19) [172].

$$\delta_v^+ = \frac{\delta}{\mu_v}\sqrt{\tau_I \rho_v} \tag{6.19}$$

SETHI AND HRNJAK [172] used experiments of R134a and R410A with a POE lubricant from SETHI [176] and ZOELLICK [177] to regress the parameters in Equation (6.15). They found the following values: $a_1 = 0.0784$, $a_2 = -0.3$, $a_3 = -0.3$ and $a_4 = 1.4$. Literature data of the fluid properties of the liquid film were used in the parameter regression. It is unclear, if the assumed fluid properties are realistic for the conducted experiments.

Point of Zero Wall Shear Stress

The shear stress in the liquid film ($R - \delta < r < R$) is described by Equation (6.20) [161, p.58].

$$\tau(r) = \tau_I \frac{R-\delta}{r} - \frac{1}{2}\left(\frac{\partial p}{\partial z} + \rho_l g\right)\left(\frac{r^2 - (R-\delta)^2)}{r}\right) \tag{6.20}$$

For the point of zero wall shear stress it is $\tau_w = \tau|_{r=R} = 0$. This leads to Equation (6.21).

$$\tau_w = \tau_I \frac{R-\delta}{R} - \frac{1}{2}\left(\frac{\partial p}{\partial z} + \rho_l g\right)\left(\frac{R^2 - (R-\delta)^2)}{R}\right) = 0 \tag{6.21}$$

Introducing Equation (6.21) to the system of Equations (6.8 - 6.12), the critical mass flux $J_{crit} = J|_{\tau_w=0}$ can be calculated.

6.4 Literature Data on Critical Mass Flux Experiments

Experimental data of the two-phase flow of refrigerant-lubricant mixtures is used in Section 6.5 to assess the correlations on the interfacial friction factor and in Section 6.6 to validate the two-phase flow simulation. In the following, experiments are summarized that either identify stability limits for lubricant return or contain data in the vicinity of the critical mass flux.

JACOBS ET AL. [27] and MACKEN ET AL. [178] conducted experiments to identify the point of flow reversal in the two-phase flow of HCFC R22 and mineral oil lubricants. Unfortunately, they do not publish all data required for the validation of the two-phase flow model.

BIANCARDI ET AL. [25] developed a test-rig with four parallel suction lines. Each suction line was equipped with ball valves. This allowed to modify the mass flux in 3 steps as they used a fixed speed compressor. Sight glasses were installed in the top and bottom manifold to observe if the oil mass flow is upwards or downwards. This enabled the authors to indicate a range of the refrigerant velocity in which the point of flow reversal is located. The upper value can be used as a conservative limit for oil return. Astonishingly, they found a lower critical velocity for an immiscible pair of R407C and POE compared to a miscible combination. The publication is not considered for validation, as the identified threshold for lubricant return cannot be related to any of the criteria defined in Section 6.2. Furthermore, the study only contains very few data points for refrigerant-lubricant mixtures that are within the scope of the present study.

CREMASCHI [23] investigated the oil retention in the suction line for higher mass fluxes and only report some qualitative results for flow reversal.

All in all, publications that can serve as validation cases are scarce. Only the publications of MEHENDALE [168], ZOELLICK AND HRNJAK [179], RAMAKRISHNAN AND HRNJAK [180], and SETHI AND HRNJAK [162] contain useful data. These publications are presented in more detail below. More experimental two-phase flow data of refrigerants and POE lubricants, especially around the point of flow reversal, would be desirable.

Experiments of Mehendale

MEHENDALE AND RADERMACHER [28] developed a vertical test section with an injection port for the lubricant oil. This allowed to modify the refrigerant and oil mass flow independently from each other. Also pressure and superheat of the refrigerant could be adjusted. The test section had an optical access above and below the injection port. The inner diameter of the test section was $D = 8\,\text{mm}$. This set-up enabled MEHENDALE AND RADERMACHER [28] to identify the point of flow reversal more precisely compared to BIANCARDI ET AL. [25].

They conducted experiments with the HFC refrigerants R410A and R407C and a POE lubricant with a VG of 32. As a benchmark, they also investigated R22 with a mineral oil lubricant. Experiments were conducted for a lower and a higher pressure level and different oil circulation ratios. Starting with stable annular flow in the test section, the vapor mass flux was reduced until either the beginning of flow reversal with an oscillatory motion of the liquid film or a completely downward flowing liquid film was observed. A significant difference in the mass flux between the onset of flow reversal and the complete downward liquid film was observed. They found that the onset of flow reversal occurs at a lower mass flux if the oil circulation ratio was increased. [168]

The experiments of MEHENDALE [168] showed a severe difference to real applications. The lubricant injected into the test section had not been in contact with the refrigerant before. The viscosity is expected to be much higher compared to a lubricant saturated with refrigerant. Therefore, the results of MEHENDALE [168] can only be used in Section 6.6.1 to validate the two-phase model without the calculation of the fluid properties[6]. Fluid properties of the pure lubricant are used instead.

[6] In the experimental investigation of the solubility of refrigerant-lubricant mixtures, it is reported that it takes several hours until the vapor pressure settles on a constant level even in a stirred vessel (see e.g. [73, 104]). Therefore, it is expected that the pure lubricant properties describe the liquid phase of the two-phase flow better than the properties of a saturated lubricant.

Experiments of Zoellick, Ramakrishnan, and Sethi

ZOELLICK AND HRNJAK [179] developed a closed loop test-rig to observe the two-phase flow of refrigerant and lubricants in horizontal and vertical segments. The test-rig did not contain a compressor and consisted of a single pressure level. This reduced vibrations that might affect the transport of the liquid film.

In the test rig, liquid refrigerant and a lubricant-rich mixture of refrigerant and lubricant are mixed. To obtain the desired oil circulation ratio, the mass flow rate can be adjusted separately for the liquid refrigerant and the lubricant-rich liquid using two gear pumps. Then, the mixture is evaporated and leaves the evaporator with an adjustable superheat. As in a refrigeration cycle, a liquid phase that contains the lubricant and dissolved refrigerant remains at the evaporator outlet. Subsequently, the two-phase flow enters first a horizontal and then a vertical test section. Both test sections can be removed from the rest of the cycle to weigh the retained oil in the test sections. Downstream of the test sections, the two-phase flow is separated. The lubricant-rich liquid phase enters a storage vessel. The vapor phase that consists of pure refrigerant is condensed. The refrigerant condenser and the storage vessel for the liquid-phase are connected to the respective gear pumps to close the cycle. [179]

The test-rig of ZOELLICK AND HRNJAK [179] was subsequently used for further studies by RAMAKRISHNAN AND HRNJAK [180] and SETHI AND HRNJAK [162].[7] The meta-data of the experiments conducted by the different authors are summarized in Table 6.1. RAMAKRISHNAN AND HRNJAK [180] focused on the influence of the viscosity on the two-phase flow by using lubricants of different viscosity grades. SETHI AND HRNJAK [162] modified the test-rig to investigate the influence of the pipe inclination and compared the refrigerants R1234yf and R134a. The only information on the lubricant given in all publications is the viscosity grade. The trade name or values for density or viscosity are not indicated.

Experiments were conducted for various mass fluxes at a fixed OCR, evapora-

[7] The publications of ZOELLICK AND HRNJAK [179], RAMAKRISHNAN AND HRNJAK [180], and SETHI AND HRNJAK [162] are related to the Master's theses of the respective first authors [176, 177, 181]. The Master's theses contain raw data of the experiments.

tion temperature T_{evap}, and superheat ΔT_{SH}. The challenge in the test-setup is to adjust the OCR to the desired value, as the lubricant-rich liquid contains dissolved refrigerant, as well. The refrigerant mass fraction was estimated based on an the ideal mixture law of the density (see Equation (3.34)) and literature data from the ASHRAE handbook of refrigeration from 2002. This version of the ASHRAE handbook was not available to the author of the present study, but in the more recent version (OWEN [26]), data of the mixture density is not published for all of the investigated refrigerant-lubricant mixtures. Thus it is unclear, how the OCR was determined in these cases.[8]

Table 6.1: Meta-data of experiments of Zoellick, Ramakrishnan, and Sethi.

Case No.	Author	Ref.	Lub. VG	D mm	T_{evap} °C	ΔT_{SH} K	OCR %	Fluid props. in [26]
1	SETHI [176]	R134a	32	10.2	13.5	15	1;3;5	✓
2	RAMAKRISHNAN [181]	R134a	100	10.2	13.0	15	1;3;5	✓
3	ZOELLICK [177]	R410A	32	7.2	12.1	5;10;15	1;3;5	✓
4	RAMAKRISHNAN [181]	R410A	32	10.2	11.7	15	1;3;5	✓
5	ZOELLICK [177]	R410A	32	18.5	14.9	15	3;5	✓
6	RAMAKRISHNAN [181]	R410A	100	10.2	11.7	15	1;3;5	-
7	SETHI [176]	R1234yf	32	10.2	13.0	15	1;3;5	-
8	RAMAKRISHNAN [181]	R1234yf	100	10.2	13.2	15	1;3;5	-

The superheat $\Delta T_{SH} = 15\,K$ used in most of the experiments is relatively high compared to practical applications. The high superheat leads to a low amount of dissolved refrigerant in the liquid phase and, thus, to a high viscosity of the liquid phase.

[8] Additionally, it was found regarding the published raw data in the thesis of ZOELLICK [177] that a recalculation of the OCR leads to different results compared to the published data. This can be related to the pure lubricant density described in Equation 3.3 of ZOELLICK [177]. If transposed digits are assumed and the reported offset-value of $\rho_0 = 9\underline{84}.1\,kg\,m^{-3}$ is modified to $\rho_0 = 9\underline{48}.1\,kg\,m^{-3}$, the calculated values for the OCR agree with the published values. Albeit, the modified offset value of $\rho_0 = 948.1\,kg\,m^{-3}$ leads to unrealistically low density values for polyol ester lubricants. Thus, it seems likely that there is a typo in the code of the process control. This would result in values of the OCR that are approximately 50% higher compared to the published values. It is not possible to recalculate the OCR with the published raw data in the theses of RAMAKRISHNAN [181] and SETHI [176]. Therefore, it is unclear, if this issue also affects the publications of RAMAKRISHNAN AND HRNJAK [180] and SETHI AND HRNJAK [162].

The experiments presented in this section are subsequently used in Section 6.5 to assess the correlations of the interfacial friction factor f_I and in Section 6.6.2 to validate the two-phase flow model. The case numbers indicated in Table 6.1 are subsequently used to refer to the respective experiments.

6.5 Assessment of Interfacial Friction Factor Correlations

In the present section, the different correlations for the interfacial friction factor f_I introduced in Section 6.3 are assessed regarding their applicability for refrigerant-lubricant mixtures. Therefore, the interfacial friction factor f_I is calculated from published raw data of the experiments presented in the previous Section 6.4. Beside these experiments, there are other publication that determined the experimental friction factor in the two phase annular flow of refrigerants and lubricants, e.g. CREMASCHI [23] or LEE [170]. Unfortunately, the required raw-data to calculate the friction-factor are not published in these studies.

To calculate the friction factor f_I from experimental data, Equations (6.9) and (6.12) are combined. This results in Equation (6.22).

$$f_\mathrm{I} = -\frac{\left(\frac{\partial p}{\partial z} + \rho_\mathrm{v} g\right)(R-\delta)}{\rho_\mathrm{v}(v_\mathrm{v} - v_\mathrm{l})^2} \tag{6.22}$$

The vapor velocity v_v and liquid velocity v_l are calculated with the cross-sectional area, mass flow rate, and density of vapor and liquid phase, respectively, according to Equations (6.23) and (6.24).

$$v_\mathrm{v} = \frac{\dot{\mathfrak{m}}_\mathrm{v}}{\pi \rho_\mathrm{v}(R-\delta)^2} \tag{6.23}$$

$$v_\mathrm{l} = \frac{\dot{\mathfrak{m}}_\mathrm{l}}{\pi \overline{\rho}_\mathrm{l} \delta (2R-\delta)} \tag{6.24}$$

The film thickness δ is calculated with the mass of the liquid film in the test section $\mathfrak{m}_\mathrm{l}$ of the experiments assuming a constant film thickness δ along the length of the test section L_TS and neglecting liquid droplet entrainment in the

vapor core flow according to Equation (6.25).

$$\delta = R - \sqrt{R^2 - \frac{\mathfrak{m}_\mathrm{l}}{\pi \overline{\rho}_\mathrm{l} L_\mathrm{TS}}} \tag{6.25}$$

The mass of the liquid film $\mathfrak{m}_\mathrm{l}$ cannot be measured directly. It is determined by the mass of lubricant $\mathfrak{m}_\mathrm{Lub}$ retained in the test section and the mass fraction of dissolved refrigerant $w_\mathrm{l,Ref}$ according to Equation (6.26).

$$\mathfrak{m}_\mathrm{l} = \frac{\mathfrak{m}_\mathrm{Lub}}{1 - w_\mathrm{l,Ref}} \tag{6.26}$$

ZOELLICK AND HRNJAK [179], RAMAKRISHNAN AND HRNJAK [180], and SETHI AND HRNJAK [162] determined the mass of retained oil m_Lub by venting and evacuating the test section.

SETHI AND HRNJAK [172] did not publish the mass fraction of dissolved refrigerant $w_\mathrm{l,Ref}$, the vapor density ρ_v, and liquid density $\overline{\rho}_\mathrm{l}$ required to calculate the friction factor. Therefore, these values are calculated with the PCP SAFT EoS. This step leads to deviations to the the friction factor depicted in SETHI AND HRNJAK [172]. The values of the properties calculated in the present study can be found in Table 6.2. The fluid properties are subsequently used in the validation of the two-phase flow model, as well. Therefore, Table 6.2 contains also the liquid viscosity $\overline{\mu}_\mathrm{l}$, calculated with Equations (5.10) and (5.15). The solubility differs significantly for the different refrigerants. R410A shows a higher solubility in the POE lubricants compared to R1234yf. The solubility of all refrigerants is higher for the lubricant 100-1 compared to lubricant 32-1. This can be explained by the composition of the lubricant that consists only of DiPEs. DiPEs show six polar carboxylic groups per molecule in contrast to four carboxylic groups per PE-molecule. These polar groups serve as preferred bonding spot for polar refrigerants [118]. The higher number of carboxylic groups leads to more dissolved refrigerant molecules in the lubricant. A comparison of *Cases 2* and *7* shows that the solubility strongly affects the liquid viscosity $\overline{\mu}_\mathrm{l}$, as the mixture viscosity of *Case 7* with a lubricant of VG = 32 is higher compared to *Case 2* with a lubricant of VG = 100 for similar conditions. The friction factor calculated from the experimental data is depicted in Figure 6.4 over the dimensionless film thickness $\delta\, D^{-1}$.

Table 6.2: Calculated fluid properties for the two-phase experiments.

Case No.	Author	Ref.	Lub. ID[a]	T_{evap} °C	ΔT_{SH} K	ρ_v $\frac{kg}{m^3}$	μ_v μPa s	$x_{l,Ref}$ %	$\overline{\rho}_l$ $\frac{kg}{m^3}$	$\overline{\mu}_l$ mPa s
1	SETHI [176]	R134a	32-1	13.5	14.5	21.02	11.85	67.1	1040	6.95
2	RAMAKRISHNAN [181]	R134a	100-1	13.0	14.9	20.63	11.85	80.2	1054	10.15
3.1	ZOELLICK [177]	R410A	32-1	12.1	5.6	43.01	13.03	89.1	1064	4.56
3.2	ZOELLICK [177]	R410A	32-1	12.1	10.0	41.63	13.21	82.9	1038	6.44
3.3	ZOELLICK [177]	R410A	32-1	12.2	15.1	40.36	13.42	76.1	1020	8.35
4	RAMAKRISHNAN [181]	R410A	32-1	11.7	15.0	39.87	13.39	76.9	1021	3.64
5	ZOELLICK [177]	R410A	32-1	14.9	13.6	44.12	13.54	79.0	1023	2.98
6	RAMAKRISHNAN [181]	R410A	100-1	11.7	15.1	39.83	13.40	85.3	1028	5.78
7	SETHI [176]	R1234yf	32-1	13.0	14.9	24.58	12.56	51.5	1013	13.84
8	RAMAKRISHNAN [181]	R1234yf	100-1	13.2	15.1	24.72	12.58	58.0	1011	41.62

a: See Table 3.10 for information on the lubricant.

Additionally, friction factor data of two-phase flow experiments with air and water or other solutions are shown. The meta-data of these experiments are summarized in Table 6.3.

The marker types in Figure 6.4 refer to the experiment as indicated in the legend. The marker color refers to the liquid ratio LR. The liquid ratio LR is

Table 6.3: Vertical two-phase flow experiments with air and water or solutions.

Case No.	Author	L_{TS}[a] m	D mm	Gas	Liquid	T °C	ρ_g $\frac{kg}{m^3}$	ρ_l $\frac{kg}{m^3}$	μ_l mPa s
A1	WOLF ET AL. [182]	10.1	31.8	Air	Water	25	1.953[b]	997[b]	0.890[b]
A2	ZABARAS ET AL. [183]	1.9	50.8	Air	Solution[c]	25	1.637[b]	1020	1.040
A3.1	FUKANO AND FURUKAWA [184]	3.5	26.0	Air	Water-Glycerol[d]	28	1.273[b]	998	0.848
A3.2								1113	3.784
A3.3								1149	6.434
A3.4								1159	9.967

a: Distance between heighest measurement probe and liquid inlet in the experimental setup.

b: Values are calculated with *CoolProp* [41].

c: Aqueous solution with 1 mol $kg^{-1}_{H_2O}$ sodium hydroxyde, 0.005 mol $kg^{-1}_{H_2O}$ potassium ferricyanide, and 0.005 mol $kg^{-1}_{H_2O}$ potassium ferrocyanide.

d: Mass fraction of glycerol in solution is $w_{A3.1} = 0$, $w_{A3.2} = 0.45$, $w_{A3.3} = 0.53$, and $w_{A3.4} = 0.60$.

defined in Equation (6.27) as the ratio of the liquid film mass flow rate $\dot{m}_l$ to the total mass flow rate $\dot{m}_l + \dot{m}_v$.

$$\mathrm{LR} = \frac{\dot{m}_l}{\dot{m}_l + \dot{m}_v} \tag{6.27}$$

The calculated values are compared to the friction factor correlations of *Wallis* (Equation (6.13)) and *Belt* (Equation (6.14)).[9]

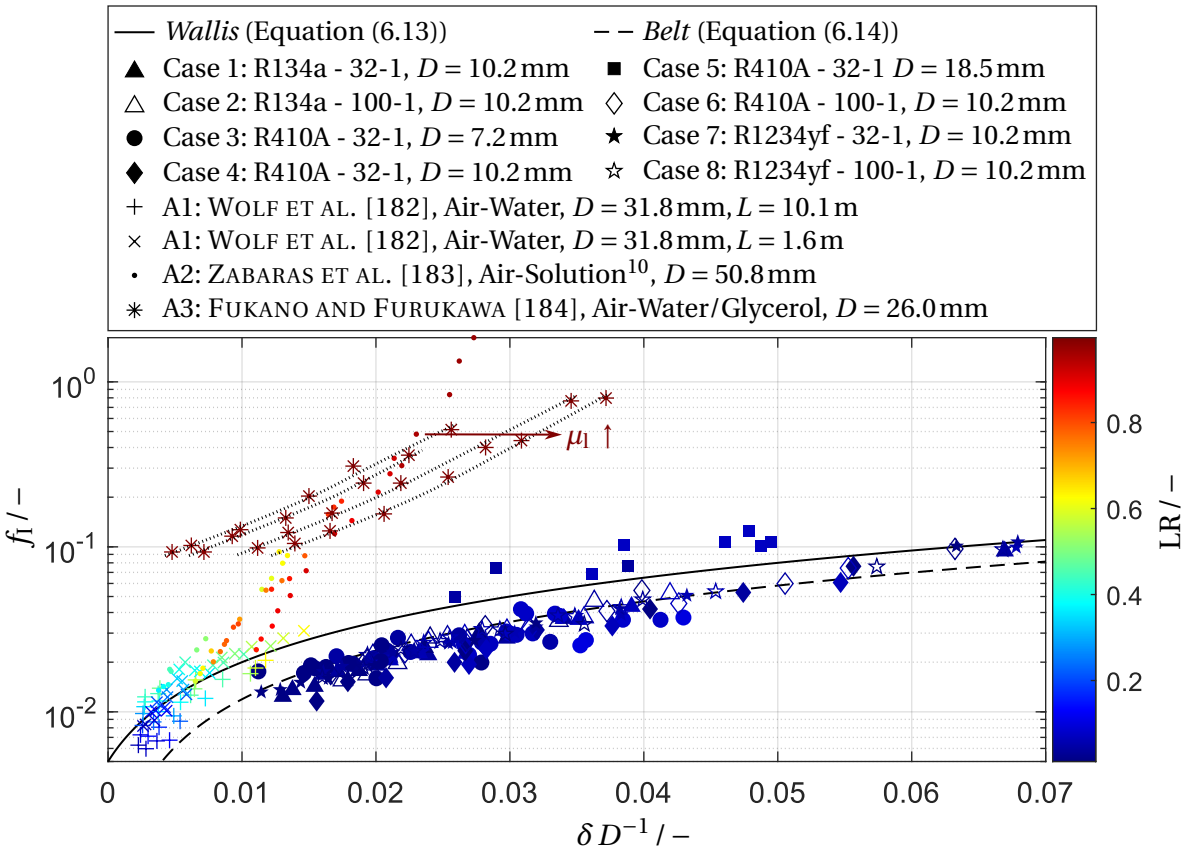

Figure 6.4: Comparison of the interfacial friction factor f_l of refrigerant-lubricant and water-air experiments.

On a first view, the refrigerant-lubricant mixture data (*Cases 1-8*) can be distinguished easily from the air - water / solution data (*Cases A1-A3*) due to the dark blue color of the data points, which stands for a low liquid ratio LR.

[9] The correlation of SETHI AND HRNJAK [172] depends on multiple parameters. Therefore, it cannot be depicted in Figure 6.4 in a way that it can be compared to the experimental friction factor values reasonably.

[10] For information on the solution refer to Table 6.3, Footnote c.

Regarding the refrigerant-lubricant *Cases 1-8*, the experimental results scatter around the correlation of *Belt* (Equation (6.14)) for a dimensionless film thickness $\delta/D < 0.05$, except for *Case 5*. There are only few results with a larger film thickness, but it seems that these are approximated better by the correlation of *Wallis* (Equation (6.13)). The higher friction factor of *Case 5* compared to the *Cases* (*1-4, 6-8*) is related to issues in the conduction of the experiments.[11]

BELT ET AL. [173] found that the correlation of *Wallis* (Equation (6.13)) is valid in the range of $0.005 < \delta/D < 0.02$. The correlation of *Belt* (Equation (6.14)) was developed with experiments on the two-phase flow of water and air in a range of $0.003 < \delta/D < 0.016$ [173]. A part of the experimental data on refrigerants and lubricants exceeds this range to a large extend.

In the following, the experiments with refrigerants and lubricants (*Cases 1-8*) are compared to the experiments with air and water or other solutions (*Cases A1-A3*). For a similar value of the friction factor f_{I}, the dimensionless film thickness δD^{-1} is much higher for the two-phase flow of refrigerants and lubricants compared to the two-phase flow of air and water or other solutions. There are some hypotheses that might explain the difference:

- The vapor density ρ_{v} of the HFC and HFO refrigerants is much higher compared to the density of air, as it can be seen comparing the respective values in Table 6.1 and in Table 6.3. The higher vapor density of the refrigerant compared to air leads to a significantly smaller friction factor (see Equation (6.5)) and liquid ratio (see Equation (6.27)). This explains the difference between the experiments with air of *Cases A1* and *A2* on the one hand and refrigerants in *Cases 1-8* on the other hand.
- The higher liquid film viscosity leads to a larger film thickness for a similar liquid ratio. This effect can be observed for *Case A3*. The same effect exists also for the refrigerant-lubricant experiments, but it is hard to see in Figure 6.4, as the markers of different experiments overlap. Therefore, the friction factor of the *Cases 1-8* is depicted in Figure G.1 in the Appendix separately for each refrigerant.

[11] For the large pipe diameter of $D = 18.5\,\mathrm{mm}$, ZOELLICK [177] faced issues with lubricant entering the connection ports of the differential pressure transducers, when the valves that separate the test sections from the rest of the cycle are actuated. Therefore, he conducted separated measurements for pressure loss and oil retention.

- At least in the lower parts of the vertical test section of *Cases 1-8*, the flow cannot be considered as hydrodynamically developed. The film thickness of the refrigerant-lubricant experiments was obtained by averaging the retained oil over the length of the test section. The difference between a hydrodynamically developed and an undeveloped flow can be observed comparing the calculated friction factor data of WOLF ET AL. [182] obtained at a height $L = 10\,\mathrm{m}$ and a height $L = 1.6\,\mathrm{m}$[12]. At the height $L = 1.6\,\mathrm{m}$, the flow is not developed hydrodynamically. This leads to higher values of friction factor and film thickness.Therefore, averaging the retained oil over the length of the test section might lead to a higher film thickness, if the flow is not developed hydrodynamically in the lower part of the test section.
- The phase interface of the refrigerant-lubricant flow might be less wavy compared to air-water or air-glycerol mixtures. There is no data for two-phase refrigerant-lubricant flow available to quantify this.
- Droplet entrainment in the vapor core was neglected in the calculation of the friction factor but occurs in the experiments (see Section 6.1). This leads to a larger calculated film thickness δ. Based on the available data, it is not possible to quantify the effect.

Further research is required to clarify the influence of different fluid combinations on the friction factor. For the thesis at hand, it is important to find a correlation for the friction factor that properly models the interfacial shear stress τ_I in the suction line of the vapor cycle. In this regard, the correlation of *Belt* (Equation (6.14)) seems promising. Nevertheless, the correlations of *Wallis* (Equation (6.13)) and *Sethi* (Equation (6.15)) are also considered in the validation of the two-phase flow model in Section 6.6 to ensure that the critical mass flux J_crit is predicted as accurate as possible.

[12] The height $L = 1.6\,\mathrm{m}$ is related to the pressure measurement. The data of the film thickness used to calculate the friction factor were obtained at $L = 1.07\,\mathrm{m}$.

6.6 Validation of the Critical Mass Flux Prediction

In this section, the two-phase flow model is validated with experimental literature data in two steps. First, only the two-phase flow model is validated with flow reversal experiments of MEHENDALE [168]. In the second step, the complete tool chain to predict the critical mass flux is validated with experiments of ZOELLICK AND HRNJAK [179], RAMAKRISHNAN AND HRNJAK [180], and SETHI AND HRNJAK [162]. The tool chain consists of the determination of the pure lubricant composition in Chapter 3, the solubility calculation of the refrigerant-lubricant mixture in Chapter 4, the calculation of the mixture viscosity in Chapter 5 and the calculation of the critical mass flux with the two-phase flow model (see Figure 1.3).

For the two-phase flow model, Equations (6.8 - 6.12) are implemented in Matlab®. The system of Equations is solved with the nonlinear least squares solver *lsqnonlin* of Matlab®. The fluid properties, inner pipe diameter D, and operation parameters pressure p, Temperature T, refrigerant mass flux J_{Ref}, and OCR are used as input parameters to the model. The critical mass flux J_{crit} is computed using Equation (6.21) with the Matlab® solver *fzero*. The pressure gradient $\partial p/\partial z$, interfacial shear stress τ_{I}, and film thickness δ of Equation (6.21) are determined with the two-phase flow model. This two-stage approach was found to be more robust compared to a the solution in a single stage.

6.6.1 Validation with Experiments of Mehendale

In the following, the experimental data of MEHENDALE [168] described in Section 6.4 are used to validate the prediction of the critical mass flux. In the publications of MEHENDALE [28, 168], the pressure loss over the test section is not reported. Nevertheless, the observed mass flux for the onset of flow reversal in the experiments can be compared to the model predictions for similar flow conditions. Analogously to the procedure in MEHENDALE [168], it is assumed that the onset of flow reversal can be described with the point of zero wall shear stress $J_{\mathrm{fr,exp}} \approx J_{\mathrm{crit}}$.

In contrast to MEHENDALE [168], the pure lubricant viscosity and density are used in this study to calculate the critical mass flux with the two-phase flow model, because MEHENDALE [168] injected pure lubricant to the test section.[13] The pure lubricant liquid density and viscosity were read from the Daniels plots in MEHENDALE [168] that belong to the lubricant used in the experiments. The density and viscosity of the refrigerant vapor were obtained from *CoolProp* [41]. The data of the fluid properties are reported in Table H.1 in the Appendix.

Subsequently, the critical mass flux is calculated with the three different friction factor correlations of *Wallis* (Equation (6.13)), *Belt* (Equation (6.14)) and *Sethi* (Equation (6.15)). The results are compared in Table 6.4. Detailed results on the deviation of each data point are summerized in Table H.1 in the Appendix.

Table 6.4: Deviation between observed mass flux for onset of flow reversal $J_{\text{fr,exp}}$ in experiments of MEHENDALE [168] and predicted critial mass flux $J_{\text{crit,mod}}$.

f_{l}-corrlation	R410A-POE			R407C-POE		
	AAD %	Bias %	MD %	AAD %	Bias %	MD %
Wallis (Equation (6.13))	8.9	-8.7	18.1	8.0	-7.2	13.6
Belt (Equation (6.14))	6.7	4.8	15.9	8.1	8.1	20.2
Sethi (Equation (6.15))	46.7	-46.7	55.5	36	-36	47

For the mixture of R410A and the POE with a VG of 32, the correlation of *Belt* shows the lowest AAD. For the mixture with R407C, the correlation of *Wallis* shows a slightly better AAD compared to the correlation of *Belt*. The correlation of *Sethi* fails to predict the critical mass flux accurately. This is related to the high liquid viscosity that is considered in form of the liquid Reynolds-number in the friction factor correlation of *Sethi*.

Figure 6.5 compares the observed mass flux for the onset of flow reversal $J_{\text{fr,exp}}$ by MEHENDALE [168] to the predicted critical mass flux $J_{\text{crit,mod}}$ with the two-phase flow model. The color of the markers represents the OCR.

[13] For the dynamics of the solution process of refrigerants in lubricants see Footnote 6 on page 141.

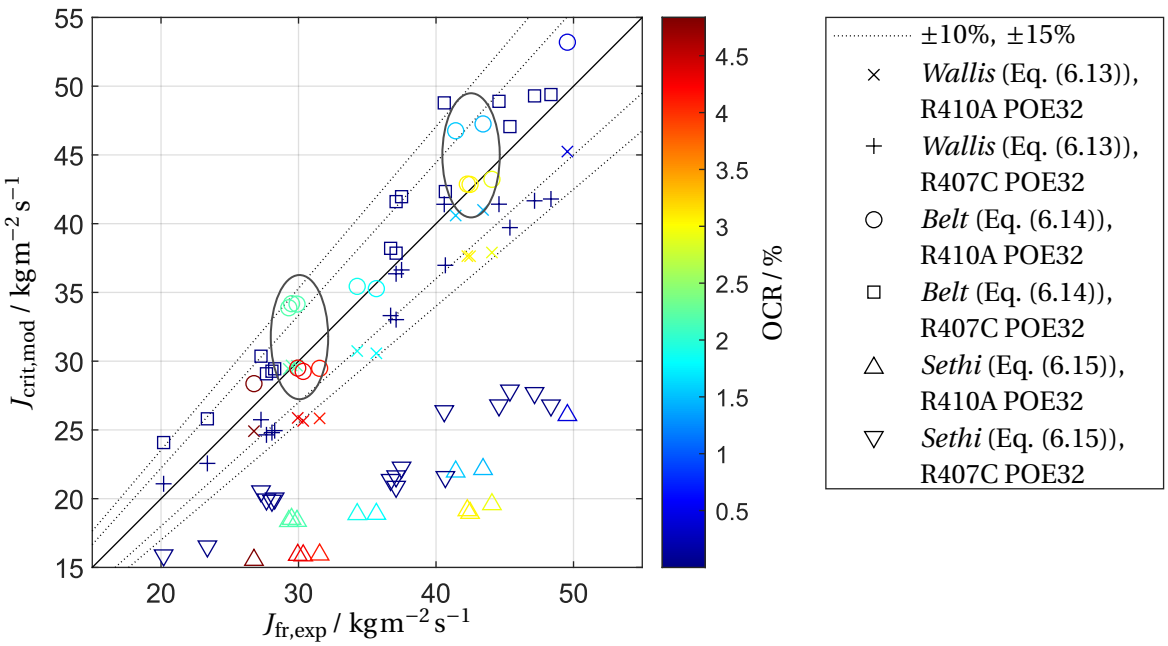

Figure 6.5: Comparison of observed mass flux for the onset of flow reversal $J_{fr,exp}$ in experiments [168] to the predicted critical mass flux $J_{crit,mod}$ for different friction factor correlations.

The predicted critical mass flux $J_{crit,mod}$ with the correlation of *Belt* (Equation (6.14)) tends to over-estimate the observed mass flux for the onset of flow reversal $J_{fr,exp}$. In contrast, $J_{fr,exp}$ is under-estimated with the correlation of *Wallis* (Equation (6.13)). The data points within the oval markings in Figure 6.5 have a similar mass flux of the onset of flow reversal $J_{fr,exp}$ but a different oil circulation ratio OCR. For these points it can be observed that the predicted critical mass flux is significantly higher for a lower OCR. This means that the two-phase flow model over-rates the influence of the oil circulation ratio on the critical mass flux.

All in all, the friction factor model of *Belt* (Equation (6.14)) is found the best option to predict the critical mass flux, because it leads to accurate results with a slight over-estimation of the critical mass flux $J_{crit,mod}$, which is preferred over an under-estimation shown by the correlation of *Wallis* (Equation (6.13)).

6.6.2 Validation with Experiments of Zoellick, Ramakrishnan, and Sethi

The experiments of ZOELLICK AND HRNJAK [179], RAMAKRISHNAN AND HRNJAK [180], and SETHI AND HRNJAK [162] presented in Section 6.4 remain the only cases to validate the complete tool chain (see Figure 1.3) containing the determination of the lubricant composition, the calculation of solubility and liquid density $\overline{\rho}_\mathrm{l}$ with the PCP SAFT EoS, the prediction of the liquid viscosity $\overline{\mu}_\mathrm{l}$ with the liquid mixture viscosity model of KENDALL AND POTTER [156] (Equation (5.10)) and the calculation of the critical mass flux J_crit with the two-phase flow model. The liquid phase is considered as a mixture of refrigerant and lubricant, which is in chemical equilibrium with the vapor phase.

The critical mass flux $J_\mathrm{crit} = J|_{\tau_\mathrm{w}=0}$ was not determined directly in the experiments, as the wall shear stress τ_w was not measured. Therefore, the mass flux at the minimum of the pressure loss $J|_{\min(-\partial p/\partial z),\mathrm{exp}}$ is compared to the prediction of the two-phase flow model $J|_{\min(-\partial p/\partial z),\mathrm{mod}}$ in the validation. The critical mass flux J_crit is close to the mass flux of the minimum in the pressure loss $J|_{\min(-\partial p/\partial z)}$ [161, p. 66].

The two-phase flow simulation is executed with the fluid properties of the different cases (see Table 6.2) and the friction factor correlations of *Wallis* (Equation (6.13)), *Belt* (Equation (6.14)), and *Sethi* (Equation (6.15)).

The mass flux of the minimum pressure loss calculated with the two-phase flow model $J|_{\min(-\partial p/\partial z),\mathrm{mod}}$ is compared to the mass flux of the lowest pressure loss found in the experiments $J|_{\min(-\partial p/\partial z),\mathrm{exp}}$. Unfortunately, the difference in the mass flux ΔJ_exp of the data-points in the experiments is not very high around the minimum pressure loss (see Figures 6.6a and 6.7a). Thus, there is a large uncertainty in the mass flux at the minimum of the pressure loss $J|_{\min(-\partial p/\partial z),\mathrm{exp}}$. The calculated deviations are summarized in Table 6.5.

The case numbers introduced in Table 6.1 are subsequently used for the comparison of the cases. *Case 3* is not considered in the validation, because the experimental data points have a significantly higher mass flux than the mass flux at the minimum pressure loss $J|_{\min(-\partial p/\partial z),\mathrm{mod}}$.

The friction factor correlation of *Belt* (Equation (6.14)) leads to the best results.

Table 6.5: Deviation of mass flux at minimum pressure loss $J|_{\min(-\partial p/\partial z)}$ between prediction and experiment for different friction factor correlations.

Case[a]	*Wallis* (Eq. (6.13))			*Belt* (Eq. (6.14))			*Sethi* (Eq. (6.15))		
	OCR in %			OCR in %			OCR in %		
	1	3	5	1	3	5	1	3	5
	Deviation[b] ϵ in %			Deviation[b] ϵ in %			Deviation[b] ϵ in %		
1	-18.2	-26.1	-26.3	-1.5	-14.7	-10.4	-5.7	-18.5	-18.4
2	-30.3	-17.4	-15.6	-16.1	0.5	-1.9	-30.3	-17.4	-20.2
4	-29.7	-27.6	-28.5	-13.8	-13.9	-14.5	-8.5	-11.2	-11.7
5		(48.3)	(53.9)		(78.1)	(80.9)		(74.3)	(77.1)
6	-28.6	-6.3	-27.7	-15.1	12.1	-16.4	-20.5	1.1	-24.9
7	-12.4	-14.2	-11.1	4.7	-1.0	2.5	-21.0	-27.4	-29.4
8	-16.7	-15.4	-17.7	-3.9	-1.6	-8.3	-42.3	-38.2	-36.5
Average	-22.7	-17.8	-21.2	-7.6	-3.1	-8.2	-21.4	-18.6	-23.5

a: Information on the different cases can be found in Table 6.1

b: Deviation calculated with Equation (3.27)

The average deviation is below 10%, which is considered acceptable. The mass flux at the minimum pressure loss $J|_{\min(-\partial p/\partial z),\mathrm{mod}}$ is slightly underestimated in most cases. Thus, a safety factor should be considered.

The table shows a high deviation for *Case 5*. In contrast to most of the other cases, the mass flux at the minimum of the pressure loss is over-predicted. The deviation cannot be explained with possible deviations in the calculation of the fluid properties, as similar properties are used in *Case 4* (see Table 6.2). *Case 4* shows a much lower deviation compared to *Case 5*. The deviations are rather related to issues in the conduction of the experiments, as reported by ZOELLICK [177].[14] Therefore, the calculated values for *Case 5* are set into brackets and are not considered in the calculation of the average deviation.

In Figure 6.6 and 6.7, pressure loss $-\partial p/\partial z$ and oil retention OR calculated with the two-phase flow model and the considered friction factor correlations are compared to experimental data for a varying mass flux J. The data at an OCR = 3% of *Case 7* and *Case 8* are selected for comparison.

[14] For the issues in the experiments of ZOELLICK [177] see Footnote 11 on page 148.

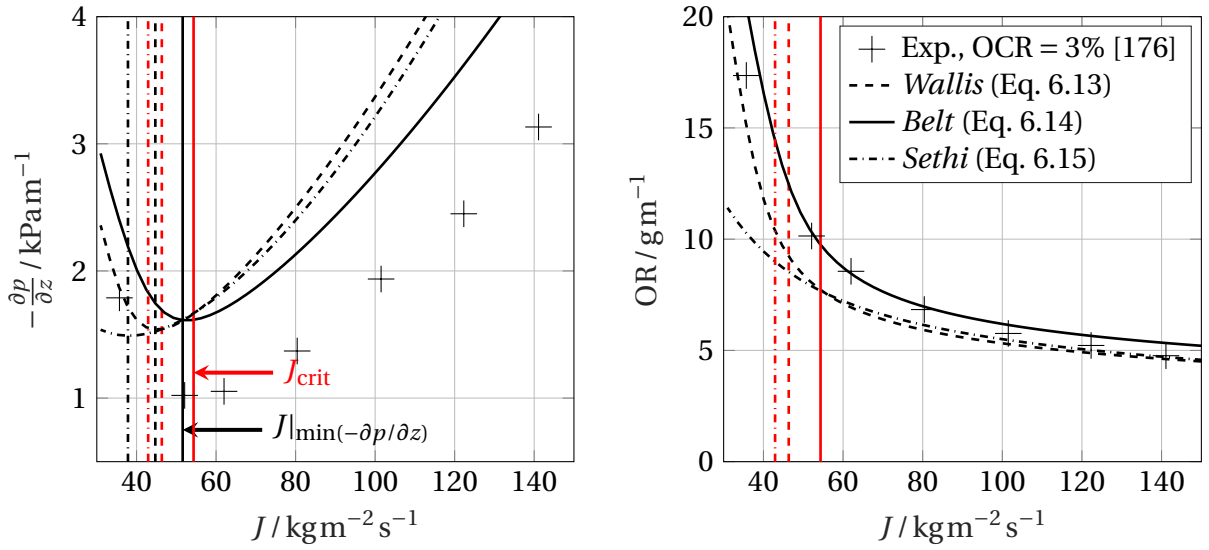

(a) Pressure loss. **(b)** Oil retention.

Figure 6.6: Comparison of experimental results with two-phase flow simulation conducted with different friction factor correlations for R1234yf and the lubricant 32-1 (*Case 7*).

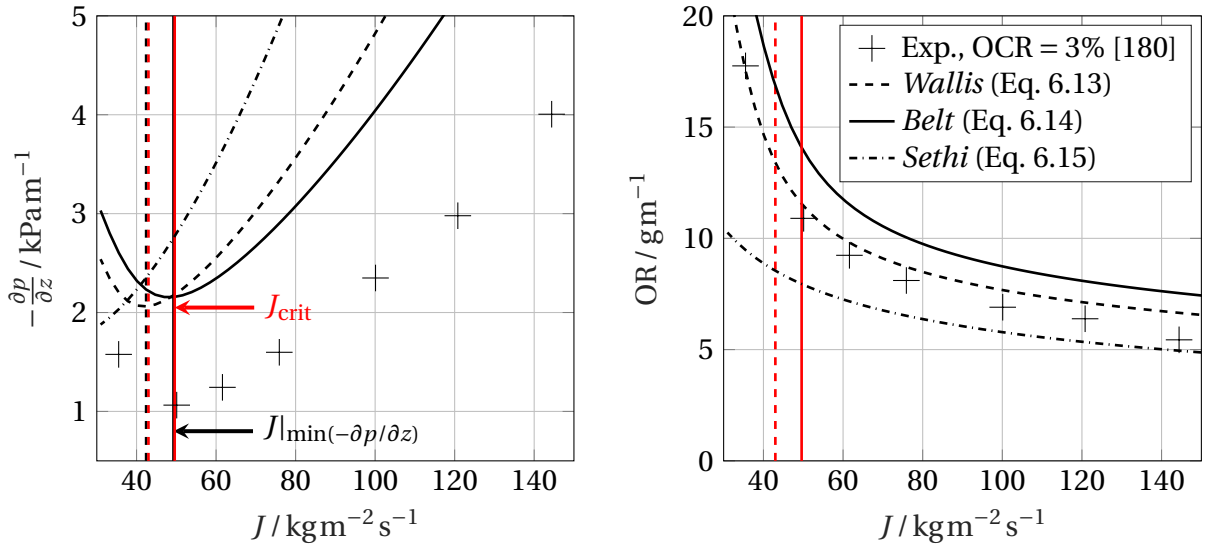

(a) Pressure loss. **(b)** Oil retention.

Figure 6.7: Comparison of experimental results with two-phase flow simulation conducted with different friction factor correlations for R1234yf and the lubricant 100-1 (*Case 8*).

Regarding the pressure loss $-\partial p/\partial z$ in Figures 6.6a and 6.7a, the values predicted with the two-phase flow model show the same trend as the experimental data. Nevertheless, there is a significant offset between predicted and experimental pressure loss for both cases and all friction factor correlations.

The model reproduces the minimum of the pressure loss $-\partial p/\partial z$ with the friction factor correlations of *Belt* and *Wallis*. The minimum in the pressure loss results from a minimum in the interfacial shear stress τ_I (see Equation (6.9)). This results from two superimposing effects. First, the friction factor f_I decreases continuously for a rising mass flux J in the correlations of *Belt* and *Wallis*, because it is a linear function of the film thickness δ. The film thickness δ decreases continuously with increasing vapor mass flux.[15] Secondly, the squared velocity difference between vapor and liquid phase $(v_\mathrm{v}-v_\mathrm{l})^2$ increases with increasing vapor mass flux. The interfacial shear stress τ_I is proportional to the product of both terms ($\tau_\mathrm{I} \sim f_\mathrm{I}(v_\mathrm{v}-v_\mathrm{l})^2$, see Equation (6.12)). For each friction factor correlation, the mass flux at the minimum of the pressure loss $J|_{\min(-\partial p/\partial z)}$ is marked with vertical black lines in Figure 6.6a and 6.7a and the critical mass flux J_crit is marked with vertical red lines in all figures. Figures 6.6a and 6.7a show that the lines for both characteristic mass fluxes are very close to each other. This confirms that it is reasonable to validate the two-phase flow model with the mass flux at the minimum pressure loss $J|_{\min(-\partial p/\partial z)}$.

In contrast to the pressure loss, the oil retention OR depicted in Figures 6.6b and 6.7b agrees better between two-phase flow model and experiments. With decreasing mass flux J, the oil retention OR increases exponentially with a strong increase around the critical mass flux.

The transition of the flow regime from annular to churn flow occurs at some point for $J < J_\mathrm{crit}$. The model is designed for annular flow only. A criterion for the transition to churn flow is not implemented. Thus, its predictions in this range can be incorrect.

The two-phase flow model is used in the Chapter 7 to calculate the critical mass flux for mixtures of low GWP-refrigerants with POE lubricants.

[15] This can be observed in Figures 6.6b and 6.7b, as the film thickness δ is closely related to the oil retention OR (see Equation (6.25), $\mathrm{OR} = \mathfrak{m}_\mathrm{l}/L_\mathrm{TS}$).

7 Critical Mass Flux of Low-GWP Refrigerants and POE Lubricants

In this chapter, the critical mass flux J_{crit} of low-GWP refrigerants with POE lubricants is calculated with the tool chain validated in Section 6.6. The influence of the fluid properties and the pipe diameter is examined in Section 7.1 for mixtures of POE lubricants with HC refrigerant R290 (propane) and the HFO refrigerant R1234yf, respectively. Based on the critical mass flux J_{crit}, the minimum cooling capacity $\dot{Q}_{\text{Evap,crit}}$ is calculated in Section 7.2. This provides a guideline to dimension the suction line for engineers in the refrigeration field. Data on the minimum cooling capacity $\dot{Q}_{\text{Evap,crit}}$ are tabulated analogously to reference books as e.g. OWEN [26].

7.1 Influence of Operation Parameters and Pipe Diameter on Critical Mass Flux

In this section, the critical mass flux is examined in detail for mixtures of polyol ester lubricants with the HC refrigerant R290 (propane) and the HFO refrigerant R1234yf, respectively. Both refrigerants are relevant alternatives for HFC refrigerants in small scale applications. The critical mass flux J_{crit} is calculated with the complete tool chain that consists of the determination of the lubricant composition in Chapter 3, the calculation of solubility and liquid density with the PCP SAFT EoS in Chapter 4, the prediction of the liquid mixture viscosity in Chapter 5 and the two-phase flow model in Chapter 6.
In Figure 7.1, the influence of the different operation and geometry parameters, superheat ΔT_{SH}, evaporation temperature T_{evap}, and the inner pipe diameter D on the critical mass flux J_{crit} is examined. In every step, one parameter is modified, while the other two are held constant.

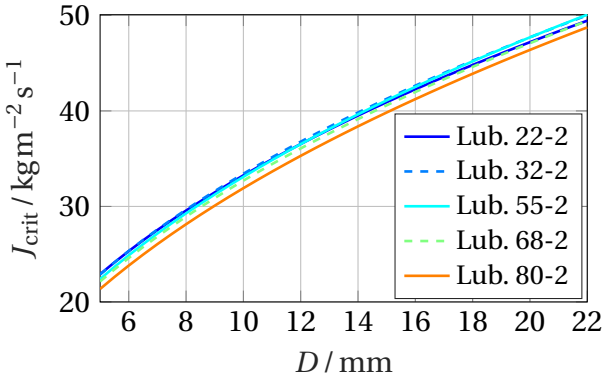

(a) Varying inner pipe diameter D, R290, $T_{Evap,out} = 20°C$, $\Delta T_{SH} = 10\,K$.

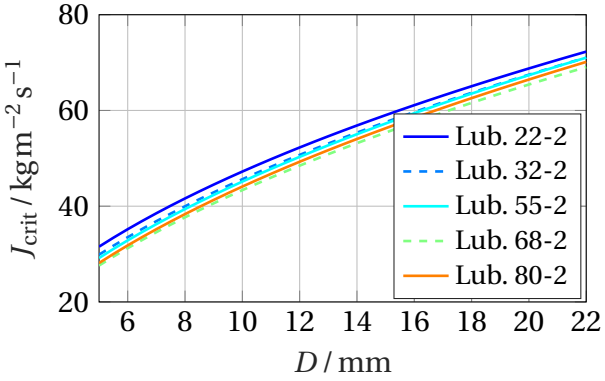

(b) Varying inner pipe diameter D, R1234yf, $T_{Evap,out} = 20°C$, $\Delta T_{SH} = 10\,K$.

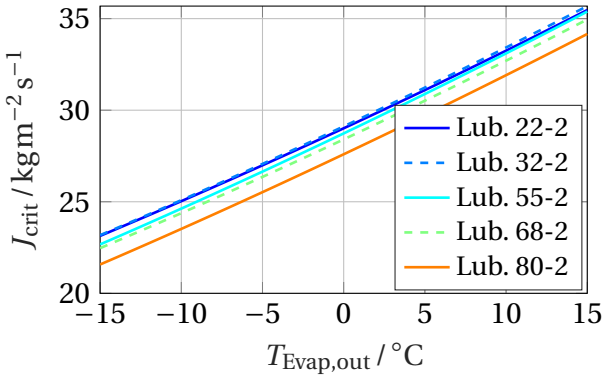

(c) Varying evap. outlet temp. $T_{Evap,out}$, R290, $D = 10\,mm$, $\Delta T_{SH} = 10\,K$.

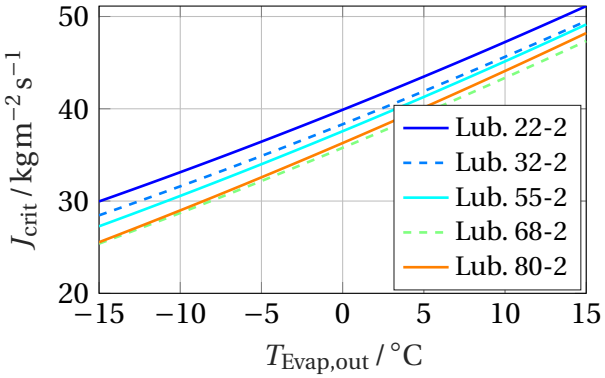

(d) Varying evap. outlet temp. $T_{Evap,out}$, R1234yf, $D = 10\,mm$, $\Delta T_{SH} = 10\,K$.

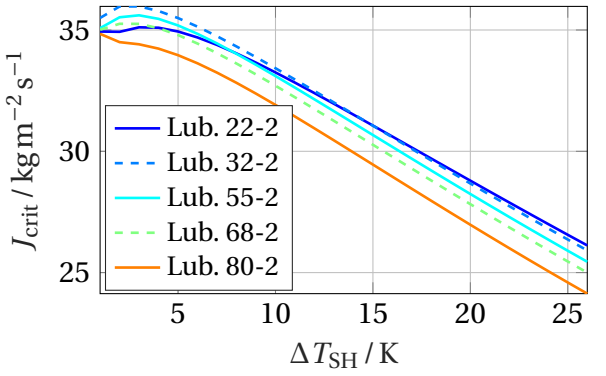

(e) Varying superheat ΔT_{SH}, R290, $D = 10\,mm$, $T_{Evap,out} = 20°C$.

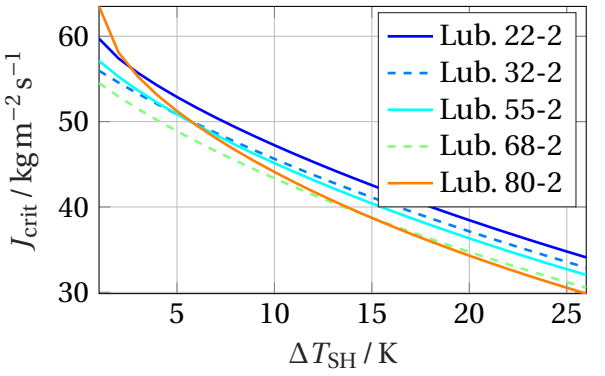

(f) Varying superheat ΔT_{SH}, R1234yf, $D = 10\,mm$, $T_{Evap,out} = 20°C$.

Figure 7.1: Critical mass flux J_{crit} depending on refrigerant, lubricant, and process parameters. The OCR is set to OCR = 3% in all calculations.

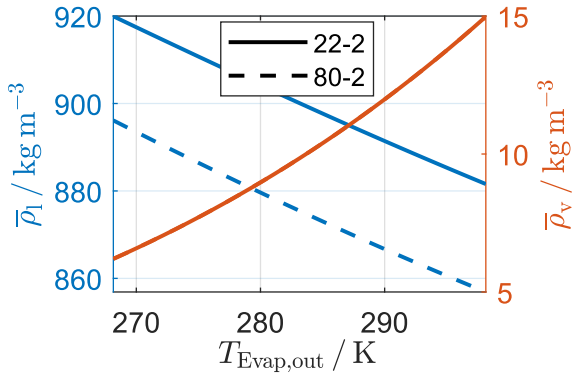

(a) Density of liquid and vapor phase, R290.

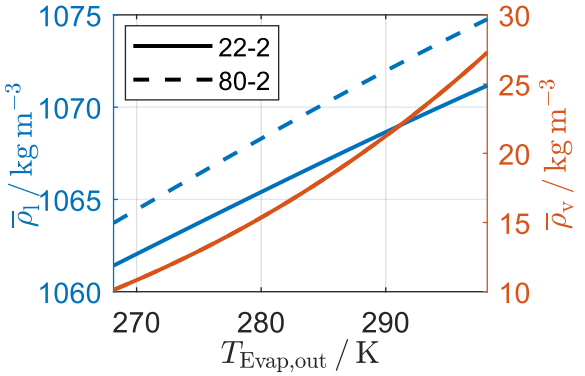

(b) Density of liquid and vapor phase, R1234yf.

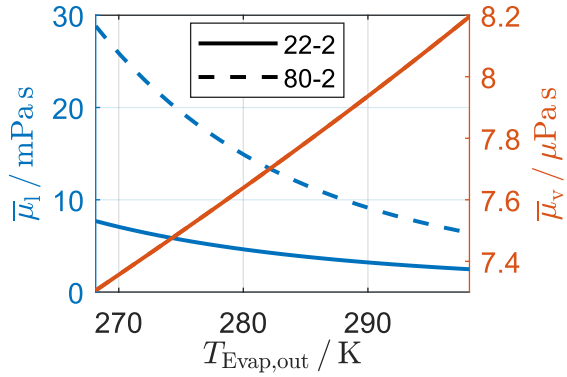

(c) Dyn. viscosity of liquid and vapor phase, R290.

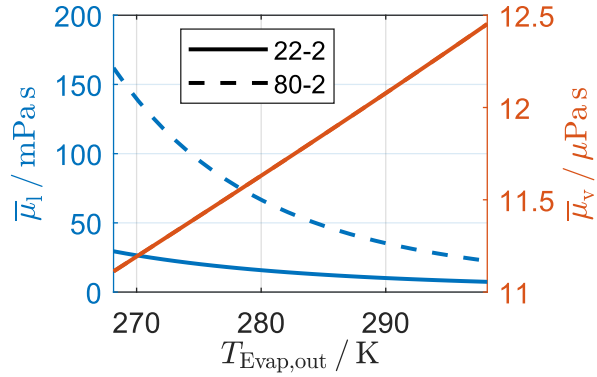

(d) Dyn. viscosity of liquid and vapor phase, R1234yf.

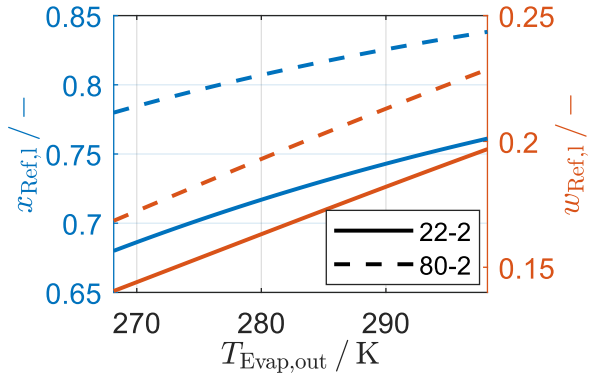

(e) Mole fraction $x_{\mathrm{Ref,l}}$ and mass fraction $w_{\mathrm{Ref,l}}$ of liquid phase, R290.

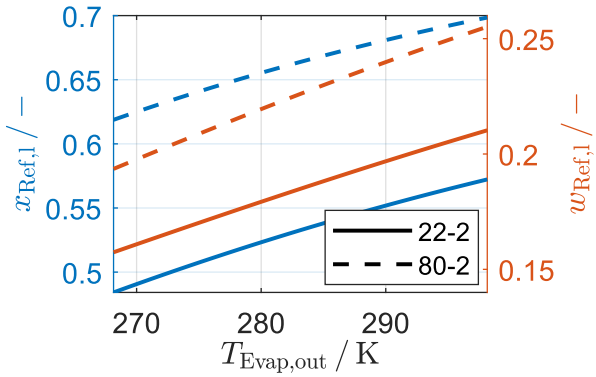

(f) Mole fraction $x_{\mathrm{Ref,l}}$ and mass fraction $w_{\mathrm{Ref,l}}$ of liquid phase, R1234yf.

Figure 7.2: Fluid properties for critical mass flux calculation with varying evaporator outlet temperature $T_{\mathrm{Evap,out}}$ and a superheat of $\Delta T_{\mathrm{SH}} = 10\,\mathrm{K}$.

The results are depicted in Figure 7.1 for R290 in the left column and for R1234yf in the right column. The lines in the sub-figures represent different POE lubricants. Lubricants with a viscosity grade in the range of $22 < \mathrm{VG} < 80$ are considered. The composition of the lubricants can be found in Table 3.10.

First, the influence of the inner pipe diameter D on the critical mass flux J_{crit} is depicted in Figures 7.1a and 7.1b. For a varying inner pipe diameter D, the fluid properties remain equal. The critical mass flux J_{crit} is proportional to $\sqrt{D}$, as predicted by the correlation of *Jacobs* (Equation (6.5)). The lines for the different lubricants are close to each other. This means that the influence of the pipe diameter D is much stronger compared to the viscosity of the liquid.

Secondly, the influence of the temperature in the suction line $T_{\mathrm{Evap,out}}$ is described in Figure 7.1c and 7.1d. The fluid properties of vapor and liquid phase are depicted in Figure 7.2. For a better comprehensibility, the fluid properties are depicted only for the lubricant with lowest (22-2) and highest (80-2) viscosity. The critical mass flux J_{crit}, depicted in Figure 7.1c and 7.1d, rises linearly due to the increasing vapor density ρ_{v} (see Figures 7.2a and 7.2b) and the decreasing mixture viscosity $\overline{\mu}_{\mathrm{l}}$ (see Figures 7.2c and 7.2d). For the different lubricants in the mixture, the critical mass flux differs by 4.5% to 7.5% for R290 and by 8% to 17% for R1234yf. The liquid density $\overline{\rho}_{\mathrm{l}}$ of mixtures with different lubricants is in a narrow range. Thus, the difference in the critical mass flux between the different lubricants can be attributed mainly to the liquid viscosity $\overline{\mu}_{\mathrm{l}}$, which differs by a factor of 3 to 5.5 between the different lubricants. The amount of dissolved refrigerant in the liquid phase is slightly increasing with rising temperature $T_{\mathrm{Evap,out}}$ for both examined refrigerants (see Figures 7.2e and 7.2f). It can be concluded from the case of varying temperature $T_{\mathrm{Evap,out}}$ that the influence of the vapor density ρ_{v} on the critical mass flux is higher compared to the influence of the liquid viscosity $\overline{\mu}_{\mathrm{l}}$.

Thirdly, the influence of varying superheat ΔT_{SH} on the critical mass flux J_{crit} is investigated in Figure 7.1e and 7.1f. In this case, the temperature in the suction line $T_{\mathrm{Evap,out}}$ is kept constant. Thus, the pressure p_{evap} decreases for rising superheat ΔT_{SH}. The fluid properties calculated for this case are depicted in Figure 7.3.

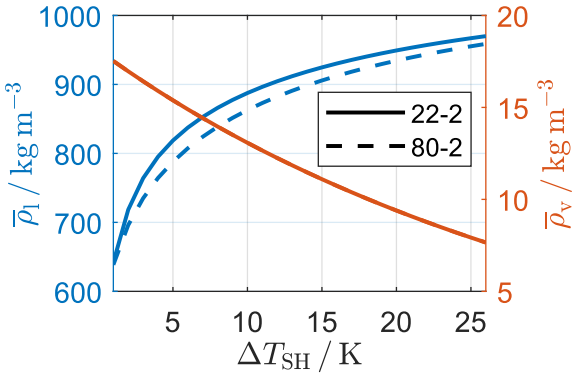

(a) Density of liquid and vapor phase, R290.

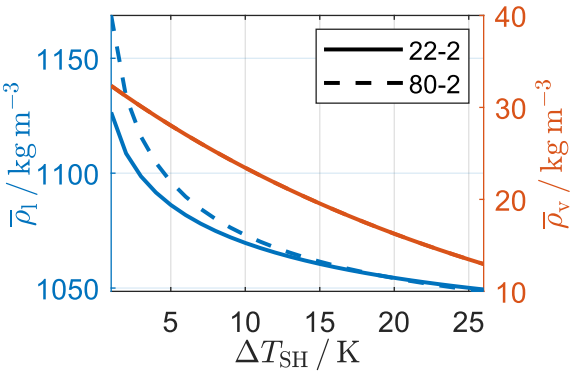

(b) Density of liquid and vapor phase, R1234yf.

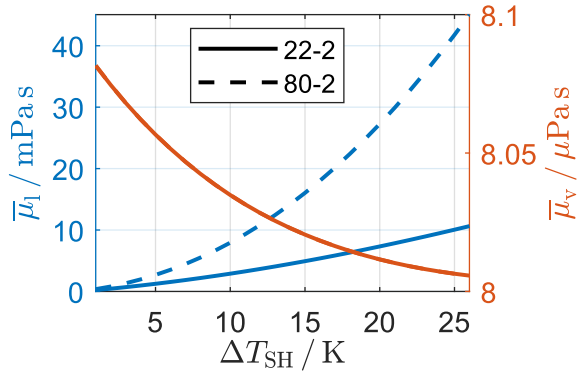

(c) Dyn. viscosity of liquid and vapor phase, R290.

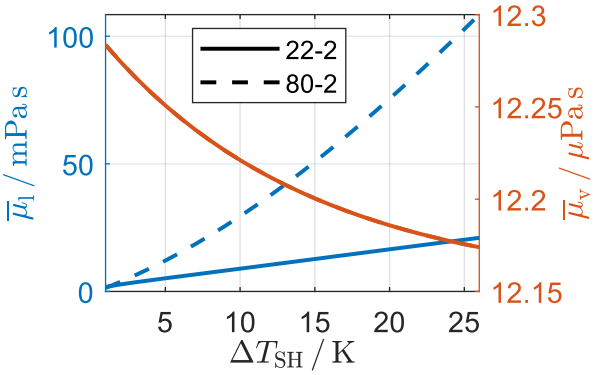

(d) Dyn. Viscosity of liquid and vapor phase, R1234yf.

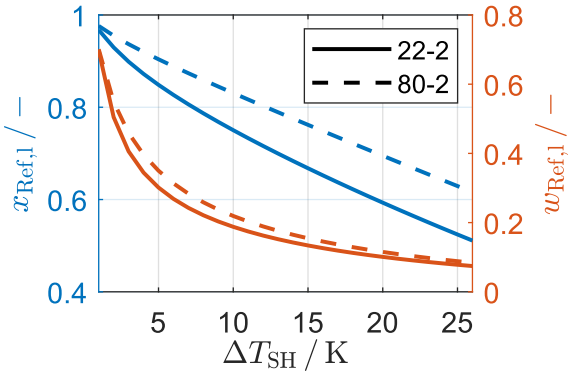

(e) Mole fraction $x_{Ref,l}$ and mass fraction $w_{Ref,l}$ of liquid phase, R290.

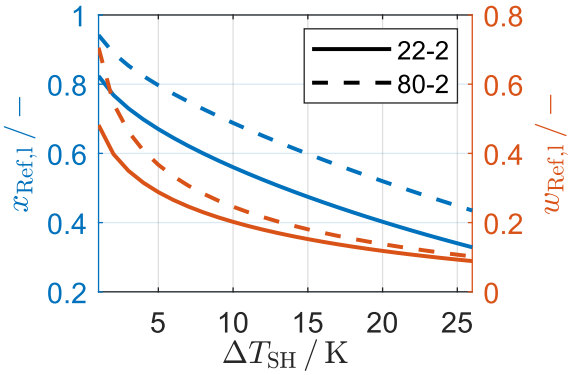

(f) Mole fraction $x_{Ref,l}$ and mass fraction $w_{Ref,l}$ of liquid phase, R1234yf.

Figure 7.3: Fluid properties for critical mass flux calculation with varying superheat ΔT_{SH} and an evaporator outlet temperature of $T_{Evap,out} = 20°C$.

This case is interesting, because the superheat ΔT_{SH} has a strong influence on the amount of dissolved refrigerant, as depicted in Figures 7.3e and 7.3f. Therefore, the viscosity of the liquid phase $\overline{\mu}_l$ depicted in Figures 7.3c and 7.3d increases significantly for rising superheat ΔT_{SH}. For the mixtures with R290, the decrease in the amount of dissolved refrigerant leads to strong increase in the liquid density $\overline{\rho}_l$ (see Figure 7.3a), because the density of pure refrigerant is much smaller compared to the density of pure POE lubricant. In contrast, the mixture density $\overline{\rho}_l$ with R1234yf remains rather constant (see Figure 7.3b). The density of liquid R1234yf is similar to the density of the pure lubricant. Due to the decreasing pressure p_{evap}, the vapor density ρ_v decreases for rising superheat ΔT_{SH}. Both, the decrease in vapor density ρ_v and the increase of the liquid mixture viscosity $\overline{\mu}_l$ lead to the decrease in the critical mass flux J_{crit} for a superheat $\Delta T_{SH} > 5\,K$. For a smaller superheat $\Delta T_{SH} < 5\,K$, a maximum can be observed for mixtures with R290 and lubricants 22-1 to 68-2. This phenomenon can be attributed to the strong increase of the liquid density $\overline{\rho}_l$ in this regime. As the liquid mixture density is very similar for the different lubricants (see Figures 7.3a and 7.3b), the difference in the critical mass flux for mixtures with different lubricants, as depicted in Figures 7.1e and 7.1f can be assigned to the difference in the mixture viscosity. For the different lubricants, the critical mass flux differs by 2% - 8% for R290 and by 14% - 17% for R1234yf.

All in all, it can be observed that R1234yf has a higher critical mass flux J_{crit} compared to R290 for similar conditions. The results presented above show that the operation parameters have a strong influence on the stability of the lubricant return. Therefore, a worst case scenario has to be considered to guarantee the lubricant return in the complete operation range. The worst case for lubricant return occurs at the highest temperature $T_{Evap,out}$ and the lowest superheat ΔT_{SH} in the operation range of the suction line.

The critical mass flux decreases for a decrease in vapor or liquid density, or an increase in the liquid mixture viscosity. An increase in the liquid mixture viscosity, resulting from the application of a lubricant with a higher VG, reduces the critical mass flux up to 16% for R1234yf and up to 8% for R290.

7.2 Minimum Cooling Capacity

In OWEN [26], the operation limit for safe lubricant return to the compressor is expressed in form of the minimum cooling capacity $\dot{Q}_{\mathrm{Evap,crit}}$. The advantage of the minimum cooling capacity is that it can be calculated balancing the enthalpy of the heat source fluid (i.e. the water or air flow, depending on the type of the heat source) between input and output of the evaporator. Thus, it is not necessary to measure the mass flow rate of the refrigerant, which is convenient for practical applications.

The minimum cooling capacity can be used in two ways: either to determine the minimum compressor power $P_{\mathrm{Comp,el,min}}$ with a given energy efficiency ratio (EER) of the refrigeration cycle for a given pipe diameter D, or to dimension the suction line diameter D for a required minimum cooling capacity $\dot{Q}_{\mathrm{Evap,crit}}$. The energy efficiency ratio relates the heat flow to the refrigerant in the evaporator $\dot{Q}_{\mathrm{Evap}}$ to the electric power of the compressor $P_{\mathrm{Comp,el}}$ according to Equation (7.1).

$$\mathrm{EER} = \frac{\dot{Q}_{\mathrm{Evap}}}{P_{\mathrm{Comp,el}}} \tag{7.1}$$

The minimum cooling capacity $\dot{Q}_{\mathrm{Evap,crit}}$ results from the critical mass flux J_{crit} according to Equation (7.2).

$$\dot{Q}_{\mathrm{Evap,crit}} = J_{\mathrm{crit}} A (h_{\mathrm{Evap,out}} - h_{\mathrm{Evap,in}}) \tag{7.2}$$

The mass specific enthalpy at the evaporator inlet $h_{\mathrm{Evap,in}}$ is calculated assuming a condensation temperature $T_{\mathrm{cond}} = 40°\mathrm{C}$ and saturated liquid refrigerant prior to the expansion valve. In the present study, the mass specific enthalpies at evaporator inlet $h_{\mathrm{Evap,in}}$ and outlet $h_{\mathrm{Evap,out}}$ are calculated with *CoolProp* [41].

The minimum cooling capacity is calculated for the pipe diameters according to DIN EN 12735-1 [185]. The evaporation temperature is set to values in the range of $-10°\mathrm{C} < T_{\mathrm{evap}} < 10°\mathrm{C}$ in steps of $\Delta T_{\mathrm{evap}} = 5\,\mathrm{K}$. The superheat is either $\Delta T_{\mathrm{SH}} = 5\,\mathrm{K}$, $\Delta T_{\mathrm{SH}} = 10\,\mathrm{K}$, or $\Delta T_{\mathrm{SH}} = 15\,\mathrm{K}$. For each refrigerant, a lubricant is selected according to the recommended viscosity grades (see Section 1.4.2). For

R290 (propane) and R1234yf, the minimum cooling capacity is summarized in Table 7.1. For all other refrigerants, similar tables can be found in Tables I.1-I.3 in the Appendix. Analogously to OWEN [26], the values are tabulated for the outer pipe diameter.

Table 7.1: Minimum cooling capacity $\dot{Q}_{\mathrm{Evap,crit}}$.

	T_{evap}	ΔT_{SH}	Outer pipe diameter[a] in mm										
			6	8	10	12	15	16	18	22	28	35	42
	°C	K	Minimum cooling capacity $\dot{Q}_{\mathrm{Evap,crit}}$ in kW										
R290 - Lubricant 80-2	-10	5	0.04	0.13	0.27	0.47	0.91	1.10	1.54	2.70	4.73	8.75	14.31
		10	0.04	0.13	0.27	0.47	0.93	1.13	1.59	2.80	4.93	9.20	15.14
		15	0.04	0.12	0.27	0.48	0.94	1.14	1.61	2.86	5.05	9.46	15.60
	-5	5	0.05	0.14	0.29	0.52	1.00	1.21	1.70	2.97	5.20	9.62	15.72
		10	0.05	0.14	0.30	0.53	1.03	1.25	1.75	3.09	5.44	10.14	16.66
		15	0.05	0.14	0.30	0.53	1.05	1.27	1.79	3.17	5.59	10.45	17.22
	0	5	0.05	0.15	0.32	0.57	1.10	1.33	1.86	3.26	5.69	10.53	17.21
		10	0.05	0.16	0.33	0.58	1.14	1.37	1.93	3.40	5.98	11.12	18.26
		15	0.05	0.16	0.33	0.59	1.16	1.41	1.98	3.50	6.16	11.49	18.91
	5	5	0.06	0.17	0.35	0.62	1.20	1.45	2.03	3.56	6.22	11.50	18.79
		10	0.06	0.17	0.36	0.64	1.25	1.51	2.12	3.73	6.54	12.16	19.95
		15	0.06	0.17	0.37	0.65	1.28	1.55	2.18	3.84	6.76	12.59	20.69
	10	5	0.06	0.18	0.38	0.68	1.31	1.58	2.22	3.88	6.77	12.52	20.45
		10	0.07	0.19	0.39	0.70	1.37	1.65	2.31	4.07	7.14	13.25	21.72
		15	0.07	0.19	0.40	0.72	1.40	1.70	2.38	4.20	7.38	13.73	22.55
R1234yf - Lubricant 32-2	-10	5	0.02	0.07	0.14	0.25	0.50	0.61	0.86	1.52	2.69	5.03	8.30
		10	0.02	0.07	0.14	0.26	0.51	0.62	0.87	1.54	2.73	5.13	8.47
		15	0.02	0.07	0.15	0.26	0.52	0.63	0.89	1.58	2.80	5.25	8.67
	-5	5	0.03	0.08	0.16	0.29	0.57	0.69	0.97	1.72	3.04	5.68	9.36
		10	0.03	0.08	0.16	0.29	0.58	0.70	0.99	1.75	3.09	5.79	9.55
		15	0.03	0.08	0.17	0.30	0.59	0.71	1.01	1.79	3.16	5.92	9.78
	0	5	0.03	0.09	0.18	0.33	0.64	0.78	1.09	1.94	3.41	6.38	10.50
		10	0.03	0.09	0.18	0.33	0.65	0.79	1.11	1.97	3.48	6.50	10.72
		15	0.03	0.09	0.19	0.34	0.66	0.81	1.14	2.01	3.55	6.65	10.97
	5	5	0.03	0.10	0.21	0.37	0.72	0.87	1.23	2.17	3.82	7.13	11.72
		10	0.03	0.10	0.21	0.37	0.73	0.88	1.25	2.20	3.89	7.27	11.97
		15	0.03	0.10	0.21	0.38	0.75	0.90	1.27	2.25	3.98	7.43	12.24
	10	5	0.04	0.11	0.23	0.41	0.80	0.97	1.37	2.42	4.25	7.93	13.03
		10	0.04	0.11	0.23	0.42	0.82	0.99	1.39	2.46	4.33	8.08	13.30
		15	0.04	0.11	0.24	0.42	0.83	1.01	1.42	2.51	4.43	8.27	13.60

a: According to DIN EN 12735-1 [185].

Additionally, the minimum cooling capacity is depicted for R290 and R1234yf over the inner pipe diameter D in Figure 7.4.

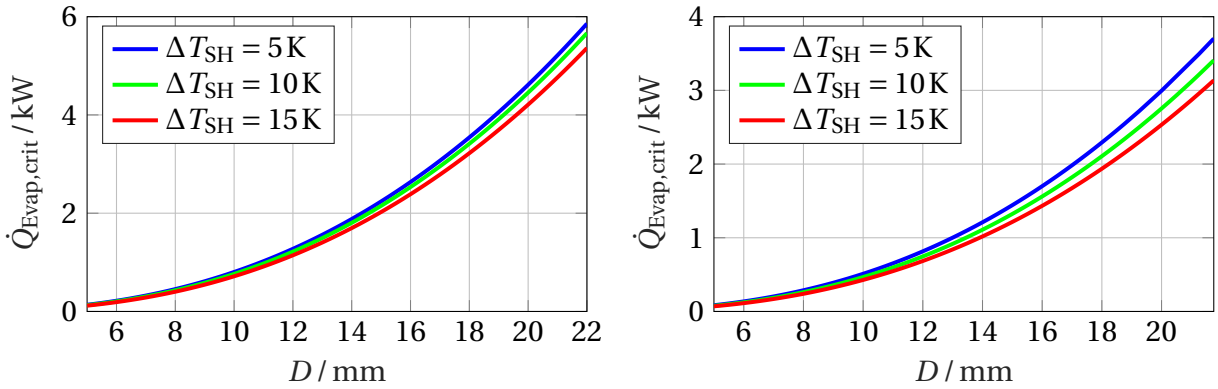

(a) R290, lubricant 80-2, $T_{\mathrm{Evap,out}} = 25°\mathrm{C}$. **(b)** R1234yf, lubricant 32-2, $T_{\mathrm{Evap,out}} = 25°\mathrm{C}$.

Figure 7.4: Minimum cooling capacity $\dot{Q}_{\mathrm{Evap,crit}}$ for varying inner pipe diameter D.

The minimum cooling capacity $\dot{Q}_{\mathrm{Evap,crit}}$ is higher for R290 compared to R1234yf, whereas it is vice-versa for the critical mass flux J_{crit}. The reason is the higher mass specific enthalpy difference over the evaporator $\Delta h_{\mathrm{Evap}} = h_{\mathrm{Evap,out}} - h_{\mathrm{Evap,in}}$ for R290 in comparison to R1234yf.

The minimum cooling capacity is $\dot{Q}_{\mathrm{Evap,crit}} = 1.65\,\mathrm{kW}$ for R290 (propane), a frequently chosen suction line outer diameter of 16 mm, an evaporation temperature of $T_{\mathrm{evap}} = 10°\mathrm{C}$, and a superheat of $\Delta T_{\mathrm{SH}} = 10\,\mathrm{K}$ (see Table 7.1). With an assumed energy efficiency ratio of EER = 2, the limit for part-load operation of the electric compressor power would be $P_{\mathrm{Comp,el,crit}} = 825\,\mathrm{W}$. This is a value that can be reached in small scale domestic applications with variable speed compressors. The example shows that lubricant return in the suction line is an issue that should be considered in the dimensioning and operation of refrigeration cycles with variable speed compressors and refrigerant R290 (propane). The same applies for other HC refrigerants, as it can be seen in the Tables I.2 and I.3. For R1234yf, the minimum cooling capacity is $\dot{Q}_{\mathrm{Evap,crit}} = 0.99\,\mathrm{kW}$ at the same conditions. Thus, lubricant return plays a less critical role compared to R290.

8 Summary and Conclusions

The lubricant return in the suction line limits part-load operation of variable speed compressors. A reduction of the load of variable speed compressors leads to a decrease of the mass flux in the suction line. If the mass flux falls below a certain threshold, the annular liquid wall-film that contains the lubricant is not dragged upwards in vertical sections anymore. This threshold is known as the critical mass flux for lubricant return. A trade-off has to be made in the dimensioning of the suction line diameter for refrigeration cycles with a variable speed compressor. On the one hand, pressure losses at full-load should be reduced. On the other hand, the critical mass flux should be low to permit a wide operation range of the compressor. The aim of this thesis was to determine the critical mass flux for refrigerants with a low global warming potential.

The influence of the molecular structure on fluid properties of polyol esters was analyzed. Based on a database for fluid properties of polyol esters, a tool chain was developed to predict thermophysical properties of the refrigerant-lubricant mixture in the liquid film of two-phase annular flow in the suction line of refrigeration cycles. The modeling procedure, the results, and the conclusions are summarized in the following for each element of the tool chain:

- **Determination of the lubricant composition:**
  An algorithm was developed to determine the composition of a mixture of different PEs and DiPEs based on target data of density, viscosity and molecular weight of e.g. a commercial lubricant of unknown composition. The algorithm comprises the mixture laws for the different properties. The mixture laws were validated with the scarce literature data available for binary polyol ester mixtures of known composition. Regarding the viscosity, high deviations from ideal mixture laws were observed for temperatures above 40°C. It remains unclear whether this effect is the

result of measurement artifacts or an effect of physical relevance. Further research on the mixture viscosity of different PEs and DiPEs is required to confirm these measurements and explain the deviations.

The algorithm was assessed with a commercial polyol ester lubricant of known composition of carboxylic acids. It was not possible to recalculate the lubricant composition with the complete dataset of PEs. Nevertheless, the algorithm determined a composition that describes the density and viscosity of the commercial lubricant well.

- **Calculation of the refrigerant solubility in the lubricant:**
  The PC(P) SAFT model of GROSS AND VRABEC [43] was used to calculate the refrigerant solubility in the lubricant. The binary interaction parameter of PEs and refrigerants was determined based on solubility data of binary mixtures. Correlations for the binary interaction parameter were developed. Significant gaps were identified for mixtures of branched PEs and HFO refrigerants, HC refrigerants with all types of polyol esters, and DiPEs with all refrigerants. To fill these gaps, the binary interaction parameter was regressed assuming a lubricant composition calculated with the previously described algorithm and using solubility data of refrigerants with commercial lubricants.

  For HC and HFO refrigerants, experiments on the solubility of refrigerants and (commercial) polyol esters are scarce. Further research in this field would significantly improve the data basis for solubility prediction.

- **Calculation of the mixture viscosity of refrigerants and lubricants:**
  The mixture viscosity of refrigerants and lubricants shows significant deviations to ideal mixture laws. This leads to challenges in the modeling process. Nine models applied for mixtures of refrigerants and lubricants in literature were presented. Adjustable parameters were regressed to literature data of the liquid mixture viscosity of refrigerants and lubricants. The empiric mixture model of KENDALL AND POTTER [156] was selected to calculate the viscosity of the refrigerant-lubricant mixture in the liquid film. This correlation showed acceptable average deviations for the database of experimental mixture viscosity. Nevertheless, the maximum deviation is high for all models including the selected approach.

- **Two-phase flow in vertical suction lines:**
  The fluid properties determined in the previously described elements of the tool chain are used in a two-phase flow model to calculate the critical mass flux. Mixtures of refrigerants and lubricants substantially differ from other fluids in two-phase annular flow. A higher ratio of film thickness to pipe diameter is observed for similar friction factors for refrigerants and lubricants compared to other fluids. The friction factor correlation of BELT ET AL. [173] best approximates the experimentally obtained values of the friction factor.

  Experiments on the critical mass flux of refrigerant-lubricant mixtures are very scarce. Only a few experiments were found to validate the complete tool chain. The model showed a slight under-prediction of the critical mass flux but lead to an average absolute deviation below 10% for all considered cases.

Finally, the critical mass flux and the minimum cooling load were calculated for refrigerants with a low global warming potential. The operation parameters evaporator outlet temperature and superheat have a significant influence on the critical mass flux. In contrast, the difference in the critical mass flux of different lubricants is small for the same refrigerant.

Especially, for hydrocarbon refrigerants the critical mass flux is within the potential operation range of variable speed compressors. This shows that the lubricant return should be considered for hydrocarbon refrigerants in the determination of the operation range of variable speed compressors.

The results of the critical mass flux calculations for the considered refrigerants with a low global warming potential are tabulated in form of the minimum cooling capacity. These tables can be used as a guideline for engineers in the refrigeration sector to dimension the diameter of the suction line to ensure a proper lubricant return.

Bibliography

[1] R. M. Lazzarin and M. Noro. “Past, Present, Future of Solar Cooling: Technical and Economical Considerations”. In: *Solar Energy* 172 (2018), pp. 2–13. DOI: 10.1016/j.solener.2017.12.055.

[2] D. Fischer, F. Rautenberg, T. Wirtz, B. Wille-Haussmann and H. Madani. “Smart Meter Enabled Control for Variable Speed Heat Pumps to Increase PV Self-Consumption”. In: *International Congress on Refrigeration*. Paper 580. Yokohama, 2015. DOI: 10.13140/RG.2.1.2566.3762.

[3] D. Fischer, J. Bernhardt, H. Madani and C. Wittwer. “Comparison of Control Approaches for Variable Speed Air Source Heat Pumps Considering Time Variable Electricity Prices and PV”. In: *Applied Energy* 204 (2017), pp. 93–105. DOI: 10.1016/j.apenergy.2017.06.110.

[4] T. Beck, H. Kondziella, G. Huard and T. Bruckner. “Optimal Operation, Configuration and Sizing of Generation and Storage Technologies for Residential Heat Pump Systems in the Spotlight of Self-Consumption of Photovoltaic Electricity”. In: *Applied Energy* 188 (2017), pp. 604–619. DOI: 10.1016/j.apenergy.2016.12.041.

[5] M. Pinamonti, A. Prada and P. Baggio. “Rule-Based Control Strategy to Increase Photovoltaic Self-Consumption of a Modulating Heat Pump Using Water Storages and Building Mass Activation”. In: *Energies* 13.23 (2020), p. 6282. DOI: 10.3390/en13236282.

[6] L. Langer and T. Volling. “An Optimal Home Energy Management System for Modulating Heat Pumps and Photovoltaic Systems”. In: *Applied Energy* 278.115661 (2020), pp. 1–15. DOI: 10.1016/j.apenergy.2020.115661.

[7] L. Cremaschi, Y. Hwang and R. Radermacher. “Experimental Investigation of Oil Retention in Air Conditioning Systems”. In: *International Journal of Refrigeration* 28.7 (2005), pp. 1018–1028. DOI: 10.1016/j.ijrefrig.2005.03.012.

[8] “Chapter 12: Lubricants in Refrigerant Systems”. In: *2018 ASHRAE Handbook - Refrigeration (SI Edition)*. Ed. by M. S. Owen. Atlanta: American Society of Heating, Refrigerating and Air-Conditioning Engineers, 2018. ISBN: 978-1-5231-2137-3.

[9] T. Toyama, H. Matsuura and Y. Yoshida. “Visual Techniques to Quantify Behavior of Oil Droplets in a Scroll Compressor”. In: *International Compressor Engineering Conference*. Paper 1788. West Lafayette, 2006.

[10] S. S. Wujek and P. S. Hrnjak. “Method for Quantitatively Analyzing Flow Phenomena in Annular-Mist Two-Phase Flows”. In: *International Compressor Engineering Conference*. Paper 1036. West Lafayette, 2010.

[11] A. J. Zimmermann and P. S. Hrnjak. “Oil Flow at Discharge Valve in a Scroll Compressor”. In: *Proceedings of the Institution of Mechanical Engineers, Part E: Journal of Process Mechanical Engineering* 229.2 (2015), pp. 104–113. DOI: 10.1177/0954408914559315.

[12] H. S. Kim and M. S. Kim. “A Review on Flow Characteristics of Refrigerant and Oil Mixture in a Heat Pump System”. In: *International Journal of Air-Conditioning and Refrigeration* 23.03 (2015), p. 1530002. DOI: 10.1142/S2010132515300025.

[13] J. Xu and P. Hrnjak. “Quantification of Flow and Retention of Oil in Compressor Discharge Pipe”. In: *International Journal of Refrigeration* 80 (2017), pp. 252–263. DOI: 10.1016/j.ijrefrig.2017.05.004.

[14] Y. Hwang, L. Cremaschi, R. Radermacher, T. Hirata, Y. Ozaki and T. Hotta. “Oil Circulation Ratio in CO2 Climate Control Systems”. In: *SAE Technical Paper* 2003–01 (2003), p. 0730. DOI: 10.4271/2003-01-0730.

[15] B. Shen and E. A. Groll. “Review Article: A Critical Review of The Influence of Lubricants on the Heat Transfer and Pressure Drop of Refrigerants—Part II: Lubricant Influence on Condensation and Pressure Drop”. In: *HVAC&R Research* 11.4 (2005), pp. 511–526. DOI: 10.1080/10789669.2005.10391152.

[16] A. Razzouk, I. Mokbel, J. García, J. Fernandez, N. Msakni and J. Jose. “Vapor Pressure Measurements in the Range 10^{-5} Pa to 1Pa of Four Pentaerythritol Esters: Density and Vapor–Liquid Equilibria Modeling of Ester Lubricants”. In: *Fluid Phase Equilibria*. 3rd Fluid Properties Challenge 260.2 (2007), pp. 248–261. DOI: 10.1016/j.fluid.2007.07.029.

[17] P. Nekså, H. Rekstad, G. R. Zakeri and P. A. Schiefloe. “CO2-heat Pump Water Heater: Characteristics, System Design and Experimental Results”. In: *International Journal of Refrigeration* 21.3 (1998), pp. 172–179. DOI: 10.1016/S0140-7007(98)00017-6.

[18] B. Shen and E. A. Groll. “Review Article: A Critical Review of the Influence of Lubricants on the Heat Transfer and Pressure Drop of Refrigerants, Part 1: Lubricant Influence on Pool and Flow Boiling”. In: *HVAC&R Research* 11.3 (2005), pp. 341–359. DOI: 10.1080/10789669.2005.10391142.

[19] L. Lin, H. Peng and G. Ding. “Influence of Oil Concentration on Wetting Behavior during Evaporation of Refrigerant–Oil Mixture on Copper Surface”. In: *International Journal of Refrigeration* 61 (2016), pp. 23–36. DOI: 10.1016/j.ijrefrig.2015.09.001.

[20] Y. Sun, J. Wang and Y. Hu. “Effect of Refrigerant/Oil Solubility on Thermodynamic Performance of the Evaporator Working with R600a and DME”. In: *The Journal of Chemical Thermodynamics* 154.106331 (2021). DOI: 10.1016/j.jct.2020.106331.

[21] H. Li and P. Hrnjak. “Effect of Lubricant on Two-phase Refrigerant Distribution in Microchannel Evaporator”. In: *SAE International Journal of Materials and Manufacturing* 6.3 (2013), pp. 567–575. DOI: 10.4271/2013-01-1508.

[22] O. Lottin, P. Guillemet and J. Lebreton. “Effects of Synthetic Oil in a Compression Refrigeration System Using R410A. Part II: Quality of Heat Transfer and Pressure Losses within the Heat Exchangers”. In: *International Journal of Refrigeration* 26.7 (2003), pp. 783–794. DOI: 10.1016/S0140-7007(03)00065-3.

[23] L. Cremaschi. “Experimental and Theoretical Investigation of Oil Retention in Vapor Compression Systems”. PhD thesis. College Park: University of Maryland, 2004.

[24] L. Cremaschi, A. S. Yatim and S. K. Mulugurthi. “Experimental Study of Oil Retention in Microchannel Type Evaporators of Air-Source Heat Pump Systems”. In: *International Journal of Refrigeration* 91 (2018), pp. 158–166. DOI: 10.1016/j.ijrefrig.2018.04.022.

[25] F. R. Biancardi, H. H. Michels, T. H. Sienel and D. Pandy R. *Study of Lubricant Circulation in HVAC Systems. Volume I - Description of Technical Effort and Results*. Final Technical Report DOE/CE/23810-71. East Hartford, CT: United Technologies Research Center, 1996.

[26] M. S. Owen, ed. *2018 ASHRAE Handbook - Refrigeration (SI Edition)*. Atlanta: American Society of Heating, Refrigerating and Air-Conditioning Engineers, 2018. ISBN: 978-1-5231-2137-3.

[27] M. Jacobs, F. Scheideman, S. Kazem and N. Macken. “Oil Transport by Refrigerant Vapour”. In: *ASHRAE Transactions* 82.2 (1976), pp. 318–329.

[28] S. S. Mehendale and R. Radermacher. “Experimental and Theoretical Investigation of Annular Film Flow Reversal In a Vertical Pipe: Application To Oil Return In Refrigeration Systems”. In: *HVAC&R Research* 6.1 (2000), pp. 55–74. DOI: 10.1080/10789669.2000.10391250.

[29] European Comission. *Regulation (EU) of the European Parliament and of the Council of 16 April 2014 on Fluorinated Greenhouse Gases and Repealing Regulation (EC) No 842/2006*. 2015.

[30] B. O. Bolaji and Z. Huan. “Ozone Depletion and Global Warming: Case for the Use of Natural Refrigerant – a Review”. In: *Renewable and Sustainable Energy Reviews* 18 (2013), pp. 49–54. DOI: 10.1016/j.rser.2012.10.008.

[31] J. M. Calm and G. C. Hourahan. “Physical, Safety, and Environmental Data for Current and Alternative Refrigerants”. In: *23rd International Congress of Refrigeration*. Paper 915. Prague: IIR/IIF, 2011, p. 22.

[32] W. P. D. Fernando. “Experimental Investigation of Refrigerant Charge Minimisation of a Small Capacity Heat Pump”. PhD thesis. Stockholm: Kungliga Tekniska högskolan, 2007.

[33] F. Hanslik and J. Süß. “Water as a Refrigerant in Centrifugal Compressor Cooling Systems for Industrial Applications”. In: *Advanced Cooling Technologies and Applications*. Ed. by S. M. Sohel Murshed. London: IntechOpen, 2018. ISBN: 978-1-78984-839-7. DOI: 10.5772/intechopen.79614.

[34] G. Briley. “A History of Refrigeration”. In: *ASHRAE Journal* (2004), pp. 31–34.

[35] W. Bock and C. Puhl. *Kältemaschinenöle*. Berlin, Offenbach: VDE Verlag, 2010. ISBN: 978-3-8007-3829-8.

[36] S. Boyde. “Esters”. In: L. R. Rudnick. *Synthetics, Mineral Oils, and Bio-Based Lubricants*. Ed. by L. R. Rudnick. 3rd ed. Boca Raton: CRC Press, 2020, pp. 45–76. ISBN: 978-1-315-15815-0. DOI: 10.1201/9781315158150-3.

[37] J. A. Karnaz. “Lubricant Development To Meet Lower GWP Refrigerant Challenges”. In: *International Compressor Engineering Conference*. Paper 1444. West Lafayette, 2014.

[38] V. Nair. “HFO Refrigerants: A Review of Present Status and Future Prospects.” In: *International Journal of Refrigeration* 122 (2021), pp. 156–170. DOI: 10.1016/j.ijrefrig.2020.10.039.

[39] Deutsches Institut für Normung e.V. *DIN ISO 2909:2004-08, Petroleum products – Calculation of viscosity index from kinematic viscosity*. Beuth Verlag GmbH, 2004. DOI: 10.31030/9556201.

[40] R. Cavestri. *Measurement of Viscosity, Density, and Gas Solubility of Refrigerant Blends in Selected Synthetic Lubricants*. Final Report DOE/CE/23810–46, 82433. Dublin, Ohio: Imaginatino Resources, Inc., 1995. DOI: 10.2172/82433.

[41] I. H. Bell, J. Wronski, S. Quoilin and V. Lemort. “Pure and Pseudo-pure Fluid Thermophysical Property Evaluation and the Open-Source Thermophysical Property Library CoolProp”. In: *Industrial & Engineering Chemistry Research* 53.6 (2014), pp. 2498–2508. DOI: 10.1021/ie4033999.

[42] E. Lemmon, M. Huber and M. McLinden. *REFPROP - Referemce Fluid Thermodynamic and Transport Properties*. Version NIST Standard Reference Database 23, Version 9.1. NIST, Applied Chemicals and Materials Division, 2013.

[43] J. Gross and J. Vrabec. “An Equation-of-State Contribution for Polar Components: Dipolar Molecules”. In: *AIChE Journal* 52.3 (2006), pp. 1194–1204. DOI: 10.1002/aic.10683.

[44] E. Jantzen. “The Origins of Synthetic Lubricants: The Work of Hermann Zorn in Germany Part 2 Esters and Additives for Synthetic Lubricants”. In: *Journal of Synthetic Lubrication* 13.2 (1996), pp. 113–128. DOI: 10.1002/jsl.3000130202.

[45] T. Mang and W. Dresel. *Lubricants and Lubrication*. 3rd ed. Weinheim: Wiley-VCH, 2017. ISBN: 978-3-527-32670-9.

[46] K. Kishore and H. K. Shobha. “Thermodynamics of Flow and Vaporization Processes in Long-Chain Liquids”. In: *The Journal of Physical Chemistry* 96.20 (1992), pp. 8161–8168. DOI: 10.1021/j100199a063.

[47] A. S. Pensado, M. J. P. Comuñas and J. Fernández. "Relationship between Viscosity Coefficients and Volumetric Properties: Measurements and Modeling for Pentaerythritol Esters". In: *Industrial & Engineering Chemistry Research* 45.26 (2006), pp. 9171–9183. DOI: 10.1021/ie0606035.

[48] L. Fedele, S. Marinetti, F. Pernechele, S. Bobbo and M. Scattolini. "Temperature and Pressure Dependence of Branched Pentaerythritol Ester Density". In: *Journal of Chemical & Engineering Data* 53.8 (2008), pp. 1779–1784. DOI: 10.1021/je800110r.

[49] M. Warman and E. Brunswick. "Synthetic Ester Lubricants". U.S. pat. 3360465A. Drew Chemical Corp. 1967.

[50] E. L. Niedzielski. "Neopentyl Polyol Ester Lubricants-Bulk Property Optimization". In: *Industrial & Engineering Chemistry Product Research and Development* 15.1 (1976), pp. 54–58. DOI: 10.1021/i360057a010.

[51] O. Fandiño, A. S. Pensado, L. Lugo, M. J. P. Comuñas and J. Fernández. "Compressed Liquid Densities of Squalane and Pentaerythritol Tetra(2-Ethylhexanoate)". In: *Journal of Chemical & Engineering Data* 50.3 (2005), pp. 939–946. DOI: 10.1021/je049580w.

[52] O. Fandiño, A. S. Pensado, L. Lugo, E. R. López and J. Fernández. "Volumetric Behaviour of the Environmentally Compatible Lubricants Pentaerythritol Tetraheptanoate and Pentaerythritol Tetranonanoate at High Pressures". In: *Green Chemistry* 7.11 (2005), p. 775. DOI: 10.1039/b508402d.

[53] O. Fandiño, J. García, M. J. P. Comuñas, E. R. López and J. Fernández. "P ρ T Measurements and Equation of State (EoS) Predictions of Ester Lubricants up to 45 MPa". In: *Industrial & Engineering Chemistry Research* 45.3 (2006), pp. 1172–1182. DOI: 10.1021/ie050818z.

[54] O. Fandiño, E. R. López, L. Lugo and J. Fernández. "Compressed Liquid Densities of Two Dipentaerythritol Esters". In: *Fluid Phase Equilibria*. Colloquium Dominique Richon 296.1 (2010), pp. 30–36. DOI: 10.1016/j.fluid.2010.01.019.

[55] L. Fedele, S. Marinetti, S. Bobbo and M. Scattolini. "PρT Experimental Measurements and Data Correlation of Pentaerythritol Esters". In: *Journal of Chemical & Engineering Data* 52.1 (2007), pp. 108–115. DOI: 10.1021/je060271a.

[56] K. R. Harris. "Temperature and Pressure Dependence of the Viscosities of Krytox GPL102 Oil and Di(Pentaerythritol) Hexa(Isononanoate)". In: *Journal of Chemical & Engineering Data* 60.5 (2015), pp. 1510–1519. DOI: 10.1021/acs.jced.5b00099.

[57] L. Lin and M. A. Kedzierski. "Density and Viscosity of a Polyol Ester Lubricant: Measurement and Molecular Dynamics Simulation". In: *International Journal of Refrigeration* 118 (2020), pp. 188–201. DOI: 10.1016/j.ijrefrig.2020.07.004.

[58] S. L. Outcalt. "Compressed-Liquid Density Measurements of Four Polyol Ester-Based Lubricants". In: *Energy & Fuels* 32.3 (2018), pp. 3775–3782. DOI: 10.1021/acs.energyfuels.8b00050.

[59] Å. Wahlström and L. Vamling. "Solubility of HFCs in Pentaerythritol Tetraalkyl Esters". In: *Journal of Chemical & Engineering Data* 45.1 (2000), pp. 97–103. DOI: 10.1021/je990171n.

[60] G. E. Bohner, J. A. Krimmel and J. J. Schmidt-Collérus. "Properties of Polyester Fluids with Desirable Synthetic Lubricant Characteristics." In: *Journal of Chemical & Engineering Data* 7.4 (1962), pp. 547–553. DOI: 10.1021/je60015a035.

[61] S. Rossi, G. Lombardo, D. Menegazzo, L. Vallese, B. Heithorst and L. Fedele. "Viscosity Measurements for Various Pentaerythritol Esters in the Range of Temperatures Between 273.65 K and 353.15 K (under revision)". 2024.

[62] T. S. Chao, M. Kjonaas and J. DeJovine. "Esters from Branched-Chain Acids and Neopentylpolyols and Phenols as Base Fluids for Synthetic Lubricants". In: *Industrial & Engineering Chemistry Product Research and Development* 22.2 (1983), pp. 357–362. DOI: 10.1021/i300010a037.

[63] S. Bair. "The Pressure and Temperature Dependence of the Low-Shear Viscosity". In: *High Pressure Rheology for Quantitative Elastohydrodynamics*. Oxford: Elsevier, 2019, pp. 97–133. ISBN: 978-0-444-64156-4. DOI: 10.1016/B978-0-444-64156-4.00005-2.

[64] A. Laesecke, C. Junker and D. S. Lauria. "Viscosity Measurements of Three Base Oils and One Fully Formulated Lubricant and New Viscosity Correlations for the Calibration Liquid Squalane". In: *Journal of Research of the National Institute of Standards and Technology* 124.124002 (2019), pp. 1–41. DOI: 10.6028/jres.124.002.

[65] R. Nutui, M. Maties and M. Nutui. "Correlations between the Structure, Physical and Rheological Properties in the Class of Neopentylpolyol Esters Used as Lubricating Oils". In: *Journal of Synthetic Lubrication* 7.2 (1990), pp. 145–154. DOI: 10.1002/jsl.3000070205.

[66] X. Paredes, A. S. Pensado, M. J. P. Comuñas and J. Fernández. "Experimental Dynamic Viscosities of Dipentaerythritol Ester Lubricants at High Pressure". In: *Journal of Chemical & Engineering Data* 55.9 (2010), pp. 3216–3223. DOI: 10.1021/je100057b.

[67] A. S. Pensado, M. J. P. Comuñas, L. Lugo and J. Fernández. "High-Pressure Characterization of Dynamic Viscosity and Derived Properties for Squalane and Two Pentaerythritol Ester Lubricants: Pentaerythritol Tetra-2-ethylhexanoate and Pentaerythritol Tetranonanoate". In: *Industrial & Engineering Chemistry Research* 45.7 (2006), pp. 2394–2404. DOI: 10.1021/ie051275w.

[68] Å. Wahlström and L. Vamling. "Viscosity for Mixtures of HFCs and Pentaerythritol Esters." In: *20th International Congress of Refrigeration: Refrigeration into the Third Millennium*. Paper 348. Vol. 2. Sydney, 1999.

[69] V. Eychenne and Z. Mouloungui. "Relationships between Structure and Lubricating Properties of Neopentylpolyol Esters". In: *Industrial & Engineering Chemistry Research* 37.12 (1998), pp. 4835–4843. DOI: 10.1021/ie9801204.

[70] Deutsches Institut für Normung e.V. *DIN EN ISO 3016:2019-09, Petroleum and Related Products from Natural or Synthetic Sources – Determination of Pour Point (ISO 3016:2019);* Beuth Verlag GmbH, 2019. DOI: 10.31030/3030984.

[71] R. Hołyst and A. Poniewierski. *Thermodynamics for Chemists, Physicists and Engineers*. Dordrecht: Springer Netherlands, 2012. ISBN: 978-94-007-2998-8.

[72] J. García, R. Abou Naccoul, J. Fernández, A. Razzouk and I. Mokbel. "Vapor-Pressure Measurements and Modeling of Dipentaerythritol Ester Lubricants". In: *Industrial & Engineering Chemistry Research* 50.8 (2011), pp. 4231–4237. DOI: 10.1021/ie102166r.

[73] A. R. C. Morais, L. D. Simoni, J. T. Douglas, A. M. Scurto and M. B. Shiflett. "Phase Equilibrium and Diffusivities of Hydrofluorocarbons in a Synthetic Polyol Ester Lubricant". In: *AIChE Journal* 66.7 (2020), e16241. DOI: 10.1002/aic.16241.

[74] D. S. Viswanath, ed. *Viscosity of Liquids: Theory, Estimation, Experiment, and Data*. Dordrecht: Springer, 2007. 660 pp. ISBN: 978-1-4020-5481-5.

[75] A. Allal, C. Boned and A. Baylaucq. "Free-Volume Viscosity Model for Fluids in the Dense and Gaseous States". In: *Physical Review E* 64.1 (2001), p. 011203. DOI: 10.1103/PhysRevE.64.011203.

[76] R. H. Ewell and H. Eyring. "Theory of the Viscosity of Liquids as a Function of Temperature and Pressure". In: *The Journal of Chemical Physics* 5.9 (1937), pp. 726–736. DOI: 10.1063/1.1750108.

[77] S. Glasstone, K. J. Laidler and H. Eyring. *The Theory of Rate Processes*. International Chemical Series. New York, London: McGraw-Hill, 1941.

[78] I. C. Wei and R. L. Rowley. "A Local Composition Model for Multicomponent Liquid Mixture Shear Viscosity". In: *Chemical Engineering Science* 40.3 (1985), pp. 401–408. DOI: 10.1016/0009-2509(85)85102-2.

[79] M. A. Marcelino Neto and J. R. Barbosa. "Viscosity Behavior of Mixtures of CO2 and Lubricant Oil". In: *Journal of the Brazilian Society of Mechanical Sciences and Engineering* 32.4 (2010), pp. 454–459. DOI: 10.1590/S1678-58782010000400007.

[80] L. Grunberg and A. H. Nissan. "Mixture Law for Viscosity". In: *Nature* 164.4175 (4175 1949), pp. 799–800. DOI: 10.1038/164799b0.

[81] S. Arrhenius. "Über die innere Reibung verdünnter wässeriger Lösungen". In: *Zeitschrift für Physikalische Chemie* 1U.1 (1887), pp. 285–298. DOI: 10.1515/zpch-1887-0133.

[82] M. H. Cohen and D. Turnbull. "Molecular Transport in Liquids and Glasses". In: *The Journal of Chemical Physics* 31.5 (1959), pp. 1164–1169. DOI: 10.1063/1.1730566.

[83] A. K. Doolittle. "Studies in Newtonian Flow. II. The Dependence of the Viscosity of Liquids on Free-Space". In: *Journal of Applied Physics* 22.12 (1951), pp. 1471–1475. DOI: 10.1063/1.1699894.

[84] T. H. Chung, M. Ajlan, L. L. Lee and K. E. Starling. "Generalized Multiparameter Correlation for Nonpolar and Polar Fluid Transport Properties". In: *Industrial & Engineering Chemistry Research* 27.4 (1988), pp. 671–679. DOI: 10.1021/ie00076a024.

[85] L. Lugo, X. Canet, M. J. P. Comuñas, A. S. Pensado and J. Fernández. "Dynamic Viscosity under Pressure for Mixtures of Pentaerythritol Ester Lubricants with 32 Viscosity Grade: Measurements and Modeling". In: *Industrial & Engineering Chemistry Research* 46.6 (2007), pp. 1826–1835. DOI: 10.1021/ie061187r.

[86] C. Zéberg-Mikkelsen, A. Baylaucq, M. Barrouhou, S. Quiñones-Cisneros and C. Boned. "Comparative Study of Viscosity Models on the Ternary System Methylcyclohexane + Cis-Decalin + 2,2,4,4,6,8,8-Heptamethylnonane up to 100MPa". In: *Fluid Phase Equilibria* 222–223 (2004), pp. 135–148. DOI: 10.1016/j.fluid.2004.06.033.

[87] S. E. Quiñones-Cisneros, C. K. Zeberg-Mikkelsen and E. H. Stenby. "The Friction Theory (f-Theory). for Viscosity Modeling". In: *Fluid Phase Equilibria* 169 (2000), pp. 249–276.

[88] S. E. Quiñones-Cisneros, C. K. Zéberg-Mikkelsen, J. Fernández and J. García. "General Friction Theory Viscosity Model for the PC-SAFT Equation of State". In: *AIChE Journal* 52.4 (2006), pp. 1600–1610. DOI: 10.1002/aic.10755.

[89] M. J. P. Comuñas, A. Baylaucq, C. Boned and J. Fernández. "High-Pressure Measurements of the Viscosity and Density of Two Polyethers and Two Dialkyl Carbonates". In: *International Journal of Thermophysics* 22.3 (2001), pp. 749–768. DOI: 10.1023/A:1010770831215.

[90] Deutsches Institut für Normung e.V. *DIN 51563:2011-04: Testing of Mineral Oils and Related Materials – Determination of Viscosity Temperature Relation – Slope m*. Beuth Verlag GmbH, 2011. DOI: 10.31030/1748810.

[91] K. Stephan and F. Mayinger. *Thermodynamik - 2 Mehrstoffsysteme*. 14th ed. Springer Lehrbuch. Berlin, Heidelberg: Springer, 1999. ISBN: 3-540-64481-4. DOI: 10.1007/978-3-662-10522-1.

[92] O. Fandiño, M. J. P. Comuñas, L. Lugo, E. R. López and J. Fernández. "Density Measurements under Pressure for Mixtures of Pentaerythritol Ester Lubricants. Analysis of a Density-Viscosity Relationship". In: *Journal of Chemical & Engineering Data* 52.4 (2007), pp. 1429–1436. DOI: 10.1021/je700121n.

[93] A. R. C. Morais, L. D. Simoni, A. M. Scurto and M. B. Shiflett. "Solubility and Diffusivity of Hydrofluoroolefin Refrigerants in a Polyol Ester Lubricant". In: *Industrial & Engineering Chemistry Research* 59.13 (2020), pp. 6279–6287. DOI: 10.1021/acs.iecr.9b06821.

[94] A. R. C. Morais, L. D. Simoni, M. B. Shiflett and A. M. Scurto. "Viscosity and Density of a Polyol Ester Lubricating Oil Saturated with Compressed Hydrofluoroolefin Refrigerants". In: *Journal of Chemical & Engineering Data* 65.9 (2020), pp. 4335–4346. DOI: 10.1021/acs.jced.0c00431.

[95] F. F. Czubinski, C. J. N. Sanchez, A. K. da Silva, M. A. M. Neto and J. R. Barbosa. "Phase Equilibrium and Liquid Viscosity Data for R-290/POE ISO 22 Mixtures between 283 and 353 K". In: *International Journal of Refrigeration* 114 (2020), pp. 79–87. DOI: 10.1016/j.ijrefrig.2020.02.029.

[96] J. Bock. "Vapour Liquid Equilibria of a Low GWP Refrigerant, R1234ze(E), Mixed With a POE Lubricant". PhD thesis. Urbana-Champaign: University of Illinois, 2015.

[97] W. L. Martz and M. Jacobi. *Refrigerant-Oil Mixtures and Local Composition Modeling*. ACRC TR-68. Urbana, Illinois, USA: Air Conditioning and Refrigeration Center University of Illinois Mechanical & Industrial Engineering Dept., 1994, p. 123.

[98] S. Gunsel and M. Pozebanchuk. *Elastohydrodynamic Lubrication with Polyolester Lubricants and HFC Refrigerants, Final Report, Volume 2*. DOE/CE/23810-102-Vol.2, 8217. The Woodlands, 1999, DOE/CE/23810-102–Vol.2, 8217. DOI: 10.2172/8217.

[99] X. Wang, Y. Sun and N. Gong. "Experimental Investigations for the Phase Equilibrium of R1234yf and R1234ze(E) with Two Linear Chained Pentaerythritol Esters". In: *The Journal of Chemical Thermodynamics* 92 (2016), pp. 66–71. DOI: 10.1016/j.jct.2015.08.038.

[100] Y. Sun, X. Wang, D. Wang, L. Jin and Z. Liu. "Absorption of Isobutane in Three Linear Chained Pentaerythritol Esters between 293.15 and 348.15 K". In: *International Journal of Refrigeration* 76 (2017), pp. 118–125. DOI: 10.1016/j.ijrefrig.2017.01.021.

[101] F. Pernechele, S. Bobbo, L. Fedele and R. Stryjek. "Solubility of Carbon Dioxide in Pentaerythritol Tetrabutyrate (PEC4) and Comparison with Other Linear Chained Pentaerythritol Tetraalkyl Esters". In: *International Journal of Thermophysics* 30.4 (2009), pp. 1144–1154. DOI: 10.1007/s10765-009-0580-8.

[102] Y. Sun, X. Wang, N. Gong and Z. Liu. "Solubility of Trans-1,3,3,3-Tetrafluoroprop-1-Ene (R1234ze(E)) in Pentaerythritol Tetrapentanoate (PEC5) in the Temperature Range from 283.15 to 353.15 K". In: *International Journal of Refrigeration* 48 (2014), pp. 114–120. DOI: 10.1016/j.ijrefrig.2014.09.013.

[103] Y. Sun, X. Wang, N. Gong and Z. Liu. "Solubility Measurement and Correlation of Isobutane with Two Pentaerythritol Tetraalkyl Esters between (293.15 and 348.15) K". In: *Journal of Chemical & Engineering Data* 60.5 (2015), pp. 1504–1509. DOI: 10.1021/acs.jced.5b00082.

[104] O. Fandiño, E. R. López, L. Lugo, M. Teodorescu, A. M. Mainar and J. Fernández. "Solubility of Carbon Dioxide in Two Pentaerythritol Ester Oils between (283 and 333) K". In: *Journal of Chemical & Engineering Data* 53.8 (2008), pp. 1854–1861. DOI: 10.1021/je800178x.

[105] Y. Sun, X. Wang, D. Wang and L. Jin. "Measurement and Correlation for Phase Equilibrium of HFO1234yf with Three Pentaerythritol Esters from 293.15K to 348.15K". In: *The Journal of Chemical Thermodynamics* 112 (2017), pp. 122–128. DOI: 10.1016/j.jct.2017.04.020.

[106] S. Bobbo, F. Pernechele, L. Fedele and R. Stryjek. "Solubility Measurements and Data Correlation of Carbon Dioxide in Pentaerythritol Tetrahexanoate (PEC6)". In: *Journal of Chemical & Engineering Data* 53.11 (2008), pp. 2581–2585. DOI: 10.1021/je800429j.

[107] Y. Sun, X. Wang, N. Gong and Z. Liu. "Solubility of Trans-1,3,3,3-Tetrafluoropropene (R1234ze(E)) in Pentaerythritol Ester Heptanoic Acid (PEC7) and in Pentaerythritol Tetranonanoate (PEC9) between 283.15K and 353.15K". In: *Fluid Phase Equilibria* 387 (2015), pp. 154–159. DOI: 10.1016/j.fluid.2014.12.030.

[108] O. Fandiño, E. R. López, L. Lugo, J. García and J. Fernández. "Solubility of Carbon Dioxide in Pentaerythritol Ester Oils. New Data and Modeling Using the PC-SAFT Model". In: *The Journal of Supercritical Fluids* 55.1 (2010), pp. 62–70. DOI: 10.1016/j.supflu.2010.05.026.

[109] L. Fedele, F. Pernechele, S. Bobbo, M. Scattolini and R. Stryjek. "Solubility of Carbon Dioxide in Pentaerythritol Tetraoctanoate". In: *Fluid Phase Equilibria* 277.1 (2009), pp. 55–60. DOI: 10.1016/j.fluid.2008.11.011.

[110] Y. Sun, G. Di, J. Wang, X. Wang and M. He. "Phase Behavior of R1234yf and R600a in Pentaerythritol Tetranonanoate". In: *International Journal of Refrigeration* 109 (2020), pp. 135–142. DOI: 10.1016/j.ijrefrig.2019.10.005.

[111] L. Fedele, S. Bobbo, F. Pernechele and R. Stryjek. "Solubility Temperature Dependence and Data Correlation of Carbon Dioxide in Pentaerythritol Tetra-2-methylbutyrate". In: *Journal of Chemical & Engineering Data* 54.11 (2009), pp. 3104–3107. DOI: 10.1021/je900201t.

[112] S. Bobbo, L. Fedele, M. Scattolini, R. Camporese and R. Stryjek. "Solubility of Carbon Dioxide in 2-Methylbutyric, 2-Methylvaleric and 2-Methylhexanoic Ester Oils". In: *Fluid Phase Equilibria*. 16th Symposium on Thermophysical Properties 256.1 (2007), pp. 81–85. DOI: 10.1016/j.fluid.2006.10.022.

[113] S. Bobbo, L. Fedele, F. Pernechele, M. Scattolini and R. Stryjek. "Solubility Measurements and Correlation of Carbon Dioxide in Pentaerythritol Tetra-2-Methylhexanoate. Comparison with Other Pentaerythritol Esters". In: *Fluid Phase Equilibria*. Proceedings of the 17th Symposium on Thermophysical Properties 290.1 (2010), pp. 115–120. DOI: 10.1016/j.fluid.2009.10.017.

[114] L. Fedele, S. Bobbo, M. Scattolini and R. Stryjek. "Solubility Measurements and Data Correlation of Carbon Dioxide in Pentaerythritol Tetra(2-Ethylbutanoate) (PEBE6)". In: *Journal of Chemical & Engineering Data* 56.1 (2011), pp. 62–64. DOI: 10.1021/je100761z.

[115] O. Fandiño, E. R. López, L. Lugo and J. Fernández. "Solubilities of Carbon Dioxide in a Dipentaerythritol Ester and in a Polyether". In: *Journal of Chemical & Engineering Data* 55.12 (2010), pp. 5483–5488. DOI: 10.1021/je1006339.

[116] W. A. Fouad and L. F. Vega. “Molecular Modeling of the Solubility of Low Global Warming Potential Refrigerants in Polyol Ester Lubricants”. In: *International Journal of Refrigeration* (2019), p. 10. DOI: 10.1016/j.ijrefrig.2019.04.004.

[117] J. García, X. Paredes and J. Fernández. “Phase and Volumetric Behavior of Binary Systems Containing Carbon Dioxide and Lubricants for Transcritical Refrigeration Cycles”. In: *The Journal of Supercritical Fluids* 45.3 (2008), pp. 261–271. DOI: 10.1016/j.supflu.2008.01.022.

[118] T. Sugii, E. Ishii and F. Müller-Plathe. “Solubility of Carbon Dioxide in Pentaerythritol Hexanoate: Molecular Dynamics Simulation of a Refrigerant–Lubricant Oil System”. In: *The Journal of Physical Chemistry B* 119.37 (2015), pp. 12274–12280. DOI: 10.1021/acs.jpcb.5b06459.

[119] J. Gross and G. Sadowski. “Perturbed-Chain SAFT: An Equation of State Based on a Perturbation Theory for Chain Molecules”. In: *Industrial & Engineering Chemistry Research* 40.4 (2001), pp. 1244–1260. DOI: 10.1021/ie0003887.

[120] J. Groß. *Entwicklung einer Zustandsgleichung für einfache, assoziierende und makromolekulare Stoffe*. Fortschritt-Berichte VDI Reihe 3, Verfahrenstechnik 684. Düsseldorf: VDI-Verlag, 2001. 157 pp. ISBN: 978-3-18-368403-8.

[121] M. A. Marcelino Neto and J. R. Barbosa. “Solubility, Density and Viscosity of a Mixture of R-600a and Polyol Ester Oil”. In: *International Journal of Refrigeration* 31.1 (2008), pp. 34–44. DOI: 10.1016/j.ijrefrig.2007.08.004.

[122] D.-Y. Peng and D. B. Robinson. “A New Two-Constant Equation of State”. In: *Industrial & Engineering Chemistry Fundamentals* 15.1 (1976), pp. 59–64. DOI: 10.1021/i160057a011.

[123] G. Soave. “Equilibrium Constants from a Modified Redlich-Kwong Equation of State”. In: *Chemical Engineering Science* 27.6-A (1972), pp. 1197–1203.

[124] P. Flory. *Statistical Mechanics of Chain Molecules*. New York: Interscience Publishers, 1968.

[125] G. M. Wilson. “Vapor-Liquid Equilibrium. XI. A New Expression for the Excess Free Energy of Mixing”. In: *Journal of the American Chemical Society* 86.2 (1964), pp. 127–130. DOI: 10.1021/ja01056a002.

[126] M. A. Monsalvo. “Phase Behavior and Viscosity Modeling of Refrigerant - Lubricant Mixtures”. PhD thesis. Lyngby: Department of Chemical Engineering, Technical University of Denmark, 2006. ISBN: 9788791435386.

[127] A. Dominik, W. G. Chapman, M. Kleiner and G. Sadowski. “Modeling of Polar Systems with the Perturbed-Chain SAFT Equation of State. Investigation of the Performance of Two Polar Terms”. In: *Industrial & Engineering Chemistry Research* 44.17 (2005), pp. 6928–6938. DOI: 10.1021/ie050071c.

[128] W. Chapman, K. Gubbins, G. Jackson and M. Radosz. "SAFT: Equation-of-state Solution Model for Associating Fluids". In: *Fluid Phase Equilibria* 52 (1989), pp. 31–38. DOI: 10.1016/0378-3812(89)80308-5.

[129] J. A. Barker and D. Henderson. "Perturbation Theory and Equation of State for Fluids: The Square-Well Potential". In: *The Journal of Chemical Physics* 47.8 (1967), pp. 2856–2861. DOI: 10.1063/1.1712308.

[130] J. A. Barker and D. Henderson. "Perturbation Theory and Equation of State for Fluids. II. A Successful Theory of Liquids". In: *The Journal of Chemical Physics* 47.11 (1967), pp. 4714–4721. DOI: 10.1063/1.1701689.

[131] P. K. Jog and W. G. Chapman. "Application of Wertheim's Thermodynamic Perturbation Theory to Dipolar Hard Sphere Chains". In: *Molecular Physics* 97.3 (1999), pp. 307–319. DOI: 10.1080/00268979909482832.

[132] V. Vinš and J. Hrubý. "Solubility of Nitrogen in One-Component Refrigerants: Prediction by PC-SAFT EoS and a Correlation of Henry's Law Constants". In: *International Journal of Refrigeration* 34.8 (2011), pp. 2109–2117. DOI: 10.1016/j.ijrefrig.2011.07.002.

[133] J. García, M. Youbi-Idrissi, J. Bonjour and J. Fernández. "Experimental and PC-SAFT Volumetric and Phase Behavior of Carbon dioxide+PAG or POE Lubricant Systems". In: *The Journal of Supercritical Fluids* 47.1 (2008), pp. 8–16. DOI: 10.1016/j.supflu.2008.05.009.

[134] S. Bobbo, L. Fedele, F. Pernechele and R. Stryjek. "Solubility of CO2 in Commercial POE Oils with Different Standard Viscosity". In: *International Compressor Engineering Conference*. Paper 988. West Lafayette, 2008, p. 9.

[135] J. Gross and G. Sadowski. "Reply to Comment on "Perturbed-Chain SAFT: An Equation of State Based on a Perturbation Theory for Chain Molecules"". In: *Industrial & Engineering Chemistry Research* 58.14 (2019), pp. 5744–5745. DOI: 10.1021/acs.iecr.9b01515.

[136] C. W. Meyer and G. Morrison. "Dipole Moments of Seven Refrigerants". In: *Journal of Chemical & Engineering Data* 36.4 (1991), pp. 409–413. DOI: 10.1021/je00004a019.

[137] W. A. Fouad and L. F. Vega. "The Phase and Interfacial Properties of Azeotropic Refrigerants: The Prediction of Aneotropes from Molecular Theory". In: *Physical Chemistry Chemical Physics* 19.13 (2017), pp. 8977–8988. DOI: 10.1039/C6CP08031F.

[138] C. C. Sampson, M. Kamson, M. G. Hopkins, P. L. Stanwix and E. F. May. "Dielectric Permittivity, Polarizability and Dipole Moment of Refrigerants R1234ze(E) and R1234yf Determined Using a Microwave Re-Entrant Cavity Resonator". In: *The Journal of Chemical Thermodynamics* 128 (2019), pp. 148–158. DOI: 10.1016/j.jct.2018.07.011.

[139] J. Gross. "An Equation-of-State Contribution for Polar Components: Quadrupolar Molecules". In: *AIChE Journal* 51.9 (2005), pp. 2556–2568. DOI: 10.1002/aic.10502.

[140] W. Fernando, H. Han, B. Palm, E. Granryd and P. Lundquist. "The Solubility of Propane (R290) with Commonly Used Compressor Lubricant Oils". In: *International Conference on Compressors and Their Systems*. Paper C615/055/2003. London: Cromwell Press, 2003, pp. 157–166.

[141] P. Ginies, P. Dewitte, M. F. Terrier and M. Charni. "Low GWP Refrigerant and Partial Miscible Lubricant". In: *International Refrigeration and Air Conditioning Conference*. Paper 1559. West Lafayette, 2014, p. 11.

[142] M. A. Marcelino Neto and J. R. Barbosa. "Phase and Volumetric Behaviour of Mixtures of Carbon Dioxide (R-744) and Synthetic Lubricant Oils". In: *The Journal of Supercritical Fluids* 50.1 (2009), pp. 6–12. DOI: 10.1016/j.supflu.2009.04.006.

[143] S. Quiñones-Cisneros, J. García, J. Fernández and M. Monsalvo. "Phase and Viscosity Behaviour of Refrigerant–Lubricant Mixtures". In: *International Journal of Refrigeration* 28.5 (2005), pp. 714–724. DOI: 10.1016/j.ijrefrig.2004.12.004.

[144] A. S. Pensado, A. a. H. Pádua, M. J. P. Comuñas and J. Fernández. "High-Pressure Viscosity and Density of Carbon Dioxide + Pentaerythritol Ester Mixtures: Measurements and Modeling". In: *AIChE Journal* 54.6 (2008), pp. 1625–1636. DOI: 10.1002/aic.11473.

[145] A. S. Pensado, A. A. H. Pádua, M. J. P. Comuñas and J. Fernández. "Viscosity and Density Measurements for Carbon Dioxide+pentaerythritol Ester Lubricant Mixtures at Low Lubricant Concentration". In: *The Journal of Supercritical Fluids* 44.2 (2008), pp. 172–185. DOI: 10.1016/j.supflu.2007.10.004.

[146] C. Thébault and L. Vamling. "A New Correlation for Viscosity of Oil/Refrigerant Mixtures". In: *20th International Congress of Refrigeration: Refrigeration into the Third Millennium*. Paper 347. Vol. 2. Sydney, 1999.

[147] J. Wu, Z. Chen, J. Lin and J. Li. "Experimental Analysis on R290 Solubility and R290/Oil Mixture Viscosity in Oil Sump of the Rotary Compressor". In: *International Journal of Refrigeration* 94 (2018), pp. 24–32. DOI: 10.1016/j.ijrefrig.2018.07.021.

[148] R. Macías-Salinas, F. García-Sánchez and G. Eliosa-Jiménez. "An Equation-of-State-Based Viscosity Model for Non-Ideal Liquid Mixtures". In: *Fluid Phase Equilibria* 210.2 (2003), pp. 319–334. DOI: 10.1016/S0378-3812(03)00169-9.

[149] M. A. M. Marcelino Neto and J. R. Barbosa. "Solubility, Density and Viscosity of Mixtures of Isobutane (R-600a) and a Linear Alkylbenzene Lubricant Oil". In: *Fluid Phase Equilibria* 292.1-2 (2010), pp. 7–12. DOI: 10.1016/j.fluid.2009.12.029.

[150] Y. Sun, J. Wang, X. Wang, M. He and Y. Hu. "An Experimental Investigation and Correlation of the Viscosity Refrigerant/Oil Solutions". In: *International Journal of Refrigeration* 121 (2021), pp. 152–158. DOI: 10.1016/j.ijrefrig.2020.10.034.

[151] P. K. Katti and M. M. Chaudhri. "Viscosities of Binary Mixtures of Benzyl Acetate with Dioxane, Aniline, and *m* -Cresol." In: *Journal of Chemical & Engineering Data* 9.3 (1964), pp. 442–443. DOI: 10.1021/je60022a047.

[152] O. Redlich and A. T. Kister. “Algebraic Representation of Thermodynamic Properties and the Classification of Solutions”. In: *Industrial & Engineering Chemistry* 40.2 (1948), pp. 345–348. DOI: 10.1021/ie50458a036.

[153] M. A. M. Marcelino Neto and J. R. Barbosa. “Experimental Characterization of Phase Equilibrium, Liquid Density and Viscosity of a Mixture of R-744 (CO2) and Polyol Ester Oil”. In: (2007), p. 12.

[154] M. A. Marcelino Neto and J. R. Barbosa. “Prediction of Refrigerant-Lubricant Viscosity Using the General PC-SAFT Friction Theory”. In: *International Journal of Refrigeration* 45 (2014), pp. 92–99. DOI: 10.1016/j.ijrefrig.2014.05.019.

[155] M. A. Monsalvo, A. Baylaucq, S. E. Quiñones-Cisneros and C. Boned. “High-Pressure Viscosity Behavior of x 1,1,1,2-Tetrafluoroethane (HFC-134a)+(1-x) Triethylene Glycol Dimethylether (TriEGDME) Mixtures: Measurements and Modeling”. In: *Fluid Phase Equilibria* 247.1-2 (2006), pp. 70–79. DOI: 10.1016/j.fluid.2006.06.015.

[156] J. Kendall and K. Potter. “The Viscosity of Liquids - The Viscosity - Composition Curve for Ideal Liquid Mixtures”. In: *Journal of the American Chemical Society* 39.9 (1917), p. 16.

[157] J. Baustian, M. Pate and A. Bergles. “Properties of Oil-Refrigerant Liquid Mixtures with Applications Ot Oil Concentration Measurement: Part I Thermophysical and Transport Properties”. In: *ASHRAE Transactions* 92.1 (1986).

[158] M. K. Jensen and D. L. Jackman. “Prediction of Nucleate Pool Boiling Heat Transfer Coefficients of Refrigerant-Oil Mixtures”. In: *Journal of Heat Transfer* 106.1 (1984), pp. 184–190. DOI: 10.1115/1.3246632.

[159] A. M. Yokozeki. “Solubility and Viscosity of Refrigerant Oil Mixtures”. In: *International Compressor Engineering Conference*. Paper 1002. West Lafayette, 1994.

[160] F. Mayinger. *Strömung und Wärmeübergang in Gas-Flüssigkeits-Gemischen*. Vienna: Springer Vienna, 1982. ISBN: 978-3-7091-3822-9. DOI: 10.1007/978-3-7091-3822-9.

[161] G. Hewitt and N. Hall-Taylor. *Annular Two-Phase Flow*. Elsevier, 1970. 327 pp. ISBN: 978-1-4832-8523-8.

[162] A. Sethi and P. Hrnjak. “Oil Retention and Pressure Drop of R1234yf and R134a with POE ISO 32 in Suction Lines”. In: *HVAC&R Research* 20.6 (2014), pp. 703–720. DOI: 10.1080/10789669.2014.930304.

[163] M. S. Owen, ed. *2014 ASHRAE Handbook - Refrigeration (SI Edition)*. Atlanta: American Society of Heating, Refrigerating and Air-Conditioning Engineers, 2014. ISBN: 978-1-68015-328-6.

[164] G. Wallis. *The Transition from Flooding to Upwards Cocurrent Annular Flow in a Vertical Pipe*. AEEW-R-142. United Kingdom, 1962, p. 22.

[165] G. B. Wallis. *One-Dimensional Two-phase Flow*. New York: McGraw-Hill, 1969. 450 pp. ISBN: 978-0-07-067942-9.

[166] H. Herwig. *Dimensionsanalyse von Strömungen*. Wiesbaden: Springer Fachmedien Wiesbaden, 2017. ISBN: 978-3-658-19773-5. DOI: 10.1007/978-3-658-19774-2.

[167] H. D. Baehr and K. Stephan. *Wärme- und Stoffübertragung*. Berlin, Heidelberg: Springer Berlin Heidelberg, 2013. ISBN: 978-3-642-36557-7.

[168] S. Mehendale. "Experimental and Theoretical Investigation of Annular Film Flow Reversal in a Vertical Pipe". PhD thesis. College Park: University of Maryland, 1998. 174 pp.

[169] S. C. Kesim, K. Albayrak and A. İleri. "Oil Entrainment in Vertical Refrigerant Piping". In: *International Journal of Refrigeration* 23.8 (2000), pp. 626–631. DOI: 10.1016/S0140-7007(99)00085-7.

[170] J.-P. Lee. "Experimental and Theoretical Investigation of Oil Retention in a Carbon Dioxide Air-Conditioning System". PhD thesis. College Park: University of Maryland, 2003. 156 pp.

[171] R. Radermacher, L. Cremaschi and R. A. Schwentker. "Modeling of Oil Retention in the Suction Line and Evaporator of Air-Conditioning Systems". In: *HVAC&R Research* 12.1 (2006), pp. 35–56. DOI: 10.1080/10789669.2006.10391166.

[172] A. Sethi and P. Hrnjak. "Modeling of Oil Retention and Pressure Drop in Vertical Suction Risers". In: *Science and Technology for the Built Environment* 21.7 (2015), pp. 1033–1046. DOI: 10.1080/23744731.2015.1026270.

[173] R. J. Belt, J. M. C. Van't Westende and L. M. Portela. "Prediction of the Interfacial Shear-Stress in Vertical Annular Flow". In: *International Journal of Multiphase Flow* 35.7 (2009), pp. 689–697. DOI: 10.1016/j.ijmultiphaseflow.2008.12.003.

[174] J. C. Asali, T. J. Hanratty and P. Andreussi. "Interfacial Drag and Film Height for Vertical Annular Flow". In: *AIChE Journal* 31.6 (1985), pp. 895–902. DOI: 10.1002/aic.690310604.

[175] A. Frohn and N. Roth. *Dynamics of Droplets*. Springer Science & Business Media, 2000. 308 pp. ISBN: 978-3-540-65887-0.

[176] A. Sethi. "Oil Retention and Pressure Drop of R1234yf and R134a with POE ISO 32 in Suction Lines". MA thesis. Urbana, Illinois, USA: University of Illinois, 2011.

[177] K. F. Zoellick. "Oil Retention and Pressure Drop in Horizontal and Vertical Suction Lines with R410A / POE ISO 32". MA thesis. Urbana, Illinois, USA: University of Illinois, 2010.

[178] D. N. A. Macken, F. C. Scheideman and M. L. Jacobs. "Pressure Loss and Liquid Transport of Oil-Refrigerant Mixtures". In: *ASHRAE Transactions* 85.2 (1979), pp. 77–92.

[179] K. F. Zoellick and P. Hrnjak. "Oil Retention and Pressure Drop in Horizontal and Vertical Suction Lines with R410A/POE". In: *International Refrigeration and Air Conditioning Conference*. Paper 1097. West Lafayette, 2010.

[180] A. Ramakrishnan and P. S. Hrnjak. “Oil Retention and Pressure Drop of R134a, R1234yf and R410A with POE 100 in Suction Lines”. In: *International Compressor Engineering Conference*. Paper 1327. West Lafayette, 2012, p. 11.

[181] A. Ramakrishnan. “Investigation of Oil Retention and Pressure Drop in Suction Lines Using R1234yf, R134a and R410A with POE ISO 100”. MA thesis. Urbana, Illinois, USA: University of Illinois, 2012.

[182] A. Wolf, S. Jayanti and G. F. Hewitt. “Flow Development in Vertical Annular Flow”. In: *Chemical Engineering Science* 56 (2001), pp. 3221–3235.

[183] G. Zabaras, A. E. Dukler and D. Moalem-Maron. “Vertical Upward Cocurrent Gas-Liquid Annular Flow”. In: *AIChE Journal* 32.5 (1986), pp. 829–843. DOI: 10.1002/aic.690320513.

[184] T. Fukano and T. Furukawa. “Prediction of the Effects of Liquid Viscosity on Interfacial Shear Stress and Frictional Pressure Drop in Vertical Upward Gas–Liquid Annular Flow”. In: *International Journal of Multiphase Flow* 24.4 (1998), pp. 587–603. DOI: 10.1016/S0301-9322(97)00070-0.

[185] Deutsches Institut für Normung e.V. *DIN EN 12735-1: Copper and Copper Alloys – Seamless, Round Tubes for Air Conditioning and Refrigeration – Part 1: Tubes for Piping Systems; German Version EN 12735-1:2020*. Berlin: Beuth Verlag GmbH, 2020.

[186] T. J. Fortin. “Density, Speed of Sound, and Heat Capacity Measurements of Polyol Ester Lubricants”. In: *Journal of Chemical & Engineering Data* 63.12 (2018), pp. 4325–4338. DOI: 10.1021/acs.jced.8b00358.

[187] S. Bobbo, L. Fedele and R. Stryjek. “Oil Structure Influence on the Solubility of Carbon Dioxide in POE Lubricants”. In: *International Compressor Engineering Conference*. Paper 776. West Lafayette, 2006.

[188] S. L. Outcalt and M. O. McLinden. “Automated Densimeter for the Rapid Characterization of Industrial Fluids”. In: *Industrial & Engineering Chemistry Research* 46.24 (2007), pp. 8264–8269. DOI: 10.1021/ie070791e.

Appendix

A Molecular Structure of Carboxlic Acids and POE Lubricants

A.1 Carboxlic Acids for Synthesis of Polyol Esters

Table A.1 gives information on the molecular structure of the carboxylic acids used in PEs and DiPEs in this study. It supplements the data given in Table 2.2 on page 22.

Table A.1: Carboxylic acids for synthesis of polyol esters.

Carbon Number in Acid	4	5	6	7
Linear	C($n+3$) 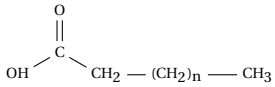			
Methyl-branching	B4M2 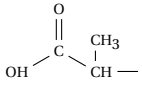	B5M2 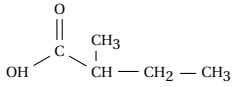	B6M2 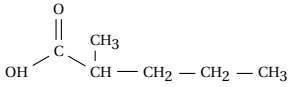	B7M2 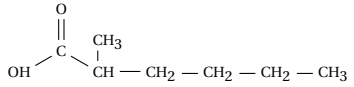
		B5M3 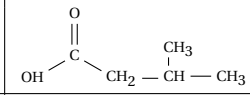	B6M4 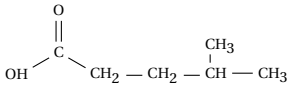	
Dimethyl-branching		B5M22 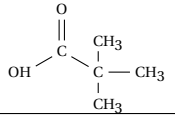	B6M22 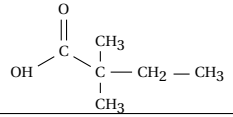	B7M22 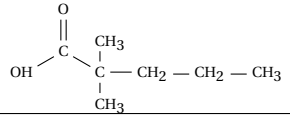
				B7M33 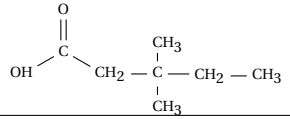
Ethyl-branching			B6E2 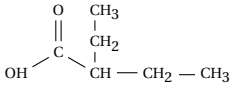	

Table A.1: (continued) Carboxylic acids for synthesis of polyol esters.

Carbon Number in Acid *c*	8	9	10
Methyl-branching	B8M6 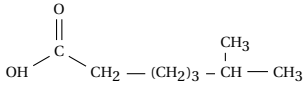	B9M7 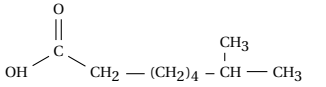	B10M8 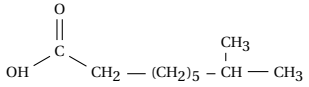
Dimethyl-branching	B8M22 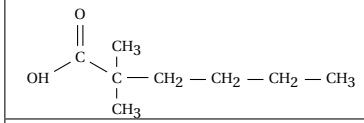		
	B8M44 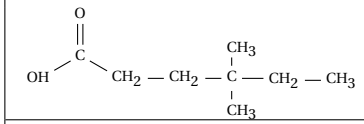		
	B8M55 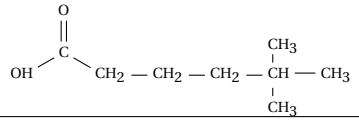		
Trimethyl-branching		B9M355 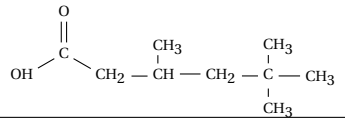	
Ethyl-branching	B8E2 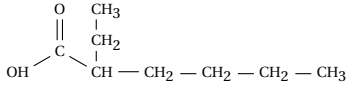		

A.2 Synthesis of Polyols and Carboxylic Acids to Polyol Esters

The reaction schemes shown in Figure A.1 supplements the reaction scheme in Figure 2.2 which is depicted in space-saving notation. Additionally, the reaction scheme for the synthesis of DiPEs is depicted in Figure A.2. To get an impression of the three-dimensional appearance of PE molecules, the reader is referred to LAESECKE ET AL. [64].

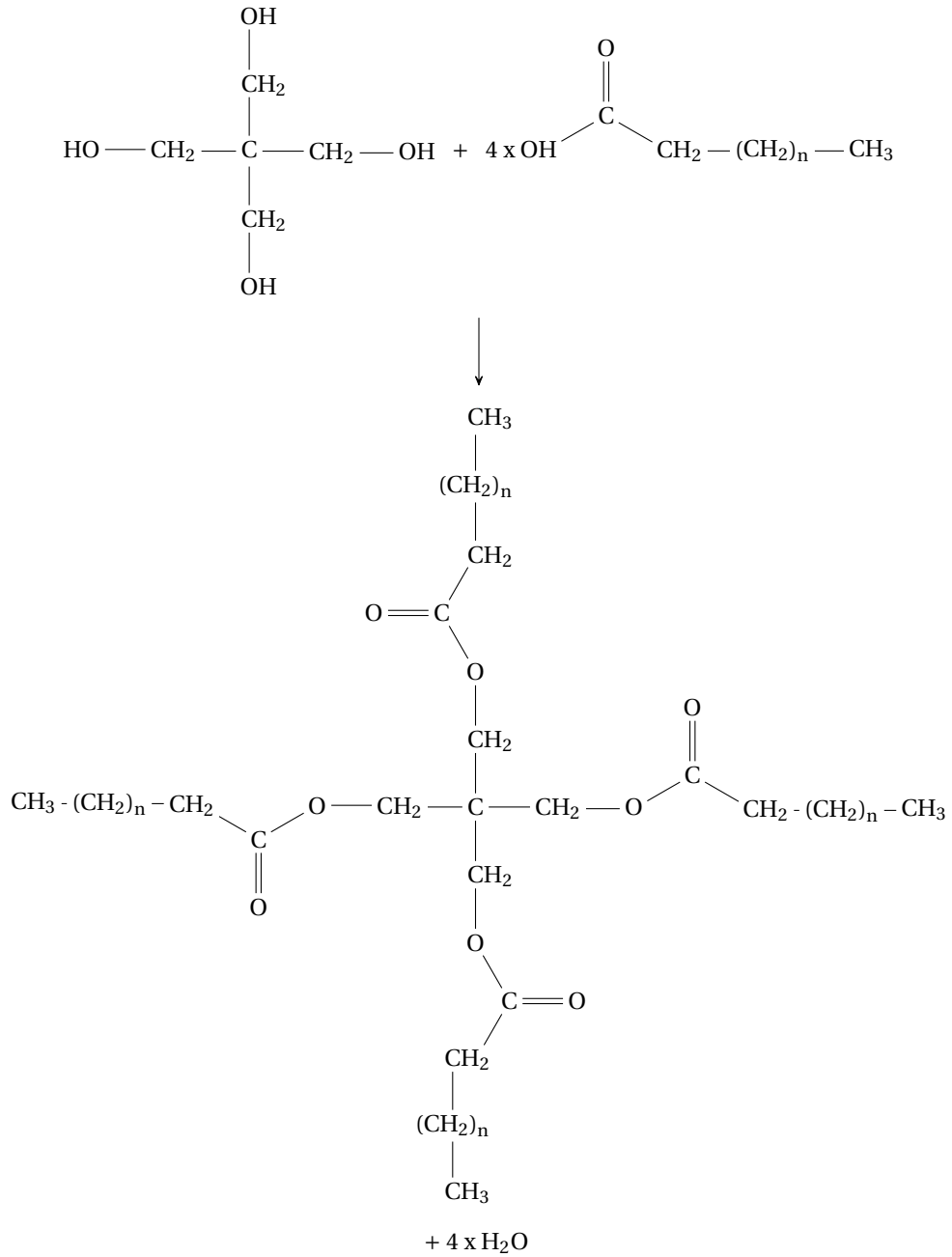

Figure A.1: Reaction of pentaerythritol and linear carboxylic acid to pentaerythritol tetraalkyl ester and water.

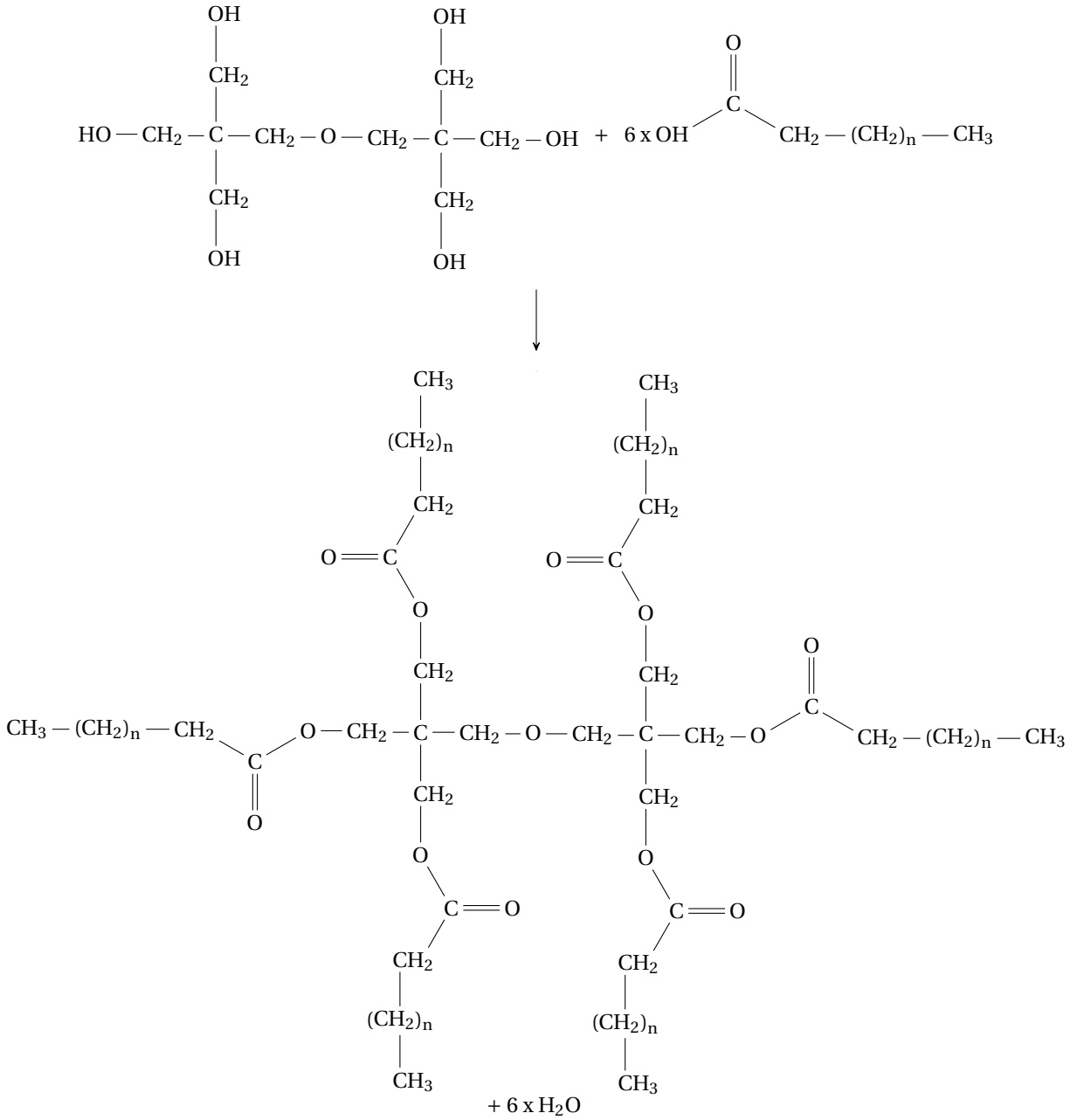

Figure A.2: Reaction of di-pentaerythritol and linear carboxylic acid to di-pentaerythritol hexaalkyl ester and water.

B Database of PEs and DiPEs in Literature

B.1 Literature-Overview on Experiments Related to Polyol Esters

Table B.1 gives an overview on the experimental data found for different PEs and DiPEs. The table shows the demand for further research that is required to model the properties of the pure component polyol ester or mixtures of the polyol ester with a refrigerant without additional assumptions.

Table B.1: Summary of literature on PE and DiPE data.

Identifier	Polyol Ester			Refrigerant - Polyol Ester Mixture			
	Density	Viscosity	Vapor Pressure	Solubility		Viscosity	
Linear Pentaerythritol Tetralkyl Ester							
PEC3	KISHORE AND SHOBHA [46]	KISHORE AND SHOBHA [46]					
PEC4	FEDELE ET AL. [55] KISHORE AND SHOBHA [46]	ROSSI ET AL. [61] KISHORE AND SHOBHA [46]		R744 R1234yf R1234ze	PERNECHELE ET AL. [101] WANG ET AL. [99] WANG ET AL. [99]		
PEC5	FANDIÑO ET AL. [53] FEDELE ET AL. [55] FORTIN [186] KISHORE AND SHOBHA [46] OUTCALT [58]	ROSSI ET AL. [61] BOHNER ET AL. [60] BOYDE [36] KISHORE AND SHOBHA [46] LAESECKE ET AL. [64] NUTUI ET AL. [65] PENSADO ET AL. [47] WAHLSTRÖM AND VAMLING [68]	RAZZOUK ET AL. [16]	R744 R600a R1234yf	FANDIÑO ET AL. [104] SUN ET AL. [103] SUN ET AL. [105]	R744 R125 R134a	PENSADO ET AL. [145]* WAHLSTRÖM AND VAMLING [68]
PEC6	FEDELE ET AL. [55]	ROSSI ET AL. [61] BOHNER ET AL. [60]		R744	BOBBO ET AL. [106]		

Table B.1: (continued) Summary of literature on PE and DiPE data.

Identifier	Polyol Ester			Refrigerant - Polyol Ester Mixture			
	Density	Viscosity	Vapor Pressure	Solubility			Viscosity
PEC7	FANDIÑO ET AL. [52] FEDELE ET AL. [55] FORTIN [186] KISHORE AND SHOBHA [46] OUTCALT [58]	ROSSI ET AL. [61] BOHNER ET AL. [60] BOYDE [36] KISHORE AND SHOBHA [46] LAESECKE ET AL. [64] NUTUI ET AL. [65] PENSADO ET AL. [47]	RAZZOUK ET AL. [16]	R600a R1234yf R744	SUN ET AL. [103] SUN ET AL. [105] FANDIÑO ET AL. [115]	R744	PENSADO ET AL. [145]*
PEC8	FEDELE ET AL. [55] KISHORE AND SHOBHA [46]	ROSSI ET AL. [61] BOHNER ET AL. [60] BOYDE [36] KISHORE AND SHOBHA [46] NUTUI ET AL. [65]		R744	BOBBO ET AL. [187]		
PEC9	FANDIÑO ET AL. [52] FORTIN [186] KISHORE AND SHOBHA [46] OUTCALT [58] WAHLSTRÖM AND VAMLING [59]	BOHNER ET AL. [60] BOYDE [36] KISHORE AND SHOBHA [46] LAESECKE ET AL. [64] NUTUI ET AL. [65] PENSADO ET AL. [67]	RAZZOUK ET AL. [16]	R1234yf R600a R32 R125 R134a R143a R152 R744	SUN ET AL. [105, 110] SUN ET AL. [110] WAHLSTRÖM AND VAMLING [59] FANDIÑO ET AL. [115]	R744	PENSADO ET AL. [145]*
PEC10	KISHORE AND SHOBHA [46]	KISHORE AND SHOBHA [46]					

Table B.1: (continued) Summary of literature on PE and DiPE data.

Identifier	Polyol Ester			Refrigerant - Polyol Ester Mixture	
	Density	Viscosity	Vapor Pressure	Solubility	Viscosity
Branched Pentaerythritol Tetralkyl Ester with Methyl Functional Group					
PEB4M2		ROSSI ET AL. [61] BOHNER ET AL. [60]			
PEB5M2	FEDELE ET AL. [48]	ROSSI ET AL. [61] CHAO ET AL. [62]		R744	BOBBO ET AL. [112, 187] FEDELE ET AL. [111]
PEB5M3		CHAO ET AL. [62]			
PEB6M2	FEDELE ET AL. [48]	ROSSI ET AL. [61] CHAO ET AL. [62]		R744	BOBBO ET AL. [112]
PEB6M4		CHAO ET AL. [62]			
PEB7M2	FEDELE ET AL. [48]	ROSSI ET AL. [61]		R744	BOBBO ET AL. [112]
PEB8M6		BOHNER ET AL. [60]			
Branched Pentaerythritol Tetralkyl Ester with Ethyl Functional Group					
PEB6E2	WAHLSTRÖM AND VAMLING [59]	ROSSI ET AL. [61] BOHNER ET AL. [60]		R744 R32 R125 R134a R143a R152	FEDELE ET AL. [114] WAHLSTRÖM AND VAMLING [59]

Table B.1: (continued) Summary of literature on PE and DiPE data.

Identifier	Polyol Ester			Refrigerant - Polyol Ester Mixture			
	Density	Viscosity	Vapor Pressure	Solubility		Viscosity	
PEB8E2	WAHLSTRÖM AND VAMLING [59] FANDIÑO ET AL. [51]	ROSSI ET AL. [61] NUTUI ET AL. [65] OWEN [8] PENSADO ET AL. [67] WAHLSTRÖM AND VAMLING [68]	RAZZOUK ET AL. [16]	R744 R32 R125 R134a R143a R152	BOBBO ET AL. [113],FANDIÑO ET AL. [104] WAHLSTRÖM AND VAMLING [59]	R744 R125 R134a	PENSADO ET AL. [144]* WAHLSTRÖM AND VAMLING [68]
Branched Pentaerythritol Tetralkyl Ester with Di-Methyl Functional Group							
PEB5M22		BOHNER ET AL. [60]					
PEB6M22		CHAO ET AL. [62]					
PEB7M33		CHAO ET AL. [62]					
PEB8M22		CHAO ET AL. [62]					
PEB8M44		CHAO ET AL. [62]					
PEB8M55		CHAO ET AL. [62]					
Branched Pentaerythritol Tetralkyl Ester with Tri-Methyl Functional Group							
PEB9M355		BOYDE [36]					
Linear Di-Pentaerythritol Hexaalkyl Ester							
DiPEC4		BOHNER ET AL. [60]					
DiPEC5	FANDIÑO ET AL. [54]	PAREDES ET AL. [66]	GARCÍA ET AL. [72]				
DiPEC6		BOHNER ET AL. [60]					
DiPEC7	FANDIÑO ET AL. [54]	PAREDES ET AL. [66]	GARCÍA ET AL. [72]	R744	FANDIÑO ET AL. [115]		

Table B.1: (continued) Summary of literature on PE and DiPE data.

Identifier	Polyol Ester			Refrigerant - Polyol Ester Mixture	
	Density	Viscosity	Vapor Pressure	Solubility	Viscosity
Branched Di-Pentaerythritol Hexaalkyl Ester with Methyl Functional Group					
DiPEB9M7	HARRIS [56]	HARRIS [56]	GARCÍA ET AL. [72]		
DiPEB10M8		BOHNER ET AL. [60]			
Branched Di-Pentaerythritol Hexaalkyl Ester with Ethyl Functional Group					
DiPEB8E2		BOHNER ET AL. [60]			
Branched Di-Pentaerythritol Hexaalkyl ester with Tri-Methyl Functional Group					
DiPEB9M355		OWEN [8]			

*: The experiments of PENSADO ET AL. [144, 145] were conducted with a low lubricant concentration beeing characteristic for the liquid line of the refrigeration cycle and the evaporator inlet.

B.2 Measurements of Density and Viscosity of Polyol Esters

The following tables contain more detailed information on measurements of the fluid properties of pentaerythritol tetraalkyl esters and di-pentaerythritol hexaalkyl esters. The tables also summarizes meta-data of the experiments in order to identify possible sources of deviations in the fluid properties for the same polyol ester between the different publications. Table B.2 contains data on the density measurements described in Section 2.2.1. Table B.3 summarizes data on the viscosity measurements described in Section 2.2.2.

Table B.2: Meta data of the density measurements of PEs and DiPEs.

Publication	PE / DiPE	Purity	Measurement device	Uncertainty
FANDIÑO ET AL. [53]	PEC5	>95%	Vibrating tube densimeter Anton Paar DMA512P	$\pm 0.14\,kg\,m^{-3}$
FANDIÑO ET AL. [52]	PEC7, PEC9	>95%		$\pm 0.1\,kg\,m^{-3}$
FANDIÑO ET AL. [51]	PEB8E2	99%		$\pm 0.1\,kg\,m^{-3}$
FANDIÑO ET AL. [54]	DiPEC5, DiPEC7	>95%	Vibrating tube densimeter Anton Paar DMA-HPM	$\pm 0.7\,kg\,m^{-3}$
FEDELE ET AL. [55]	PEC4-8	>98%	Vibrating tube densimeter Anton Paar DMA512	$\pm 0.452\,kg\,m^{-3}$
FEDELE ET AL. [48]	PEB5M2, PEB6M2, PEB7M2	>98%		
HARRIS [56]	DiPEB9M7	>95%	Vibrating tube densimeter Anton-Paar DMA	±0.02%
KISHORE AND SHOBHA [46]	PEC3-5, PEC7-10	n/a	Mercury calibrated dilatometer	±0.2%
LIN AND KEDZIERSKI [57]	PEC6	95±2%	n/a	±0.1%
OUTCALT [58]	PEC5 PEC7 PEC9	96.7% 97.3% 93.0%	Vibrating tube densimeter Anton Paar DMA-HPM [188]	$\pm 0.8\,kg\,m^{-3}$
WAHLSTRÖM AND VAMLING [59]	PEC9 PEB6E2 PEB8E2	>95% >95% >90%	Vibrating tube densimeter Anton Paar DMA602	±0.1%

Some data on viscosity was found in the reference books of BAIR [63], BOYDE [36], and OWEN [8]. Unfortunately, the origin of the published viscosity data is unclear and details on the viscosity measurement technique or measurement uncertainty are not given in these cases.

Table B.3: Meta data of the viscosity measurements of PEs. (In alphabetical order of the first authors names.)

Publication	PE / DiPE	Purity	T	p	Viscometer	Uncert.
BAIR [63]	PEC6	n/a	40°C-165°C	0.1 MPa - 1200 MPa	n/a	n/a
BOHNER ET AL. [60]	PEC5...9, PEB4M22, PEB5M22, PEB6E2, PEB8M6[1], DiPEC4, DiPEC6, DiPEB8E2, DiPEB10M8	n/a	100°F, 210°F	atm	Fenske-Ostwald	n/a
BOYDE [36]	PEC5, PEC7, PEC8, PEC9, PEB8E2, PEB9M355	n/a	40°C, 100°C	atm	n/a	n/a
CHAO ET AL. [62]	PEB5M2, PEB5M3, PEB6M2, PEB6M4, PEB6M22, PEB7M22, PEB7M33, PEB8M22, PEB8M44, PEB8M55	n/a	100°F, 210°F	atm	n/a	n/a
HARRIS [56]	DiPEB9M7	≥ 95%	20°C-90°C	0.1 MPa - 200 MPa	Falling body viscometer	± 2%
KISHORE AND SHOBHA [46]	PEC2...5, PEC7...10	n/a	30°C-140°C	atm	Rotational viscometer	± 2.5%

[1]Prepared from technical pentaerythritol. Technical pentaerythritol contains about 5% of di- and tri-pentaerythritol.

Table B.3: (continued) Meta data of the viscosity measurements of PEs.

Publication	PE / DiPE	Purity	T	p	Viscometer	Uncert.
LAESECKE ET AL. [64]	PEC5, PEC7, PEC9	96.7%, 97.3%, 93.0%	2°C - 177°C	0.12 MPa - 138 MPa	Oscillating piston viscometer	± 2%
LIN AND KEDZIERSKI [57]	PEC6	95±2%	-15°C - 100°C	atm	Stabinger viscometer	±2.1%
NUTUI ET AL. [65]	PEC5-9, PEB8E2, PEB9M355	n/a	100°F, 210°F	atm	n/a	n/a
OWEN [26]	PEB8E2, DiPEB9M355	n/a	40°C	atm	n/a	n/a
PAREDES ET AL. [66]	DiPEC5, DiPEC7	≥ 95%	30°C - 100°C	0.1 MPa - 60 MPa	Rolling ball viscometer	± 3%
PENSADO ET AL. [47, 67]	PEC5, PEC7, PEC9 PEB8E2	≥ 95%, ≥ 95%, ≥ 95%, 99%	30°C - 80°C	0.1 MPa - 60 MPa	Rolling ball viscometer	± 3%
ROSSI ET AL. [61]	PEC5-8, PEB5M2, PEB6M2, PEB7M2, PEB8E2	n/a	0.5°C - 100°C	atm	n/a	n/a
WAHLSTRÖM AND VAMLING [68]	PEC5, PEB8E2	≥ 95%, ≥ 90%	30°C, 45°C, 60°C	atm	Capillary viscometer	± 4%

C Density of PEs

Figure C.1 shows the temperature influence on the density described in Section 2.2.1. It supplements Figure 2.3b on page 26 that shows the gradient of the density data depicted in Figure C.1 with respect to temperature.

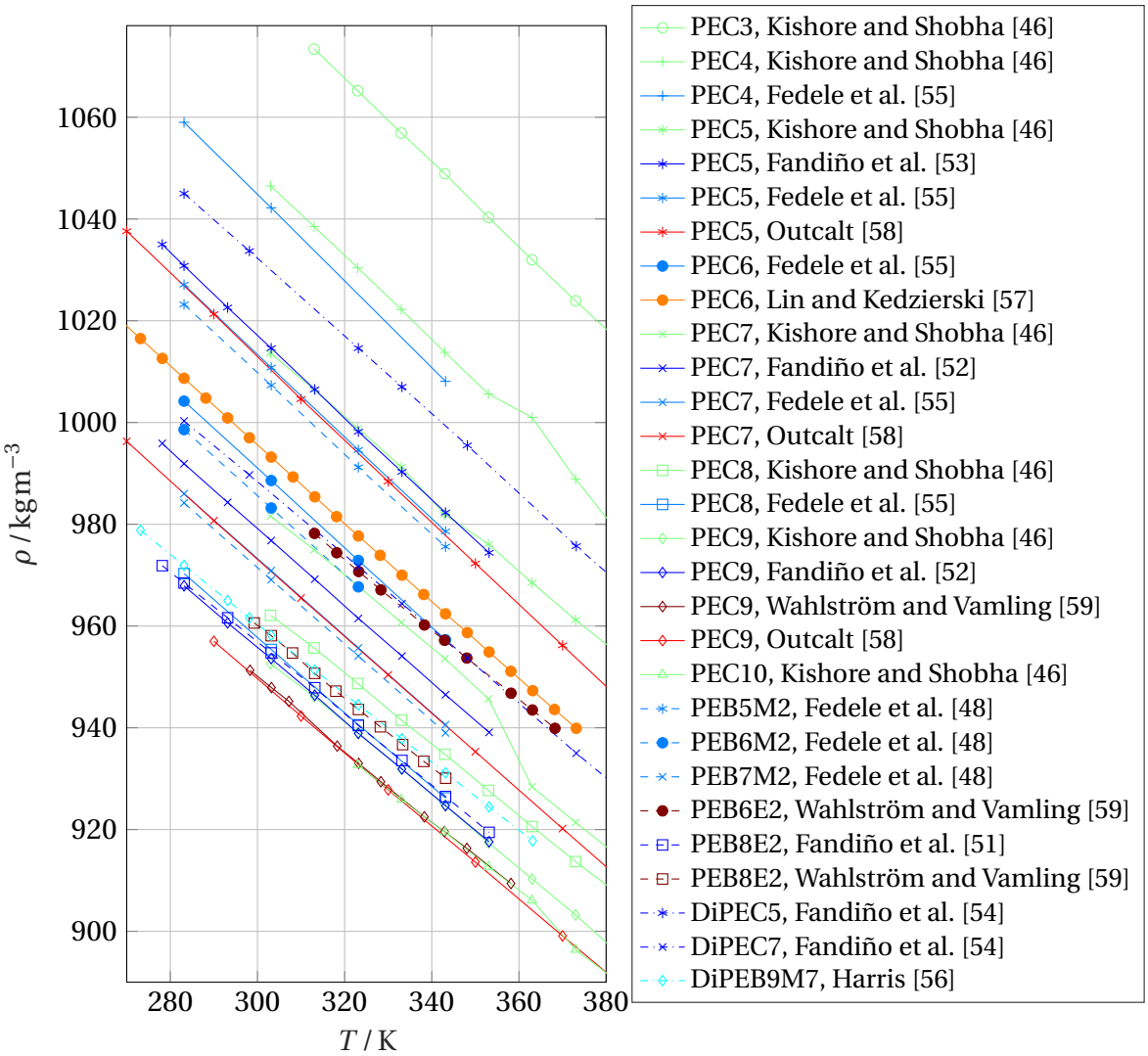

Figure C.1: Density of PEs in literature over temperature.

D Pure Component Parameters of Viscosity Models

D.1 Model Parameters of the Free Volume Theory

For a better overview, the parameters of the free volume theory of ALLAL ET AL. [75] (see page 45) are summarized in Table D.1 for all substances used in the mixture viscosity calculation. The values for the refrigerants are fitted

Table D.1: Pure component parameters of polyol esters and refrigerants for the free volume theory model of ALLAL ET AL. [75].

Component	Free Volume Parameters			Deviation		
	α	l	B	AAD	MD	Bias
	$\mathrm{J\,m^3\,mol^{-1}\,kg^{-1}}$	Å	10^{-3}	%	%	%
PEC5	395	0.202	2.57	1.76	2.85	-0.04
PEC7	563	0.183	1.65	0.93	2.03	-0.01
PEC9	792	0.141	1.12	3.09	5.84	-0.13
PEB5M2	176	0.149	11.6	8.35	18.69	-0.94
PEB8E2	687	0.041	1.78	2.86	5.01	-0.1
PEB9M355	460	0.0139	4.56	8.7	18.49	-1.05
DiPEC5	952	0.0825	0.863	3.04	4.49	-0.11
DiPEC7	1240	0.0795	0.614	2.78	4.53	-0.1
DiPEB9M7	792	0.0168	2.1	6.91	20.52	-0.72
R32	26.5	56.3	10.1	5.1	4.4	15
R125	26.5	61.5	10.7	2.6	2	6.8
R134a	26.5	72	12.6	2	1.7	11.4
R1234yf	26.5	78.2	12.8	2.4	2.1	12
R1234ze	26.5	85.3	13.2	1.2	−1	8.4
R290	27.1	162	31.2	1.6	1.1	6.6
R1270	25.3	181	22.1	1.2	0.8	5.2
R600a	27.2	197	40.2	0.9	0.4	6.6
R744	26.5	39.8	13.4	1.4	1.1	5.3

to viscosity data of vapor and liquid phase obtained from *REFPROP* [42] in a temperature range of 240 K < T < 350 K and a pressure range for R744 (CO_2) of 0.55 MPa < p < p_{crit} and for all other refrigerants of 0.1 MPa < p < p_{crit}.

D.2 Model Parameters of the F-Theory

For a better overview, the scaling parameters μ_a and μ_r of the f-theory of QUIÑONES-CISNEROS ET AL. [88] (see page 47) are summarized in Table D.2 for all substances used in the mixture viscosity calculation.

Table D.2: Pure component parameters of polyol esters and refrigerants for the f-theory model of QUIÑONES-CISNEROS ET AL. [88].

Component	f-theory Parameters		Deviation		
	μ_a	μ_r	AAD	MD	Bias
	10^{-7} Pa s	10^{-7} Pa s	%	%	%
PEC5	−129.3	174	10.04	31.14	−1.59
PEC7	8.288	104.5	5.66	24.04	−0.59
PEC9	21.43	69.38	7.44	15.83	−0.74
PEB5M2	−1490	78.44	22.86	50.45	−7.05
PEB8E2	−373.1	80.4	12.55	32.79	−2.41
PEB9M355	7877	2742	41.58	76.32	−22.34
DiPEC5	−75.19	171.1	7.64	12.88	−0.71
DiPEC7	−17.65	51.59	6.87	11.14	−0.55
DiPEB9M7	−1099	505.8	16.76	66.88	−5.67
R32	6.202	60.55	5.57	15.66	4.67
R125	−24.83	138.8	9.28	21.3	5.43
R134a	−48.42	159.8	9.93	47.16	7.57
R1234yf	−18.36	114.4	10.07	38.02	7.58
R1234ze	−58.77	165.4	1.18	9.18	0.16
R290	2.082	63.77	0.62	3.59	−0.17
R600a	−12.99	89.46	0.93	4.12	0.04
R1270	9.851	55.91	0.89	8.58	−0.09
R744	23.94	57.17	12.38	143	8.33

The values for the refrigerants are fitted to viscosity data of vapor and liquid phase obtained from *REFPROP* [42] in a temperature range of 240 K < T <

350 K and a pressure range for R744 (CO_2) of 0.55 MPa < p < p_{crit} and for all other refrigerants of 0.1 MPa < p < p_{crit}.

D.3 Model Parameters for Viscosity Model of Comuñas et al.

The values of the parameters of Equation 3.21 and 3.22 on page 48 are summarized in Table D.3.

Table D.3: Pure component parameters of PEs and DiPEs for the model of COMUÑAS ET AL. [89].

Component	Data Source	$10^6 a_1$ Pa s	a_2 K	a_3 K	$10^{-6}\ a_{5,0}$ Pa	$10^{-6}\ a_{5,1}$ Pa K^{-1}	$10^{3}\ a_{5,2}$ Pa K^{-2}	a_4 -
PEC5	LAESECKE ET AL. [64]	41.6	533	12.6	-361	2.74	-538	8.41
PEC7		47.9	533	15.3	-361	2.74	-195	10.50
PEC9		125	404	73.8	-361	2.74	655	8.33
PEB5M2	ROSSI ET AL. [61]	43.9	519	31.8	-361	2.74	3.4	8.00
PEB8E2	PENSADO ET AL. [67]	37.7	550	29.9	-361	2.74	-168	10.50
DiPEC5	PAREDES ET AL. [66]	46.6	621	-4.85	-361	2.74	-4080	8.18
DiPEC7		44.0	643	-14.0	-361	2.74	-631	8.30
DiPEB9M7	HARRIS [56]	84.5	548	56.2	-361	2.74	28.5	16.6

The parameters of PEB9M355 for the *Ubbelohde-Walter* Equation (3.23) are $a_1 = 9.7109$ and $a_2 = -3.7607$.

E Procedure to Read Data of Daniels Plots

The procedure to read Daniels plots is used in Section 3.5 to gather information on the temperature influence on the kinematic viscosity of commercial POE lubricants described in Table 3.9 on page 68. The procedure is described step-by-step in the following.

1. The Daniels plot image (Figure 1.2 shows an example) is read with the Matlab® function *imread*. Subsequently, it is cropped, so that it only contains the coordinate system and data for both solubility and viscosity plot.
2. Grid lines of the coordinate system are recognized by averaging the pixel values of the image in horizontal and vertical direction, respectively. A value is assigned to every grid line according to the original image.
3. In a calibration function, the pixel position in horizontal direction is related to the Temperature T and in vertical direction to the kinematic viscosity ν and vapour pressure p, respectively.
4. The grid lines of the coordinate grid are deleted from the image. So, only the viscosity or solubility information remains.
5. The remaining pixels that have a value above a certain threshold are designated to a lubricant mass-fraction w_{Lub} level as indicated in the original image.
6. CAVESTRI [40] use the following extension of Raoult's law to represent the solubility data:

$$\begin{aligned} p(x_{\mathrm{Ref}}, T) = & x_{\mathrm{Ref}} p_{\mathrm{v,Ref}}(T) + x_{\mathrm{Ref}}(1 - x_{\mathrm{Ref}}) \ldots \\ & (a_1 + a_2 T + a_3 T^2 + a_4 x_{\mathrm{Ref}} + a_5 x_{\mathrm{Ref}} T + a_6 x_{\mathrm{Ref}} T^2)\, p_{\mathrm{Ref,sat}}(T) \end{aligned} \tag{E.1}$$

To obtain the vapor pressure of the refrigerant $p_{\mathrm{v,Ref}}$, the Antoine equation is fitted with data of the pure refrigerant obtained from *CoolProp* [41]. As the composition of the lubricant is unknown, the mole fraction of the refrigerant x_{Ref} is replaced by the mass fraction of the refrigerant w_{Ref}. This way, the equation loses its physical background. Nevertheless, it is still suited to represent the solubility data:

$$\begin{aligned} p(w_{\mathrm{Ref}}, T) = & w_{\mathrm{Ref}} p_{\mathrm{sat,Ref}}(T) + w_{\mathrm{Ref}}(1 - w_{\mathrm{Ref}}) \ldots \\ & (a_1 + a_2 T + a_3 T^2 + a_4 w_{\mathrm{Ref}} + a_5 w_{\mathrm{Ref}} T + a_6 w_{\mathrm{Ref}} T^2)\, p_{\mathrm{sat,Ref}}(T) \end{aligned} \tag{E.2}$$

The coefficients a_i of Equation (E.2) are fit to the vapor pressure p data obtained from the Daniels plot.

7. The coordinate system of Daniels plots is often distorted such that the kinematic viscosity data is depicted as a straight line. Therefore, the pixel position of the temperature (horizontal direction) is fitted to a polynom of 1st order. The kinematic viscosity ν can subsequently be calculated with the calibration function obtained in step 3.

F Correlations for the Binary Interaction Coefficient k_{ij}

Figures F.1 and F.2 show the values of the binary interaction coefficient k_{ij} calculated with binary solubility data of refrigerants with PEs and DiPEs in Section 4.5.1. They complete the information given in Figure 4.5 on page 96.

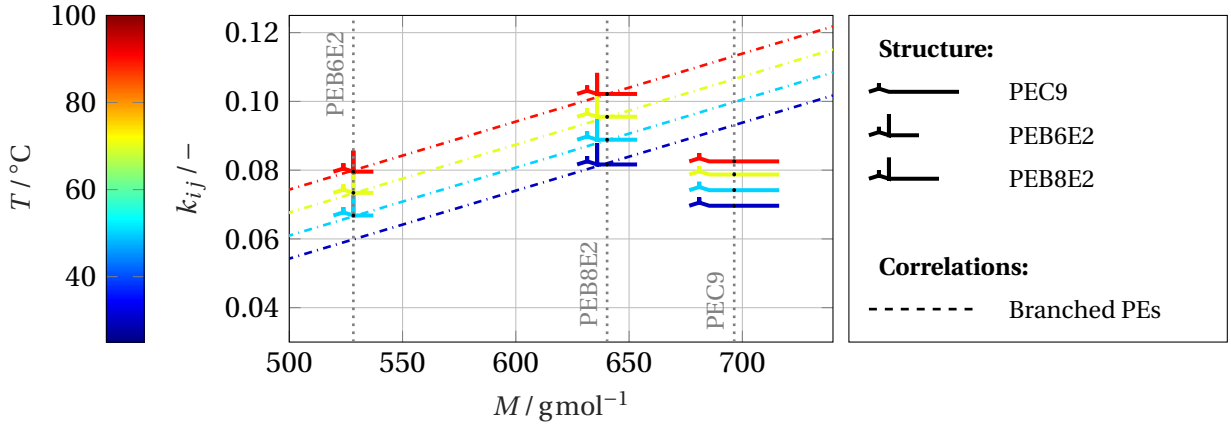

(a) R32

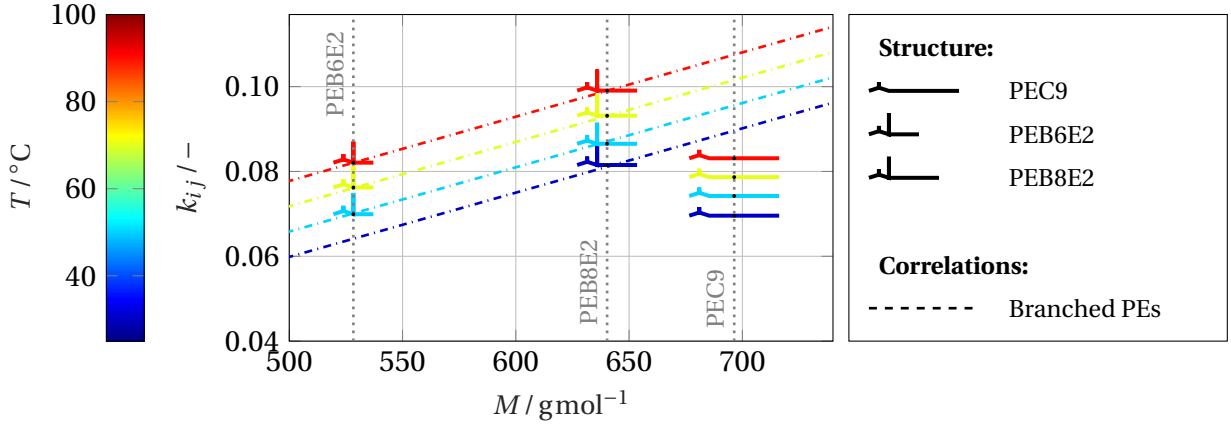

(b) R125

Figure F.1: Binary interaction parameter k_{ij} of HFCs and PEs.

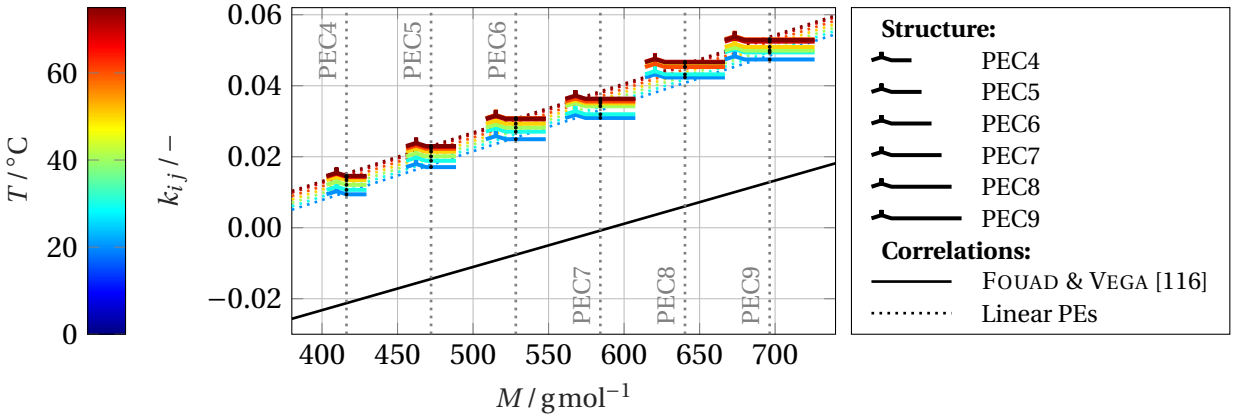

(a) R1234yf

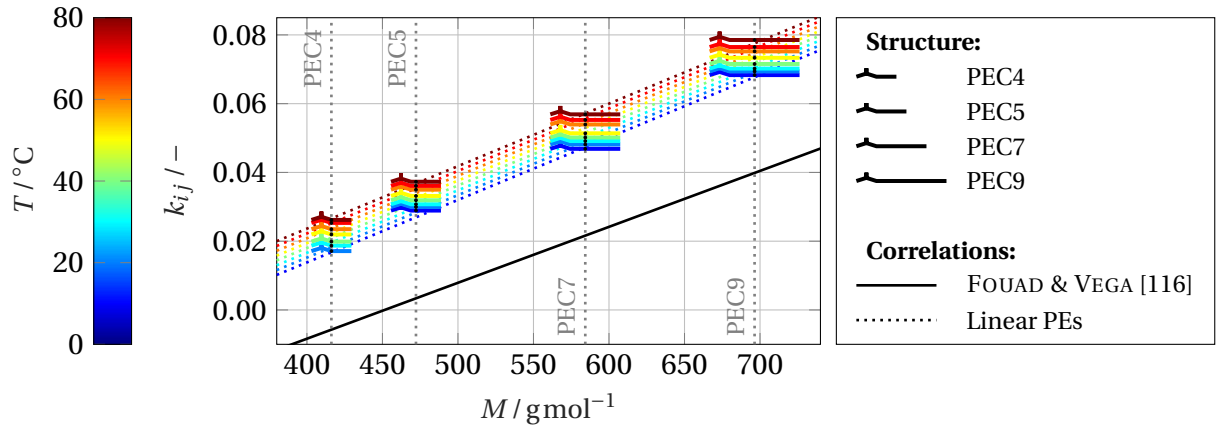

(b) R1234ze

Figure F.2: Binary interaction parameter k_{ij} of HFOs and PEs.

A large difference between the correlation of Fouad and Vega [116] and the correlation developed in this thesis can be observed in Figure F.2. The reason for the difference is that Fouad and Vega [116] used the Polar PC SAFT EoS of Dominik et al. [127], whereas the PCP SAFT EoS of Gross and Vrabec [43] was used in the present study.

Figure F.3 shows a graphical representation of the correlations for the interfacial fricition factor f_{I} summarized in Table 4.7 on page 103.

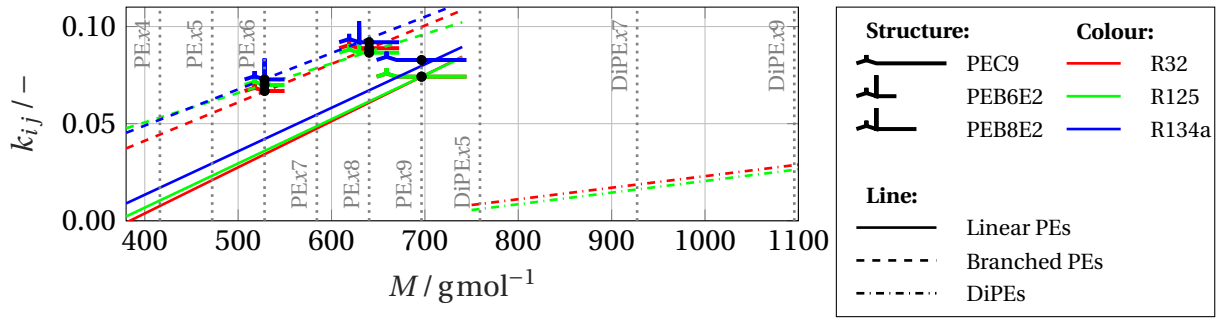

(a) HFCs, $T = 50°C$.

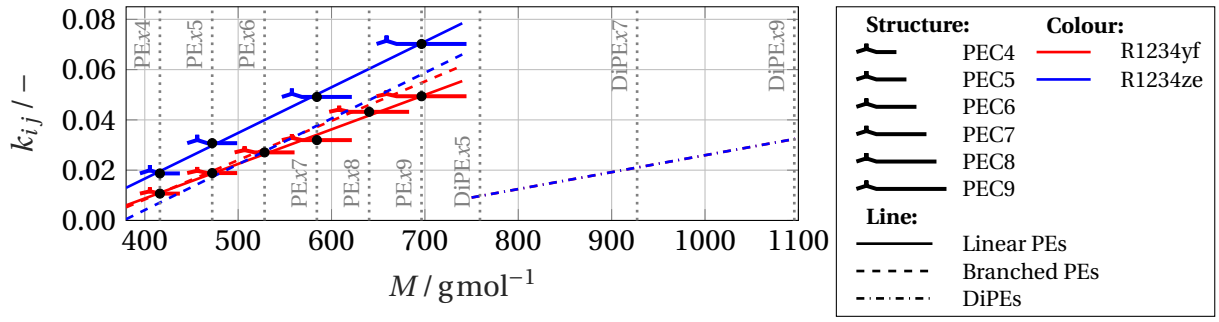

(b) HFOs, $T = 30°C$.

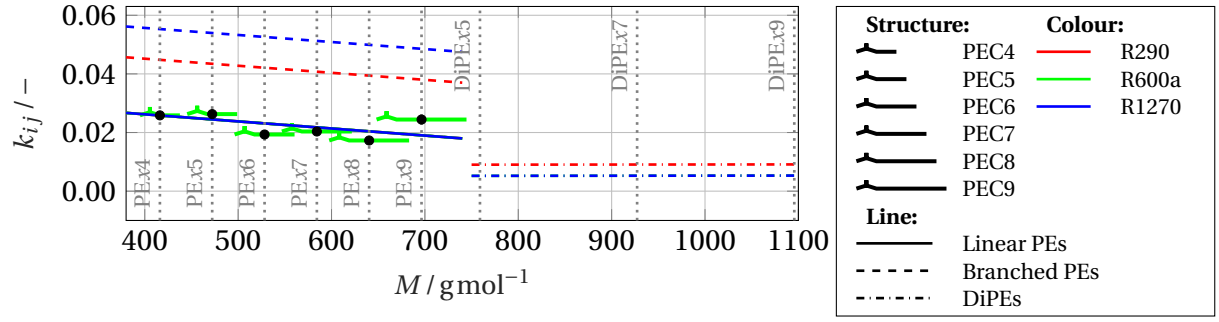

(c) HCs, $T = 30°C$.

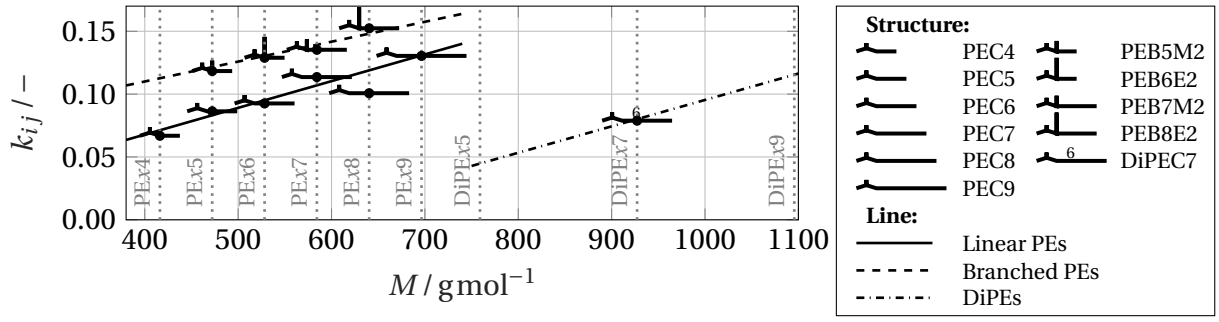

(d) R744, $T = 30°C$.

Figure F.3: Correlations for the binary interaction parameter k_{ij} of linear and branched PEs as well as DiPEs.

G Interfacial Friction Factor of Experiments of Zoellick, Ramakrishnan, and Sethi

To allow the reader to better distinguish the data points of the different refrigerant-lubricant mixtures in Figure 6.4 on page 147, the data is plotted separately for the different refrigerants used in the experiments in Figure G.1.

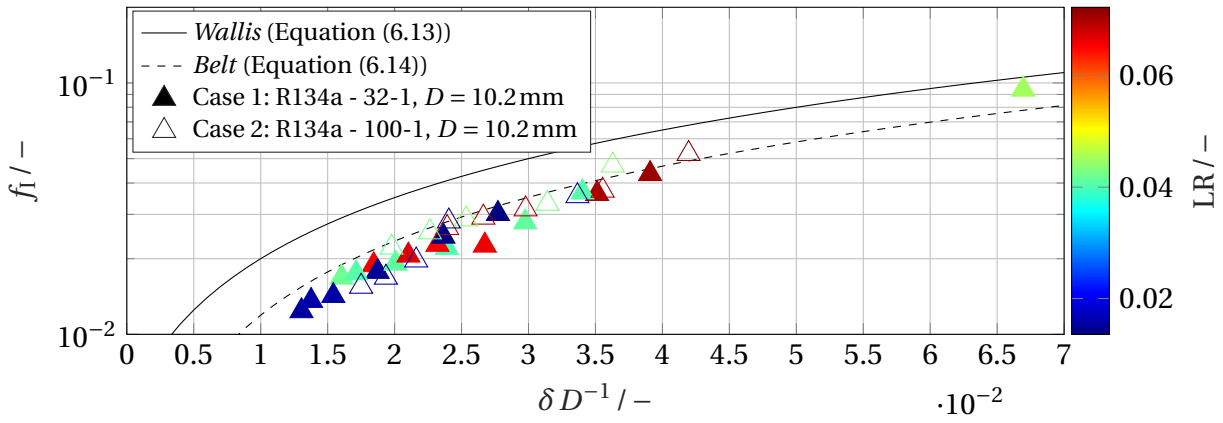

(a) R134a

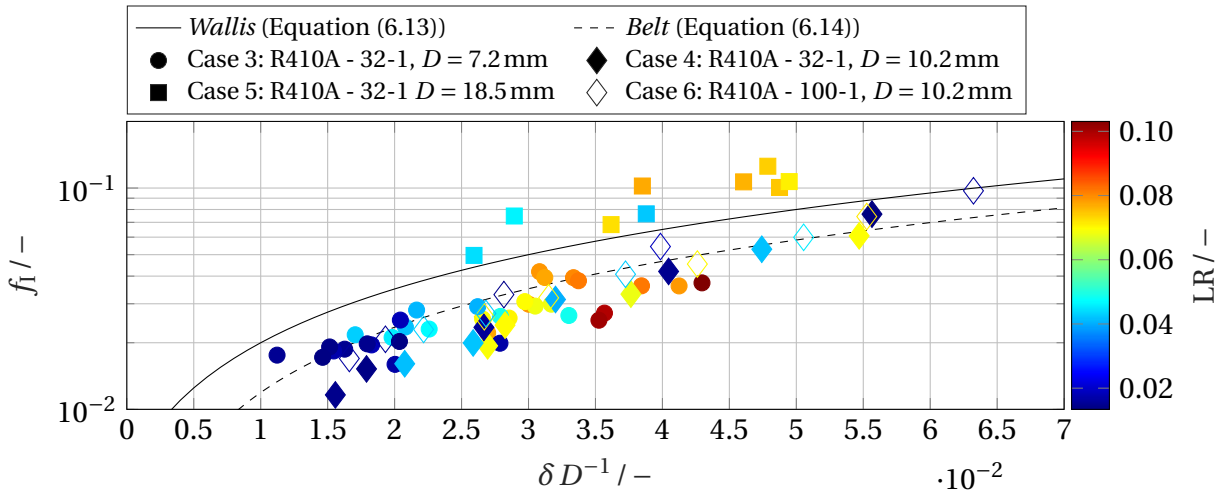

(b) R410A

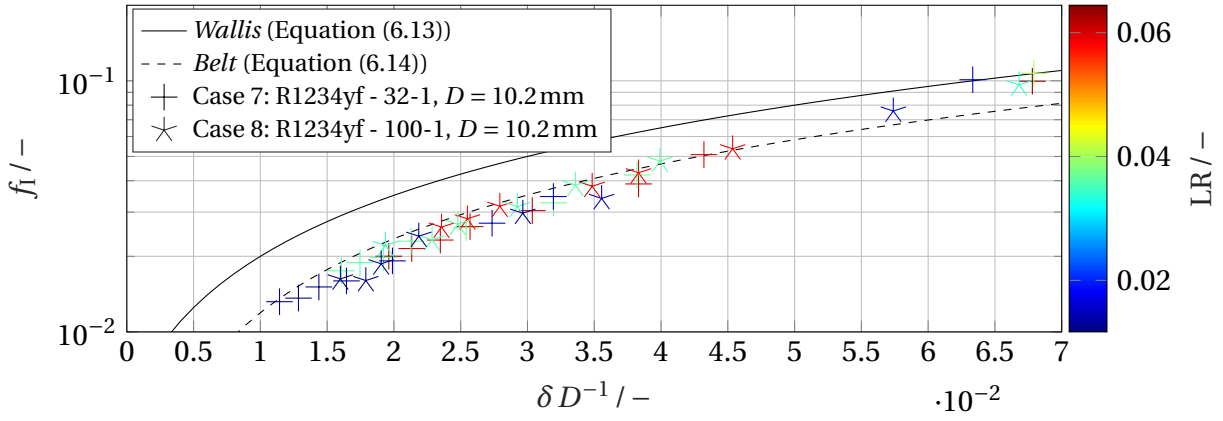

(c) R1234yf

Figure G.1: Calculated interfacial friction factor f_l for experiments with the same refrigerant.

H Fluid Properties and Deviation in Validation of Mehendale

Table H.1 details the fluid properties of the vapor phase calculated with *CoolProp* [41] and the liquid phase read from the Daniels plots in MEHENDALE [168, p. 34ff] for the pure lubricant. These fluid properties are used in Section 6.6.1 to calculate the critical mass flux J_{crit} with the two-phase flow model of the present study. Additionally, more detailed results compared to Table 6.4 on page 151 are given regarding the deviation between the critical mass flux $J_{\mathrm{crit,pred}}$ predicted with the two-phase flow model of the present study and the mass flux for the onset of flow reversal $J_{\mathrm{FR,exp}}$ observed in the experiments of MEHENDALE [168]. The deviation is calculated for each experiment of MEHENDALE [168] and the different friction factor correlations considered in the present work.

Table H.1: Fluid properties and deviation between observed mass flux for onset of flow reversal $J_{\mathrm{FR,exp}}$ in experiments of MEHENDALE [168] and predicted critial mass flux $J_{\mathrm{crit,pred}}$.

Ref./ Lub.	No[a]	ρ_{v} $\frac{\mathrm{kg}}{\mathrm{m}^3}$	μ_{v} μPa s	ρ_{l} $\frac{\mathrm{kg}}{\mathrm{m}^3}$	μ_{l} mPa s	$\varepsilon_{\mathrm{Wallis}}$ %	$\varepsilon_{\mathrm{Belt}}$ %	$\varepsilon_{\mathrm{Sethi}}$ %
R410A POE32	33	33.0	13.0	974.1	58.7	-8.7	7.4	-47.4
	36	31.6	12.9	975.0	62.4	-5.6	8.8	-49.0
	37	31.1	12.9	975.0	62.4	-2.0	12.9	-47.0
	39	16.0	12.7	975.5	64.5	0.5	15.7	-37.3
	40	16.9	12.7	975.7	65.2	-14.3	-1.1	-47.0
	41	16.3	12.7	975.7	65.2	-0.7	14.3	-38.5
	42	17.3	12.7	975.7	65.2	-10.3	3.4	-44.9
	43	16.3	12.7	975.4	63.9	0.7	15.9	-37.2
	44	13.5	12.6	976.6	69.1	-15.4	-3.6	-47.7
	45	12.9	12.6	976.5	68.7	-6.9	6.0	-41.9
	46	13.8	12.6	976.6	69.1	-13.6	-1.5	-46.9
	48	13.6	12.6	976.6	69.5	-18.1	-6.5	-49.5
	49	30.8	12.9	976.1	66.8	-14.0	-1.9	-55.5
	52	31.1	12.8	976.9	70.7	-11.4	0.9	-55.4
	53	30.9	12.8	976.6	69.1	-11.0	1.4	-54.7
R407C POE32	54	27.0	12.4	969.9	46.3	-7.1	9.7	-39.9
	55	26.5	12.4	969.4	44.5	-2.3	11.9	-40.6
	58	24.4	12.5	968.3	40.6	-12.5	3.7	-38.6
	59	27.1	12.4	969.1	43.6	-11.7	4.5	-41.3
	61	27.4	12.4	970.3	47.4	-13.6	2.1	-44.6
	62	27.2	12.4	970.3	47.4	2.0	20.2	-35.1
	63	10.2	12.2	971.0	48.9	-5.6	11.3	-24.7
	64	9.3	12.2	971.4	50.1	-10.9	5.1	-27.9
	65	9.6	12.2	971.6	50.5	-11.7	4.2	-29.2
	67	9.4	12.2	971.8	51.1	-11.6	4.3	-29.2
	69	21.3	12.4	969.4	44.5	-9.2	4.1	-41.8
	71	21.1	12.3	970.0	46.6	-11.0	2.0	-43.7
	72	26.4	12.4	970.2	47.0	-2.0	12.2	-41.7
	74	27.2	12.3	970.9	48.7	-9.1	4.1	-47.0
	75	9.7	12.2	971.6	50.5	-3.4	10.4	-29.3
	76	8.4	12.2	971.6	50.5	4.4	19.3	-21.3

a: Number of experiment designated by MEHENDALE [168] in Table 10. The operation parameters for the respective experiment can be found in MEHENDALE [168], Table 10.

I Minimum Cooling Capacity of Low-GWP Refrigerants

Tables I.1-I.3 contain the calculated values of the minimum cooling capacity $\dot{Q}_{c,min}$ for the refrigerants R1234ze, R600a, and R1270. The structure of the tables is similar to Table 7.2 on page 163 for refrigerants R290 and R1234yf.

Table I.1: Minimum cooling capacity $\dot{Q}_{c,min}$ for R1234ze and lubricant 32-2.

		Outer pipe diameter[a] in mm										
T_{evap}	ΔT_{SH}	6	8	10	12	15	16	18	22	28	35	42
°C	K	Minimum cooling capacity $\dot{Q}_{c,min}$ in kW										
	5	0.03	0.08	0.16	0.28	0.54	0.65	0.91	1.59	2.77	5.10	8.30
-10	10	0.03	0.07	0.16	0.27	0.53	0.64	0.90	1.58	2.77	5.12	8.38
	15	0.03	0.07	0.15	0.27	0.53	0.64	0.90	1.59	2.78	5.17	8.48
	5	0.03	0.09	0.18	0.32	0.61	0.74	1.03	1.80	3.13	5.76	9.38
-5	10	0.03	0.08	0.18	0.31	0.60	0.73	1.02	1.78	3.12	5.78	9.45
	15	0.03	0.08	0.17	0.31	0.60	0.73	1.02	1.79	3.14	5.84	9.56
	5	0.03	0.10	0.20	0.36	0.69	0.83	1.16	2.02	3.51	6.47	10.54
0	10	0.03	0.09	0.20	0.35	0.68	0.82	1.14	2.00	3.50	6.49	10.60
	15	0.03	0.09	0.20	0.35	0.68	0.82	1.15	2.01	3.53	6.55	10.73
	5	0.04	0.11	0.23	0.40	0.77	0.93	1.29	2.26	3.93	7.24	11.79
5	10	0.04	0.11	0.22	0.39	0.76	0.91	1.28	2.24	3.92	7.25	11.85
	15	0.04	0.11	0.22	0.39	0.76	0.92	1.28	2.25	3.95	7.32	11.98
	5	0.04	0.12	0.25	0.44	0.86	1.03	1.44	2.51	4.37	8.06	13.13
10	10	0.04	0.12	0.25	0.43	0.84	1.02	1.43	2.50	4.36	8.07	13.18
	15	0.04	0.12	0.25	0.43	0.85	1.02	1.43	2.51	4.40	8.15	13.33

a: According to DIN EN 12735-1 [185].

Table I.2: Minimum cooling capacity $\dot{Q}_{c,min}$ for R600a and lubricant 22-2.

T_{evap}	ΔT_{SH}	Outer pipe diameter[a] in mm										
		6	8	10	12	15	16	18	22	28	35	42
°C	K	Minimum cooling capacity $\dot{Q}_{c,min}$ in kW										
-10	5	0.03	0.08	0.17	0.30	0.58	0.70	0.97	1.70	2.96	5.46	8.90
	10	0.03	0.08	0.17	0.31	0.60	0.72	1.01	1.77	3.09	5.72	9.35
	15	0.03	0.08	0.18	0.31	0.61	0.74	1.04	1.82	3.19	5.90	9.66
-5	5	0.03	0.09	0.19	0.33	0.65	0.78	1.09	1.90	3.30	6.09	9.92
	10	0.03	0.09	0.20	0.34	0.67	0.81	1.13	1.98	3.46	6.39	10.44
	15	0.03	0.10	0.20	0.35	0.69	0.83	1.16	2.04	3.56	6.60	10.79
0	5	0.04	0.10	0.21	0.37	0.72	0.87	1.21	2.11	3.67	6.76	11.01
	10	0.04	0.10	0.22	0.39	0.75	0.90	1.26	2.20	3.85	7.11	11.60
	15	0.04	0.11	0.22	0.40	0.77	0.93	1.30	2.27	3.97	7.34	12.00
5	5	0.04	0.11	0.24	0.41	0.80	0.96	1.34	2.34	4.07	7.48	12.18
	10	0.04	0.12	0.24	0.43	0.83	1.00	1.40	2.45	4.27	7.87	12.84
	15	0.04	0.12	0.25	0.44	0.85	1.03	1.44	2.52	4.40	8.14	13.29
10	5	0.04	0.13	0.26	0.46	0.88	1.06	1.48	2.58	4.49	8.25	13.43
	10	0.05	0.13	0.27	0.47	0.92	1.11	1.55	2.70	4.71	8.69	14.17
	15	0.05	0.13	0.28	0.49	0.95	1.14	1.60	2.79	4.87	8.98	14.66

a: According to DIN EN 12735-1 [185].

Table I.3: Minimum cooling capacity $\dot{Q}_{c,min}$ for R1270 and lubricant 80-2.

T_{evap}	ΔT_{SH}	Outer pipe diameter[a] in mm										
°C	K	6	8	10	12	15	16	18	22	28	35	42
		Minimum cooling capacity $\dot{Q}_{c,min}$ in kW										
	5	0.05	0.14	0.30	0.53	1.02	1.23	1.72	3.02	5.27	9.73	15.89
-10	10	0.05	0.14	0.30	0.54	1.05	1.27	1.78	3.14	5.51	10.26	16.85
	15	0.05	0.14	0.30	0.54	1.06	1.28	1.81	3.20	5.65	10.55	17.37
	5	0.06	0.16	0.33	0.58	1.12	1.35	1.89	3.30	5.76	10.65	17.38
-5	10	0.05	0.16	0.33	0.59	1.15	1.39	1.96	3.44	6.05	11.24	18.43
	15	0.05	0.16	0.33	0.60	1.17	1.42	2.00	3.53	6.21	11.58	19.05
	5	0.06	0.17	0.36	0.63	1.22	1.47	2.06	3.60	6.29	11.61	18.96
0	10	0.06	0.17	0.36	0.65	1.26	1.53	2.14	3.76	6.60	12.26	20.10
	15	0.06	0.17	0.37	0.66	1.29	1.56	2.19	3.87	6.80	12.67	20.81
	5	0.07	0.19	0.39	0.69	1.33	1.60	2.24	3.92	6.84	12.63	20.61
5	10	0.07	0.19	0.40	0.71	1.38	1.66	2.34	4.10	7.19	13.34	21.85
	15	0.07	0.19	0.41	0.72	1.41	1.71	2.40	4.22	7.42	13.80	22.65
	5	0.07	0.20	0.42	0.74	1.44	1.74	2.43	4.25	7.42	13.70	22.36
10	10	0.07	0.21	0.44	0.77	1.50	1.81	2.54	4.46	7.80	14.47	23.68
	15	0.07	0.21	0.44	0.79	1.54	1.86	2.61	4.59	8.06	14.98	24.56

a: According to DIN EN 12735-1 [185].